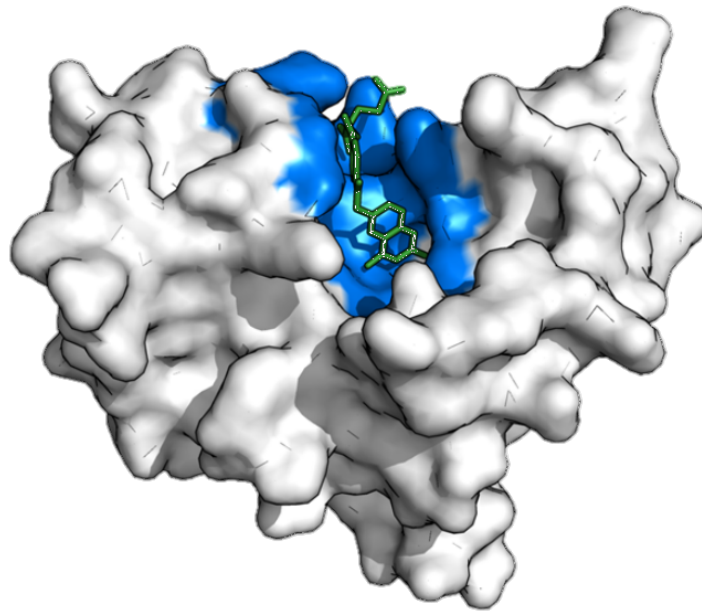




UNIVERSITA' DEGLI STUDI DI PAVIA

Dipartimento di Biologia e Biotecnologie "L. Spallanzani"

Targeting cellular kinases and viral factors for molecular therapy of cancer, neurodegenerative diseases and viral infections.



Jorge Isaac Armijos-Rivera

Dottorato di Ricerca in
Genetica, Biologia Molecolare e Cellulare
Ciclo XXX – A.A. 2014-2017



UNIVERSITA' DEGLI STUDI DI PAVIA

Dipartimento di Biologia e Biotecnologie "L. Spallanzani"

**Targeting cellular kinases and viral
factors for molecular therapy of cancer,
neurodegenerative diseases and viral
infections.**

Jorge Isaac Armijos-Rivera

Supervised by Prof. Giovanni Maga

Dottorato di Ricerca in
Genetica, Biologia Molecolare e Cellulare
Ciclo XXX – A.A. 2014-2017.

Abstract

Cells do not live in isolation; they are actually bombarded continuously by innumerable stimuli from their environment which cause signal cascades in the whole cell. Kinases are key factors in mediating this "rhapsody" of signals in the extra and intracellular communication network. Due the massive list of cellular processes in which kinases are involved with, it is not surprising that their physiological malfunction or deregulation is related with a number of human pathologies, including different cancers types, neurodegenerative diseases as well as viral infections. The identification of the role of specific kinases in the progression of specific diseases give us the possibility of exploiting their inhibition as a therapeutic strategy.

The Parkinson's disease (PD) related kinase leucine-rich repeat kinase 2 (LRRK2) and its pathogenic mutant form *G2019S* have been extensively studied in the last decade, because their importance as enzymatic targets against the neurodegenerative disease PD. Although, a few LRRK2 inhibitors having been published in the last years, to the best of our knowledge, only a few reports have been published on the selective inhibition of the *G2019S* mutant over wild type LRRK2. In this regard, we design and characterize a library of small molecules able to inhibit the enzymatic activity of LRRK2. We were able to identify promising compounds selective towards the *G2019S* form, which are good candidates for further biological investigations.

On the other hand, traditionally antiviral drug discovery has been mainly focused on the inhibition of viral targets, leading to the development of highly specific drugs to fight specific infections. As a consequence of the high mutation rate of RNA viruses, the major problem with compounds that directly target specific viral proteins is the rapid emergence of new drug-resistant viral strains. Using *in vitro* assays, we identified active compounds that were able to inhibit the kinase activity of the cellular enzyme Phosphatidylinositol 4 kinase III beta (PI4KIII β) at micromolar concentrations. Because this kinase has been described to be exploit by several ssRNA+ virus to their replication, we propose these inhibitors as a valuable starting point in the developing of novel broad-spectrum antivirals.

Indeed, in cell based experiments some of the tested compounds demonstrate to be active against a representative panel of enteroviruses.

The last part of my work during my PhD internship has been focused on the characterization of new Indolyl aryl sulfone (IAS) as HIV-1 nonnucleoside reverse transcriptase inhibitors. IAS have been shown to potently inhibit RNA-dependent DNA polymerization of wild type (*wt*) and drug resistant mutants of HIV-1. Herein, we describe the mechanism of inhibition of a selected IAS derivative (**RS5187**) that shows high inhibitory potency against the *wt* and the drug resistant mutant *K103N-Y181C* forms of HIV-1 reverse transcriptase (RT). Our results demonstrate that these compounds inhibit RT displaying a different mechanism against the *wt* or the mutated form, suggesting new strategies for the development of inhibitors showing high potency of action towards mutants resistant to the current antiretroviral therapy.

Acknowledgements

My sincere thanks and gratitude to my mentor and supervisor Prof. Maga, an outstanding scientist, for having me provided the opportunity to work in his laboratory of molecular virology and DNA enzymology in Pavia. His continuous support and scientific advice motivated me to carry out my doctoral thesis and helped me to overcome troublesome experimental situations. I highly appreciate his patience and every precious thought of his immense wisdom he shared with me throughout my three-year PhD studies. I would like to thank Prof. Maga for reviewing my thesis manuscript, for his critical view and suggestions, which altogether led to creation of a better manuscript.

I don't have enough words to express gratitude to Dr. Crespan for having me introduced into the world of the enzymatic assays, for his inputs on data analysis, for his comments and vigilance on my experiments and for all these hours reviewing my thesis manuscript. Thank you for having always been incredibly supportive and for being always willing to discuss my results and provide me with useful suggestions and comments.

I gratefully acknowledge to all my laboratory colleagues, in particular to Elisa Mentegari and Nadia Garibaldi; thank you for your suggestions, support and for your valuable friendship.

I would also like to thank Dr. Miroslava Kissova for all the advice regarding my experiments.

Finally, I would like to thank the support of the Secretaria Nacional de Educación Superior Ciencia y Tecnología del Ecuador (SENESCYT), who funded my study grant.

Abbreviations

3TC: Lamivudine;
ABC: Abacavir;
ACBD3: Acyl- CoA-Binding Domain Containing Protein 3
AIDS: Acquired Immunodeficiency Syndrome
Arf1: ADP-Ribosylation Factor 1
ATV: Atazanavir
AZT: Azidothymidine
AZTTP: Azidothymidine triphosphate
BBB: Blood-Brain Barrier
CD4: Cluster of quadruple Differentiation
CDP-DG: Cytidine Diphosphate-Diacylglycerol
CNS: central nervous system
COMT: Catechol-O-methyltransferase inhibitors
D4T: Stavudine
DBS: Deep Brain Stimulation
DDI: Didanosine;
eEF1A2: Effector of Eukaryotic Elongation Factor 1 Alpha 2
EFV: Efavirenz
ER: Endoplasmic Reticulum
ETR: Etravirine
FAPP: Four-Phosphate-Adaptor Protein
FDA: Food and Drug administration
FPV: Fosamprenavir;
Fq: Frequenin
FTC: emtricitabine
GBD: Global burden disease
GBF1: Golgi-Specific Brefeldin A-Resistance Guanine Nucleotide
Exchange Factor 1
HAART: High Activity Anti-Retroviral Therapy
HCV: Hepatitis C virus
HIV: Human Immunodeficiency Virus
Hsp90: Heat shock protein 90
IAS Indolyl Aryl Sulfones

IDV: Indinavir
I κ B α : Inhibitor of κ B
IN: Integrase
L-DOPA: Levodopa
LKU: Lipid Kinase Unique Domain
LPV: Lopinavir
LRRK2: Leucine Rich Repeat Kinase 2
LTR Long-Terminal-Repeats
MA: HIV matrix
MAO: Monoamine oxidase inhibitors
MLV: Murine leukemia virus
MRI: Magnetic Resonance Imagine
NA (Substrate): Nucleic acid
NCS-1: Neuronal Calcium Sensor-1
NF- κ B: nuclear factor κ B
NFV: Nelfinavir
NNBS: NNRTIS binding site
NNRTIS: Non-nucleoside reverse transcriptase inhibitors
NRTIS: Nucleoside reverse transcriptase inhibitors
NVP: Nevirapine
Pbs: Primer-binding-site
PD: Parkinson's disease
PET: Positron Emission Tomography
PH: Pleckstrin Homology
PI3Ks: Phosphoinositide 3 lipid kinases
PI4KIII β : Phosphatidylinositol 4 kinase type III beta
PI4KIII α : Phosphatidylinositol 4 kinase type III alpha
PI4Ks: Phosphoinositide 4 lipid kinases
PIC: pre-integration-complex
PIKs: Phosphoinositide lipid kinases
PIP5Ks: Phosphoinositide Phosphate 5 lipid kinases
PIP3Ks: Phosphoinositide Phosphate lipid kinases
PIs: Phosphoinositides
PI: protease inhibitors
PKD: Vesicular-Transport-Regulator Protein Kinase D
Ppt: polypurine track

PR: Protease
Pro-Rich: Proline Rich Sequences
PtdIns: phosphatidylinositol
PtdIns4P: Phosphatidylinositol 4-phosphate
Rdrp 3D^{pol} : RNA-dependent RNA polymerase
ROS. Reactive oxygen species
RPV: Rilpivirine
RT: Reverse Transcriptase
Rtis: Reverse Transcriptase Inhibitors
SHIP1: Phosphatidylinositol-3,4,5-trisphosphate 5-phosphatase 1
SIV: Simian Immunodeficiency Virus
SNCA: Synuclein alpha gene
SPR: Sepiapterin reductase
TDF: Tenofovir disoproxil fumarate;
TGFA: Transforming growth factor- α
TGN: *Trans*-Golgi Network
TPV: Tipranavir
TRPV1: Transient Receptor Potential Vanilloid 1
Vpr: Viral-protein-R
ZDV: Zidovudine

CONTENTS

ABSTRACT 3

ACKNOWLEDGEMENTS..... 5

ABBREVIATIONS 6

CONTENTS 9

1. INTRODUCTION 12

1.1. PART I: LEUCINE RICH REPEAT KINASE 2 (LRRK2) IN PARKINSON'S DISEASE 13

1.1.1. Parkinson's disease:..... 13

1.1.2. PD diagnostic..... 14

1.1.3. Treatments for Parkinson's disease. 15

1.1.3.1. Pharmacotherapy..... 16

1.1.3.1.1. Dopaminergic therapy..... 16

1.1.3.1.2. Non- dopaminergic therapy..... 17

1.1.3.2. New approved drugs..... 18

1.1.3.3. Deep brain stimulation. 18

1.1.4. Genetics of Parkinson's disease 19

1.1.4.1. Leucine-Rich Repeat Kinase 2 and Parkinson's disease 21

1.2. PART II: PHOSPHATIDYLINOSITOL KINASES AND THEIR ROLES IN CANCER AND VIRAL INFECTIONS 24

1.2.1. PI4KIII β 27

1.2.2. PI4KIII β structure..... 29

1.2.3. PI4KIII β and cancer..... 29

1.2.4. PI4KIIIβ and viral diseases	33
1.3. PART III: HIV-1 Reverse Transcriptase	35
1.3.1. HIV/AIDS.....	35
1.3.2. Human Immunodeficiency Virus (HIV)	36
1.3.2.1.1. HIV structure and genome	37
1.3.2.1.2. HIV replication cycle and tropism	38
1.3.2.1.3. Entry to the cell.....	38
1.3.2.1.4. HIV Nuclear import.....	39
1.3.2.1.5. HIV Genetic expression	40
1.3.2.1.6. HIV-1 reverse transcriptase (RT)	41
1.3.2.1.7. RT synthesis and structure	41
1.3.2.1.8. The process of reverse transcription	42
1.3.3. HIV-1 control strategies and the drug resistance problem.....	44
1.3.4. High Activity Anti-Retroviral Therapy (HAART).....	45
1.3.5. HIV Reverse Transcriptase Inhibitors (RTIs).....	46
1.3.5.1. Nucleoside reverse transcriptase inhibitors (NRTIs).....	46
1.3.5.1.1. Non-nucleoside reverse-transcriptase inhibitors (NNRTIs)	48
2. AIMS OF THE RESEARCH.....	51
3. MATERIALS AND METHODS	52
3.1. PART I: Leucine Rich Repeat Kinase 2 (LRRK2)	50
3.1.1. In vitro LRRK2 inhibition assay	50
3.1.2. Inhibition mechanism	50
3.1.3. Kinase panel	51
3.2. PART II: PHOSPHATIDYLINOSITOL KINASES.....	54
3.3. In vitro kinase inhibition assays.	54
3.4. Kinase panel.	54
3.5. PART III: HIV-1 REVERSE TRANSCRIPTASE	55
3.5.1. Chemical reagents.....	55

3.5.2.	Protein purification.....	55
3.5.3.	In vitro RT enzymatic assays.....	56
3.5.4.	Inhibition mechanism.....	57
3.5.5.	Association / dissociation rate analysis.	58
4.	RESULTS.....	60
4.1.	PART I: targeting LRRK2.....	60
4.1.1.	Characterization of heteroaryl-hydrazones derivatives by a multicomponent pharmacophore fragment decoration approach	60
4.2.	PART II: Targeting PI4KIIIβ:.....	68
4.2.1.	Identification of multitarget agents active as broad-spectrum antivirals.	68
4.3.	PART III: Targeting HIV-1 RT.....	77
4.3.1.	RT purification.....	77
4.3.2.	Evaluation of the inhibition potency of a library of new IAS derivatives.....	77
4.3.3.	The mechanism of action of RS5187.	80
4.3.3.1.	Kinetic parameters of RS5187 toward HIV-1 RT <i>wt</i>.....	80
4.3.3.2.	Kinetic parameters of RS5187 toward HIV-1 RT drug resistant mutant <i>K103N-Y181C</i>.	84
6.	DISCUSSION.....	88
	REFERENCES.....	93
	LIST OF ORIGINAL MANUSCRIPTS.....	108

1. Introduction

Kinases are by definition enzymes with the capability to phosphorylate a receptor aminoacidic residue located on a protein substrate or a lipidic residue. The reversible phosphorylation of proteins and lipids is a modulator mechanism of several cellular functions across all the living organisms. Until now, due to the understanding of the human genome sequence, more than 500 protein and lipid kinases have been identified (Manning G *et al.*, 2002). According to the type of substrate, kinases can be classified into two large groups: protein kinases and lipid kinases. Protein kinases are further divided into Serine-Threonine Kinases, which phosphorylate the -OH group of the serine or threonine residues, and Tyrosine Kinases, which phosphorylate the -OH group of the aminoacidic residue tyrosine on their substrates. Phosphoinositide lipid kinases (PIKs) phosphorylate lipids present in the cell, both on the plasma membrane and on the membranes of the organelles, generating phosphorylated variants of phosphatidylinositol (PtdIns), that are critical for second messenger signaling and cellular remodeling (Brown J and Auger K, 2011).

The phosphorylation cascades orchestrated by kinases regulate important and critical cell pathways and, for this reason, the activities of kinases are finely regulated in cells. However, mutations and dysregulation of kinases are well-known to contribute to the development of many human disorders, including neurodegenerative disorders and several types of cancer (Manning G *et al.*, 2002). Therefore, kinases are considered important targets against different oncologic, neurodegenerative and even viral diseases.

The knowledge of the role of kinases in normal and pathological conditions led to the development of several drugs directed against the enzymatic activity of target kinases in order to treat the disease by correcting their deregulation.

1.1. PART I: LEUCINE RICH REPEAT KINASE 2 (LRRK2) IN PARKINSON'S DISEASE

1.1.1. PARKINSON'S DISEASE:

Pathological and Clinical features of PD

Parkinson's disease (PD) is a chronic and progressive movement disorder of the central nervous system (CNS), typically represented by tremor rigidity and slowness of the movement (Massano J and Bhatia K, 2012) PD is the second most common neurodegenerative disease worldwide just after Alzheimer's disease, affecting 5 million people (GBD 2015 disease and injury incidence and prevalence collaborators, 2016) and resulting in about 117,400 deaths globally (GBD 2015 mortality and causes of death collaborators, 2016).

The predominant motor symptoms are collectively named "parkinsonian syndrome" or "parkinsonism" (Samii A *et al*, 2004), but mental and behavioral problems may also occur even if PD has been traditionally consider as a motor disorder (de Lau L and Breteler M, 2006). The specific group of symptoms of PD varies from person to person, but usually, the primary motor signs of PD include tremor of the hands, arms, legs, jaw and face as well as bradykinesia or slowness of movement, rigidity and postural instability accompanied to impaired balance and coordination.

The motor symptoms are known to be the consequence of the neuronal degeneration caused by the cell death in the *substantia nigra* pars compacta region, which is defined as the main pathological characteristic of the PD patients (Samii A *et al*, 2004). The main effects of cell degeneration in this area are the low levels of dopamine, as well as the pathological depigmentation of this area, caused by the loss of nigrostriatal dopaminergic neurons, typical of several neuropathologies (Segura-Aguilar J, 2017). In most of cases the disease symptoms are manifested when about 80% of dopamine at striatum and 50% of dopaminergic neurons in the *substantia nigra* are lost (Fearnley J and Lees A, 1991).

The cause of the cell death in this region is still poorly understood but coincides with the formation and accumulation of protein in inclusions bodies, known as Lewy bodies, in the affected neurons. These intracellular structures are the pathological hallmarks of the disease (Christine C and Aminoff M, 2004).

The neurologist Frederic Lewy (1885-1950) in 1912 detected for the first time the Lewy bodies in the brains of PD patients. Nowadays these eosinophilic inclusions are classified by their morphology and location, into those found within the *substantia nigra* in the brain stem, with a characteristic dense core surrounded by a halo of radiating fibrils, and cortical Lewy bodies that not exhibit particular distinctions between the nucleus and the halo (Uversky V, 2017).

In general, Lewy bodies are spherical masses mainly composed by the protein α -synuclein associated with neurofilament proteins (i.e. keratin). Moreover, ubiquitin and tau proteins, which stabilize microtubules in neurons of the central nervous system, may also be present (Massano J and Bhatia K, 2012).

The α -synuclein is a protein particularly abundant in neurons, especially in presynaptic terminals. Recent studies showed that high concentration of α -synuclein and ubiquitinated proteins in Lewy bodies suggest a fault in protein degradation pathway, such as proteosomal degradation or autophagy (de Lau L and Breteler M, 2006; Uversky V, 2017). However, the mechanism that leads, from the accumulation of proteins in the neuron's cytoplasm to the formation of Lewy bodies is still unclear. Although Lewy bodies are a pathological characteristic of PD, they are also characteristic of some variants of dementia and Alzheimer's disease (Christine C and Aminoff M, 2004).

1.1.2. PD Diagnostic.

The pathophysiology behind cognitive and neuropsychiatric symptoms in PD is undoubtedly complex and individually variable. Reliable biomarkers that can be applied for early diagnosis and for the surveillance of disease

progression are the basis of clinical treatments and the discovery of several genetic factors linked to PD offer the opportunity to use them as biomarkers for the identification of individuals at risk. However, given the polymorphism present in idiopathic PD where normal aging, genetics and environmental factors are involved, definitive biomarker and diagnostic laboratory tests are current not yet available. For this reason, the clinical diagnosis in the early stages of the disease represent an open challenge, being based mainly on physical examination that evaluates the improvement of symptoms after dopamine treatment. Some neuroimaging technologies, like Magnetic Resonance Imagine (MRI) or Positron Emission Tomography (PET), using markers to trace the dopamine levels on the brain, can be used to a more accurate diagnosis and rule out disorders that could give rise to similar symptoms (Samii A *et al*, 2004; Christine C and Aminoff M, 2004; Mandel S *et al.*, 2010; Gerlach M *et al.*, 2012; Barber T *et al.*, 2017). Unfortunately, such lack of biomarker for PD leads to a high the rate of misdiagnosis (Atashrazm F and Dzamko N, 2016; Gerlach M *et al*, 2012).

1.1.3. Treatments for Parkinson's Disease.

Finding a suitable treatment for PD patients is very difficult for several reasons. The PD is a degenerative disease with a progressive development, which means that it will worsen over time and, as the disease progresses, the effectiveness of the drugs decreases becoming increasingly difficult to control the symptoms. Over the years, many agents and therapeutic approaches have been tested. As a result, there are currently new therapies and approaches available to treat PD in its different stages, moreover nowadays many promising treatments continue to be evaluated either in the laboratory or clinical trials in order to meet the unmet needs of this disease. In a general view, there is widespread consensus in the classification of treatments for PD: non-pharmacological therapy, pharmacotherapy, functional neurosurgery, transplantation and gene therapy (Kakkar A and Dahiya N, 2015).

1.1.3.1. Pharmacotherapy.

Among the forms of treatment, pharmacotherapy is considered the most efficient in the early stages of PD (Chieng L *et al*, 2015), it can be divided into dopaminergic and non-dopaminergic treatments.

1.1.3.1.1. Dopaminergic Therapy.

Many of the characteristic symptoms of PD are due to a deficiency of dopamine in the brain (Samii A *et al*, 2004). So, the first option to contain the early symptoms of the disease consists of dopamine compensation strategies (administration dopamine agonist). Despite its efficacy, this therapy just works as a palliative measure for early motor symptoms since it does not influence the continuous neuronal loss (Clarimón J and Kulisevsky J, 2013; Kakkar A and Dahiya N, 2015).

Levodopa (L-DOPA), and other dopamine agonists, are widely used instead of dopamine (Chieng L *et al*, 2015) since it is unable to cross the blood-brain barrier (BBB). However, when administered alone, only 5–10% of L-DOPA reach the dopaminergic neurons. The rest is metabolized into dopamine elsewhere, causing several of the side effects of Levodopa treatment, including nausea, dyskinesia and hypotension (Samii A *et al*, 2004).

Pharmacological treatment, especially the long-term use of levodopa, can lead to some motor complications. In these circumstances “on” periods can manifest, in which the patient has an adequate response to antiparkinson medication with an improvement of the clinical symptoms. Subsequently “off” periods occur, in which the response to levodopa decreases and the symptomatology of the disease, such as tremor or difficulty walking, return despite the treatment (Nutt J, 2001; Brodsky M *et al.*, 2010). The short half-life of levodopa may be the main cause of these fluctuations (Samii A *et al*, 2004; Elshoff J *et al.*, 2015).

Akinesia of awakening and wearing-off phenomenon are considered as predictable motor fluctuations as they follow a clear dose-response pattern. On the other hand, non-predictable “on-off” phenomenon has a complex

relationship with medication intakes where the “on” and “off” periods alternate without an apparent relation with levodopa doses. (Lees A, 1989; Samii A *et al*, 2004)

There are other drugs that may be useful in the treatment of motor symptoms that are usually administered if one dopamine agonist is not well tolerated by the patient. However, levodopa remains the most potent drug and the backbone along the antiparkinson treatment despite its severe side effects observed after long term treatment (Elshoff J *et al.*, 2015; Patil A *et al.*, 2017).

1.1.3.1.2. Non– dopaminergic therapy.

In general, peripheral dopadecarboxylase inhibitors (carbidopa or bencerazide) are given in combination with levodopa to prevent its anticipated conversion into dopamine, thus increasing the amount of L-DOPA in the central nervous system (Etminan M *et al*, 2003). In addition, other drugs are included into the therapy in order to decrease the side effects due to peripheral dopamine accumulation derived from dopamine agonist treatments.

Domperidone is a drug that acts as a dopamine antagonist, blocking selectively the dopaminergic receptors. Domperidone does not cross the BBB, therefore it blocks the dopamine receptor D2 (Lees A, 1989; Elshoff J *et al.*, 2015) without worsen the disease. In PD patients under PD treatment the drug is used to relieve nausea and vomiting (Elshoff J *et al.*, 2015).

Monoamine oxidase (MAO)-B inhibitors, as Azilect (rasagiline) and Zelapar (selegiline), act against the enzymatic activity of MAO, which is found mainly in both neurons and astroglia, and outside the CNS in brain, in liver and in intestinal mucosa. MAO regulates the metabolic degradation of catecholamines and serotonin in the CNS and peripheral tissues and is divided in types A and B, with the latter representing the major form in the human brain (Kakkar A and Dahiya N, 2015; Elshoff J *et al.*, 2015). Therefore, inhibition of MAO-B, specifically avoids dopamine degradation in the brain.

Catechol-O-methyltransferase (COMT) inhibitors prevent the peripheral breakdown of levodopa. This increases the overall bioavailability of levodopa and its concentration in the brain, prolonging the clinical response to dopaminergic therapy.

Anticholinergic drugs block the neurotransmitter acetylcholine in the central and the peripheral nervous system. Restoring the balance between the levels of acetylcholine and dopamine, in PD patients this treatment decreases tremor, and may alleviate rigidity and bradykinesia.

1.1.3.2. New approved drugs.

Safinamide (Xadago) has been approved in 2017 as a complement in the treatment of PD with levodopa/carbidopa in patients with “off” episodes. Xadago significantly increases daily “on” time without dyskinesia. It is a selective, reversible MAO-B inhibitor with favorable pharmacokinetic and side-effect profiles (Dézsi L and Vécsei L, 2014). Differently from other MAO-B inhibitors, other than increasing the stability of dopamine in the brain, it also blocks the release of glutamate, an important neurotransmitter which in PD acts as a neurotoxin (Blandini F *et al.*, 1996).

1.1.3.3. Deep Brain Stimulation.

As mentioned above the use of dopaminergic and non-dopaminergic drugs could effectively improve mobility and reduce dyskinesias, but long-term medical management is often complicated. Similar to the pharmacological treatments currently available, surgical options offer symptomatic benefits.

Deep brain stimulation (DBS) consist in electric stimulation of specific areas of the brain exerted by electrodes placed on one or both cerebral hemisphere, connected to a neurostimulator device. Through the electrodes, electrical impulses are send to the areas of the brain that control movement, located in subthalamic nucleus or the *globus pallidus interna*. The electrical pulses block signals that cause the motor symptoms of PD (Chieng L *et al.*, 2015; Kakkar A and Dahiya N, 2015; Sidiropoulos C *et al.*, 2017; Fang J and Tolleson C, 2017).

DBS represent a treatment choice for patients with advanced PD motor symptoms, particularly those in whom symptoms cannot be adequately controlled with drugs. In terms of mobility, emotional well-being, bodily discomfort and activities of daily living, neurostimulation has proven to be more effective than medication alone (Deuschl G *et al.*, 2006; Kurtis M *et al.*, 2016). Although DBS has been approved by the FDA since 1997 as a useful tool to counteract the motor symptoms of PD, the exact mechanism with which DBS acts as well as the impact on non-motor symptoms continues to be ambiguous (Kurtis M *et al.*, 2016).

1.1.4. Genetics of Parkinson's Disease

Although the etiology of most of PD cases is still unknown, the identification of specific genetic defects on PD familiar cases contributed to shed light on the molecular mechanisms that determine PD pathogenesis (Chen C *et al.*, 2012; Gatto E *et al.*, 2013; Hardy J *et al.*, 2009).

Some factors such as the natural aging, diet and lifestyle, over the years, have been considered as risk agents for PD, even if none of them is considered essential for PD outcome and progression. Only in 1997 it was discovered that recurrent mutations occur in the SNCA gene in patients with PD (Mata I *et al.*, 2006; de Stefano A *et al.*, 2002). The SNCA gene encodes alpha-synuclein, the major component of Lewi Bodies (Massano J and Bhatia K, 2012; Du T *et al.*, 2015; Uversky V, 2017). Since then, several families have been identified with parkinsonism with a clear Mendelian inheritance and other "PD genes" associated with familiar forms of PD have been discovered. About 10% of PD cases are caused by monogenetic forms (de Lau L and Breteler M, 2006; Gatto E *et al.*, 2013).

Nowadays, inherited mutations that cause familial PD, mostly missense mutations, have been identified in 18 genes (Atashrazm F and Dzamko N, 2016), which are predominantly involved in protein quality control and mitochondrial metabolism (Table. 1). All these mutations are associated with altered function(s) of the associated genetic product (Table. 1).

Table 1: Monogenic forms of Parkinson's disease

LOCUS	GENE	CHROMOSOME	INHERITANCE	PROTEIN	PROTEIN FUNCTION	PD PHENOTYPE	OTHER PHENOTYPE
PARK1	SNCA	4q21-23	AD	α -synuclein	Dopamine release and transport.	Young onset, rapid progression	
PARK2	<i>Parkin</i>	6q5.5-q27	AR	Parkin	Ubiquitin ligase	Young onset, slow progression	Early dystonia, and dyskinesia
PARK3	Unknown*	2p13	AD			Similar to idiopathic PD	Dementia
PARK4	<i>SNCA</i>	4p16	AD	SNCA		Young onset, dementia	Dementia
PARK5	<i>UCHL1</i>	4p14	AD	UCHL-1	Ubiquitin C-terminal hydrolase	Similar to idiopathic PD	
PARK6	<i>PINK1</i>	1p36	AR	PINK1	PTEN-induced kinase, protection against mitochondrial dysfunction	Young onset, benign course, levodopa responsive	
PARK7	<i>DJ-1</i>	1p36	AR	DJ-1	Protection against oxidative stress	Similar to idiopathic PD, levodopa responsive	
PARK8	<i>LRRK2</i>	12p11.2-q13.1	AD	LRRK2	Membrane trafficking, role in cytoskeletal dynamics	Late-onset, indistinguishable from idiopathic PD	
PARK9	<i>ATP13A2</i>	1p36	AR			Parkinsonism with spasticity, dementia, and supranuclear palsy	Dementia, pyramidal syndrome
PARK10	Unknown	1p32	Unknown				
PARK11	<i>GIGYF2</i>	2q36-37	Unknown			No definite	
NURR1	Unknown	2q22-q23	AD	NR4A2	Nuclear receptor		

Data were extrapolated from: De Stefano A *et al.*, 2002; Cuervo A *et al.*, 2004; Bonini N and Giasson B, 2005; de Lau L and Breteler M, 2006; Clarimón J and Kulisevsky J, 2013; and Gasser, 2015.

*Candidate genes in this region: Transforming growth factor- α (TGFA), cytochrome P450 retinoid metabolizing protein (P450RAI- 2), sepiapterin reductase (SPR, or 7,8-dihydrobiopterin: NADP oxidoreductase), and the N-acetyltransferase 8 (putative) 2 (CML2)

Familial PD forms usually exhibit some differences in the symptoms and disease progression rather than idiopathic PD. For example, mutations in α -synuclein are often associated with a more aggressive form than idiopathic PD (Bonini N and Giasson B, 2005; Uversky V, 2017). On the contrary, recessively inherited PINK1 mutations displays a much earlier onset and often a more severe course of the disease (de Lau L and Breteler M, 2006).

1.1.4.1. Leucine-Rich Repeat Kinase 2 and Parkinson's Disease

Leucine-Rich Repeat Kinase 2 (LRRK2) is a large (280 kDa) multi-domain serine-threonine kinase, encoded in humans by the PARK8 gene. LRRK2 belongs to leucine rich repeat kinase family, since it contains several copies of a signature aminoacidic repeat module called leucine-rich domain (Göring S *et al.*, 2014). The expression of LRRK2 has been identified on several brain regions as cerebral cortex, *substantia nigra* and caudate putamen (Westerlund M *et al.*, 2008; Chen C *et al.*, 2012) but seems to be more abundant in kidney, lung, spleen and testis of mammals (Maekawa T *et al.*, 2010). LRRK2 also, appears to be a relatively abundant protein of human peripheral blood mononuclear cells including, CD14⁺ monocytes, CD19⁺ B-cells, and CD4⁺ as well as CD8⁺ T-cells. Moreover, *LRRK2* expression is up-regulated in cultured macrophages in the presence of microbial structures and lentiviral particles, and its activity contributes to interferon γ signaling (Hakimi M *et al.*, 2011).

LRRK2 influences the activity of several transcription factors. It has been shown that LRRK2 positively regulates microglial inflammation via the nuclear factor κ B (NF- κ B) pathway by stimulation of expression and by phosphorylation of the inhibitor I κ B α (inhibitor of κ B) (Gardet A *et al.*, 2010; Kim B *et al.*, 2012; Hongge L *et al.*, 2015). Furthermore, Recent studies demonstrate that Na⁺/K⁺-ATPase activity is considerably lower in dendritic cells isolated from mice lacking functional LRRK2 (*LRRK2*^{-/-}). By direct phosphorylation LRRK2 is able to up-regulate the activity of the forkhead box transcription factor FoxO1, in addition, LRRK2 activity also contributes in the regulation of reactive oxygen species (ROS) production

and in the monocyte maturation (Gardet A *et al.*, 2010; Thévenet J *et al.*, 2011). Some studies report that LRRK2 deficiency leads to nuclear up-regulation of NFAT (Jabri B *et al.*, 2011; Liu Z *et al.*, 2011) which is expressed in most cells of the immune system but it is also involved in the development of cardiac, skeletal muscle, and nervous systems.

Table 2: LRRK2 pathogenic and putatively pathogenic mutations.

Location	Aminoacid substitution	Aminoacid conservation across vertebrates	Domain	Disease segregation
Exon 19	R793M	Yes ^a	Ankyrin repeat	NR
Exon 21	Q930R	Yes		NR
Exon 24	R1067Q	Yes	LRR	NR
Exon 24	S1096C	In mammals	LRR	NR
Exon 24	L1114L	NA	Splicing	Yes
Exon 25	I1122V	Yes	LRR	Yes
Exon 27	S1228T	Yes ^b	LRR	NR
Exon 29	I1371V	Yes	Roc	NR
Exon 31	R1441C	Yes	Roc	Yes
Exon 31	R1441G	Yes	Roc	Yes
Exon 31	R1441H	Yes	Roc	NR
IVS31	NA	NA	Splicing	NR
Exon 32	R1514Q	In mammals	COR	NR
IVS33	NA	NA	Splicing	NR
Exon 35	Y1699C	Yes	COR	Yes
Exon 38	M1869T	Yes	COR	NR
Exon 40	R1941H	Yes	Kinase	NR
Exon 41	I2012T	Yes	Kinase	Yes
Exon 41	G2019S	Yes	Kinase	Yes
Exon 41	I2020T	Yes	Kinase	Yes
Exon 48	T2356I	No	WD40	NR
Exon 48	G2385R	No	WD40	NR

^a Except M in mouse, ^b Except in chicken.

Abbreviations: IVS=intervening sequence; NA=not applicable; NR=Not reported.

Data were extrapolated from Mata I *et al.*, 2006.

In neurobiology and pathology, LRRK2 became an important target since its mutations has been associated with both autosomal-dominant and late-onset sporadic PD cases (Yun H *et al.*, 2011; Cookson M, 2010). Importantly, differently from all the other familial PDs, the clinical features of LRRK2 PD are indistinguishable from the idiopathic form (Shen J, 2004; Hardy J *et al.*, 2009) (Table 1). The most common LRRK2 mutations in PD are the missense mutations located within the catalytic kinase domain or in the ROC-COR tandem GTPase domain (Tab. 2). These mutations are present in ratio of 5–13% of familial PD and 1–5% of sporadic PD (Chen C *et al.*, 2012; Fell M *et al.*, 2015). All these mutations increase the level of auto-phosphorylation of LRRK2 (Atashrazm F and Dzamko N, 2016), enhancing its kinase activity. Among those mutation, G2019S is the most common pathological one. The other four LRRK2 mutations (*R1441C*, *R1441G*, *Y1699C*, and *I2020T*) are much less common, having been identified in only a small number of patients (Hardy J *et al.*, 2009; Clarimón J and Kulisevsky J, 2013). The biological consequence of enhanced LRRK2 activity is still poorly understood. However, studies in cell lines or in animal models such as in flies, worms, and mice have shown that overexpression of *G2019S* LRRK2 may favor neuronal degeneration (Hardy J *et al.*, 2009).

Inhibition of LRRK2 kinase activity, and in particular of the pathogenic mutant *G2019S*, has been proposed as an attractive therapeutic strategy for the treatment of PD (Hatano T *et al.*, 2009; Mark *et al.*, 2010). Among the first-generation selective compounds, LRRK2-IN-1 appeared to be a promising agent for PD therapeutic studies. In fact, it presents high selectivity and potency against both LRRK2 *wt* and its mutant form *G2019S*. However, its bulky size and impermeability through the BBB limited the LRRK2-IN-1 use *in vivo*. Moreover, LRRK2-IN-1 cause a number of off-target effects relating to inflammatory pathways (Deng X *et al.*, 2011; Luerman G *et al.*, 2014). Among the second generation of LRRK2 inhibitors, HG-10-102-1 shows interesting features. During *in vivo* examination, following intraperitoneal administration at a dose of 100 mg/kg, this inhibitor was able to cross the BBB and completely inhibit

LRRK2 activity in mouse brain. However, with lower doses of 10 and 30 mg/kg, HG-10-102-1 could only partially inhibit LRRK2 in brain (Choi H *et al.*, 2012). Despite a few LRRK2 inhibitors having been published in the last years (Kirrane T *et al.*, 2012; Kramer T *et al.*, 2012), only a few reports have been published on the selective inhibition of the *G2019S* mutant over wild type LRRK2 (Franzini M *et al.*, 2013; Lang C *et al.*, 2015). Considering that the physiological and pathological functions of this kinase remain poorly understood, it would be desirable to identify novel chemical probes able to selectively inhibit the pathogenic *G2019S* LRRK2 mutant.

1.2.PART II: PHOSPHATIDYLINOSITOL KINASES AND THEIR ROLES IN CANCER AND VIRAL INFECTIONS

Phosphoinositide lipid kinases (PIKs) are the enzymes responsible for the production of the different species of phosphatidylinositol (PtdIns) (Scheme 1). PIKs are widely distributed throughout the cell where their enzymatic activity on PtdIns can change their reactivity and localization. PI3Ks purified from rat liver were the first mammalian lipid kinases to be discovered (Carpenter C *et al.*, 1990); today, a total of 18 PIKs have been described divided into three major subfamilies PI3Ks, PI4Ks and PIPK / PIP5Ks (Scheme 1).

PtdIns and its derivatives known as phosphoinositides (PIs), consist in a family of lipids of the class of the phosphatidylglycerides. They represent only 10 to 20% of total cellular phospholipids (Balla T, 2013) and a very small part of total lipids present in the cellular membrane compartments. The biosynthesis of PtdIns is catalyzed by phosphatidylinositol synthase in the endoplasmic reticulum (ER) (Kim Y *et al.*, 2011) from *myo*-inositol and CDP-diacylglycerol (CDP-DG) (Agranoff B *et al.*, 1958; Benjamins J and Agranoff B, 1969).

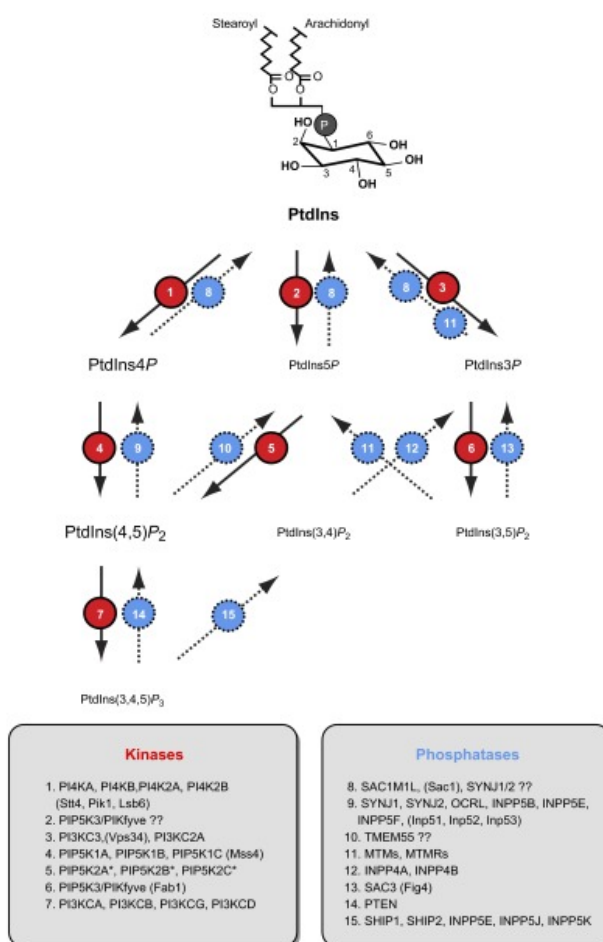
Structurally PtdIns consist of a glycerol backbone esterified to two fatty acids chains and a phosphate group attached to a cyclic polyol *myo*-inositol at the position D1. This inositol head group possesses five hydroxyls ready

for phosphorylation located in positions D2 through D6. However, only -OH groups located at positions D3, D4 and D5 (Top of Scheme 1) are naturally phosphorylated, giving rise to seven PtdIns derivatives (Balla T, 2013) (Scheme 1).

There is a hierarchical organization in the production of PIs as well as of its distribution between the various membrane compartments. As a PI moves outward from the nucleus toward the plasma membrane, the extent of inositol lipid phosphorylation is increased. In this manner, the endoplasmic reticulum and nuclear envelope mainly contain PtdIns. The endosomal compartments, including the Golgi, contain monophosphorylated PtdIns, such as PtdIns4P or PtdIns3P. The plasma membrane has the PtdIns(4,5)P₂ and PtdIns(3,4,5)P₃. The only exception is PtdIns(3,5)P₂ that is formed at the multivesicular body, which is an endomembrane compartment (Balla T, 2013).

The phosphorylation of PtdIns is a key determinant for a wide variety of cellular functions including cell growth and proliferation. Several signaling proteins are recruited to specific cellular locations through interaction with the PIs via inositide-binding protein modules, such as the pleckstrin homology domains (PH-domains) (Moravcevic K *et al.*, 2012). PIs can also regulate particular ion channels by interacting with molecules that reside in the membrane, such is the case of PtdIns4P and PtdIns(4,5)P₂ that regulate the transient receptor potential vanilloid 1 (TRPV1) cation channel (Hammond G *et al.*, 2012).

The deregulation on the activity of PIKs may allow the development of many pathologies particularly related to their physiological functions, including some forms of cancer and diabetes (Brown J and Auger K, 2011). An example is, gain-of-function mutations in *PIK3CA*, which encodes the catalytic subunit p110 α of PI3K, these mutations are related with endometrial (Cheung L *et al.*, 2011) and colorectal cancer (Jaiswal B *et al.*, 2009).



Scheme 1: Phosphatidylinositol (PtdIns) structure and interconversions between various phosphoinositides and the enzymes catalyzing these reactions. The yeast enzymes are listed in parentheses. Where there is some ambiguity it is indicated by “?”. * PIP5K2s are 4-kinases that act on PtdIns5P. (Scheme extrapolated from Balla T, 2013)

1.2.1. PI4KIII β

In mammals, four enzymes (PI4Ks) are able to phosphorylate the 4-OH of PtdIns to generate PtdIns4P (Scheme 1). PI4Ks fall into two classes, defined as type II and type III. In first place Type II PI4Ks (PI4KII α and β) are enzymes of ~55 kDa, that showed high affinity for ATP ($K_m = \sim 10\text{-}50 \mu\text{M}$). One of the most noteworthy characteristics of PI4KIIs is that they can be strongly inhibited by adenosine ($K_i = \sim 10\text{-}70 \mu\text{M}$). On the other hand, the isoforms PI4KIII α and PI4KIII β constitute the Type III of the PI4Ks family. These enzymes are less sensitive to adenosine ($K_i > 1 \text{ mM}$) but they are instead inhibited by wortmannin ($IC_{50} = \sim 50\text{-}100 \text{ nM}$). PI4KIII α and PI4KIII β have similar primary structures, with a molecular mass greater than 200 kDa, but differ in tissue and subcellular distribution (Balla T *et al.*, 1997; Balla A and Balla T, 2006; Chu K *et al.*, 2010; Gehrman T and Heilmayer L, 1998; Nakagawa T *et al.*, 1996).

Experiments in yeast demonstrate that PI4KIII β is mainly Golgi and nucleus located (Strahl T *et al.*, 2005). The localization of PI4KIII β at Golgi can be attributed to the interactions of PI4KIII β (at residues 125–169), with a small Ca^{2+} binding protein frequenin (NCS-1 in mammalian cells), and Arf1 (GTPase ADP-ribosylation factor 1) (Bourne Y *et al.*, 2001; Hilfiker S, 2013), these interactions promote the recruitment and binding of PI4KIII β to the Golgi. Instead, the localization of PI4KIII β in the cytoplasm is mediated by Rab11, a protein involved in a large number of cellular trafficking processes (Prekeris R *et al.*, 2000; Takahashi S *et al.*, 2012). In particular, Rab11 binds to PI4KIII β at residues 401-516, without affecting the PI4KIII β enzymatic activity (de Graaf P *et al.*, 2002). From the cytoplasm, PI4KIII β can be recruited to the Golgi by Acyl- CoA-binding domain containing protein 3 (ACBD3). Even if PI4KIII β can shuttle to the nucleus from cytoplasm, its nuclear function(s) remain unclear (de Graaf P *et al.*, 2004). However, it was demonstrated that PKD (vesicular-transport-regulator protein kinase D) mediated the phosphorylation of PI4KIII β at Ser268 (Hausser A *et al.*, 2005). Such modification promotes the interaction of

PI4KIII β with 14-3-3 proteins, an event that inhibits the nuclear localization of PI4KIII β (Demmel L *et al.*, 2008).

The phosphorylated product of PI4KIII β , Phosphatidylinositol 4-phosphate (PtdIns4P), is a monophosphorylated form of PtdIns. This lipid is bound by pleckstrin homology (PH) domains of oxysterol-binding proteins, ceramide transfer proteins, or by four-phosphate-adaptor protein 1 and 2 (FAPP1 and FAPP2) (Dornan G *et al.*, 2016), all involved in lipid transfer functions. The positively charged surface of PH domains on these proteins mediates the interactions with the negatively charged PtdIns4P and its derivatives (Bottomley M *et al.*, 1998). Through these interactions, PI4KIII β and its phosphorylated products are thought to play a critical role in mediating membrane trafficking in the *Trans*-Golgi Network (TGN).

PtdIns4P is also an essential precursor of the secondary messengers PtdIns(4,5)P₂ and PtdIns(3,4,5)P₃. The first one is an important component in the formation of the cleavage furrow during cytokinesis (Field S *et al.*, 2005), while PtdIns(3,4,5)P₃, that diffuses through the cytoplasm, which, because of its solubility, interacts with inositol triphosphate receptors on the ER, causing the release of calcium and raising the level of intracellular calcium. PtdIns(3,4,5)P₃ also participates in signal transduction processes. In immune cells for example, PtdIns(3,4,5)P₃ interacts with the phosphoinositide phospholipase C (PLC γ 1) activity via activation of Tec-family tyrosine kinases, in a process controlled by SHIP1 (Phosphatidylinositol-3,4,5-trisphosphate 5-phosphatase 1) (Fluckiger A *et al.*, 1998).

Moreover, PtdIns(4,5)P₂ and PtdIns(3,4,5)P₃ interact with different binding domains (including PH domain) rich in basic residues of cytoskeletal proteins such as cortexillin I, gelsolin, N-WASP, vinculin and profilin (Niggli V, 2001). As a result, serving as an anchor to the plasma membrane for all these proteins, both PtdIns(4,5)P₂ and PtdIns(3,4,5)P₃ are able to influence the cytoskeletal organization. The levels of these lipids in cell can be increased or decreased upon stimulation, depending on cell type and

stimulus (Czech, 2000), contributing to modulation of cell membrane organization.

1.2.2. PI4KIII β Structure

PI4KIII β is a large (92 kDa) multi-domain enzyme (Nakagawa T *et al.*, 1996) (Fig. 1) and, similarly to PI4KIII α , it contains a conserved catalytic domain that shows similarity to the catalytic domain of PI3Ks. It also possesses a lipid kinase unique domain (LKU), which is predicted to be helical. The LKU domain is followed by the frequenin (Fq)/NCS-1 binding site. Moreover, PI4KIII β present a conserved Ser-rich segment that contains several phosphorylation sites, including PKD phosphorylation site at Ser268, where PI4KIII β can be phosphorylated and, consequently, activated (Hausser A *et al.*, 2005). PI4KIII β in its structure also presents a loop within the N-lobe, located in its kinase domain (Fig. 1) (Dornan G *et al.*, 2016). PI4KIII β also contains N-terminal proline rich sequences (Pro-rich), whose function is the less known among the PI4KIII β domains (Balla T, 2013) of the kinase domain. Finally, PI4KIII β shuttles between the nucleus and the cytoplasm, in its structure PI4KIII β possess several Leu-rich sequences that could serve as binding sites for nuclear localization and nuclear export (Heilmeyer L *et al.*, 2003).

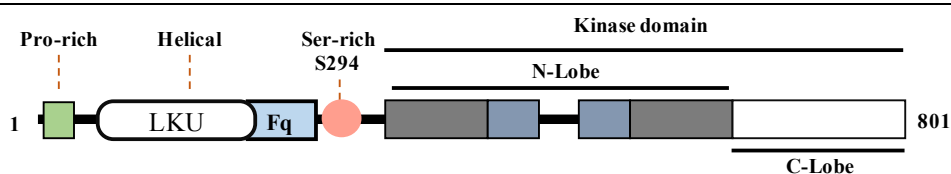


Figure 1: PI4KIII β domain organization.

1.2.3. PI4KIII β and Cancer

As mentioned above, among PIKs family, PI3K has been largely associated with diverse cancer onset (Table 3) promoted by gain-of-function mutations in the catalytic subunit p110 α of PI3K. Moreover, there are many activators

of PI3K that in cancer are mutated or overexpressed as *KRAS* mutations in endometrial and colorectal cancer (Cheung L *et al.*, 2011) or *ERBB2* overexpression, in breast cancer (Slamon D *et al.*, 1989; Lynch T *et al.*, 2004; Oda K *et al.*, 2008).

Even if PI3K is the main PIK associated with different types of cancer, the deregulation of PI4KIII β or malfunction of its PI products can also lead to a malignant transformation. It has been suggested that PI4KIII β , like PI3Ks, also plays a role in breast cancer oncogenesis, since *PI4KB*, the gene encoding PI4KIII β , has been found to be highly expressed in breast tumors (Curtis C *et al.*, 2012; Morrow A *et al.*, 2014). It is well known that PI4KIII β regulates breast epithelial morphogenesis (Pinke D and Lee J, 2011). In breast cancer PI4KIII β overexpression increases the PI3K-dependent Akt activation, a serine-threonine kinase that regulates multiple biologic processes that is found deregulated in many cancers (Cheng J *et al.*, 1996; Franke *et al.*, 1997; Vivanco I and Sawyers C, 2002; Carpten J *et al.*, 2007; Chu K *et al.*, 2010;). The mechanism underlying this process is still unclear but it was found that the higher level of Akt kinase activity following PI4KIII β overexpression is independent from its kinase function (Morrow A *et al.*, 2004). PI4KIII β is also a downstream effector of eukaryotic elongation factor 1 alpha 2 (eEF1A2), a transforming gene that is highly expressed in both breast and ovarian cancer (Anand N *et al.*, 2002; Tomlinson V *et al.*, 2005).

Table 3: The PIKs, physiological role and associated diseases

	NAME	S	P	ROLE	Pathogenic associates	
PHOSPHOINOSITIDE KINASES	PI4KIIIa/ PI4KA	Type III PI 4-Kinases	PtdIns	PtdIns4P	Cytoskeletal organization, cell wall integrity, sphingolipids metabolism, transfer mediator between Golgi and ER.	Viral diseases, Hepatitis C Virus (HCV).
	PI4KIIIb / PI4KB		PtdIns	PtdIns4P	Golgi related functions, cytokinesis, trafficking regulator in the late secretory pathway.	Breast cancer, cystic fibrosis, Viral diseases.
	PI4K2 α	Type II PI 4-Kinases	PtdIns	PtdIns4P	Membrane recruiter of clathrin adaptors AP-1, AP-3 and GGAs, endocytosis, Lysosomal trafficking of glucocerebrosidase enzyme.	Gaucher disease, late onset spinocerebellar degeneration.
	PI4K2 β	Class III PI 3-Kinase	PtdIns	PtdIns4P		NID
	PI3KC3		PtdIns	PtdIns3P	Golgi-prevacuolar compartments-vacuola trafficking, Membrane rearrangement in multivesicular bodies, autophagy, endocytosis.	NID
	PIP5K1A	Type I PIP Kinases	PtdIns4P	PtdIns(4,5)P ₂	FcgR-mediated phagocytosis, actin cycle.	NID
	PIP5K1B		PtdIns4P	PtdIns(4,5)P ₂	Transferrin receptor endocytosis	NID
	PIP5K1C		PtdIns4P	PtdIns(4,5)P ₂	Clathrin-mediated endocytosis in neurons, production of vesicles in chromaffin cells.	Breast cancer
	PIP5K2A	Type II PIP Kinases a	PtdIns5P	PtdIns(4,5)P ₂		NID
	PIP5K2B		PtdIns5P	PtdIns(4,5)P ₂		NID
PIP5K2C	PtdIns5P		PtdIns(4,5)P ₂		NID	
PIP5K3	Type III PIP Kinases	PtdIns3P	PtdIns(3,5)P ₂	Multivesicular body pathway, autophagy.	NID	

PtdIns(4,5)P ₂ Kinases	PI3Kα/ PI3KCA	Class I PI 3-Kinases	PtdIns(4,5)P ₂	PtdIns(3,4,5)P ₂	Insulin/IGF1-mediated regulation of cellular growth and metabolism, angiogenesis.	Colorectal and endometrial cancer, glioblastoma and other cancer forms	
	PI3Kβ/ PI3KCB		PtdIns(4,5)P ₂	PtdIns(3,4,5)P ₂	Clathrin-mediate endocytosis, insulin-mediate signals, B-cells development.	Can induce tumorigenesis under PTEN loss.	
	PI3Kγ/ PI3KCG		PtdIns(4,5)P ₂	PtdIns(3,4,5)P ₂	Protein kinase activity, phosphorylation of MEK protein, Chemotaxis of neutrophils and macrophages, chemokine responses, inflammation, patelet aggregation, T-cell signaling.	Inflammatory diseases, colorectal cancer.	
	PI3Kδ/ PI3KCD		PtdIns(4,5)P ₂	PtdIns(3,4,5)P ₂	Support immune cells functions.	Allergic, autoimmune and pulmonary diseases, chronic lymphocytic leukemia, multiple myeloma,	
	PI3K2α / PI3K2A		Class II PI 3-Kinases	PtdIns	PtdIns3P	Clathrin-mediated endocytosis and trafficking, insulin-related functions, liver regeneration.	NID

Classification of PIKs according to their substrate, enzymatic function in cell and associated diseases.

^aType II PIPKs seem to be more important in the control of PtdIns5P than in the production of new PtdIns(4,5)P₂ but its specific roll remain elusive (Clarke J *et al.*, 2010).

NID: Non-independent diseases related with this specific enzyme have been reported, **P:** Product, **S:** Substrate. Data in this table were obtained from: Audhya A *et al.*, 2000; Babst M *et al.*, 2002; Bairstow S *et al.*, 2006; Balla T, 2013 Berger P *et al.*, 2006; Bielas S *et al.*, 2009; Bohnacker T *et al.*, 2009; Carpten J *et al.*, 2007; Clarke J *et al.*, 2010; Coppolino M *et al.*, 2002; Cheung L *et al.*, 2011; Czech M, 2000; Dominguez V *et al.*, 2006; Foukas L *et al.*, 2006; Gaidarov I *et al.*, 2001; Garcia-Bustos J *et al.*, 1994; Itakura E *et al.*, 2008; Jia S *et al.*, 2008; Jovic M *et al.*, 2012; Krauss M *et al.*, 2003; Padron D *et al.*, 2003; Rozelle A *et al.*, 2000; Sasaki T *et al.*, 2000a; Sasaki T *et al.*, 2000b; Simons J *et al.*, 2009; Sun Y *et al.*, 2010; Trotter P *et al.*, 1998 ; Yamamoto A *et al.*, 1995 and Yoshida S *et al.*, 1994.

1.2.4. PI4KIII β and viral diseases

Traditionally, antiviral drug discovery has been mainly focused on the inhibition of viral targets, leading to the development of highly specific drugs to fight specific infections. As a consequence of the high mutation rate of RNA viruses, the major problem with compounds that directly target specific viral proteins is the rapid emergence of new drug-resistant viral strains. A strategy to overcome this issue is to target host factors that are essential for the viral replication cycle but dispensable for host cell survival. Other than avoid resistance onset, this approach has another important advantage: since viruses belonging to the same genus or family usually share the same cellular pathways for replication, targeting a host factor may allow the development of effective broad-spectrum antiviral compounds (Ujjan I *et al.*, 2015).

Human enterovirus infections are considered one of the major causes of acute exacerbations in chronic pulmonary diseases like asthma, chronic obstructive pulmonary disorder and cystic fibrosis in children and adults (Leigh R and Proud D, 2015). In most enteroviruses, the membrane protein 3A interacts with host proteins Arf1 (ADP-ribosylation factor 1) and GBF1 (Golgi-specific brefeldin A-resistance guanine nucleotide exchange factor 1) (Wessels E *et al.*; 2007; Teterina N *et al.*, 2011), to enhance the recruitment of PI4KIII β to host membranes. After its recruitment, PI4KIII β generates a PtdIns4P lipid-enriched microenvironment to which the viral RdRp 3D^{pol} (RNA-dependent RNA polymerase) can bind and initiate the viral RNA replication (Hsu N *et al.*, 2010). However, the viral 3A activation of PI4KIII β is far from being fully understood because different enteroviral 3A proteins have different capacities to activate PI4KIII β . For example, in Cocksackie virus B which also belongs to enterovirus genus, the 3A-dependent recruitment of PI4KIII β has been shown to be independent of both, GBF1 and Arf1 (Dorobantu C *et al.*, 2014), highlighting the complexity of viral activation of PI4KIII β .

Even if the viral activation of PI4KIII β is not fully understood, its relevance for viral infections is clear as well as its relevance as broad-spectrum viral

target. Importantly, chemical inhibition of PI4KIII β does not influence cell viability, probably because the PtdIns4P amount produced by other PI4Ks could support cell trafficking and signaling, but it is not sufficient to sustain viral RNA synthesis (Altan-Bonnet N and Balla T, 2012; la Marche M *et al.*, 2012).

A major aim in the development of PI4KIII β inhibitors is to achieve selective inhibition of the β isoforms over the α one. In fact, unselective inhibition of α and β isoforms lead to cell toxicity. Among the PI4KIII β inhibitors with antiviral activity against enterovirus, PIK93 is the most relevant one (IC₅₀=19 nM). Even if PIK93 can inhibit the catalytic activity of PI4KIII β isoform at nanomolar concentrations, it is not selective because it is able to effectively inhibit PI4KIII α too (IC₅₀=39 nM) (Arita M *et al.*, 2011; MacLeod A *et al.*, 2013; Boura E and Nencka N, 2015).

1.3. PART III: HIV-1 Reverse Transcriptase

1.3.1. HIV/AIDS

From its "public appearance" in 1981, the global pandemic caused by the human immunodeficiency virus (HIV) infection and its consequent Acquired Immunodeficiency Syndrome (AIDS) have become one of the most relevant public health issues around the world. In 2016 were reported 1.8 millions of new infections and 1.2 millions deaths due to HIV-related infections. In the same year, it has been estimated that approximately 36.7 million people are infected with HIV worldwide (Cohen M *et al.*, 2008; GBD 2015 disease and injury incidence and prevalence collaborators, 2016; GBD 2015 mortality and causes of death collaborators, 2016).

Table 4: HIV/AIDS in numbers

	HIV/AIDS IN NUMBERS			
	Global prevalence (thousands)		Number of deaths (thousands)	
	2015	2005 / 2015 Variation (%)	2005	2015
HIV/AIDS	37 277	21,1	1 791	1 192
Tuberculosis	8 861	9,2	1 347	1 112
HIV/AIDS— tuberculosis	258	17,9	351	211
HIV/AIDS resulting in other diseases	37 543	23,6	1 440	980
Sexually transmitted diseases excluding HIV	1145527	16,9	135	108

Prevalence: Global prevalence for 2015, percentage change of counts between 2005 and 2015 for all causes. Percentage change in counts between 2005 and 2015.

HIV/AIDS—tuberculosis: Tuberculosis in HIV-positive people

Deaths: Global deaths in 2005 and 2015 for all ages and both sexes combined between 2005 and 2015

Sub-Saharan Africa region continues to be the most affected by the virus. On the other hand, more recent epidemiological data (Cohen M *et al.*, 2008; GBD 2015 mortality and causes of death collaborators, 2016) show that some countries in this same region had very large gains in life expectancy from 2005 to 2015, due to the better accessibility to antiretroviral drugs. In Asia and Latin America, the percentage of infected people has also declined due to increasingly effective preventive and informative campaigns. Nowadays, AIDS mortality has reduced worldwide mainly because of the great efforts made to make antiretroviral drugs more accessible around the world, greatly improving the quality of life of infected patients (GBD 2015 mortality and causes of death collaborators, 2016).

1.3.2. Human Immunodeficiency Virus (HIV)

HIV is a retrovirus of the genus *Lentivirus*, of which two main types have been identified: HIV-1 and HIV-2, which are the only human *Lentiviruses*. their genetic identity is about 40%, and are differentiated by the antibody response that their respective envelope proteins induce in the host organism (Sharp P and Hahn B, 2011; Garg H and Joshi A, 2017)

The HIV-1 serotype is the most widely diffused worldwide and is classified into many subgroups. The sub-group M (main) contains 8 different subtypes (nominated with the letters from A to H), which exhibit difference in their sequence of the glycoprotein gp120 around 30 and 40%. HIV-1 sub-group M is the responsible for most infections worldwide, with sub-type B being the most frequent in infected populations in North America and Europe. Finally, the sub-group O (out-group), which is relatively rare, is found just in Cameroon, Gabon and France. On the other hand, the less frequent type HIV-2 is prevalently isolated in Western-Africa, Portugal and Brazil (Gallo R, 2000).

HIV is phylogenetically related with the Simian Immunodeficiency Virus (SIV), a *Lentivirus* HIV-related that infects non-human primates. Several strains of SIV have been isolated from different species of African-monkeys. These viruses seem non-pathogenic for some host species, such as

the case of genus of primates *Cercopithecus*. At the same time, SIV-strain that are non-pathogenic for some species could result pathogenic to other ones (Sharp P and Hahn B, 2011). In the case of *Cercopithecus*, the abundant presence of the virus among the populations of this genus suggest a long co-existence history that allowed them to evolve in parallel.

1.3.2.1. HIV structure and genome

HIV have an outer surface predominantly spherical, with a diameter about of 100 nm. Externally is surrounded by the viral envelope which derives from portions of the host cell membrane. This lipid layer includes some copies of the HIV envelope glycoproteins gp120 and gp41. More inwardly, it exhibits a structure called matrix (MA) that is composed by p17 protein and contain the conical viral capsid that is composed by p24 protein (Frankel A and Young J, 1998).

Table 5: HIV Viral proteins

Structural Proteins	Regulatory Proteins	Auxiliary Proteins	Proteins with enzymatic Activity
-Gag	-Tat	-Vpr	-Reverse Transcriptase (RT) -Protease (PR) -Integrase (IN)
-MA	-Rev	-Vpu	
-CA	-Nef	-Vif	
-NC			
p6			
-Env			
-SU			
-TM			
-Gag-Pol precursor			

Summary of the main viral proteins in HIV-1. Table adapted from Frankel A and Young J, 1998.

Inside the capsid there are two copies of the positive single-stranded RNA genome of about 9,7 kb. The three polycistronic genes of the retrovirus family *gag*, *pol* and *env*, and other six additional genes: *tat*, *vpr*, *rev*, *vif*, *nef*,

and *vpu* (*vpx* in HIV-2, also found in SIV), constitute the viral genome (Frankel A and Young J, 1998).

Each terminal end of the genome possesses repeated sequences or Long-Terminal-Repeats (LTR), of approximately 640bp, that include regulatory elements for gene expression such as sites for polyadenylation, transcription factors binding sites, regulatory sequences, as well as transactivation and inhibitory regulation sequences. The viral core also contains the viral enzymes reverse transcriptase (RT), integrase (IN), protease (PR) and, additionally, the proteins p6, p7, vif, vpr, nef (Fig. 2) (Frankel A and Young J, 1998).

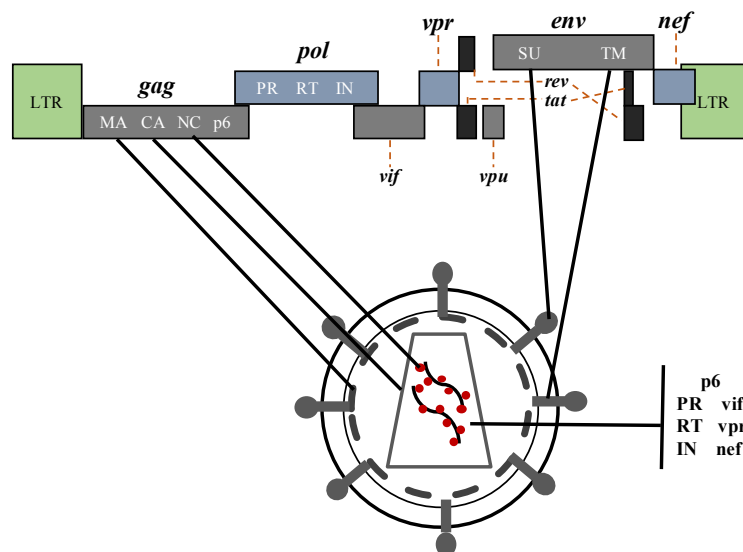


Figure 2: HIV-1 genome and virion.

1.3.2.2. HIV replication cycle and tropism:

1.3.2.2.1. Entry to the cell

Viral particles can initiate the infection to the host as a virion or through the contact with other infected cells, bloodstream and / or through the mucous membranes represent to be the most effective routes of transmission, being

the main targets immune cells such as CD4⁺ T-cells, macrophages, and microglial cells.

HIV-1 entry to target cells through interaction of the virion envelope glycoproteins gp120 with the membrane receptor CD4 (Cluster of quadruple Differentiation). Such receptor is a 55 kDa cell surface glycoprotein expressed mainly in mature T lymphocytes, which represent the main HIV target, as well as on monocytes and macrophages (Chan D *et al.*, 1997; Zeitlmann L *et al.*, 2001; Sudharshan S and Biswas J, 2008; Arrildt K *et al.*, 2012). CD4 exerts a fundamental role in the immune response. It possesses four domains (D1- D2- D3- D4) and acts binding to relatively invariant sites on class II major-histocompatibility-complex outside the peptide binding site (Maddon P *et al.*, 1985; Wang J *et al.*, 1990; Bui V and Nguyen T, 2016).

Gp120 forms a complex with gp41. Upon the interaction between gp120 and CD4 a vast conformational change take place in gp120 itself and in gp41. In particular, such rearrangements involve hydrophobic regions in the N-terminal sequence of gp41 that take contacts with the cellular membrane, allowing the fusion with the viral envelope (Chan D and Kim P, 1998; Gallo S *et al.*, 2003; Blumenthal R *et al.*, 2012).

However, the solely presence of CD4 is not sufficient for viral entry (Doms R and Peiper S, 1997). Membrane surface receptors CXCR4 or CCR5, which are receptors for chemokine SDF-1 and chemokine MIP-1 alpha, MIP-1 β and RANTES, are also critical factors in the entry process, acting as co-receptors during the virus-cell fusion. (Chan D and Kim P, 1998).

1.3.2.2.2. HIV Nuclear import

Soon after the entry of the virus into the cytoplasm, the viral core undergoes to an uncoating process, during which most of the capsid is eliminated, while nucleocapsid, viral-protein-R (Vpr), integrase, and a small portion of matrix remain still associated (Miller M *et al.*, 1997; Fassati A and Goff S, 2001). As uncoating goes on, the viral RT reverse transcribes the single stranded RNA genome into a double stranded DNA, named provirus. At this

point, the provirus associates with viral and cellular proteins to form a high molecular weight nucleoprotein complex called pre-integration-complex (PIC). PIC translocation to perinuclear compartment is greatly facilitated by the cytoskeleton-dependent active intracytoplasmic movement (McDonald D *et al.*, 2002; Jayappa K *et al.*, 2012). Subsequently, PIC reaches the nucleus through nuclear pore complexes and integrates into genomic DNA through the activity of IN (Lewis P *et al.*, 2002; Greene W and Peterlin B, 2002).

Other retroviruses, such as murine leukemia virus (MLV), are only able to infect dividing cells because lacks nuclear import ability and depends solely on nuclear membrane dissolution during mitosis to access host cell genomic DNA (Springett G *et al.*, 1989; Roe T *et al.*, 1993; Lewis P and Emerman M, 1994). On the contrary, HIV-1 has the ability to successfully infect non-dividing cells (Gartner S *et al.*, 1986) as well as dividing cells (Christ F *et al.*, 2008); a feature that plays a crucial role in infection establishment, disease progression, and AIDS pathogenesis.

In a single infected cell, only one to three provirus are integrated in the host genome. After integration, the HIV provirus lies transcriptionally silent and immunologically inert (Dahabieh M *et al.*, 2015). This latent phase lasts as long as the infected cell life, so the period of time of viral latency can vary between few hours to years depending of the cellular type.

1.3.2.2.3. HIV Genetic expression

Under circumstances that are not entirely clear, but that in T cells may be controlled by the heat shock protein 90 (Hsp90) (Anderson I *et al.*, 2014), the T cell adopts a cellular state that promotes and sustains productive HIV transcription, and virus production resumes.

The gene expression of HIV-1 genes can be distinguished in an early and a late phase. The regulatory genes encoding for *tat* and *rev* are first expressed. Tat and Rev protein are then imported in the nucleus where they fulfill their regulatory function. Tat, in particular, increases the transcription frequency and increases the elongation efficiency of viral mRNA. Rev, on the other

hand, has the function of stabilizing and transporting transcripts of structural genes into the cytoplasm, both unspliced or partially spliced. Rev accumulation inhibits the further synthesis of its mRNA and that of Tat, allowing late phase to take place. In this phase, coding transcripts are produced for the Gag and Gag-Pol polyproteins that are sent to the cell membrane where the protease process them to mature proteins. Part of the full-length RNAs, is not translated, but will be used as a single stranded positive RNA genome in new viral particles (Jacks T, 1990; Coffin J *et al.*, 1997).

When the synthesis of structural proteins is completed, they are assembled in new virions at the inner face of the cell membrane. The glycoproteins gp120 and gp41 are inserted into the cell membrane through exocytotic vesicles. Then, by “budding”, the virus acquires the envelope consisting of portions of the cytoplasmic cell membrane. Finally, a large number of new virions are released from the cell surface, which alters the ionic and osmotic flow of the cell, resulting in lysis of the cell surface (Rosenberg Z and Fauci A, 1989; Levy J, 1993; Sundquist W and Kräusslich H, 2012).

1.3.2.2.4. HIV-1 reverse transcriptase (RT)

Reverse transcriptase (RT) was discovered more than 40 years ago and until now it is considered the most important target in the antiviral therapy against HIV.

Before the viral genome can be integrated into the host chromosome, it must first be reverse transcribed into a DNA duplex. This event is essential in the life cycle of the virus. Moreover, retro transcriptase activity is unique to the retrovirus and it is not present in human cells. For this reason, after HIV was discovered, the reverse transcription / DNA-polymerization step in HIV replication was immediately considered as a primary therapeutic target.

1.3.2.2.5. RT synthesis and structure

The first RT-structure of HIV-1 was obtained in the early 1990s, where the enzyme was present in complex with the non nucleosidic inhibitor

nevirapine. Since then, it has been known that HIV-1 RT is composed by a 66 and a 51 kDa subunit polypeptide heterodimer (p66 / p51), which is encoded by a single open reading frame of the Gag-Pol precursor polyprotein. During viral assembly, PR cleaves such polypeptide releasing the mature proteins, including p66. At this point, p66 forms a homodimer that is further recognized by PR. This time the protease cleaves a single p66 subunit, generating the mature heterodimer p66/p51. Subunit p66 catalyzes the DNA polymerase and Ribonuclease H activities of RT. This subunit presents an open extended structure with a large active-site cleft resembling a right hand and composed of palm, thumb and fingers subdomains. On the other hand, p51 forms a closed compact structure incapable of participating in catalysis. Instead, p51 has a complementary support role providing structural support to p66, facilitating p66 loading onto a template-primer and stabilizing the appropriate p66 conformation during tRNA-primed initiation of reverse transcription (Le Grice S *et al.*, 1991; Kohlstaedt L *et al.*, 1992; Jacobo-Molina A *et al.*, 1993; Amacker Mand Hübscher, 1998).

1.3.2.2.6. The process of reverse transcription

Many viral and cellular factors are involved in the process of reverse transcription, but the two essential enzymatic activities that are necessary to carry out reverse transcription are both present in RT: the RNA and DNA-dependent DNA polymerase activity and the RNase H that degrades RNA if it is part of an RNA–DNA duplex (Gallo R, 2000; Hu and Hughes, 2012).

To perform the retro-transcription RT needs both a *primer* and a template. While the single stranded viral RNA constitutes the template, a host tRNA₃^{Lys} serves as a *primer* for the synthesis of the first strand of DNA. tRNA₃^{Lys} anneals to a sequence near the 5' end of the viral RNA (LTR region) known as primer-binding-site (Pbs). Reverse transcription initiates from the annealed 3' end of tRNA₃^{Lys} primer. DNA synthesis creates an RNA–DNA hybrid that is substrate for RNase H activity. Degradation of the 5' end of the viral RNA (Fig. 3B) partially exposes the newly synthesized minus-strand DNA (Fig. 3B). This DNA portion is then annealed to the 3'

end of the viral RNA using as a bridge the direct repeats (R) ends of the viral RNA (Fig. 3C). After that, the DNA synthesis can continue along the length of the genome simultaneously with RNase H dependent RNA degradation (Fig. 3C) (Panganiban and Fiore, 1988, Hu and Temin, 1990, Hu and Hughes, 2012). The polypurine track, a purine-rich sequence in the RNA genome (ppt) is not processed by RNase H and serves as the *primer* for the synthesis of the second DNA strand. Interestingly, there are two ppt sequence in HIV-1, one at the 3' end of the RNA and the other near the middle of the genome. It is not fully clear the function of this second one, but the 3' ppt is essential for viral replication. The synthesis of the second strand of DNA continues until it reaches the annealed tRNA₃^{Lys} (Charneau *et al.*, 1992) (Fig. 3E), which is then removed by RNase H. The subsequent extension of the plus and minus strands is the final step of the formation of a new double stranded viral DNA (Hu and Temin, 1990) (Fig. 3F).

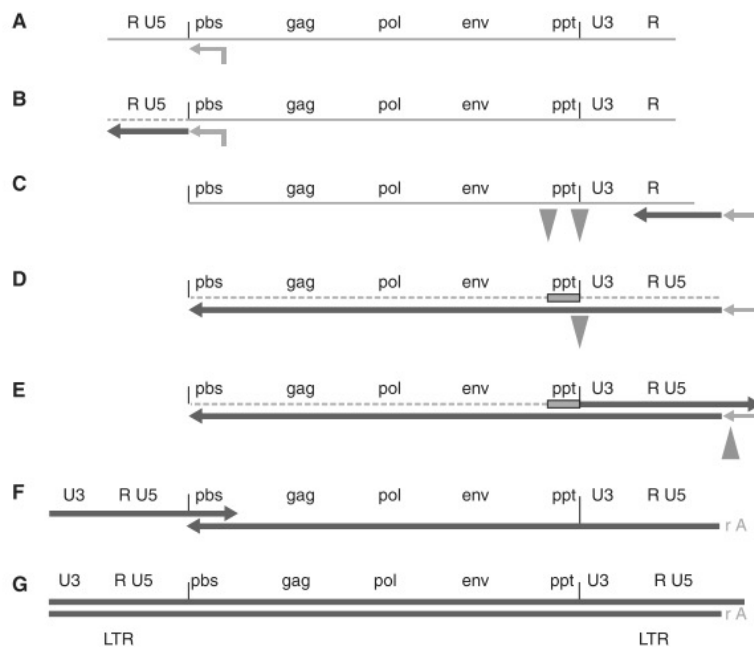


Figure 3: Retroviral reverse transcription

1.3.3. HIV-1 control strategies and the drug resistance problem.

HIV/AIDS is one of the leading infectious causes of death for adults worldwide (GBD 2015 mortality and causes of death collaborators, 2016). In general, to control the spread of a viral infection the main objectives are the development of an antiviral treatment capable of eradicating the disease and the preparation of an effective vaccine to prevent the infection. Unfortunately, none of these goals have been achieved yet with HIV-1 infection. At present, only pharmacological therapy can slow down the course of infection.

One of the biggest problems in the development of antiviral therapies lies in the ability of viruses to exploit the host metabolic machinery, which makes difficult to identify active molecules that selectively inhibit viral replication without affecting the normal functions in the host cell. This can be achieved by targeting viral enzymes not present in the cells, such as reverse transcriptase. The other major problem is the ability of RNA viruses to acquire resistance mutations, which lead to poor efficacy of the therapies over time.

Currently, none of the approved drugs is able alone to suppress successfully the HIV infection. Unfortunately, when these drugs are used alone, the viral burden in infected patients increases again in a short period of time. The reason for this event is that drug-resistant HIV-1 variants evolve under the selective pressure of the pharmacological regimen, making the monotherapy an ineffective approach.

Currently, HIV-1 therapy is based in the simultaneous administration of cocktails of different drugs but, despite the efficiency of this treatment and even if with a slower rate, resistant mutations are still selected. The reasons that underline the onset of resistant mutations rely in the error prone DNA synthesis by RT. In fact, lacking a proofreading activity, RT introduces one misincorporation per 10^4 nucleotides incorporated. Moreover, HIV-1 exhibits a high replication rate, allowing the rapid generation of many new variants, thus enhancing the probability to select a resistant mutant. Not surprisingly, the reverse transcription/DNA polymerization step in HIV-1

replication was immediately considered as a prime drug target (Das K and Arnold E, 2013; Garbelli A *et al.*, 2017).

Nowadays, HIV/AIDS therapy includes antiretroviral drugs that inhibit the viral proliferation, drugs used in the treatment and prevention of various opportunistic infections or tumors and also, drugs focused on strengthening the patient's immune system.

1.3.4. High Activity Anti-Retroviral Therapy (HAART).

Currently, the most effective treatment for HIV-1 infection is HAART. During this treatment, drugs with different mechanism against HIV-1 RT belonging to three families, nucleoside and non-nucleoside reverse transcriptase inhibitors (NRTIs and NNRTIs), and protease inhibitors (PIs), are administered at the same time to the patient (Clumeck N and De Wit S, 2000). The therapy usually includes the combination of two NRTIs with one NNRTI, two NRTIs in combination with one PI, or the combination of three NRTIs (Gulick R *et al.*, 1997; Hammer S *et al.*, 1997; Detels R *et al.*, 2001; Beck E *et al.*, 2004; Garbelli A *et al.*, 2017).

The combined antiretroviral regimens have proved to be more effective against viral replication. Nowadays, most of the HIV drug resistance emerges because of incomplete adherence. As new drugs have been developed, HAART regimens became more efficient and better tolerated, with the emergence of resistance that became less frequent. (Gill V *et al.*, 2010).

Other pharmacological approaches complementary to HAART have been proposed. Mega-antiretroviral-therapy consists in the administration of a higher number of drugs than those normally supplied with HAART. Although this therapeutic option is difficult to apply because the odds of developing intolerance are higher. Another option is the programmed interruption of therapy. In this therapeutic scheme, the treatment is interrupted in order to control the selective pressure produced by the continuous use of drugs, thus avoiding the frequent appearance of new mutant forms resistant to the therapy. However, this approach lacks of

experimental confirmation (Loutfy M and Walmsley S, 2002; Wang Y *et al.*, 2007).

1.3.5. HIV Reverse Transcriptase Inhibitors (RTIs).

1.3.5.1. Nucleoside reverse transcriptase inhibitors (NRTIs).

NRTIs are analogs of canonical nucleosides. After entering in the cells, cellular kinases phosphorylate these compounds turning them to their active form. In this triphosphated form NRTIs compete with the natural nucleotides for incorporation by RT. However, these inhibitors lack the –OH group in the C-3 of the sugar ring. For this reason, once incorporated in a nascent DNA strand they avoid further additional phosphodiester bond formation, acting as chain terminators

The first NRTI discovered was azidothymidine (AZT), also known as Zidovudine, a thymidine analogue modified by the substitution of the hydroxyl group at C-3 of the ribose with an azide (N₃) group. Cellular enzymes convert AZT into the effective 5'-triphosphate (AZTTP) form that is incorporated preferably by RT that, differently from mammalian DNA polymerase (pols), poorly discriminate AZTTP, as well as the others NRTIs, from the natural nucleotides (Huang P *et al.*, 1990). AZT is still used in clinic and is the most widely used drug in symptomatic and asymptomatic patients with low levels of CD4+ T-lymphocytes. Currently, many other NRTIs are approved for the clinical use (Table 6).

Table 6: Common drug-resistant mutations in HIV-1 RT and Protease and their effects on viral fitness

Mutation	Drugs most affected	Fitness compared with wt virus (%)
HIV-1 reverse transcriptase		
NRTIs		
M41L	D4T, ZDV	80
K65R	ABC, DDI, TDF	55–68
K70R	D4T, ZDV	97
L74V	ABC, DDI	90
Q145M/L	all NRTIs and NNRTIs	1
Q151M	all NRTIs (except TDF, 3TC and FTC)	100
M184V	3TC, FTC	10–57
M184V/K65R	3TC, FTC, ABC, DDI, TDF	30
L210W	all NRTIs (except 3TC, FTC)	21
T215Y	D4T, ZDV	85
NNRTIs		
L100I	NVP, EFV, ETR, RPV	100
K103N	NVP, EFV	100
V106A	NVP, EFV	65–100
Y181C/I	NVP, EFV, ETR	100
Y188C/L	NVP, EFV, RPV	50–100
G190A	NVP, EFV	83
G190S	NVP, EFV	21–50
P225H	EFV	100
P236L	NVP, EFV	35–50
Mutation	Drugs most affected	Fitness compared with wt virus (%)
Protease		
M46I/L	ATV, FPV, IDV, LPV, NFV, TPV	79
I54V	All PIs	90
V82A/F/T	All PIs	79–100
I84V	All PIs	90

Table extracted from Garbelli A *et al.*, 2017.

D4T, stavudine; ZDV, zidovudine; ABC, abacavir; DDI, didanosine; TDF, tenofovir disoproxil fumarate; 3TC, lamivudine; FTC, emtricitabine; NVP, nevirapine; EFV, efavirenz; ETR, etravirine; RPV, rilpivirine; ATV, atazanavir; FPV, fosamprenavir; IDV, indinavir; LPV, lopinavir; NFV, nelfinavir; TPV, tipranavir.

An essential feature of NRTIs is their selectivity for RT over host polymerases. However, even if with a low frequency, they are also incorporated by cellular polymerases, especially by DNA polymerase γ . Such characteristic determines NRTIs induced adverse effects, especially hepatotoxicity. To improve NRTIs selectivity, chemical modifications have been explored not only in the sugar moiety, but also in the nucleobases structure. Moreover, some NRTIs take advantage from the poor ability of RT to discriminate between D and L ribose form. (Soudeyns H *et al.*, 1991).

1.3.5.1.1. Non-nucleoside reverse-transcriptase inhibitors (NNRTIs)

NNRTIs (Table 6) are RT inhibitors that do not resemble the nucleotide structure and, therefore, do not compete with natural nucleotides and are not incorporated in the nascent DNA strand. NNRTIs are important components of several combination therapies. These compounds do not require metabolic activation, they are extremely selective for HIV-1 RT, thus restricting their interaction with cellular enzymes and reducing the drug associated toxicity.

NNRTIs bind RT in a hydrophobic pocket (NNRTIs binding site –NNBS) nearby but distinct from the polymerase active site at the base of the thumb of p66. Such compounds interact with the amino acids in this pocket, which rotate outwards. This movement produces a conformational change in the p66 thumb that remain in an over-extended conformation, disturbing the catalytic site, blocking the incorporation of the incoming nucleotide and so the synthesis of DNA (Kohlstaedt L *et al.*, 1992; Ren J *et al.*, 1995). Structural differences of various NNRTIs can influence their mode of binding, making it possible that different NNRTIs might have slight differences in their mechanism of inhibition. Due to difference in conformational shape, there is no NNRTI binding pocket in p51.

The first generation of NNRTI, such as nevirapine and delavirdine (Campiani G *et al.*, 2002), has been discovered through large-scale screening of libraries molecules. However, a single amino acid substitution

in the NNBP can confer full resistance towards these drugs. Efavirenz and, more recently, etravirine, are second- and third-generation, respectively, NNRTIs that were selected not only based on their activity against RT *wt*, but also evaluating their potency against RT resistant mutants toward first generation NNRTIs (Clotet B, 1999). However, despite the efforts made to select inhibitors active towards all the RT resistant mutants, under the selective pressure of the therapy, HIV is able to select mutations that confer resistance against all the currently approved RTIs (Clotet B, 1999). Mutations conferring resistance to NNRTIs generally consist of amino acid substitutions within the binding pocket (Maga G *et al.*, 1997; Baldanti F *et al.*, 2003), which reduces the number of interactions between drug and enzyme, decreasing their affinity. Because different NNRTIs bind to the same enzyme site, such mutations confer cross-resistance to multiple inhibitors.

Among the new synthesized NNRTIs, derivatives belonging to the category of Indolyl Aryl Sulfones (IAS) have been shown to be of considerable interest. IAS are endowed with potent inhibitory activities against HIV-1 RT *wt* and most of clinically relevant RT mutant strains. Studies of conformational behavior of IAS demonstrate that compounds belonging to this family are capable to retain the pharmacophoric interactions with the enzyme because of the plasticity of their structure, being even capable to reorient themselves within the NNBS (Massarotti A and Coluccia A, 2016). Furthermore, it is well known that IAS do not display a unique mechanism of action. Drug binding studies (Cancio R *et al.*, 2005) demonstrated that the IAS affinity is highly dependent on the inhibition association rate. Indeed, based on the substituents introduced on the common drug pharmacophore, IAS derivatives demonstrated to selectively target the NNBS upon its structural reorganization caused by the formation of the RT (*wt* or mutated) binary and ternary complexes (Silvestri R *et al.*, 2003; Cancio R *et al.*, 2005; Silvestri R and Artico M, 2005; de Martino G *et al.*, 2006; Famigliani V *et al.*, 2017). The ability of IAS to bypass the steric barriers within NNBS imposed by mutations *K103N*, *Y181C*, and *K103N-Y181C*, make them an

interesting option to fight back the evolutionary capacity of HIV-1 to acquire resistance toward the approved NNRTIs. Moreover, the study of IAS mechanism of action will provide new insights in the knowledge of the capacities of their structure, which will help in the development of improved generations of these derivatives.

2. Aims of the research

Target therapy is nowadays one of the most used approaches for the development of new drugs for the treatment of different pathologies, including neurodegenerative diseases, different cancers and viral infections. The goals of my research during my PhD internship were to contribute in the development of new inhibitors of different enzymes that are validated targets in different pathologies, providing useful information on their mechanisms of action. Our research group, in collaboration with the group lead by Professor M. Radi, from University of Parma and with the group from university “La Sapienza” of Rome lead by Professor R. Silvestri, participate in the discovery and improvement of novel inhibitors. Our collaboration network starts with the development of virtual models of target enzymes in complex with their substrates. This allows the identification of the binding sites and the design of new drugs. Then, a structural-based virtual screening is employed applying different filters such as pharmacophore modelling, drug-like property calculations and docking simulations. It is important to underline that, already in this phase, several important parameters like water solubility, membrane permeability, molecular stability and cytochrome 450 toxicity, are being estimated. Only compounds capable to overcome these filters are then synthesized and sent to our laboratory in Pavia for the analysis of their inhibitory potency by *in vitro* enzymatic assays. The compounds with better profiles are tested for their selectivity against other related and unrelated enzymatic targets. The candidate compounds are further investigated for their mechanism of inhibition, in order to elucidate the kinetic properties underlying the interaction with their target. Once our analyses are completed, our results are sent back to University of Parma (in the case of compounds analyzed in PART I and II) or to University “La Sapienza” (in the case of the compounds analyzed in PART III). There, based on the biological results, the virtual models undergo to a re-evaluation and a further improvement. Starting from the identified lead compounds, new libraries of molecules are designed, virtually screened, synthesized and biological evaluated (both *in vitro* and *ex vivo*). Such iterative process continues for multiple cycle, improving the potency and selectivity of the compounds. The final goal is the identification of highly active molecules showing biological features that allow their investigation in animal models and, hopefully, in clinical trials.

3. Materials and methods

3.1.PART I: Leucine Rich Repeat Kinase 2 (LRRK2)

3.1.1. In vitro LRRK2 inhibition assay.

Recombinant LRRK2 *wt* (968-end) was purchased from Signalchem, recombinant *G2019S* mutant (970-end) was from Life Technologies.

Assay conditions: LRRK2 reaction were performed in 10 mM MOPS/NaOH pH 7.2, 0.8 mM EDTA, 2mM EGTA, 50 ng/μl BSA, 0,0013% NP40, 3 μM Na-orthovanadate, 10% DMSO, 10 mM MgCl₂, 12.5 μM ATP/[γ-33P]ATP, 100 μM LRRKtide (Signalchem) RLGRDKYKTLRQIRQ, 10ng active enzyme. To avoid plastic adsorption of enzymes and peptide, all reactions were performed using protein low-binding tubes (LoBind, Eppendorf).

All reactions were performed in 10 μl at 30 °C for 10 min. Reactions were stopped by adding 5μl of phosphoric acid 0.8%. Aliquots (10 μL) were then transfer into a P30 Filtermat (PerkinElmer), washed five times with 75 mM phosphoric acid and once with acetone for 5 min. The filter was dried and transferred to a sealable plastic bag, and scintillation cocktail (4 mL) was added.

Spotted reactions were read in a scintillation counter (Trilux, Perkinelmer). Data were plotted using GraphPad Prism 5.0. IC₅₀ values were obtained according to Equation (1), where *v* is the measured reaction velocity, *V* is the apparent maximal velocity in the absence of inhibitor, *I* is the inhibitor concentration, and IC₅₀ is the 50% inhibitory dose.

$$\text{Eq. 1} \quad v = V / \{1 + (I / IC_{50})\}$$

3.1.4. Inhibition mechanism.

G2019S kinase activity assays were performed in the presence of different fixed amounts of inhibitor with varying ATP substrate concentrations. Data were plotted using GraphPad Prism 5.0. Data were analyzed according to Michaelis–Menten equation and *K_{m,app}* and *V_{max,app}* were derived. *K_i'* and *K_i''* values were determined using equation (2) and (3) respectively.

$$\text{Eq. 2} \quad K_{m,app} = K_m (1 + [I] / K_i')$$

$$\text{Eq. 3} \quad V_{max,app} = V_{max} / (1 + [I] / K_i'')$$

All experiments were repeated three times

3.1.5. Kinase Panel.

All Tyrosine and Serine/Threonine kinases reaction were performed according to manufacturer's instructions, using 10-50 ng of enzyme. The nature of the substrates and their concentration are reported in Table 6. For some kinases, NP-40 or BSA was added. All reactions were performed in 10 μ l at 30 °C for 10 min using protein low-binding tubes (LoBind, Eppendorf). Reactions were stopped, transferred to filter and counted as in LRRK2 in vitro assay. PI4K β was purchased from Proqinase. Reaction was performed according to manufacturer's instruction and detected using ADP-Glo™ Lipid Kinase Assay (Promega).

Table 6. Kinase panel. Additional reaction condition and substrates.

Kinase	Peptide substrate	Peptide substrate [μ M]	ATP [μ M]	NP-40 %	BSA [mg/ml]
Src (Millipore)	KVEKIGEGTYGVVYK	250	100	0.00087	
GSK3 β (Signalchem)	GSK3 Substrate (Signalchem)	4	1	0.0013	
Hck (Proqinase)	KVEKIGEGTYGVVYK	50	2		
FAK (Proqinase)	KVEKIGEGTYGVVYK	50	1	0.0013	
DYRK1A (Millipore)	KKISGRLSPIMTEQ-NH2	50	170		
ABL (Promega)	KKGEAIYAAPFA-NH2	38	20	0.0013	
FLT3 (Proqinase)	KVEKIGEGTYGVVYK	50	2	0.013	
CDK2/CycA2 (Proqinase)	Histone H1	0.02mg/ml	2		1
CDK9/CycT1 (Proqinase)	CDKtide (Signalchem)	20	1		1
CDK9/CycK (Signalchem)	CDKtide (Signalchem)	20	1		1
CDK6/CycD1 (Signalchem)	RB-CTF (Proqinase)	1.22	1		1
CDK4/CycD1 (Signalchem)	RB-CTF (Proqinase)	1.525	1		1
Pim1 (Millipore)	S6 Kinase/Rsk2 Substrate Peptide 2 (Millipore)	50	1	0.013	
Pi4K β (Proqinase)	PI:PS (1:3)	200	20		

3.2. PART II: Phosphatidylinositol Kinases

3.2.1. In Vitro Kinase Inhibition Assays.

Recombinant full length, HIS6-tagged PI4KIII β was purchased from ProQinase (Germany); recombinant full-length, GST tagged PI4KIII α was from Life Technologies. Recombinant full-length, HIS6-tagged (PI3K- α) and full-length, myc-tagged (p85 α) PI3K- α /p85 α were purchased from ProQinase (Germany).

Assay Conditions: PI4KIII β , PI4KIII α , and PI3K- α /p85 α reactions were performed in 10 μ L using 20 mM Tris-HCl pH 7.5, 0.125 mM EGTA, 2 mM DTT, 0.04% Triton, 3 mM MgCl₂, 3 mM MnCl₂, 20 μ M ATP, 0.01 μ Ci γ -P33 ATP, 200 μ M Pi:3PS, 10% DMSO, 0.4 ng/ μ L of PI4KIII β , 16 ng/ μ L of PI4KIII α , and 7.6 ng/ μ L of PI3K- α /p85 α . All reactions were performed at 30 °C for 10 min. Reactions were stopped by adding 5 μ L of phosphoric acid 0.8%. Aliquots (10 μ L) were then transferred into a P30 Filtermat (PerkinElmer) and washed five times with 0.5% phosphoric acid and four times with water for 5 min. The filter was dried and transferred to a sealable plastic bag, and scintillation cocktail (4 mL) was added. Spotted reactions were read in a scintillation counter (Trilux, Perkinelmer). IC₅₀ values were obtained according to eq 1.

Lipidic Substrate Preparation: Phosphatidylinositol (PI, Sigma) and 2-oleoyl-1-palmitoyl-sn-glycero-3-phospho-L-serine (PS, Sigma) were dissolved in chloroform/methanol 9:1 and mixed at a 1:3 ratio. After chloroform/methanol evaporation, water was added to 1:62.5 w/v and the mixture was sonicated to clarity.

3.2.2. Kinase Panel.

All tyrosine and serine/threonine kinase reactions were performed according to the manufacturer's instructions, using 10– 50 ng of enzyme. Details on the nature of the substrates and their concentration are reported in table 6. For some kinases, NP-40 or BSA was added. All reactions were performed in 10 μ L at 30 °C for 10 min using protein low-binding tubes (LoBind, Eppendorf). Reactions were stopped, transferred to filter, and counted as described in PART I.

3.3.PART III: HIV-1 Reverse Transcriptase

3.3.1. Chemical reagents

The labelled nucleotide [methyl-3H] Thymidine Triphosphate ($^3\text{[H]TTP}$) 30Ci/nmol, the poly(rA) homopolymer and oligo(dT) oligomers were provided by GE Healthcare-Amersham Biosciences, while the unlabeled dTTPs were purchased from Boehringer and from Roche Molecular Biochemicals. The glass fibre filter FILTERMAT A were provided by PerkinElmer. All the other ultra-pure reagents were provided by Applichem, Merck, Sigma-Aldrich and VWR.

3.3.2. Protein purification

RT *wt* and its mutant forms *K103N*, *Y181C* and the double mutant *K103N-Y181C* were purified by fast protein liquid chromatography (FPLC).

Purification buffers

Lysis buffer: KPO4 pH 7.4 0,1 M; NP40 0,01 % and H₂O. *Equilibrium buffer*: Tris HCl pH 7.5 25 mM; NaCl 50 mM; Imidazole pH 8 5mM; Glycerol 5 % and H₂O. *Elution buffer*: Tris HCl pH 7.5 25 mM; NaCl 50 mM; Imidazole 500 mM; Glycerol 5% and H₂O.

Expression and purification of reverse transcriptase (RT) enzyme:

The plasmids containing the genes of RT *wt* and of the drug resistant mutants *K103N*, *Y181C* and the double mutant *K103N/Y181C* were employed to transform *E. coli* cells (BL21 strain), for the production and purification of the recombinant RT enzyme, tagged with a histidine tail (His-tag) at the N-terminus.

E. coli BL21 transformed with the corresponding expression plasmid were cultured in LB with 50 µg/ml of ampicillin at 37°C in agitation for 12 hours. 10 mL of this culture were then transferred into 1 L of LB until OD₆₀₀= 0.4. 1mM Isopropyl-β-D-Thiogalactoside (IPTG) was added for the induction of RT gene expression. After that, culture was grown in agitation for 4 hours at 37°C and then centrifuged at 10.000 rpm for 15 minutes at 4 °C. The obtained pellets were lysed with 2.5 ml of lysis buffer for each 1g of centrifuged bacteria pellet and 0.1 mg/mL lysozyme for 30 minutes on ice.

The liquid phase was then sonicated and centrifuged at 36000 rpm, for 60 min at 4°C.

The supernatant, containing the enzyme was thus loaded into a NiNTA Hitrap column (GE Healthcare) in which the matrix is associated with nitroacetic acid that interacts with the nickel ion, forming four bounds with it. Now, the ion still possesses two couples of free electrons that coordinate imidazole groups of histidine side chains in His-tag (in the N-ter of the protein). The elution of RT was executed through a gradient solution of imidazole (50mM – 0.5M) that competed with His tails in coordinating ions of the NiNTA complex on the matrix.

Before loading the supernatant, the column was equilibrated with 10 column volume of equilibrium buffer. During the elution were recovered 50 fraction of 200 µl each. In order to verify the presence of the enzyme, the fractions were analysed through SDS-PAGE assay, using 10% of polyacrylamide gel and Comassie Blue staining. The fractions containing active enzyme, identified through an activity assay, were divided in aliquots and stored at -80°C.

3.3.3. In vitro RT enzymatic assays

The oligo(dT)/poly(rA) hybrid was used as primer/template in the RNA-dependent DNA polymerase reaction of RT while ³[H]TTP constituted the nucleotidic substrate. The reaction was monitored through a radiolabelled incorporation.

Nucleic acids substrate: The poly(rA) homopolymers and the complementary oligo(dT) oligomers were mixed in a 1:10 ratio with Tris-HCl 25 mM (pH 8.0) containing KCl 22 mM. The sample was heated at 70°C for 5 minutes and it was cooled down to room temperature.

Nucleotide substrate: 100 µL of ³[H]TTP ethanol:water 50:50, 30 Ci/nmol (Perkinelmer) were dried in a vacuum centrifuge (SAVANT) and resuspended in 64 µL H₂O and 3.1 µL dTTP 10mM. The obtained ³[H]TTP solution was 500uM, 1490 cpm/pmol.

Assay conditions: RT reaction was performed in 50 mM Tris-HCl pH 7.5; 1mM DTT; BSA 0.2 mg/mL; Glycerol 2 %; 10 mM MgCl₂; 10% DMSO;

200nM Poly(rA)/oligo(dT); 10 μ M ³[H]TTP 1490 cpm/pmol and 0.125 μ L of Purified enzyme.

Reactions were performed in 15 μ l at 37 °C for 20 min. Aliquots (10 μ L) were then transfer into a glass fibre filter FILTERMAT A, washed three times with cold trichloroacetic acid 5% (TCA) and once with ethanol (EtOH). The filter was dried and transferred to a sealable plastic bag, and scintillation cocktail was added.

Spotted reactions were read in a scintillation counter (Trilux, Perkinelmer). Data were plotted using GraphPad Prism 5.0. IC₅₀ values were obtained according to eq. 1

3.3.4. Inhibition mechanism

RT RNA-dependent DNA polymerase activity assays of HIV-1 RT *wt* and *K103N-Y181C* mutant were performed in the presence of different fixed amounts of inhibitor with varying one of the two substrate concentrations while the other one was kept at a fixed saturating concentration. Data were plotted using GraphPad Prism 5.0. Data were analyzed according to Michaelis–Menten equation and $K_{m.app}$ and $V_{max.app}$ were derived.

Data of initial V (V_0) of these experiments where also represented by the double reciprocal Lineweaver-Burk plots (1/V vs 1/[Poly(rA)oligo dT]) of the inhibition of HIV-1 RT *wt* by **RS5187** (Fig. 13).

For the evaluation of the K_i values relative to the different mechanistic RT forms, $K_{m.app}$ and $V_{max.app}$ variation. obtained from Michaelis–Menten analysis of **RS5187** toward HIV-1 RT *wt*, were then used in the following equations.

- Relatively to the free enzyme [E]:

$$\text{Eq. 4} \quad V_{max.app}^{[NA]} = V_{max} / (1 + [I] / K_i^A)$$

Where K_i^A was derived analyzing $V_{max.app}^{[NA]}$ as a function of **RS5187** concentration.

- For the binary complex [E:NA]:

$$\text{Eq. 5} \quad V_{max.app}^{[TTP]} = V_{max} / (1 + [I] / K_i^B)$$

Where K_i^B was estimate analyzing the variation of $V_{\max.app}^{[TTP]}$ as function of the concentration of **RS5187**.

- For the ternary complex [E:NA:TTP]:

$$\text{Eq. 6} \quad K_{m.app}^{[NA]} = K_m(1 + [I]/K_i^C)$$

$$\text{Eq. 7} \quad K_{m.app}^{[TTP]} = K_m(1 + [I]/K_i^C)$$

Where K_i^C was derived studying the variation of both substrate affinities $K_{m.app}^{[NA]}$ and $K_{m.app}^{[TTP]}$ as function of the concentration of **RS5187**. The final value of K_i^C is represented by the media of the values obtained from equation 6 and equation (7).

The K_i value of **RS5187** toward HIV-1 RT *K103N-Y181C* mutant form was estimated using the equation (8)

$$\text{Eq. 8} \quad V_{m.app} = V_{max}(1 + [I]/K_i)$$

All experiments were repeated three times

3.3.5. Association / dissociation rate analysis.

The analysis of association (k_{on}) and dissociation (k_{off}) rates of **RS5187** toward HIV-1 RT *wt* and the drug resistant mutant form *K103N-Y181C* was perform in association assays at different time points, toward each mechanistic form of the enzymes.

Assay conditions: In first place this analysis was apply to the free enzyme [E], where 0.25 μ L of purified enzyme were pre-incubated at 37 $^{\circ}$ C, for different period of times with **RS5187** (100nM vs RT *wt* and 300nM vs *K103N-Y181C*), in a solution containing 50 mM Tris-HCl pH 7.5; 1mM DTT; BSA 0.2 mg/mL; Glycerol 2 %; MgCl₂ 20mM. Subsequently, such mixture was diluted with a mixture containing 50 mM Tris-HCl pH 7.5; 1mM DTT; BSA 0.2 mg/mL; Glycerol 2 %; MgCl₂ 20mM and the substrates Poly(rA)/oligo(dT) and ³[H]TTP 1490 cpm/pmol for the final concentration of 150nM and 10 μ M respectively. This avoids later enzyme–inhibitor association and allows the reaction to start. To evaluate the association/dissociation rates toward the binary complex [E:NA], 0.25 μ L of purified enzyme were pre-incubated at different time points with **RS5187** (100nM vs RT *wt* and 300nM vs *K103N-Y181C*) and 1 μ M

Poly(rA)/oligo(dT) at 37 °C, in order to promote the formation of the binary complex, in a solution containing 50 mM Tris-HCl pH 7.5; 1mM DTT; BSA 0.2 mg/mL; Glycerol 2 %; MgCl₂ 20mM. Then, a solution containing 50 mM Tris-HCl pH 7.5; 1mM DTT; BSA 0.2 mg/mL; Glycerol 2 %; MgCl₂ 20mM and ³[H]TTP 1490 cpm/pmol for a final concentration of 10μM, was used to dilute the preliminary-solution and to allow the reaction to start. Finally, RNA-dependent DNA polymerase assay to evaluate the ternary complex [E:NA:TTP] was performed pre-incubating at 37 °C, 0.25 μL of purified enzyme with 1μM Poly(rA)/oligo(dT) and 5μM dTTP at different time points, in a solution containing 50 mM Tris-HCl pH 7.5; 1mM DTT; BSA 0.2 mg/mL; Glycerol 2 %; MgCl₂ 20mM. After pre-incubation, such mixture was diluted with a second solution containing 50 mM Tris-HCl pH 7.5; 1mM DTT; BSA 0.2 mg/mL; Glycerol 2 %; MgCl₂ 20mM and ³[H]TTP 1490 cpm/pmol in a final concentration of 10μM, which allowed the start of the reaction. All reactions were incubated at 37 °C for 10 min. Aliquots (10 μL) were then transfer into a glass fibre filter FILTERMAT A and acid-precipitated radioactivity was measured as described above.

Data, representing the percentage of residual enzymatic activity after inhibitor exposure at the zero-time point and at different time points, was then plotted against time using GraphPad Prism 5.0. and analyzed by one phase decay analysis through the equation (9), where Y0 is the percentage of residual enzymatic activity when the pre-incubation time is zero. AMPLITUDE is the residual enzymatic activity value at infinite times, expressed in the same units as Y0. k_{app} is the rate constant, expressed in inverse seconds. Results of this analysis were used to estimate the k_{on} and k_{off} parameters using the equation (10) and (11)

$$\text{Eq. 9} \quad Y = (Y_0 - \text{AMPLITUDE}) * \exp(-k_{\text{app}} * X) + \text{AMPLITUDE}$$

$$\text{Eq. 10} \quad k_{\text{app}} = k_{\text{on}} / ([I] + K_i)$$

$$\text{Eq. 11} \quad k_{\text{off}} = k_{\text{on}}(K_i)$$

4. Results

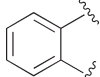
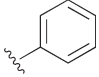
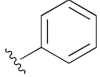
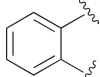
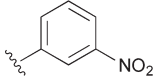
The synthesis of the compounds evaluated in PART I (Table 7) and PART II (Fig. 10 and Table 9) has been performed by the laboratory of Prof. Marco Radi at the University of Parma (see the attached original manuscripts for detailed information about the synthesis of these compounds). Compound **RS5187**, a derivative belonging to the indolyl-aryl-sulfone family, analyzed in PART III was synthesized by the laboratory of Prof. Romano Silvestri at University “La Sapienza”, Rome.

4.1. PART I: Targeting LRRK2

4.1.1. Characterization of heteroaryl-hydrazones derivatives by a multicomponent pharmacophore fragment decoration approach.

The inhibition potency of the heteroaryl-hydrazones compounds **9c–l**, **12** and **13** synthesized by multicomponent approaches (Table 7) towards both LRRK2 wild type (*wt*) and the G2019S mutated form was evaluated in cell-free assays. A preliminary screening was initially conducted to select the most promising compounds for additional biological studies (Fig. 5).

Table 7: Heteroaryl-hydrazone derivatives

Cpd	R ₁	R ₂	R ₃	R ₄	R ₅	R ₆	Yield ^a (%)
9b			H	H			53
9c			H	H	CH ₃		33

9d		CH ₃	H	H		39
9e		H	H	CH ₃		32
9f		H	H	CH ₃		41
9g		CH ₃	H	H		42
9h	H	H	H	H		45
9i	H	H	H	Cl		40
9j	CH ₃	H	CH ₃	CN		48
9k			CN	H		44
9l			CN	H		51
9m		H	H	H		38
9n		H	H	H		41
						12
						13^c

^a Isolated yield. ^b Compound **12** is the result of copper-catalyzed oxidation and ulterior microwave-assisted Buchwald amination with 4-(2-aminoethyl)morpholine of **9i**.

^c Compound **13** derived from reacting the latter compound **9g** with 4-(4-methylpiperazin-1-yl)benzoic acid under standard coupling conditions. (For detailed information concerning to the process of compounds synthesis please refer to the original manuscripts).

Among the quinoline derivatives, the most interesting compounds were found to be those bearing a hydroxyl or methoxy substituent on the right part of the molecule (**9d**, **f**, **g**) while pyridine derivatives (**9h–j**) generally showed poor inhibitory potency. Despite its high micromolar activity, the novel tetrahydroquinoline-3-carbonitrile derivative **9k** could be also considered as an interesting starting point for future chemical exploration.

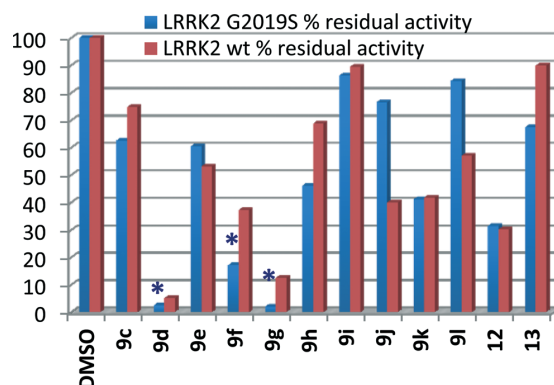


Figure 5: Inhibitory effect of synthesized compounds against LRRK2 *wt* (red bars) and *G2019S* (blue bars) expressed as % residual activity at 100 μ M concentration of the inhibitors. *% residual activity for compounds **9d**, **f**, **g** was reported at 50 μ M

Another promising result was obtained from the screening of the triazolo[4,3-*a*]pyridine derivative **12** while the complete loss of activity converting compound **9g** into **13** may provide useful indications to refine the docking models.

Table 8: Potency of compounds 9d, f, g and 12 against LRRK2 (wt and G2019S mutant) and their inhibitory effect on selected kinases.

Kinase	ID ₅₀ (μM) ^a				K _i (μM) ^b	
	9d	9f	9g	12	Bosutinib	Sorafenib
LRRK2 wt	3.0 (4) ^c	32.6 (7.5) ^c	2.7 (2.4) ^c	32.0 (3.5) ^c	0.3 (1.5) ^c	0.7 (0.07) ^c
LRRK2 G2019S	0.9	4.8	1.3	9.1	0.2	9.7

Kinase	% Inhibition at 100 μM				K _d (nM) ^d	
	9d	9f	9g	12	Bosutinib	Sorafenib
Src	31	5	21	40	1	NA
GSK3β	0	1	0	14	NA ^e	NA
Hck	0	0	0	0	3.4	8500
FAK	11	1	13	8	570	NA
DYRK1A	0	9	22	26	NA	NA
ABL	43	6	24	19	0.1	130
FLT3	50	3	62	0	2200	13
CDK2/cycA2	9	3	12	22	NA	8700
CDK9/cycT1	0	1	0	24	NA	NA
CDK9/cycK	53	2	24	38	NA	NA
CDK6/cycD1	42	1	40	18	ND ^f	ND
CDK4/cycD1	9	7	16	10	NA	NA
Pi4Kβ	32	0	31	3	NA	NA
Pim1	20	3	43	29	NA	NA

^a EC50 values are the mean of at least three independent experiments. Standard errors were all within 10% of the mean. ^b K_i values were extrapolated from Garofalo A *et al*, 2013. ^c wt/G2019S activity ratio (LRRK2 specificity index). ^d K_d values were extrapolated from Davis M *et al*, 2011. ^e NA = not active. ^f ND = not determined.

In the next phase, inhibition potencies of compounds **9d**, **f**, **g** and **12** were further investigated in dose-dependent experiments and ID₅₀ values for LRRK2 *wt* and *G2019S* were determined. Furthermore, the specificity of the compounds was tested against a panel of selected kinases (Table 8). Two well-known kinase-targeting drugs (Bosutinib and Sorafenib), recently investigated as LRRK2 inhibitors, (Liu Z *et al*, 2014) were also included in Table 8 for comparison purposes. It was interesting to note that, compared

to Bosutinib and Sorafenib, our compounds showed a better selectivity profile for the mutant form, as indicated by the higher *wt/G2019S* activity ratio (LRRK2 specificity index) and by the very low inhibitory potency against all the tested kinases. Although Bosutinib and Sorafenib were not developed as LRRK2 inhibitors, their good inhibitory efficacy against a few of the kinases reported in Table 8 is representative of the incomplete selectivity that characterizes most of the common kinase-targeting drugs.

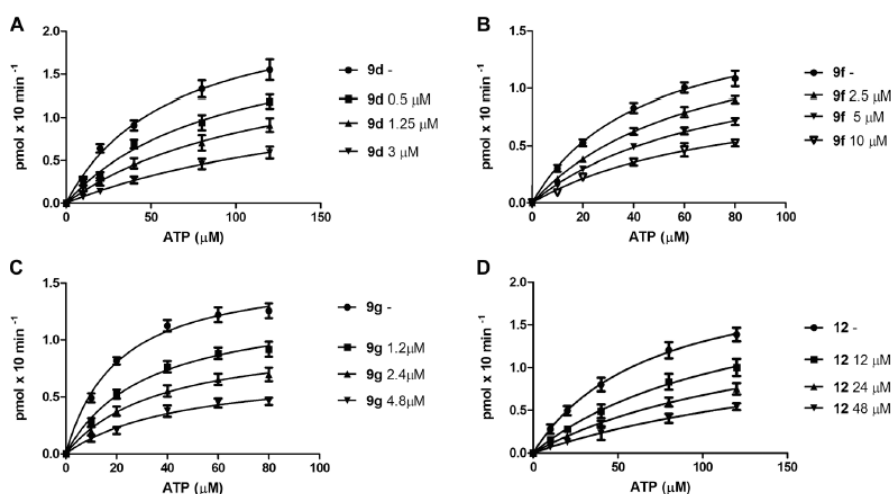


Figure 6: Kinetic analysis of the kinase reaction in the presence of different concentrations of LRRK2 *G2019S* inhibitors **9d**, **f**, **g** and **12**. Variation of the reaction velocity of LRRK2 *G2019S* as a function of ATP concentration at different fixed concentrations of **9d** (A), **9f** (B), **9g** (C) and **12** (D). Each reaction was performed as described in the methods section. Values are the means of three independent experiments. Error bars represent \pm S.D.

We then investigated the mechanism of inhibition of compounds **9d**, **f**, **g** and **12** toward the pathogenic *G2019S* mutant. LRRK2 *G2019S* kinase reactions were conducted by titrating ATP at different fixed doses of the compounds (Fig. 6, eqn. 2). Trends of the apparent affinities ($K_{m,app}$) and

apparent maximal velocities ($V_{\max,app}$) obtained from this analysis were then studied as a function of inhibitor concentration (Fig. 7 and 8).

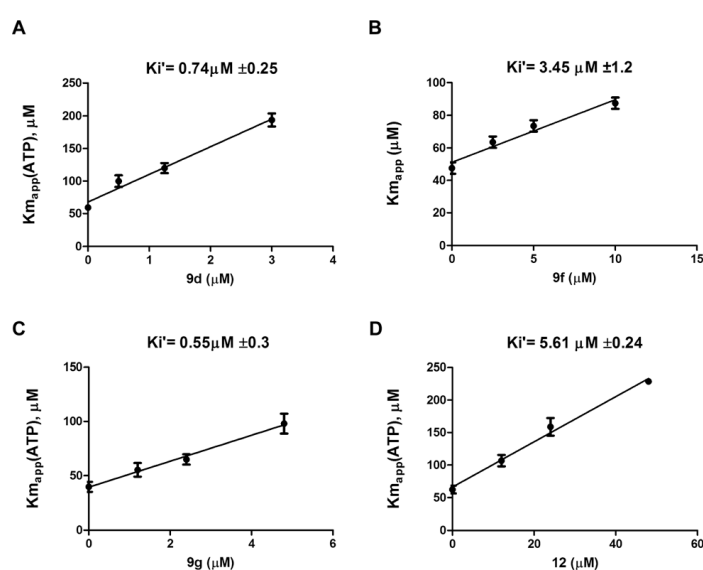


Figure 7: Determination of inhibitors' affinities for the LRRK2 *G2019S* free enzyme complex. Variation of the $K_{m,app}$ values of LRRK2 *G2019S* determined as shown in Fig. 6 as a function of **9d** (A), **9f** (B), **9g** (C) and **12** (D) concentration. K_i' values are reported at the top of each graph. Data analysis was performed as described in methods section. Values are the means of three independent experiments. Error bars represent \pm S.D.

For all these compounds, the $K_{m,app}$ values increased with increasing dose of inhibitor, underlying a competitive mechanism of action toward ATP. In particular, compound **12** inhibited the *G2019S* reaction without affecting the $V_{\max,app}$ parameter (Fig. 8D), thus resulting in a pure *ATP-competitive* mechanism of inhibition. On the other hand, increasing the concentration of compounds **9d**, **f** and **g** resulted in a decrease in $V_{\max,app}$ values, revealing these compounds as *mixed-type* inhibitors against *G2019S*, being able to

compete with ATP to form a complex with the free enzyme ($[E] \rightarrow [E : I]$) and also to bind to the enzyme in complex with ATP ($[E:ATP] \rightarrow [E:ATP:I]$).

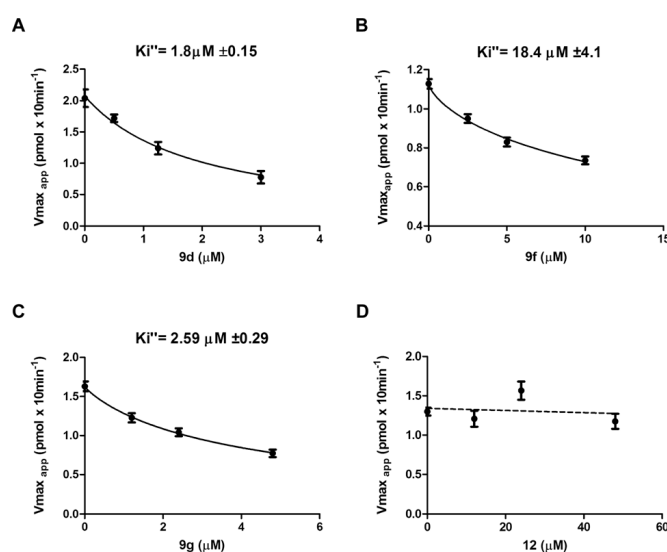


Figure 8: Determination of inhibitors' affinities for the [LRRK2 *G2019S* : ATP] complex. Variation of the $V_{max,app}$ values of LRRK2 *G2019S* determined as shown in Fig. 6 as a function of **9d** (A), **9f** (B), **9g** (C) and **12** (D) concentration. K_i'' values are reported at the top of each graph. Dotted line in (D) was obtained from data linear interpolation. Data analysis was performed as described in methods section. Values are the means of three independent experiments. Error bars represent \pm S.D.

The affinity for the free enzyme (K_i') was calculated for each compound according to eqn (2) and reported in Fig. 7; the affinity for the binary complex was calculated according to eqn (3) and reported in Fig. 8. The *mixed*-type inhibitors **9f** and **9g** showed a higher affinity toward the free enzyme than toward the [E:ATP] complex, with K_i' values about 5-fold lower than their K_i'' . Interestingly, compound **9d**, which exhibited the highest affinity toward the [E:ATP] complex among the tested compounds,

showed also comparable K_i' and K_i'' values. This is of particular interest since the intracellular ATP concentration is quite higher than that used in the in vitro assays, and this could affect the activity of purely ATP-*competitive* inhibitors. The *mixed*-type inhibitor **9d** (and to a lesser extent **9f** and **9g**) showed the ability to inhibit the catalytic activity of the LRRK2 G2019S mutant at low micromolar concentrations even when the enzyme is already bound to the ATP. This peculiar mechanism of action makes **9d** a promising candidate for further biological investigations and an interesting tool to identify a possible allosteric pocket on the LRRK2 kinase.

4.2.PART II: PHOSPHATIDYLINOSITOL KINASES: Targeting PI4KIII β

4.2.1. Identification of multitarget agents active as broad-spectrum antivirals.

Complete information about design and synthesis of PI4KIII β inhibitors, analyzed in this section is detailed in the attached original manuscripts.

Compound selection was based mainly on the ranking score and visual inspection of the PI4KIII β catalytic site. Thirteen commercially available compounds (5–17, Figure 9), were selected for biological investigation. These computational results were confirmed on the recently released crystal structure of PI4KIII β co-crystallized with PIK93, a known PIKs inhibitor, and this structure (PDB ID: 4D0L) was used for all the following simulations (Burke J *et al*, 2014)

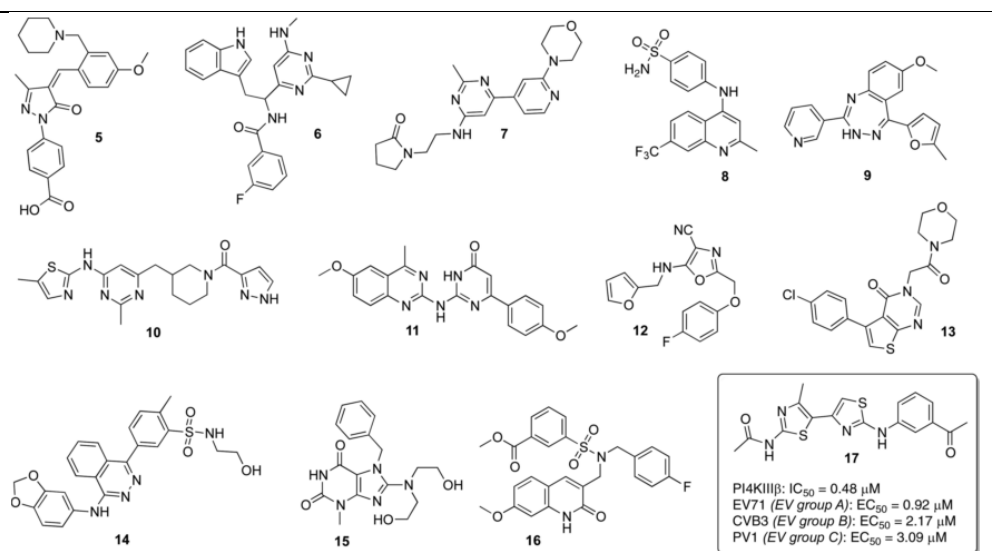
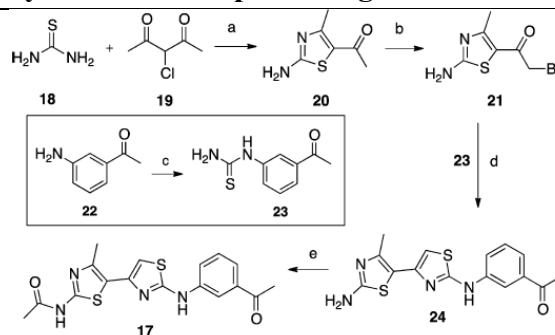


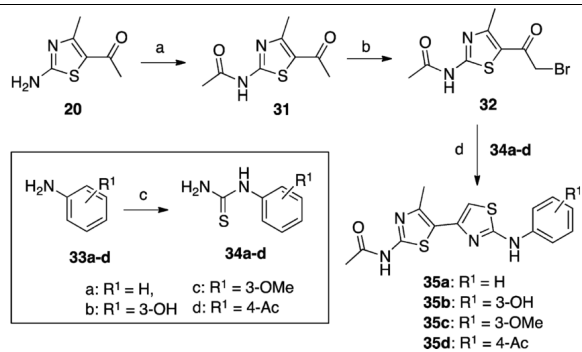
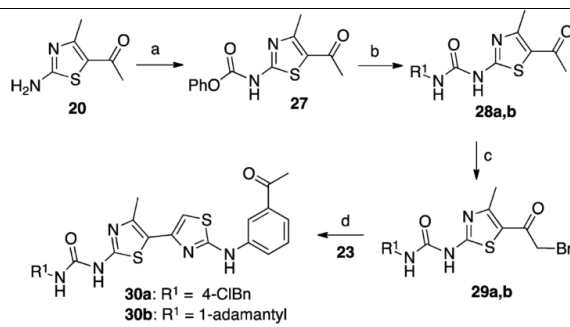
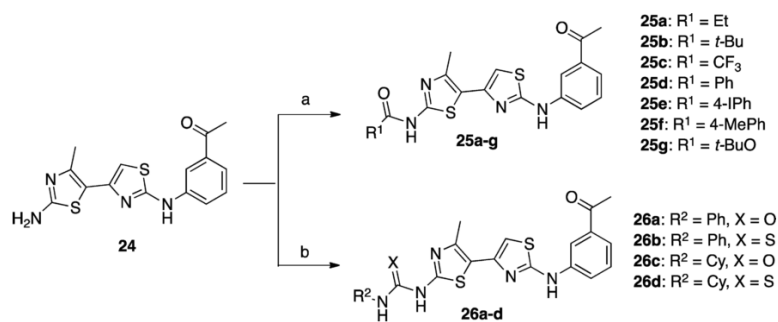
Figure 9. Chemical structure of compounds selected by virtual screening and activity profile of the hit compound 17.

These commercially available compounds were then tested both against the PI4KIII β enzyme and in a virus-cell-based replication assay (laboratory of virology and experimental chemotherapy of the Rega Institute for Medical Research, Leuven, Belgium). In particular, these compounds were evaluated for antiviral activity against a panel of Enteroviruses (EVs) that are representative of all major species: EV group A (EV71), group B (coxsackievirus B3, CVB3, and echovirus 11, ECHO11), group C (poliovirus 1, PV1), group D (enterovirus 68, EV68), rhinovirus group A (RV02) and rhinovirus group B (RV14). Among the selected compounds, only the bithiazole **17** showed activity in cell-free and cell-based assays (Figure 9) and possesses a chemical scaffold (the bithiazole) of a known family of CFTR correctors (Figure 9) (Pedemonte N *et al*, 2005a; Pedemonte N *et al*, 2005b; Yoo C *et al*, 2008). Compound **17** was therefore selected as a promising starting point for further structure-based optimization.

Chemical structure of compounds synthesized and evaluated in this section are represented in Figure 10.

Synthesized compounds against PI4KIII β





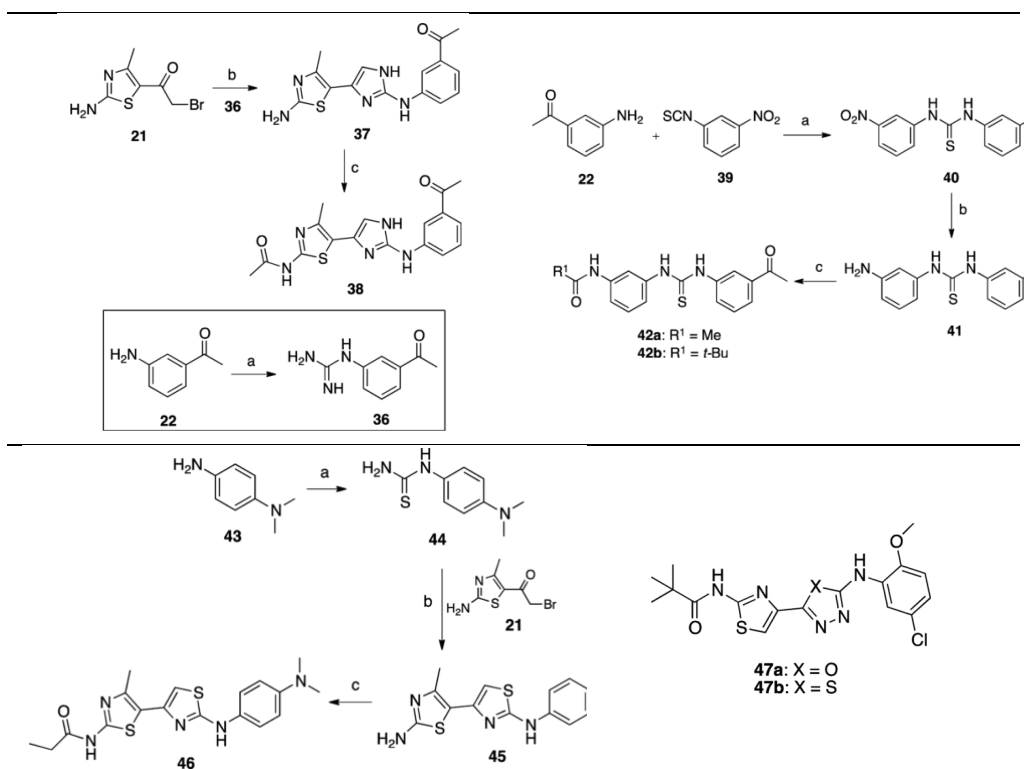


Figure 10: Schematic representation of compounds synthesis and chemical structure. (For detailed information please refer to the original manuscripts).

Biological analysis and antiviral activity.

All the synthesized compounds were initially evaluated for their inhibitory potency against PI4KIII β kinase *in vitro* and for their cell-based antiviral activity: EV71 was used as the primary target for SAR exploration since compound **17** revealed the best and most reproducible antiviral activity against this virus. In particular, the antiviral activity against EV71 was evaluated in EV71-induced CPE-reduction assay in rhabdomyosarcoma (RD) cells. Both the EC₅₀ values and the CC₅₀ values were measured. Uninfected, treated cells were also inspected under the microscope to evaluate whether the compounds altered normal cell morphology. The EC₅₀ and CC₅₀ values allowed us to calculate the selectivity index (SI), defined as

CC₅₀/EC₅₀. Compound **3** was used as a positive control. Results are summarized in Table 9.

Table 9: Activity of synthesized derivatives in PI4KIII β Inhibition assay and in virus-cell-based EV71 assay.

compd	PI4K III β IC ₅₀ (μ M) ^a	EV71 EC ₅₀ (μ M)	EV71 CC ₅₀ (μ M) ^b	EV71 CC ₅₀ (μ M) ^c	SI ^d	SI ^d
17	0.48	0.92 \pm 2.75	16.5 \pm 9.04	9.73 \pm 0.87	17.9	10.6
25a	0.27	0.38 \pm 0.10	10.1 \pm 4.82	6.37 \pm 2.46	26.6	23.6
25b	0.32	0.27 \pm 0.05	7.94 \pm 1.24	8.83 \pm 0.89	29.4	32.7
25c	21.89	2.0 \pm 0.95	25.8 \pm 5.06	30.1 \pm 9.93	12.9	15.0
25d	18.85	0.51 \pm 0.14	5.75 \pm 2.12	11.8 \pm 4.56	11.3	23.1
25e	>50	>44.6	ND ^e	ND	ND	ND
25f	>50	>55.7	ND	ND	ND	ND
25g	4.67	1.42 \pm 0.04	42.3 \pm 4.94	101.0 \pm 15.8	29.7	71.1
26a	7.69	NA ^f	ND	ND	ND	ND
26b	>50	NA	ND	ND	ND	ND
26c	1.82	2 \pm 0.04	8.87 \pm 3.85	ND	4.4	ND
26d	>50	NA	ND	ND	ND	ND
30a	3.95	4.77 \pm 0.28	20.9 \pm 6.97	ND	4.4	ND
30b	12.40	NA	ND	ND	ND	ND
35a	2.48	1.93 \pm 0.81	18.6 \pm 6.01	ND	9.64	ND
35b	2.63	NA	ND	ND	ND	ND
35c	1.55	1.2 \pm 0.16	9.17 \pm 0.85	ND	5.9	ND
35d	3.71	0.68 \pm 0.04	5.59 \pm 0.32	ND	8.2	ND
38	>50	>90.2	85.7	64.2	ND	ND
42a	NA	NA	ND	ND	ND	ND
42b	NA	NA	ND	ND	ND	ND
46	50.00	8.58 \pm 0.77	51.6 \pm 27.1	142.0 \pm 62.8	6	ND
47a	NA	NA	ND	ND	ND	ND
47b	NA	NA	ND	ND	ND	ND
3 ^g	0.06	0.73	>125			

^aValues are the mean of at least three independent experiments. ^bCC₅₀ values were assessed by MTS method. ^cCC₅₀ values were determined by microscopically detectable alteration of cell morphology. ^dSelectivity index (SI = CC₅₀/EC₅₀). ^eND = not determined. ^fNA = not active.

A close correlation between the antiviral activity measured in the cell-based assay and the inhibitory potency of the PI4KIII β kinase was observed, with only a few exceptions. The best results were obtained via modifying the left part of the molecule. In particular, compounds **25a, b**, bearing respectively a

Table 10: Evaluation of the broad-spectrum antiviral activity of the most potent derivatives against a representative panel of enteroviruses.

compd	CVB3			ECHO11			PVI			EY68		RV14		RV02	
	EC ₅₀ (μM)	CC ₅₀ (μM)	EC ₅₀ (μM)	CC ₅₀ (μM)	EC ₅₀ (μM)	CC ₅₀ (μM)	EC ₅₀ (μM)	CC ₅₀ (μM)	EC ₅₀ (μM)	CC ₅₀ (μM)	EC ₅₀ (μM)	CC ₅₀ (μM)	EC ₅₀ (μM)	CC ₅₀ (μM)	
17	2.17	101 ± 33.6	1.57 ± 0.23	>268	3.09	>269	NA ^a	ND ^b	>268	ND	NA ^b	ND	ND	ND	
25a	2.16	89.1 ± 16.2	0.97	12 ± 4.07	<1.52	5.49 ± 1.42	NA	ND	NA	ND	NA	ND	>259	ND	
25b	ND	20.9 ± 3.83	0.72 ± 0.05	5.07 ± 1.24	<1.41	5.07 ± 1.3	1.38	3.09	4.85 ± 1.09	ND	2.01 ± 0.05	ND	2.01 ± 0.05	ND	
25c	3.87 ± 0.23	58.8 ± 7.14	3.51	29.3 ± 1.78	2.86 ± 0.36	30.3 ± 3.66	ND	ND	10.6 ± 0.7	ND	10.6 ± 0.2	ND	10.6 ± 0.2	ND	
25d	2.19 ± 0.23	45.1 ± 4.44	1.77 ± 0.13	145 ± 27.6	2.23 ± 0.4	145 ± 27.6	NA	ND	>230	ND	2.05 ± 0.36	ND	2.05 ± 0.36	ND	
25g	2.74 ± 0.17	80.1 ± 6.97	2.93	124 ± 7.94	13.3 ± 1.9	124 ± 7.94	ND	ND	>232	ND	ND	ND	ND	ND	

^aNA = not active. ^bND = not determined

propanamide and a pivalamide moiety instead of the acetamide function of compound **17**, showed a very promising antiviral activity.

Compounds **25a, b** inhibited PI4KIII β and exhibited a significant antiviral effect at sub-micromolar concentrations, demonstrating a better activity than compound **17**. Compound **25g**, characterized by the Boc amino group, proved to be the most interesting compound of the entire series showing the highest selectivity index in the EV71 cell-based assay. Also changing the right portion of hit compound **17** gave interesting results (compounds **35a, c, d**). The central bithiazole scaffold proved to be essential for antiviral activity, as changing it gave inactive compounds (compounds **38, 42a, b**). Finally, the reported compounds **46, 47a, b** were devoid of antiviral activity and PI4KIII β inhibition activity.

Table 11: Evaluation of the antiviral activity of compound **25g** against EV71 clinical isolates

Genogroup	strain	Genbank	EC ₅₀ (μ M) ^a
			compd 25g
B2	11316	AB575927	<1.39
B5	TW/96016/08	GQ231942	21.00
	TW/70902/08	GQ231936	3.58
C2	H08300 461#812		0.97
C4	TW/1956/05	GQ231926	<1.39
	TW/2429/04	GQ231927	1.17

^aAll values are based on at least three independent dose–response curves.

On the basis of these activity data, and considering that the SI of a promising antiviral candidate should be at least greater than **10**, compounds **17, 25a–d**, and **25g** were selected for further studies. The broad-spectrum activity of the six selected compounds was evaluated against a panel of EVs representative of all major groups: EV group B (coxsackievirus B3 and echovirus11, ECHO11), group C (poliovirus 1), group D (enterovirus 68),

rhinovirus group A (RV02), and rhinovirus group B (RV14). Results are reported in Table 10.

The selected compounds showed micromolar and sub-micromolar activity against different EVs within the tested panel. In addition, the antiviral activity of the less toxic compound **25g** was confirmed against a representative panel of EV71 clinical isolates. As shown in Table 11, we could confirm the activity of compounds **25g** against the clinically relevant EV71 specimens. Only the (sub)genogroup B5 appeared to be less sensitive. Furthermore, we evaluated the lipid kinase isoform selectivity of our best PI4KIII β inhibitors by testing them in an in vitro inhibition assay on the related enzyme PI4KIII α and PI3K- α /p85 α (Table 12).

Table 12 Inhibitory effect of selected compounds against members of PIK family and profiling of compound **25g** against a small panel of unrelated kinases

compd	PI4KIII β	PI4KIII α	PI3K- α /p85 α	compd	kinase	% residual activity at 100 μ M ^a
	IC ₅₀ (μ M) ^a	% residual activity at 100 μ M ^a				
17	0.48	52	37	25g	Src FL	32
25a	0.27	72	40		GSK3 β	79
25b	0.32	71	93		Hck FL	100
25c	21.89	73	85		FAK	82
25d	18.85	81	54		DYRK1A	88
25g	4.67	69	64		ABL FL	53
35a	2.48	58	81		FLT3	59
35c	1.55	71	51		CDK2/cA2	62
35d	3.71	73	100		CDK9/cT1	57
					CDK9/cK	49
					CDK6/cD1	25
					Pim1	70

^a Values are the mean of two independent replicates.

Results showed a higher specificity of the tested bithiazole derivatives for the PI4KIII β isoform with poor inhibition of both PI4KIII α and PI3K- α /p85 α at 100 μ M concentration of each compound. The specificity of compound **25g** was also tested on a small panel of unrelated kinases: it shows only a low inhibitory effect on Src and CDK6. Despite the latter enzymes being involved in cell cycle regulation and representing common

targets of antitumor compounds, **25g** did not show any toxicity or morphology alteration at antiviral concentration in the tested cell lines. In addition, recent studies indicated that Src inhibitors have no effect on EV71 replication (Ford-Siltz L *et al*, 2014), while CDK6 seems to be down-regulated in response to EV71 infection (Leong V and Chow W, 2006).

Overall, the collected biological data indicate that a fine chemical tuning of the bithiazole substituents is needed to generate compounds able to specifically inhibit the PI4KIII β kinase and block the replication of different EVs.

4.3.PART III: Targeting HIV-1 RT

4.3.1. RT purification

We took advantage of the 6xHis tag at the N-terminal of recombinant RTs to purify each RT form (*wt*, *K103N*, *Y181C* and *K103N/Y181C*) through a single affinity chromatographic step (see *Materials and methods* section). For each purification, the eluted fractions were tested for the presence of the recombinant protein by coomassie stained SDS page. Subsequently, Bradford quantification and enzymatic activity of each positive fraction were performed. Fraction showing high purity and high activity were pooled, stored at -80°C and used for the subsequent analysis. Typical pool concentrations were between 60 and 80 mg/mL with a purity that exceed 90%.

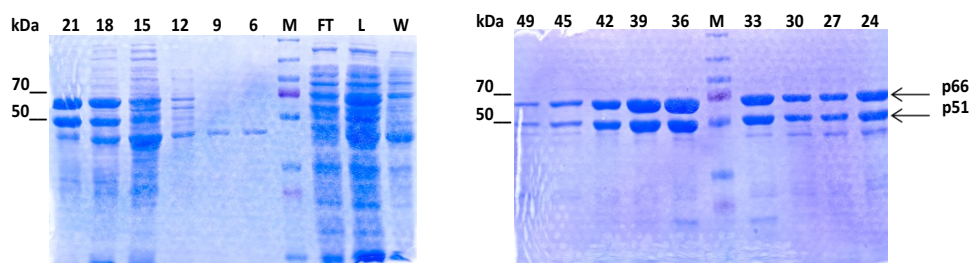


Figure 12: Example of RT purification outcome: Coomassie staining SDS-PAGE of *K103N/Y181C*. M: marker; L: supernatant; FT: flow through; W: wash; 6-49: eluate fractions. Arrows indicate bands of about 51 and 66 kDa, corresponding to the molecular weight of the two monomers that compose HIV-1 RT

4.3.2. Evaluation of the inhibition potency of a library of new IAS derivatives.

We evaluated a library of new IAS derivatives synthesized in the laboratory of Prof. R. Silvestri at University “La Sapienza” in Rome, for their ability to inhibit NNRTIs resistant mutants both *in vitro* and *in vivo*.

Inhibition assays using recombinant enzymes showed that the majority of the compounds were highly active toward RT *wt*, as well as toward the single mutants *K103N* (Lys103Asn) and *Y181C* (Tyr181Cys) (Table 13). However, the tested molecules exhibited inhibition potencies about an order of magnitude lower against the double mutant *K103N-Y181C*. This observation was expected, since this feature was common for other IAS library that we previously characterized (Famiglini V *et al.* 2017). **RS5187** and **RS5561** represents an exception, showing IC₅₀ values in the same range against both RT *wt* (**RS5187** IC₅₀ =83) and *K103N-Y181C* (**RS5187** IC₅₀ =76) enzymes. The results are summarized in Table 13, in which we also reported the IC₅₀ values for the compounds reference nevirapine (NVP), efavirenz (EFV) and etravirine (ETV), NNRTIs currently used in the clinic, as well as AZT, an approved NRTI.

Similar results were obtained by our collaborator at the University of Barcelona when the different IASs were evaluated for their ability to inhibit viral proliferation in MT-4 cells. The obtained EC₅₀ (Effective concentration of compound to inhibit by 50% cell death induced by the viral replication) well correlated with the results obtained *in vitro* (table 13). Most of the compounds were highly active toward the *wt* and single mutant forms of the enzyme. On the other hand, they generally inhibited the *K103N-Y181C* strain growth with a lower potency (from one order of magnitude to the complete loss of activity). This was not the case of **RS5187** and **RS5561**, which did not lose their activity against the double mutant.

To understand the molecular reasons that underline such activity against *K103N-Y181C*, we decided to investigate the mechanism of action of **RS5187** against the RT *wt* and toward the drug resistant double mutant form *K103N-Y181C*.

Table 13: IAS derivatives (RS) tested *in vitro* and *in vivo* against HIV-1 RT *wt* and its drug resistant mutant forms *K103N*, *Y181C* and *K103N-Y181C* double mutant.

RS	<i>Wt</i>	<i>K103N</i>		<i>Y181C</i>		<i>K103N-Y181C</i>	
	IC ₅₀ (nM)	EC ₅₀ (nM)	IC ₅₀ (nM)	EC ₅₀ (nM)	IC ₅₀ (nM)	EC ₅₀ (nM)	IC ₅₀ (nM)
5196	nd	>0.7	nd	20±8	nd	na	nd
5029	nd	<0.7	nd	44±22	nd	6089 ± 6946	nd
5194	69	<0.7	106	<0.7	81	967 ±154	375
5187	83	<0.7	73	<0.7	61	6,2 ± 0	76
5561	19	<0.7	7	<0.7	57	23.5 ± 4.3	15
5431	nd	<0.7	nd	19±2	nd	662 ± 103	nd
5103	68	<0.6	2	11±22	33	110 ± 88	45
5422	nd	<0.7	nd	0.7	nd	na	nd
5188	61	<0.7	45	<0.7	50	704 ± 85.3	628
5105	92	<0.7	nd	22±7	nd	na	nd
5111	38	<0.7	79	22±7	178	na	188
5386	nd	37±9	nd	41±11	nd	na	nd
5384	nd	437±456	nd	47.6±9.5	nd	3555±1818	nd
5286	208	18.5±0	12	7.4±0.12	34	3667 ± 907	842
5328	nd	<0.7	nd	21±14	nd	1008±816	nd
5363	nd	<0.7	nd	10±10	nd	600 ±703	nd
5364	nd	<0.6	nd	2±0.4	nd	1123 ± 1194	nd
5393	nd	<0.7	nd	4.1±6.0	nd	na	nd
5432	nd	<0.7	nd	<0.7	nd	331± 145	nd
5365	nd	166±0	nd	85±19	nd	4307 ± 2816	nd
5394	nd	151±1.7	nd	1.9±1.9	nd	4621 ± 2348	nd
NVP	400	>3756	7000	>3756	>20000	>3756	nd
EFV	80	130±180	>20000	160±180	400	>317	nd
AZT	10	16 ± 12	20	6.0 ± 3,4	164	16 ± 13	nd
ETV	23	nd	16	nd	25	nd	68

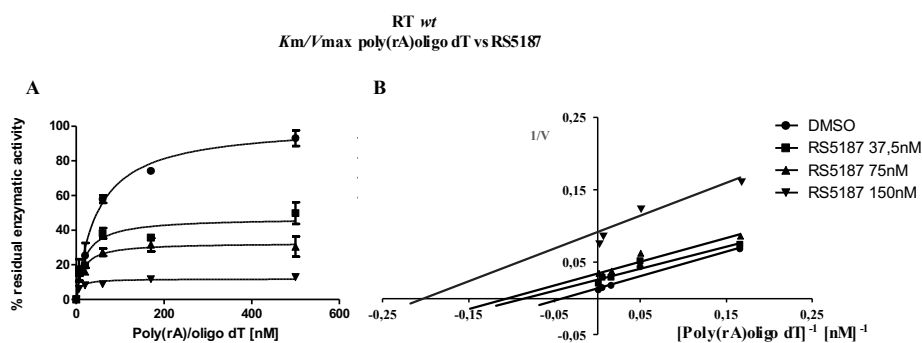
EC₅₀ represents the Anti-HIV-1 activity of RS compounds and reference compounds NVP, EFV and AZT against mutant HIV-1 strains. EC₅₀: effective concentration (nM) to inhibit by 50% cell death induced by the indicated mutant HIV-1 strain, as evaluated with the MTT method in MT-4 cells. Data are mean values of two to three independent experiments each one in triplicate. IC₅₀: The half maximal inhibitory concentration obtained by *in vitro* assays against HIV-1 RT *wt* and its mutant forms *K103N*, *Y181C* and *K103N-Y181C* double mutant. Data are mean values of three independent experiments. nd: no data. na: non active

4.3.3. The Mechanism of Action of RS5187.

4.3.3.1. Kinetic parameters of RS5187 toward HIV-1 RT *wt*.

To evaluate the mechanisms of action of **RS5187** we performed a reverse transcriptase reaction maintaining the inhibitor and a reaction substrate (nucleic acid or nucleotide) at fixed concentrations, while increasing the concentrations of the other substrate (see Method section). The variations of the apparent $V_{\max,app}$ and $K_{m,app}$ values for each substrate were studied as a function of the inhibitor concentration. The collected data are summarized in figure 13.

During the RNA-dependent DNA polymerization, catalyzed by HIV-1 RT, the enzyme displays an obligatory order of substrate binding. Initially, RT binds the nucleic acid (NA) to form the binary complex [E:NA]. The formation of this complex induces the subsequent binding of the nucleotide (TTP) with the formation of the ternary complex [E:NA:TTP].



	DMSO	RS5187 37,5nM	RS5187 75nM	RS5187 150nM
$V_{\max,app}^{[NA]}$ (%)	100	46.97	32.6	11.86
$K_{m,app}^{[NA]}$ (nM)	48.57	19.56	14.39	7.359
Std. Error				
$V_{\max,app}$	5.64	3.663	2.204	0.6755
$K_{m,app}$	9.159	6.609	4.526	2.455

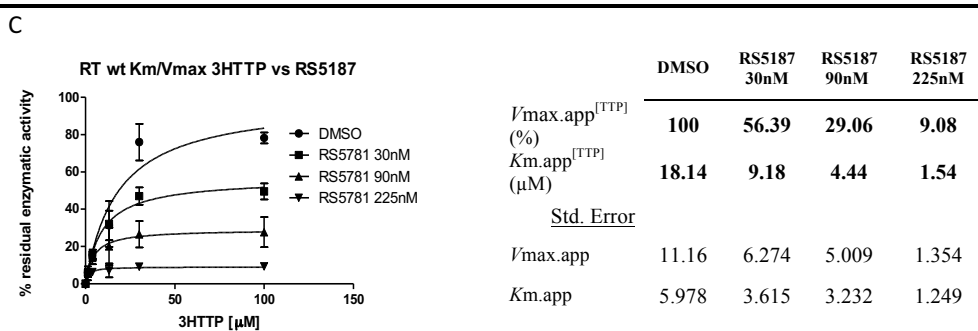


Figure 13. RS5187 Mechanism of Action Against RT wt in Increasing Concentrations of (A and B) Poly(rA)/oligo dT and (C) 3HTTP: Kinetic analysis of DNA polymerase activity in the presence of different concentrations of non-nucleoside reverse transcriptase inhibitor **RS5187**. (A) Variation of the reaction velocity of RT *wt* as a function of nucleic acid (NA) substrate concentration at different fixed concentrations of **RS5187**. Values above are the means of three independent experiments. (B) Same data used in the analysis in (A) were used to exemplify the mechanism displayed by **RS5187** against RT *wt* in a linear plot representation through the Lineweaver-Burk double-reciprocal analysis. (C) Variation of the reaction velocity of RT *wt* as a function of TTP concentration at different fixed concentrations of **RS5187**. Values are the means of three independent experiments. Error bars represent \pm S.D

To evaluate the analysis of the mechanism of action of **RS5187** against RT *wt*, toward the free enzyme [E], as well as toward the binary and ternary complexes, we performed the reverse transcriptase reaction maintaining a substrate at a fix concentration while titrating the second one at different concentrations of the inhibitor. In this way, we demonstrated that in both cases $V_{\max.app}$ and $K_{m.app}$ values decreased (Fig. 13), according to a *mixed-type* mechanism of action against both substrates. This means that **RS5187** would bind reversibly to the allosteric site of the enzyme without competing with the substrates. Moreover, according to this mechanism of action, the inhibitor can bind preferentially to the enzyme bound to its substrates, both in the binary complex or in the ternary one (Fig. 14), increasing the apparent affinity of RT *wt* for its substrates. This is likely due to an effect of the inhibitor on the rate of dissociation of the substrates from the enzyme.

remain in contact with the binding site, defined by the dissociation rate constant (k_{off}). High k_{on} and/or low k_{off} describes a high affinity inhibitor.

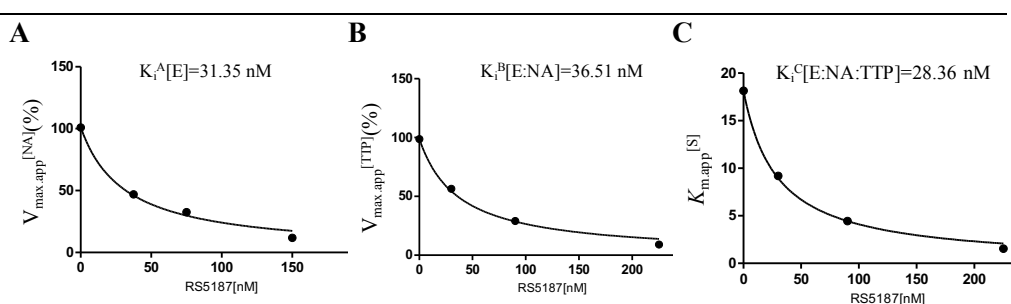


Figure 15: Dissociation constants of RS5187 and the free enzyme (A), the binary complex (B), or the ternary complex (C). Trends of the apparent affinities and apparent maximal velocities obtained from the analysis of Mechanism of action on Fig. 13 were then studied as a function of inhibitor concentration.

In order to determine the binding stability of **RS5187** to the allosteric site of the enzyme, the rates of association (k_{on}) and dissociation (k_{off}) were analyzed for all the three catalytic complexes of RT wt in the presence of 100 nM RS5187 (see methods section for analysis details). Results of such analysis is summarized in Fig. 16 and Table 14.

One Phase Decay

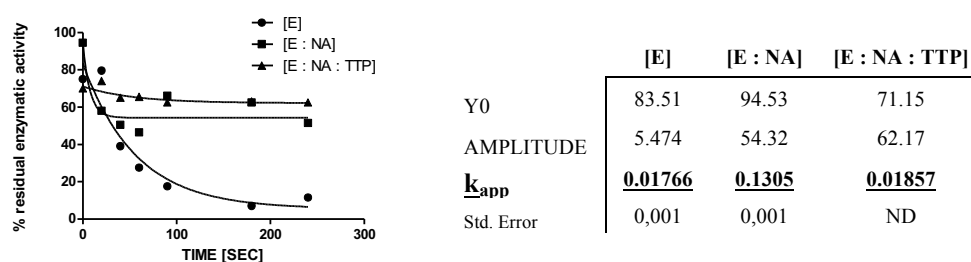


Figure 16: One phase decay analysis of RS5187 tested against the HIV-1 RT wt. 100 nM RS5187 where pre-incubated with the free enzyme (circles), RT and NA (squares) or RT, NA and TTP (triangles) at different time points. Data where analyzed as described in materials and methods section.

Table 14: Binding affinities and kinetic parameters of the Indolyl-Aryl-Sulfone derivative inhibitor **RS5187** against HIV-1 RT *wt*.

	IC ₅₀ [nM]	K _i [nM]			k _{on} (nM ⁻¹ s ⁻¹)			k _{off} (s ⁻¹)		
		[E]	[E:NA]	[E:NA:TTP]	[E]	[E:NA]	[E:NA:TTP]	[E:NA]	[E:NA:TTP]	
RS5187	83	31.4	36.5	28.4	13 x10 ⁻⁵	96 x10 ⁻⁵	15 x10 ⁻⁵	42 x10 ⁻⁴	349 x10 ⁻⁴	41 x10 ⁻⁴

Relationships among the association and dissociations rates of RS5187 for the different enzymatic forms of RT *wt*

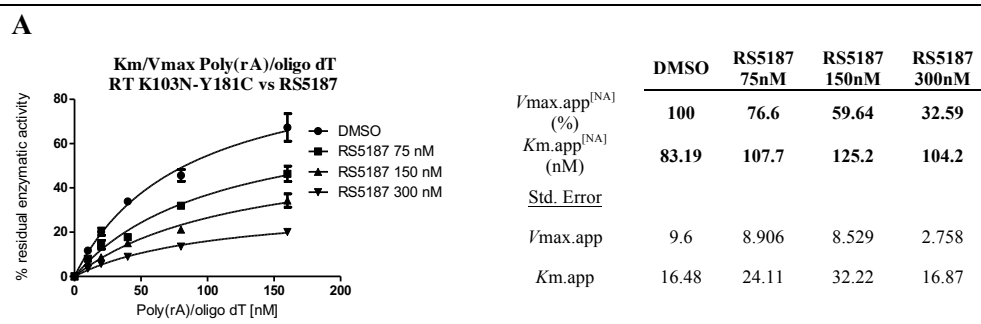
$$k_{on} = [E; NA] > [E: NA: TTP] > [E]$$

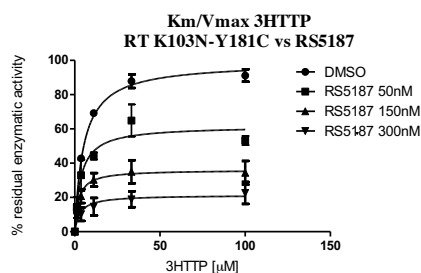
$$k_{off} = [E: NA] > [E] \geq [E: NA: TTP]$$

RS5187 demonstrate to associate about 6.7-fold faster, to the binary complex [E:NA] than to the ternary complex [E:NA:TTP] or toward the free enzyme [E]. However, other than binding more quickly to the binary complex, RS5187 remains associated about 10-fold less to the same complex with respect to free enzyme and to the ternary complex (Table 14).

4.3.3.2. Kinetic parameters of RS5187 toward HIV-1 RT drug resistant mutant *K103N-Y181C*.

Analysis of the mechanism of action of the indolyl-aryl-sulfone derivative **RS5187** tested against the RNA-dependent DNA polymerase activity of HIV-1 drug-resistant mutant RT *K103N/Y181C* was performed as in the analysis above against the *wt* form.



B

	DMSO	RS5187 50nM	RS5187 150nM	RS5187 300nM
$V_{\max.app}^{[TTP]}$ (%)	100	61.68	36.06	21.32
$K_{m.app}^{[TTP]}$ (μ M)	5.16	3.47	2.27	3.16
Std. Error				
$V_{\max.app}$	2.70	5.07	2.84	2.95
$K_{m.app}$	0.565	1.24	0.856	1.947

Figure 17: RS5187 Mechanism of Action Against RT Drug Resistant Mutant Form K103N-Y181C with Increasing Concentrations of (A) Poly(rA)/oligo dT and (B) 3HTTP: Kinetic analysis of RNA-dependent DNA polymerase activity of RT K103N-Y181C in the presence of different concentrations of non-nucleoside reverse transcriptase inhibitor **RS5187**. (A) Variation of the reaction velocity of RT *K103N-Y181C* as a function of Poly(rA)/oligo dT concentration at different fixed concentrations of **RS5187**. Values are the means of three independent experiments. (B) Variation of the reaction velocity of RT *K103N-Y181C* as a function of ³HTTP concentration at different fixed concentrations of **RS5187**. Values are the means of three independent experiments. Error bars represent \pm S.D

Variation of the reaction velocity of RT double mutant *Y181C-K103N* as a function of Poly(rA)/oligo dT concentration at different fixed concentrations of **RS5187** shows that the $V_{\max.app}^{[NA]}$ values decrease markedly while $K_{m.app}^{[NA]}$ values remain more or less stable. Interestingly the complementary analysis on the second substrate (TTP) exhibit the same trend, in this case $V_{\max.app}^{[TTP]}$ values decreases five-fold in contrast with the $K_{m.app}^{[TTP]}$ values, which variation is insignificant. This disturbance in the apparent velocity of reaction without altering the affinity of the both substrates demonstrate that non-nucleoside HIV-1 reverse transcriptase inhibitor **RS5187**, reversibly binding the allosteric site, with a *non-competitive* mechanism of action against the NA and TTP substrates of HIV-1 RT double mutant *Y181C-K103N*. Therefore, theoretically it can bind to both the free enzyme and the enzyme-substrate complexes, in this way neither [E:I] nor [E:S:I] forms products.

One Phase Decay

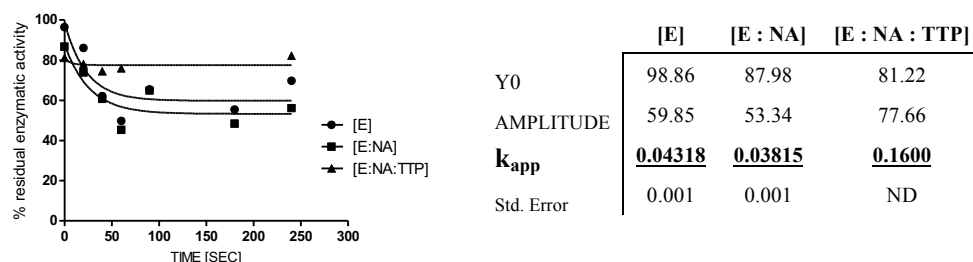


Figure 18: One phase decay analysis of RS5187 tested against the HIV-1 RT drug resistant mutant *K103N-Y181C*, obtained at 37 °C from association assays with RS5187 300nM were pre-incubated at different time points with the free enzyme [E], with the [E:NA] and [E:NA:TTP] complexes (see methods section).

Being a *non-competitive* inhibitor, the dissociation constant (K_i) of **RS5187** is equal to the IC_{50} value ($IC_{50}=76$ nM). Taking this premise into consideration and using the k_{app} values provided by the one phase decay analysis in figure 18 we proceeded to determine the velocity of association / dissociation (k_{on} / k_{off}) described in table 15.

Table 15: Binding Affinities and Kinetic Parameters of the Indolyl-Aryl-Sulfone Derivative *non-competitive* Inhibitor RS5187 against HIV-1 RT drug resistant mutant *K103N-Y181C*.

	K_{i50} [nM]	k_{on} ($nM^{-1} s^{-1}$)			K_{off} (s^{-1})		
		[E]	[E:NA]	[E:NA:TTP]	[E]	[E:NA]	[E:NA:TTP]
RS5187	76	11×10^{-3}	10×10^{-3}	43×10^{-3}	87×10^{-4}	77×10^{-4}	323×10^{-4}

Relationships among the association and dissociations rates of RS5187 for the different enzymatic forms of RT *K103N/Y181C*

$$k_{on} = [E: NA: TTP] > [E] > [E: NA]$$

$$k_{off} = [E: NA: TTP] > [E] > [E: NA]$$

RS5187 displays a velocity of association toward the ternary complex [E:NA:TTP] greater than those toward the free enzyme [E] and the [E:NA]

complex. A similar trend was found in the dissociation velocity parameters (k_{off}) which means that theoretically, the indolyl-aryl-sulfone derivative **RS5187** could bind the ternary complex [E:NA:TTP] four-fold faster than to the other complexes but could remain associated to this complex for a shorter time than to the free enzyme or the binary complex.

5. Discussion

Due to the number of cellular processes in which protein and lipid kinases are involved, their physiological malfunction or deregulation are related with numerous human pathologies including different cancer types and neurodegenerative diseases. Furthermore, they can also act as essential mediator factors during viral infections. The discovery of diseases caused by alteration of kinases activity allows the possibility of exploiting kinases inhibition as a therapeutic strategy.

In recent years, it has been shown that mutations in LRRK2 are recurrent in familial Parkinson's disease. For this reason, LRRK2 is considered as an important molecular target for the development of an effective therapy. Actually, several highly active inhibitors have been developed. However, such molecules are not able to discriminate between the *wt* and the mutated LRRK2 forms. Despite the biological function of LRRK2 is still not completely elucidated, it is possible that its inhibition would lead to adverse effects in the long term. In collaboration with Dr. Radi from the University of Parma, we evaluated a new library of heteroaryl-hydrazone derivatives as LRRK2 inhibitors through *in vitro* studies resulting in the identification of compounds with different anti-LRRK2 activity against both the *wt* and *G2019S* mutant form. Among them, the most interesting compounds were found to be those bearing a hydroxyl or methoxy substituent on the right part of the molecule (**9d**, **f** and **g**) and the triazolo[4,3-*a*]pyridine derivative compound **12**. These compounds are endowed with a low micromolar activity, and when were tested against a small panel of selected kinases showed good LRRK2 specificity index (*wt/G2019S* activity ratio), showing even better selectivity profile than two well-known kinase-targeting drugs, Bosutinib and Sorafenib. In order to elucidate the molecular mechanism that underlie the inhibition preference toward the LRRK2 mutant, we investigated the mechanism of inhibition of those molecules. Not surprisingly, we found different mechanism of inhibition among the

compounds. Compound **12** demonstrated to be able to inhibit the catalytic activity of *G2019S* displaying a pure ATP-competitive mechanism of inhibition. Furthermore, Compounds **9d**, **9f** and **9g** displayed a mixed-type inhibition when tested against the activity of the pathogenic mutant *G2019S*. This mechanism of inhibition allows the compounds to bind the free enzyme competing with the ATP, but also to bind to the enzyme when it is already in complex with ATP. Among them, compound **9d**, prove to be of particular interest since displayed comparable affinities toward the free enzyme (K_i') and the enzyme in complex with the ATP (K_i''). This result could be important because the high concentration of ATP in physiological conditions, could affect the performance of purely ATP-competitive inhibitors. All together, these results place the synthesized heteroaryl-hydrazone derivatives as good candidates for the development of new, higher potent and *G2019S* selective derivatives.

In recent years, the focus on the development of antiviral compounds is shifting from a strategy based on targeting viral proteins, to an approach considering host cell targets as well. This, because viruses are obligatory intracellular parasites, whose replicative cycle heavily depends on host cell factors. This approach might have two main advantages: since cellular proteins are less prone to mutate, drug resistance may be less likely to occur; in addition, different viruses often depend on the same host cell proteins, thus targeting these essential cofactors might allow the development of broad spectrum antiviral agents, currently lacking in the clinics.

PI4KIII β is considered a valuable target for the treatment of many viral infections. PI4KIII β converts PtdIns into PtdIns4*P* and is involved in vesicular trafficking and membrane remodeling pathways in different tissues. Enteroviruses (EV) hijack PI4KIII β to produce membrane platforms enriched in PtdIns4*P* which serve as molecular anchoring for the EV replication machinery. The most important issue regarding the development of PI4KIII β inhibitors rely on their selectivity. In fact, chemical inhibition of PI4KIII β does not influence cell viability, probably because the PtdIns4*P*

amount produced by the related PI4KIII α could support cell trafficking and signaling. However, poorly selective inhibitors targeting both PI4KIII β and PI4KIII α kinases could induce cellular toxicity. Twenty-five compounds synthesized by Prof. Marco Radi at the University of Parma, were tested against the PI4KIII β enzyme in cell-free assays. The best inhibitory profile was that displayed by compound **25a**, which contains a propanamide moiety and **25b** compound bearing a pivalamide substituent in the same location. **25a** and **25b** were able to inhibit PI4KIII β at nanomolar concentrations, closely matching data obtained in cell-based assays where these inhibitors exhibit a significant antiviral effect at the same concentration range. The activity of compounds **25a-d**, **25g** and **17** against a panel of enteroviruses also place these compounds as interestingly broad-spectrum antivirals. On the other hand, compounds **38**, **42a** and **42b** were inactive when were tested against the viral replication. Interestingly, the central bithiazole scaffold was substituted in these compounds, demonstrating that this structure is critical for antiviral activity and PI4KIII β inhibition. *In vitro* specificity assay demonstrated that compounds **25a**, **25b** and **25g** selectively target the isoform β . This is of particular interest since some toxicity risks may be expected as result of off-target inhibition of other PI4K isoforms, which could support cell trafficking and signaling when PI4KIII β is inhibited (Balla T, 2013). At the same time and despite its high micromolar activity, compound **25g** proved to be the most interesting compound of the entire series, showing the highest selectivity index and less toxicity during cell-based assays. The features of compounds **25a**, **25b** and **25g** in this study represent a valuable starting point to develop novel broad-spectrum antiviral compounds based on the host targets.

HIV-1 RT continue to be the main anti-HIV-1 target in the HAART regimen. However, despite the efficacy of the actual treatment, its selective pressure leads to resistant mutants development. We thus evaluated a set of NNRTIs of the IAS family against *wt* RT as well as against the main resistant forms that emerged during the therapy. These IAS derivatives

result in variable potency in the nanomolar range against RT *wt*, but also displayed interesting potencies against the double mutant *K103N-Y181C*. Compound **RS5187** was selected because the inhibitory potency displayed against both RT *wt* and the drug resistant mutant form *K103N-Y181C*. **RS5187** is endowed with high inhibitory potency, being able to effectively inhibit the RT *wt* activity (IC₅₀=83nM) and the drug resistant mutant *K103N-Y181C* (IC₅₀=76nM) with comparable efficiency.

When the mechanisms of inhibition were analyzed, **RS5187** demonstrated a *mixed-type* mechanism toward the *wt* form. This mechanism suggests that **RS5187** binds to the [E:NA] and/or [E:NA:TTP] complexes, affecting their breakdown. The study of the affinities of **RS5187** for each mechanistic form of RT *wt* showed that the inhibitor targeted with similarly affinities the different reaction intermediates [E], [E:NA] and [E:NA:TTP]. Interestingly, the main determinant for this mechanism was the inhibitor association rate. **RS5187** binds 6.7-fold faster, but dissociates about 10-fold faster from the binding site of the [E:NA] secondary complex of RT *wt*, than the free RT or the ternary complex, which remained unchanged.

In contrast, **RS5187** resulted to possess a fully *non-competitive* mechanism of inhibition toward *K103N-Y181C* mutant form. Thus, in principle this compound can inhibit the *K103N-Y181C* enzymatic activity without influencing the affinity for the substrates. Contrary to that observed against RT *wt*, **RS5187** is capable of discriminating against the [E:NA:TTP] ternary complex, binding it 4- folds faster than the free enzyme or the secondary complex, but dissociating 5-folds faster from the same complex. Thus, **RS5187** against both *wt* or *K103N-Y181C* mutant displays higher association rates when the enzyme was already in complex with one or two of its substrates. This, however, is compensated by a faster dissociation rate, which explains why the equilibrium constants K_i are similar for all three enzymatic forms. **RS5187** thus displays two diverse mechanisms of inhibition against two forms of the same enzyme which could mean that this IAS derivative possesses a flexible and adaptable structure that can interact dynamically with the allosteric site of HIV-1 RT making it able to bypass the steric barriers imposed by the *K103N-Y181C* mutation. Moreover

is evident that in certain mode, the structural changes in the binding site due to *K103N-Y181C* mutation and / or due conformational changes occurring during formation of the ternary complex plus the flexible and dynamical structure that accompanied to IAS derivatives allows to **RS5187** to bind [E:NA:TTP] faster in *K103N-Y181C* than in *wt*. Thus, this scaffold could be the basis for further structure-activity relationship studies, in order to make derivatives which retain the faster association rates, but achieve also slow dissociation from the ternary complex. Improving the knowledge of the mechanisms of inhibition surrounding the IAS derivatives structure helps in the selection of new compounds with improved inhibitory profiles against the drug resistant form of HIV-1 RT *K103N-Y181C*.

References

- Agranoff B, Bradley R, Brady R.** The enzymatic synthesis of inositol phosphatide. *J Biol Chem.* 1958; 233: 1077–1083
- Altan-Bonnet N Balla T.** Phosphatidylinositol 4-kinases: hostages harnessed to build panviral replication platforms. *Trends in Biochemical Sciences*, 2012; 37:293-302.
- Amacker M and Hübscher U.** Chimeric HIV-1 and feline immunodeficiency virus reverse transcriptases: critical role of the p51 subunit in the structural integrity of heterodimeric lentiviral DNA polymerases. *J. Mol. Biol.* 1998; 278, 757–765
- Anand N, Murthy S, Amann G, Wernick M, Porter L, Cukier I, Collins C, Gray J, Diebold J, Demetrick D, Lee J.** Protein elongation factor EEF1A2 is a putative oncogene in ovarian cancer. *Nat Genet.* 2002; 31:301–305.
- Anderson I, Low J, Weston S, Weinberger M, Zhyvoloup A, Labokha A, Corazza G, Kitson R, Moody C, Marcello A, Fassati A.** Heat shock protein 90 controls HIV-1 reactivation from latency. *Proc Natl Acad Sci U S A.* 2014, 15:1528-1537.
- Arita M, Kojima H, Nagano T, Okabe T, Wakita T, Shimizu H.** Phosphatidylinositol 4-kinase III beta is a target of enviroxime-like compounds for antipoliiovirusactivity. *J Virol.* 2011; 85:2364-2372.
- Arrildt K, Joseph S, Swanstrom R.** The HIV-1 Env protein: A coat of many colors. *Curr HIV/AIDS Rep.* 2012; 9:52-63.
- Atashrazm F and Dzamko N.** LRRK2 inhibitors and their potential in the treatment of Parkinson's disease. *Current Perspectives.* 2016; 177–189
- Audhya A, Foti M, Emr S.** Distinct roles for the yeast phosphatidylinositol 4-kinases, stt4p and pik1p, in secretion, cell growth, and organelle membrane dynamics. *Mol Biol Cell.* 2000; 11: 2673–2689,
- Babst M, Katzmann D, Snyder W, Wendland B, Emr S.** Endosome-associated complex, ESCRT-II, recruits transport machinery for protein sorting at the multivesicular body. *Dev Cell.* 2002; 3: 283–289.
- Bairstow S, Ling K, Su X, Firestone A, Carbonara C, Anderson R.** Type Igamma661 phosphatidylinositol phosphate kinase directly interacts with AP2 and regulates endocytosis. *J Biol Chem.* 2006; 281: 20632–20642.
- Baldanti F, Paolucci S, Maga G, Labo N, Hübscher U, Skoblov A, Victorova L, Spadari S, Minoli L, Gerna G.** Nevirapine-selected mutations Y1811/C of HIV-1 reverse transcriptase confer cross-resistance to stavudine. *AIDS.* 2003; 17:1568-1570.
- Balla A and Balla T.** Phosphatidylinositol 4-kinases: old enzymes with emerging functions. *Trends Cell Biol.* 2006; 16:351-361.
- Balla T, Downing G, Jaffe H, Kim S, Zolyomi A, Catt K.** Isolation and molecular cloning of wortmannin-sensitive bovine type-III phosphatidylinositol 4-kinases. *J Biol Chem.* 1997; 272: 18358–18366.
- Balla, T.** Phosphoinositides: tiny lipids with giant impact on cell regulation. *Physiol Rev.* 2013; 93:1019-137.

- Barber T, Klein J, Mackay C, Hu M.** Neuroimaging in pre-motor Parkinson's disease. *Neuroimage Clin.* 2017; 15:215-227.
- Beck E, Mandalia S, Gaudreault M, Brewer C, Zowall H, Gilmore N, Klein M, Lalonde R, Piché A, Hankins C.** The cost-effectiveness of highly active antiretroviral therapy, Canada 1991-2001. *AIDS.* 2004; 18:2411-2418.
- Benjamins J and Agranoff B.** Distribution and properties of CDP-diacylglycerol: inositol transferase from brain. *J Neurochem.* 1969, 16: 513–527.
- Berger P, Berger I, Schaffitzel C, Tersar K, Volkmer B, Suter U.** Multi-level regulation of myotubularin-related protein-2 phosphatase activity by myotubularin-related protein-13/set-binding factor-2. *Hum Mol Genet,* 2006; 15: 569–579.
- Bielas S, Silhavy J, Brancati F, Kisseleva M, Al-Gazali L, Sztriha L, Bayoumi R, Zaki M, Abdel-Aleem A, Rosti R, Kayserili H, Swistun D, Scott L, Bertini E, Boltshauser E, *et al.*** Mutations in INPP5E, encoding inositol polyphosphate-5-phosphatase E, link phosphatidyl inositol signaling to the ciliopathies. *Nat Genet.* 2009; 41: 1032–1036
- Blandini F, Porter RH, Greenamyre J .** Glutamate and Parkinson's disease. *Mol Neurobiol.* 1996; 12:73-94
- Blumenthal R, Durell S, Viard M.** HIV entry and envelope glycoprotein-mediated fusion. *J Biol Chem.* 2012; 287:40841-9.
- Bohnacker T, Marone R, Collmann E, Calvez R, Hirsch E, Wymann M.** PI3Kgamma adapter subunits define coupling to degranulation and cell motility by distinct PtdIns(3,4,5)P3 pools. *Sci Signal.* 2009; 2:ra27.
- Bonini NM and Giasson B.** Snaring the function of alpha-synuclein. *Cell.* 2005; 123:359-361.
- Bottomley MJ, Salim K, Panayotou G.** Phospholipid-binding protein domains. *Biochim Biophys Acta.* 1998; 1436:165-183.
- Boura E and Nencka R.** Phosphatidylinositol 4-Kinases: Function, Structure, and Inhibition. *Exp. Cell Res.* 2015; 337: 136–145
- Bourne Y, Dannenberg J, Pollmann V, Marchot P, Pongs O.** Immunocytochemical localization and crystal structure of human frequenin (neuronal calcium sensor 1). *J. Biol. Chem.* 2001 276: 11949-11955.
- Brodsky MA, Park B, Nutt J.** Effects of a dopamine agonist on the pharmacodynamics of levodopa in Parkinson disease. *Arch Neurol.* 2010; 67:27-32.
- Brown JR and Auger KR.** Phylogenomics of phosphoinositide lipid kinases: perspectives on the evolution of second messenger signaling and drug Discovery, *BMC Evol Biol.* 2011; 11: 4.
- Bui VC and Nguyen TH.** The role of CD4 on mechanical properties of live cell membrane. *J Biomed Mater Res A.* 2016; 104:239-424.
- Burke JE, Inglis AJ, Perisic O, Masson GR, McLaughlin SH, Rutaganira F, Shokat KM, Williams RL.** Structures of PI4KIII β complexes show simultaneous recruitment of Rab11 and its effectors. *Science.* 2014, 344: 1035–1038.
- Campiani G, Ramunno A, Maga G, Nacci V, Fattorusso C, Catalanotti B, Morelli E, Novellino E .** Non-nucleoside HIV-1 reverse transcriptase (RT) inhibitors: past, present, and future perspectives. *Curr Pharm Des.* 2002;8:615-657.

- Cancio R, Silvestri R, Ragno R, Artico M, De Martino G, La Regina G, Crespan E, Zanolli S, Hübscher U, Spadari S, Maga G**. High potency of indolyl aryl sulfone nonnucleoside inhibitors towards drug-resistant human immunodeficiency virus type 1 reverse transcriptase mutants is due to selective targeting of different mechanistic forms of the enzyme. *Antimicrob Agents Chemother*. 2005; 49:4546-4554.
- Carpenter CL, Duckworth BC, Auger KR, Cohen B, Schaffhausen BS, Cantley LC**. Purification and Characterization of Phosphoinositide 3-Kinase from Rat Liver *J Biol Chem*. 1990; 265:19704-19711
- Carpten JD, Faber AL, Horn C, Donoho GP, Briggs SL, Robbins CM, Hostetter G, Boguslawski S, Moses TY, Savage S, Uhlik M, Lin A, Du J, Qian YW, Zeckner DJ, et al**. A transforming mutation in the pleckstrin homology domain of AKT1 in cancer. *Nature*. 2007; 448: 439-444.
- Chan D and Kim P**. HIV Entry and Its Inhibition. *Cell*, 1998. 93, 681–684,
- Chan D, Fass D, Berger JM, Kim P**. Core Structure of gp41 from the HIV Envelope Glycoprotein. *Cell*. 1997;89:263-273.
- Chen CY, Weng YH, Chien KY, Lin KJ, Yeh TH, Cheng YP, Lu CS, Wang HL**. (*G2019S*) LRRK2 activates MKK4-JNK pathway and causes degeneration of SN dopaminergic neurons in a transgenic mouse model of PD. *Cell Death Differ*. 2012; 10:1623-1633
- Cheng JQ, Ruggeri B, Klein WM, Sonoda G, Altomare DA, Watson DK, Testa JR**. Amplification of AKT2 in human pancreatic cells and inhibition of AKT2 expression and tumorigenicity by antisense RNA. *Proc Natl Acad Sci U S A* 1996; 93:3636–3641
- Cheung LW, Hennessy BT, Li J, Yu S, Myers AP, Djordjevic B, Lu Y, Stemke-Hale K, Dyer MD, Zhang F, Ju Z, Cantley LC, Scherer SE, Liang H, Lu KH, et al**. High frequency of PIK3R1 and PIK3R2 mutations in endometrial cancer elucidates a novel mechanism for regulation of PTEN protein stability. *Cancer Discov*. 2011; 1:170-185.
- Chieng LO, Madhavan K, Wang M**. Deep brain stimulation as a treatment for Parkinson's disease related camptocormia. *J Clin Neurosci*. 2015; 22:1555-61.
- Choi H, Zhang J, Deng X, Hatcher JM, Patricelli MP, Zhao Z, Alessi DR, Gray NS**. Brain penetrant LRRK2 inhibitor. *ACS Med Chem Lett*. 2012; 3:658–662
- Christ F, Thys W, De Rijck J, Gijssbers R, Albanese A, Arosio D, Emiliani S, Rain JC, Benarous R, Cereseto A, Debyser Z**: Transportin-SR2 imports HIV into the nucleus. *Curr Biol*, 2008; 18:1192-1202
- Christine C and Aminoff MJ**. Clinical differentiation of parkinsonian syndromes: prognostic and therapeutic relevance. *Am J Med*. 2004; 117:412-419.
- Chu K, Minogue S, Hsuan JJ, Waugh MG**. Differential effects of the phosphatidylinositol 4-kinases, PI4KIIalpha and PI4KIIbeta, on Akt activation and apoptosis. *Cell Death Dis*. 2010; 1:106.
- Clarimón J and Kulisevsky J**. Parkinson's disease: from genetics to clinical practice. *Curr Genomics*. 2013;14:560-567.
- Clarke JH, Wang M, Irvine RF**. Localization, regulation and function of type II phosphatidylinositol 5-phosphate 4-kinases. *Adv Enzyme Regul*. 2010; 50: 12–18,

- Clotet B.** Efavirenz: resistance and cross-resistance. *Int J Clin Pract Suppl.* 1999; 103:21-25.
- Clumeck N and de Wit S.** Update on highly active antiretroviral therapy: progress and strategies. *Biomed Pharmacother.* 2000; 54:7-12.
- Coffin JM, Hughes SH, Varmus HE** (editors). *Retroviruses.* Cold Spring Harbor (NY): Cold Spring Harbor Laboratory Press; 1997.
- Cohen MS, Hellmann N, Levy J, de Cock K, Lange J.** The spread, treatment, and prevention of HIV-1: evolution of a global pandemic". *The Journal of Clinical Investigation.* 2008; 118:1244–1254.
- Cookson MR.** The role of leucine-rich repeat kinase 2 (LRRK2) in Parkinson's disease. *Nat Rev Neurosci.* 2010; 11:791-797.
- Coppolino MG, Dierckman R, Loijens J, Collins RF, Pouladi M, Jongstra-Bilen J, Schreiber AD, Trimble WS, Anderson R, Grinstein S.** Inhibition of phosphatidylinositol-4-phosphate 5-kinase Ialpha impairs localized actin remodeling and suppresses phagocytosis. *J Biol Chem.* 2002; 277: 43849–43857.
- Cuervo AM, Stefanis L, Fredenburg R, Lansbury PT, Sulzer D.** Impaired degradation of mutant alpha-synuclein by chaperone-mediated autophagy. *Science.* 2004; 305:1292-1295.
- Curtis C, Shah SP, Chin SF, Turashvili G, Rueda OM, Dunning MJ, Speed D, Lynch AG, Samarajiwa S, Yuan Y, Gräf S, Ha G, Haffari G, Bashashati A, Russell R, et al.** The genomic and transcriptomic architecture of 2,000 breast tumours reveals novel subgroups. *Nature* 2012; 486:346–352
- Czech M.** PIP2 and PIP3: complex roles at the cell surface. *Cell.* 2000; 100:603–606
- Dahabieh MS, Battivelli E, Verdin E.** Understanding HIV latency: the road to an HIV cure. *Annu Rev Med.* 2015; 66:407-421.
- Das K and Arnold E.** HIV-1 Reverse Transcriptase and Antiviral Drug Resistance. *Curr Opin Virol.* 2013; 3: 111–118.
- Davis MI, Hunt JP, Herrgard S, Ciceri P, Wodicka LM, Pallares G, Hocker M, Treiber DK, Zarrinkar PP.** Comprehensive analysis of kinase inhibitor selectivity. *Nat. Biotechnol.* 2011; 29: 1046–1051.
- De Graaf P, Klapisz EE, Schulz TK, Cremers AF, Verkleij AJ, van Bergen en Henegouwen PM.** Nuclear localization of phosphatidylinositol 4-kinase beta. *J Cell Sci.* 2002; 115: 1769–1775,
- De Graaf P, Zwart WT, van Dijken RA, Deneka M, Schulz TK, Geijsen N, Coffe PJ, Gadella BM, Verkleij AJ, van der Sluijs P, van Bergen en Henegouwen PM.** Phosphatidylinositol 4-kinase beta is critical for functional association of rab11 with the Golgi complex. *Mol Biol Cell.* 2004; 15: 2038–2047
- De Lau LM and Breteler M.** Epidemiology of Parkinson's disease. *Lancet Neurol.* 2006; 5:525-535
- De Martino G, La Regina G, Ragno R, Coluccia A, Bergamini A, Ciapri C, Sinistro A, Maga G, Crespan E, Artico M, Silvestri R.** Indolyl Aryl Sulphones as HIV-1 Non-Nucleoside Reverse Transcriptase Inhibitors: Synthesis, Biological Evaluation and Binding Mode Studies of New Derivatives at Indole-2-carboxamide. *Antivir Chem Chemother.* 2006;17:59-77.

- De Stefano AL, Lew MF, Golbe LI, Mark MH, Lazzarini AM, Guttman M, Montgomery E, Waters CH, Singer C, Watts RL, Currie LJ, Wooten GF, Maher NE, Wilk JB, Sullivan KM, et al.** PARK3 influences age at onset in Parkinson disease: a genome scan in the GenePD study. *Am J Hum Genet.* 2002; 70:1089-1095.
- Demmel L, Beck M, Klose C, Schlaitz AL, Gloor Y, Hsu PP, Havlis J, Shevchenko A, Krause E, Kalaidzidis Y, Walch-Solimena C.** Nucleocytoplasmic shuttling of the Golgi phosphatidylinositol 4-kinase Pik1 is regulated by 14-3-3 proteins and coordinates Golgi function with cell growth. *Mol Biol Cell.* 2008, 19: 1046–1061.
- Deng X, Dzamko N, Prescott A, Davies P, Liu Q, Yang Q, Lee JD, Patricelli MP, Nomanbhoy TK, Alessi DR, Gray NS.** Characterization of a selective inhibitor of the Parkinson's disease kinase LRRK2. *Nat Chem Biol.* 2011; 7:203–205
- Detels R, Tarwater P, Phair JP, Margolick J, Riddler SA, Muñoz A .** Effectiveness of potent antiretroviral therapies on the incidence of opportunistic infections before and after AIDS diagnosis; Multicenter AIDS Cohort Study. *AIDS.* 2001; 15:347-355
- Deuschl G, Schade-Brittinger C, Krack P, Volkmann J, Schäfer H, Bötzel K, Daniels C, Deutschländer A, Dillmann U, Eisner W, Gruber D, Hamel W, Herzog J, Hilker R, Klebe S, et al.** A randomized trial of deep-brain stimulation for Parkinson's disease. German Parkinson Study Group, Neurostimulation Section. *N Engl J Med.* 2006; 355:896-908.
- Dézi L and Vécsei L .** Safinamide for the treatment of Parkinson's disease. *Expert Opin Investig Drugs.* 2014; 23:729-742.
- Dominguez V, Raimondi C, Somanath S, Bugliani M, Loder MK, Edling CE, Divecha N, da Silva-Xavier G, Marselli L, Persaud SJ, Turner MD, Rutter GA, Marchetti P, Falasca M, Maffucci T.** Class II phosphoinositide 3-kinase regulates exocytosis of insulin granules in pancreatic beta cells. *J Biol Chem,* 2011; 286: 4216–4225
- Doms RW and Peiper SC:** Unwelcomed guests with master keys: how HIV uses chemokine receptors for cellular entry. *Virology.* 1997; 235:179-190
- Dornan GL, McPhail JA, Burke JE.** Type III phosphatidylinositol 4 kinases: structure, function, regulation, signalling and involvement in disease. *Biochem Soc Trans.* 2016; 44:260-266.
- Dorobantu C, Van der Schaar H, Ford L, Strating J, Ulferts R, Fang Y, Belov G and van Kuppeveld F.** Recruitment of PI4KIII β to Cocksackievirus B3 replication organelles is independent of ACBD3, GBF1, and Arf1. *J. Virol.* 2014; 88, 2725–2736
- Du TT, Wang L, Duan CL, Lu LL, Zhang JL, Gao G, Qiu XB, Wang XM, Yang H.** GBA deficiency promotes SNCA/ α -synuclein accumulation through autophagic inhibition by inactivated PPP2A. *Autophagy.* 2015; 11:1803-1820.
- Elshoff JP, Cawello W, Andreas JO, Mathy FX, Braun M.** An update on pharmacological, pharmacokinetic properties and drug-drug interactions of rotigotine transdermal system in Parkinson's disease and restless legs syndrome. *Drugs.* 2015 ;75:487-501.

- Etmnan M, Gill S, Samii A.** Comparison of the risk of adverse events with pramipexole and ropinirole in patients with Parkinson's disease: a meta-analysis. *Drug Saf.* 2003; 26:439-444
- Famiglini V, La Regina G, Coluccia A, Masci D, Brancale A, Badia R, Riveira-Muñoz E, Esté JA, Crespan E, Brambilla A, Maga G, Catalano M, Limatola C, Formica FR, Cirilli R, Novellino E, Silvestri R.** Chiral Indolylarylsulfone Non-Nucleoside Reverse Transcriptase Inhibitors as New Potent and Broad Spectrum Anti-HIV-1 Agents. *J Med Chem.* 2017; 60:6528-6547.
- Fang JY and Tolleson C.** The role of deep brain stimulation in Parkinson's disease: an overview and update on new developments. *Neuropsychiatr Dis Treat.* 2017; 13:723-732.
- Fassati A and Goff SP:** Characterization of intracellular reverse transcription complexes of human immunodeficiency virus type 1. *J Virol.* 2001; 75:3626-3635.
- Fearnley JM and Lees A.** Ageing and Parkinson's disease: substantia nigra regional selectivity. *Brain.* 1991; 114: 2283–2301
- Fell M, Mirescu C, Basu K, Cheewatrakoolpong B, DeMong DE, Ellis JM, Hyde LA, Lin Y, Markgraf CG, Mei H, Miller M, Poulet FM, Scott JD, Smith MD, Yin Z, et al.** MLI-2, a potent, selective and centrally active compound for exploring the therapeutic potential and safety of LRRK2 kinase inhibition. *J Pharmacol Exp Ther.* 2015; 355:397-409.
- Field SJ, Madson N, Kerr ML, Galbraith KA, Kennedy CE, Tahiliani M, Wilkins A, Cantley LC.** PtdIns(4,5)P₂ functions at the cleavage furrow during cytokinesis. *Curr Biol.* 2005; 15: 1407–1412,
- Fluckiger AC, Li Z, Kato RM, Wahl MI, Ochs RM, Longnecker R, Kinet JP, Witte ON, Scharenberg AM, Rawlings DJ.** Btk/Tec kinases regulate sustained increases in intracellular Ca²⁺ following B-cell receptor activation. *EMBO J.* 1998; 17: 1973–1985,
- Ford-Siltz LA, Viktorova EG, Zhang B, Kouivskaia D, Dragunsky E, Chumakov K, Isaacs L, Belov GA.** New small-molecule inhibitors effectively blocking picornavirus replication. *J. Virol.* 2014; 88: 11091–11107.
- Foukas LC, Claret M, Pearce W, Okkenhaug K, Meek S, Peskett E, Sancho S, Smith AJ, Withers DJ, Vanhaesebroeck B.** Critical role for the p110alpha phosphoinositide-3-OH kinase in growth and metabolic regulation. *Nature.* 2006; 441: 366–370
- Franke TF, Kaplan DR, Cantley LC, Toker A.** Direct regulation of the Akt proto-oncogene product by phosphatidylinositol-3,4-bisphosphate. *Science.* 1997; 275:665–668.
- Frankel AD and Young J.** HIV-1: fifteen proteins and an RNA. *Annu Rev Biochem.* 1998; 67:1-25.
- Franzini M, Ye X, Adler M, Aubele D, Garofalo A, Gauby S, Goldbach E, Probst G, Quinn K, Santiago P, Sham H, Tam D, Truong A, Ren Z.** Triazolopyridazine LRRK2 kinase inhibitors. *Bioorg Med Chem Lett.* 2013; 23:1967-1973.

- Gaidarov I, Smith ME, Domin J, Keen JH.** The class II phosphoinositide 3-kinase C2alpha is activated by clathrin and regulates clathrin-mediated membrane trafficking. *Mol Cell.* 2001; 7: 443–449
- Gallo RC.** The path to the discoveries of human retroviruses. *J Hum Virol.* 2000; 3:1-5
- Gallo SA, Finnegan CM, Viard M, Raviv Y, Dimitrov A, Rawat SS, Puri A, Durell S, Blumenthal R.** The HIV Env-mediated fusion reaction. *Biochimica et Biophysica Acta.* 2003; 1614:36-50.
- Garbelli A, Riva V, Crespan E, Maga G.** How to win the HIV-1 drug resistance hurdle race: running faster or jumping higher?. *Biochem J.* 2017; 474:1559-1577.
- Garcia-Bustos JF, Marini F, Stevenson I, Frei C, Hall MN.** PIK1, an essential phosphatidylinositol 4-kinase associated with the yeast nucleus. *EMBO J.* 1994; 13: 2352–2361,
- Gardet A, Benita Y, Li C, Sands BE, Ballester I, Stevens C, Korzenik JR, Rioux JD, Daly MJ, Xavier RJ, Podolsky DK.** LRRK2 is involved in the IFN-gamma response and host response to pathogens. *J Immunol.* 2010; 185, 5577–5585
- Garg H and Joshi A.** Host and Viral Factors in HIV-Mediated Bystander Apoptosis. *Viruses. J Immunol.* 2010; 185:5577-5585.
- Garofalo AW, Adler M, Aubele DL, Bowers S, Franzini M, Goldbach E, Lorentzen C, Neitz RJ, Probst GD, Quinn KP, Santiago P, Sham HL, Tam D, Truong AP, Ye XM, Ren Z.** Novel cinnoline-based inhibitors of LRRK2 kinase activity *Bioorg. Med. Chem. Lett.*, 2013, 23: 71–74.
- Gartner S, Markovits P, Markovitz DM, Kaplan MH, Gallo RC, Popovic M:** The role of mononuclear phagocytes in HTLV-III/LAV infection. *Science* 1986; 233:215-219.
- Gatto EM, Parisi V, Converso DP, Poderoso JJ, Carreras MC, Martí-Massó JF, Paisán-Ruiz C.** The LRRK2 G2019S mutation in a series of Argentinean patients with Parkinson's disease: clinical and demographic characteristics. *Neurosci Lett.* 2013; 537:1-5
- GBD 2015 Disease and Injury Incidence and Prevalence Collaborators.** Disease and Injury Incidence and Prevalence Collaborators. Global, regional, and national incidence, prevalence, and years lived with disability for 310 diseases and injuries, 1990–2015: a systematic analysis for the Global Burden of Disease Study 2015. *Lancet.* 2016; 388: 1545–1602.
- GBD 2015 Mortality and Causes of Death Collaborators.** Mortality and Causes of Death Collaborators Global, regional, and national life expectancy, all-cause mortality, and cause-specific mortality for 249 causes of death, 1980–2015: a systematic analysis for the Global Burden of Disease Study 2015. *Lancet.* 2016; 388:1459-1544.
- Gehrmann T and Heilmayer LG.** Phosphatidylinositol 4-kinases. *Eur J Biochem.* 1998; 253: 357–370.
- Gerlach M, Maetzler W, Broich K, Hampel H, Rems L, Reum T, Riederer P, Stöfler A, Streffer J, Berg D.** Biomarker candidates of neurodegeneration in Parkinson's disease for the evaluation of disease-modifying therapeutics. *J Neural Transm.* 2012; 119:39-52.

- Gill VS, Lima VD, Zhang W, Wynhoven B, Yip B, Hogg RS, Montaner JS, Harrigan PR.** Improved virological outcomes in British Columbia concomitant with decreasing incidence of HIV type 1 drug resistance detection. *Clin Infect Dis.* 2010; 50:98-105.
- Göring S, Taymans JM, Baekelandt V, Schmidt B.** Indolinone based LRRK2 kinase inhibitors with a key hydrogen bond. *Bioorg Med Chem Lett.* 2014; 19:4630-4637
- Greene WC and Peterlin BM:** Charting HIV's re- markable voyage through the cell: Basic science as a passport to future therapy. *Nat Med.* 2002, 8:673-680.
- Gulick RM, Mellors JW, Havlir D, Eron JJ, Gonzalez C, McMahon D, Richman DD, Valentine FT, Jonas L, Meibohm A, Emini EA, Chodakewitz JA.** Treatment with indinavir, zidovudine, and lamivudine in adults with human immunodeficiency virus infection and prior antiretroviral therapy. *N Engl J Med.* 1997; 337:734-739.
- Hakimi M, Selvanantham T, Swinton E, Padmore RF, Tong Y, Kabbach G, Venderova K, Girardin SE, Bulman DE, Scherzer CR, LaVoie MJ, Gris D, Park DS, Angel JB, Shen J, *et al.*** Parkinson's disease-linked LRRK2 is expressed in circulating and tissue immune cells and upregulated following recognition of microbial structures. *J Neural Transm.* 2011; 118:795-808.
- Hammer SM, Squires KE, Hughes MD, Grimes JM, Demeter LM, Currier JS, Eron JJ Jr, Feinberg JE, Balfour HH Jr, Deyton LR, Chodakewitz JA, Fischl MA.** A controlled trial of two nucleoside analogues plus indinavir in persons with human immunodeficiency virus infection and CD4 cell counts of 200 per cubic millimeter or less. AIDS Clinical Trials Group 320 Study Team. *N Engl J Med.* 1997 11; 337:725-733.
- Hammond GR, Fischer MJ, Anderson KE, Holdich J, Koteci A, Balla T, Irvine RF.** PI4P and PI(4,5)P2 are essential but independent lipid determinants of membrane identity. *Science.* 2012; 337:727–730.
- Hardy J, Lewis P, Revesz T, Lees A, Paisan-Ruiz C.** The genetics of Parkinson's syndromes: a critical review. *Curr Opin Genet Dev.* 2009; 3:254-365
- Hatano T, Kubo S, Sato S, Hattori N.** Pathogenesis of familial Parkinson's disease: new insights based on monogenic forms of Parkinson's disease. *J Neurochem.* 2009; 111:1075-93.
- Hausser A, Storz P, Martens S, Link G, Toker K, Pfizenmaier K.** Protein kinase D regulates vesicular transport by phosphorylating and activating phosphatidylinositol-4 kinase IIIbeta at the Golgi complex. *Nat. Cell Biol.* 2005; 7, 880–886
- Heilmeyer LM Jr, Vereb G Jr, Vereb G, Kakuk A, Szivák I.** Mammalian phosphatidylinositol 4- kinases. *IUBMB Life.* 2003; 55, 59–65
- Hilfiker S.** Neuronal calcium sensor-1: a multifunctional regulator of secretion. *Biochem Soc Trans.* 2003; 31: 828–832
- Hongge L, Kexin G, Xiaojie M, Nian X, Jinsha H.** The role of LRRK2 in the regulation of monocyte adhesion to endothelial cells. *J Mol Neurosci.* 2015; 55, 233–239
- Hsu NY, Ilnytska O, Belov G, Santiana M, Chen YH, Takvorian PM, Pau C, van der Schaar H, Kaushik-Basu N, Balla T, Cameron CE, Ehrenfeld E, van Kuppeveld FJ, Altan-Bonnet N.** Viral reorganization of the secretory pathway generates distinct organelles for RNA replication. *Cell.* 2010; 141:799-811.

- Huang P, Farquhar D, Plunkett W.** Selective action of 3'-azido-3'-deoxythymidine 5'-triphosphate on viral reverse transcriptases and human DNA polymerases. *J Biol Chem.* 1990; 265:11914-11918.
- Itakura E, Kishi C, Inoue K, Mizushima N.** Beclin 1 forms two distinct phosphatidylinositol 3-kinase complexes with mammalian Atg14 and UVRAG. *Mol Biol Cell.* 2008; 19: 5360–5372
- Jabri B, and Barreiro, LB.** Don't move: LRRK2 arrests NFAT in the cytoplasm. *Nat Immunol.* 2011; 12, 1029–1030
- Jacks T.** Translational suppression in gene expression in retroviruses and retrotransposons. *Curr. Top. Microbiol. Immunol.* 1990;157:93–124
- Jacobo-Molina A, Ding J, Nanni RG, Clark AD Jr, Lu X, Tantillo C, Williams RL, Kamer G, Ferris AL, Clark, P., Hizi A, Hughesi SH, Arnold E.** Crystal structure of human immunodeficiency virus type 1 reverse transcriptase complexed with double-stranded DNA at 3.0 Å resolution shows bent DNA. *Proc. Natl. Acad. Sci. U.S.A.* 1993; 90: 6320 – 6324
- Jaiswal B, Janakiraman V, Kljavin NM, Chaudhuri S, Stern HM, Wang W, Kan Z, Dbouk HA, Peters BA, Waring P, Dela Vega T, Kenski DM, Bowman KK, Lorenzo M, Li H, et al.** Somatic mutations in p85alpha promote tumorigenesis through class IA PI3K activation. *Cancer Cell.* 2009; 16: 463–474,
- Jayappa K, Ao Z, Yao X.** The HIV-1 passage from cytoplasm to nucleus: the process involving a complex exchange between the components of HIV-1 and cellular machinery to access nucleus and successful integration. *Int J Biochem Mol Biol* 2012; 3:70-85
- Jia S, Liu Z, Zhang S, Liu P, Zhang L, Lee SH, Zhang J, Signoretti S, Loda M, Roberts TM, Zhao JJ.** Essential roles of PI(3)K-p110beta in cell growth, metabolism and tumorigenesis. *Nature.* 2008; 454: 776–779
- Jovic M, Kean MJ, Szentpetery Z, Polevoy G, Gingras AC, Brill JA, Balla T.** Two PI 4-kinases control lysosomal delivery of the Gaucher disease enzyme, beta-glucocerebrosidase. *Mol Biol Cell.* 2012; 23: 1533–1545
- Kakkar A and Dahiya N.** Management of Parkinson's disease: Current and future pharmacotherapy. *Eur. J. Pharmacol.* 2015; 750, 74–81.
- Kim B, Yang MS, Choi D, Kim JH, Kim HS, Seol W, Choi S, Jou I, Kim EY, Joe EH.** Impaired inflammatory responses in murine Lrrk2-knockdown brain microglia. *PLoS One.* 2012; 7:e34693.
- Kim Y, Guzman-Hernandez ML, Balla T.** highly dynamic ER-derived phosphatidylinositol-synthesizing organelle supplies phosphoinositides to cellular membranes. *Dev Cell.* 2011; 21: 813–824.
- Kirrane T, Boyer S, Burke J, Guo X, Snow R, Soleymanzadeh L, Swinamer A, Zhang Y, Madwed J, Kashem M, Kugler S, O'Neill M.** Indole RSK inhibitors. Part 2: optimization of cell potency and kinase selectivity. *Bioorg Med Chem Lett.* 2012; 22:738-42.
- Kohlstaedt L, Wang J, Friedman JM, Rice PA, Steitz TA.** Crystal structure at 3.5 Å resolution of HIV-1 reverse transcriptase complexed with an inhibitor. *Science.* 1992; 256: 1783–1790.

- Kramer T, Lo Monte F, Göring S, Okala GM, Schmidt B.** Small molecule kinase inhibitors for LRRK2 and their application to Parkinson's disease models. *ACS Chem Neurosci.* 2012; 3:151-160.
- Krauss M, Kinuta M, Wenk MR, De Camilli P, Takei K, Haucke V.** ARF6 stimulates clathrin/AP-2 recruitment to synaptic membranes by activating phosphatidylinositol phosphate kinase type Iγ. *J Cell Biol.* 2003; 162: 113–124
- Kurtis M, Rajah T, Delgado LF, Dafsari H.** The effect of deep brain stimulation on the non-motor symptoms of Parkinson's disease: a critical review of the current evidence. *NPJ Parkinsons Dis.* 2017; 3:16024.
- La Marche M, Borawski J, Bose A, Capacci-Daniel C, Colvin R, Dennehy M, Ding J, Dobler M, Drumm J, Gaither L, Gao J, Jiang X, Lin K, McKeever U, Puyang X, et al.** Anti-Hepatitis C Virus Activity and Toxicity of Type III Phosphatidylinositol-4-Kinase Beta Inhibitors. *Antimicrob. Agents Chemother.* 2012; 56: 5149-5156
- Lang C, Ray S, Liu M, Singh A, Cuny G.** Discovery of LRRK2 inhibitors using sequential in silico joint pharmacophore space (JPS) and ensemble docking. *Bioorg Med Chem Lett.* 2015; 25:2713-2719.
- Langron E, Simone MI, Delalande CM, Reymond JL, Selwood DL, Vergani P.** Improved fluorescence assays to measure the defects associated with F508del-CFTR allow identification of new active compounds. *Br. J. Pharmacol.* 2017; 174:525-539.
- Le Grice S, Naas T, Wohlgensinger B, Schatz O.** Subunit-selective mutagenesis indicates minimal polymerase activity in heterodimer-associated p51 HIV-1 reverse transcriptase. *EMBO J.* 1991; 10:3905–3911
- Lees A.** The on-off phenomenon. *J Neurol Neurosurg Psychiatry.* 1989; Suppl:29-37.
- Leigh R and Proud D.** Virus-Induced Modulation of Lower Airway Diseases: Pathogenesis and Pharmacologic Approaches to Treatment. *Pharmacol. Ther.* 2015; 148: 185–198.
- Leong W and Chow VT.** Transcriptomic and proteomic analyses of rhabdomyosarcoma cells reveal differential cellular gene expression in response to Enterovirus 71 infection. *Cell. Microbiol.* 2006; 8:565–580
- Levy J.** Pathogenesis of human immunodeficiency virus infection. *Microbiol.* 1993; 57:183–289
- Lewis P, Emerman M:** Passage through mitosis is required for oncoretroviruses but not for the human immunodeficiency virus. *J Virol.* 1994; 68:510-516
- Lewis P, Hensel M, Emerman M.** Human immunodeficiency virus infection of cells arrested in the cell cycle. *EMBO J.* 1992; 11:3053-3058.
- Liu Z, Galembo RA Jr, Fraser KB, Moehle MS, Sen S, Volpicelli-Daley LA, DeLucas LJ, Ross LJ, Valiyaveetil J, Moukha-Chafiq O, Pathak AK, Ananthan S, Kezar H, White EL, Gupta V, et al.** Unique functional and structural properties of the LRRK2 protein ATP-binding pocket. *J. Biol. Chem.*, 2014, 289: 32937–32951.
- Liu Z, Lee J, Krummey S, Lu W, Cai H, Lenardo MJ.** The kinase LRRK2 is a regulator of the transcription factor NFAT that modulates the severity of inflammatory bowel disease. *Nat Immunol.* 2011; 12:1063–1070

- Loutfy M and Walmsley S** . Salvage antiretroviral therapy in HIV infection. *Expert Opin Pharmacother.* 2002; 3:81-90..
- Luerman G, Nguyen C, Samaroo H, Loos P, Xi H, Hurtado-Lorenzo A, Needle E, Stephen G, Galatsis P, Dunlop J, Geoghegan KF, Hirst WD.** Phosphoproteomic evaluation of pharmacological inhibition of leucine-rich repeat kinase 2 reveals significant off-target effects of LRRK2-IN-1. *J Neurochem.* 2014; 128:561–576
- Lynch T, Bell DW, Sordella R, Gurubhagavatula S, Okimoto RA, Brannigan BW, Harris PL, Haserlat SM, Supko JG, Haluska FG, Louis DN, Christiani DC, Settleman J, Haber DA.** Activating mutations in the epidermal growth factor receptor underlying responsiveness of non-small-cell lung cancer to gefitinib. *N Engl J Med.* 2004; 350:2129–2139.
- MacLeod A, Mitchell DR, Palmer NJ, Van de Poël H, Conrath K, Andrews M, Leysen P, Neyts J.** Identification of a series of compounds with potent antiviral activity for the treatment of enterovirus infections. *ACS Med. Chem. Lett.* 2013; 4: 585–589
- Maddon P, Littman DR, Godfrey M, Maddon DE, Chess L, Axel R.** The isolation and nucleotide sequence of a cDNA encoding the T cell surface protein T4: A new member of the immunoglobulin gene family. *Cell.* 1985; 42:93–104.
- Maekawa T, Kubo M, Yokoyama I, Ohta E, Obata F.** Age-dependent and cell-population-restricted LRRK2 expression in normal mouse spleen. *Biochem Biophys Res Commun.* 2010; 392:431–435.
- Maga G, Amacker M, Ruel N, Hübscher U, Spadari S** . Resistance to nevirapine of HIV-1 reverse transcriptase mutants: loss of stabilizing interactions and thermodynamic or steric barriers are induced by different single amino acid substitutions. *J Mol Biol.* 1997; 274:738-47.
- Mandel S, Morelli M, Halperin I, Korczyn AD.** Biomarkers for prediction and targeted prevention of Alzheimer's and Parkinson's diseases: evaluation of drug clinical efficacy. *EPMA J.* 2010; 1:273-292.
- Manning G, Whyte DB, Martinez R, Hunter T, Sudarsanam S.** The protein kinase complement of the human genome. *Science.* 2002; 298:1912-1934
- Massano J and Bhatia K.** *Clinical Approach to Parkinson's Disease: Features, Diagnosis, and Principles of Management.* Cold Spring Harb Perspect Med. 2012; 2: a008870.
- Massarotti A and Coluccia A.** An in-silico approach aimed to clarify the role of Y181C and K103N HIV-1 reverse transcriptase mutations versus Indole Aryl Sulphones. *J Mol Graph Model.* 2016; 63:49-56.
- Mata I, Wedemeyer WJ, Farrer MJ, Taylor JP, Gallo KA.** LRRK2 in Parkinson's disease: protein domains and functional insights. *Trends Neurosci.* 2006 May;29:286-293.
- McDonald D, Vodicka MA, Lucero G, Svitkina TM, Borisy GG, Emerman M, Hope TJ:** Visualization of the intracellular behavior of HIV in living cells. *J Cell Biol* 2002, 159:441-452
- Miller M, Farnet CM, Bushman FD.** Human immunodeficiency virus type 1 preintegration complexes: studies of organization and composition. *J Virol.* 1997; 71:5382-5390.

- Moravcevic K, Oxley CL, and Lemmon MA.** Conditional peripheral membrane proteins: facing up to limited specificity, *Structure*. 2012; 20:15-27.
- Morrow A, Alipour M, Bridges D, Yao Z, Saltiel A, Lee J.** The Lipid Kinase PI4KIII β is highly expressed in breast tumors and activates Akt in cooperation with Rab11a. *Research Mol Cancer Res*. 2014;. 12:1492-1508.
- Nakagawa T, Goto K, Kondo H.** Cloning, expression, and localization of 230-kDa phosphatidylinositol 4-kinase. *J. Biol. Chem*. 1996; 271: 12088–12094
- Niggli V.** Structural properties of lipid-binding sites in cytoskeletal proteins. *Trends Biochem Sci*. 2001; 26:604-611.
- Nutt J.** Motor fluctuations and dyskinesia in Parkinson's disease. *Parkinsonism Relat Disord*. 2001; 8:101-118.
- Oda K, Okada J, Timmerman L, Rodriguez-Viciana P, Stokoe D, Shoji K, Taketani Y, Kuramoto H, Knight ZA, Shokat KM, McCormick F.** PIK3CA cooperates with other phosphatidylinositol 3' kinase pathway mutations to effect oncogenic transformation. *Cancer Res*. 2008; 68:8127-8136.
- Padron D, Wang YJ, Yamamoto M, Yin H, Roth MG.** Phosphatidylinositol phosphate 5-kinase I β recruits AP-2 to the plasma membrane and regulates rates of constitutive endocytosis. *J Cell Biol*. 2003; 162: 693–701,
- Patil A, Sood SK, Goyal V, Kochhar K.** Cortical potentials prior to movement in Parkinson's disease. *J Clin Diagn Res*. 2017; 11:13-16.
- Pedemonte N, Lukacs GL, Du K, Caci E, Zegarra-Moran O, Galiotta LJ, Verkman AS.** Small-molecule correctors of defective deltaF508-CFTR cellular processing identified by high-throughput screening. *J. Clin. Invest*. 2005a, 115: 2564–2571.
- Pedemonte N, Sonawane ND, Taddei A, Hu J, Zegarra-Moran O, Suen YF, Robins LI, Dicus CW, Willenbring D, Nantz MH, Kurth MJ, Galiotta LJ, Verkman AS.** Phenylglycine and sulfonamide correctors of defective delta F508 and G551D cystic fibrosis transmembrane conductance regulator chloride-channel gating. *Mol Pharmacol*. 2005b; 67:1797-1807.
- Pinke D and Lee J.** The lipid kinase PI4KIII β and the eEF1A2 oncogene co-operate to disrupt three-dimensional in vitro acinar morphogenesis. *Exp Cell Res*. 2011; 317:2503–2511
- Prekeris R, Klumperman J, Scheller RH.** A Rab11/Rip11 protein complex regulates apical membrane trafficking via recycling endosomes. *Molec. Cell*. 2000; 6: 1437-1448
- Ren J, Esnouf R, Garman E, Somers D, Ross C, Kirby I, Keeling J, Darby G, Jones Y, Stuart D.** High resolution structures of HIV-1 RT from four RT-inhibitor complexes. *Nat. Struct. Biol*. 1995, 2: 293–302.
- Roe T, Reynolds TC, Yu G, Brown PO.** Integration of murine leukemia virus DNA depends on mitosis. *EMBO J*. 1993; 12:2099-2108.
- Rosenberg Z and Fauci A.** The immunopathogenesis of HIV infection. *Adv. Immunol*. 1989; 47:377–431
- Rozelle A, Machesky LM, Yamamoto M, Driessens MH, Insall RH, Roth MG, Luby-Phelps K, Marriott G, Hall A, Yin HL.** Phosphatidylinositol 4,5-bisphosphate

- induces actin-based movement of raft-enriched vesicles through WASP-ArP2/3. *Curr Biol*. 2000; 10: 311–320
- Samii A, Nutt J, Ransom B.** Parkinson's disease. *Lancet*. 2004; 363:1783-1793.
- Sasaki T, Irie-Sasaki J, Horie Y, Bachmaier K, Fata JE, Li M, Suzuki A, Bouchard D, Ho A, Redston M, Gallinger S, Khokha R, Mak TW, Hawkins PT, Stephens L, et al.** Colorectal carcinomas in mice lacking the catalytic subunit of PI(3)Kgamma. *Nature*. 2000a; 406: 897–902
- Sasaki T, Irie-Sasaki J, Jones RG, Oliviera-dos-Santos AJ, Stanford WL, Bolon B, Wakeham A, Itie A, Bouchard D, Kozieradzki I, Joza N, Mak TW, Ohashi PS, Suzuki A, Penninger JM.** Function of PI3Kgamma in thymocyte development, T cell activation, and neutrophil migration. *Science*. 2000b; 287: 1040–1046,
- Segura-Aguilar J.** Aminochrome as preclinical model for Parkinson's disease. *Oncotarget*. 2017; 8:45036-45037.
- Sharp P and Hahn B.** Origins of HIV and the AIDS pandemic. *Cold Spring Harb Perspect Med*. 2011; 1:a006841.
- Shen J.** Protein kinases linked to the pathogenesis of Parkinson's disease. *Neuron*. 2004 Nov 18;44:575-577
- Sidiropoulos C, Bowyer SM, Zillgitt A, LeWitt PA, Bagher-Ebadian H, Davoodi-Bojd E, Schwalb JM, Rammo R, Air E, Soltanian-Zadeh H .** Multimodal imaging in a patient with hemidystonia responsive to GPi deep brain stimulation. *Case Rep Neurol Med*. 2017; 2017:9653520.
- Silvestri R and Artico M.** Indolyl Aryl Sulfones (IASs): Development of highly potent NNRTIs active against *wt*-HIV-1 and clinically relevant drug resistant mutants. *Curr Pharm Des*. 2005; 11: 3779-3806.
- Silvestri R, De Martino G, La Regina G, Artico M, Massa S, Vargiu L, Mura M, Loi AG, Marceddu T, La Colla P.** Novel indolyl aryl sulfones active against HIV-1 carrying NNRTI resistance mutations: synthesis and SAR studies. *J Med Chem*. 2003; 46:2482-2493.
- Simons J, Al-Shawi R, Minogue S, Waugh MG, Wiedemann C, Evangelou S, Loesch A, Sihra TS, King R, Warner TT, Hsuan JJ.** Loss of phosphatidylinositol 4-kinase 2alpha activity causes late onset degeneration of spinal cord axons. *Proc Natl Acad Sci USA*. 2009; 106: 11535–11539
- Slamon D, Godolphin W, Jones LA, Holt JA, Wong SG, Keith DE, Levin WJ, Stuart SG, Udove J, Ullrich A.** Studies of the HER-2/neu proto-oncogene in human breast and ovarian cancer. *Science*. 1989; 244:707–712.
- Soudeyans H, Yao XI, Gao Q, Belleau B, Kraus JL, Nguyen-Ba N, Spira B, Wainberg MA.** Anti-human immunodeficiency virus Type 1 activity and in vitro toxicity of 2'-Deoxy-3'-Thiacytidine (BCH-189), a novel heterocyclic nucleoside analog. *Antimicrob Agents Chemother*. 1991; 35:1386-1390.
- Springett G, Moen RC, Anderson S, Blaese RM, Anderson WF:** Infection efficiency of T lymphocytes with amphotropic retroviral vectors is cell cycle dependent. *J Virol*. 1989, 63:3865-3869
- Strahl T, Hama H, Dewald DB, Thorner J.** Yeast phosphatidylinositol 4-kinase, Pik1, has essential roles at the Golgi and in the nucleus. *J Cell Biol*. 2005; 171: 967–979

- Sudharshan S and Biswas J.** Introduction and immunopathogenesis of acquired immune deficiency syndrome, *Indian J Ophthalmol.* 2008; 56:357-362.
- Sun Y, Turbin DA, Ling K, Thapa N, Leung S, Huntsman DG, Anderson RA.** Type I gamma phosphatidylinositol phosphate kinase modulates invasion and proliferation and its expression correlates with poor prognosis in breast cancer. *Breast Cancer Res.* 2010; 12:6.
- Sundquist W and Kräusslich H.** HIV-1 assembly, budding, and maturation. *Cold Spring Harb Perspect Med.* 2012; 2:a006924.
- Takahashi S, Kubo K, Waguri S, Yabashi A, Shin HW, Katoh Y, Nakayama K.** Rab11 regulates exocytosis of recycling vesicles at the plasma membrane. *J Cell Sci.* 2012; 125:4049-4057.
- Teterina N, Pinto Y, Weaver JD, Jensen KS, Ehrenfeld E.** Analysis of poliovirus protein 3A interactions with viral and cellular proteins in infected cells. *J Virol.* 2011; 85:4284-4296.
- Thévenet J, Pescini Gobert R, Hoof van Huijsduijnen R, Wiessner C, Sagot YJ.** Regulation of LRRK2 expression points to a functional role in human monocyte maturation. *PLoS One.* 2011;6:e21519.
- Tomlinson V, Newbery HJ, Wray NR, Jackson J, Larionov A, Miller WR, Dixon JM, Abbott CM.** Translation elongation factor eEF1A2 is a potential onco-protein that is overexpressed in two-thirds of breast tumours. *BMC Cancer.* 2005; 5:113.
- Trotter P, Wu WI, Pedretti J, Yates R, Voelker DR.** A genetic screen for aminophospholipid transport mutants identifies the phosphatidylinositol 4-kinase, Stt4p, as an essential component in phosphatidylserine metabolism. *J Biol Chem.* 1998; 273: 13189–13196
- Ujjan I, Akhund A, Saboor M, Qureshi M, Khan S.** Cytogenetic and Molecular Analyses of Philadelphia Chromosome Variants in CML (chronic myeloid leukemia) Patients from Sindh using Karyotyping and RT-PCR. *Pak J Med Sci.* 2015; 4:936-940
- Uversky V.** Looking at the recent advances in understanding α -synuclein and its aggregation through the proteoform prism. *F1000Research* 2017; 6:525.
- Vivanco I and Sawyers CL.** The phosphatidylinositol 3-kinase AKT pathway in human cancer. *Nat Rev Cancer.* 2002; 2:489–501.
- Wang J, Yan YW, Garrett TP, Liu JH, Rodgers DW, Garlick RL, Tarr GE, Husain Y, Reinherz EL, Harrison SC.** Atomic structure of a fragment of human CD4 containing two immunoglobulin-like domains. *Nature.* 1990; 348:411–418
- Wang Y, Dyer WB, Workman C, Wang B, Peng NK, Lachireddy K, Chew CB, Sullivan J, Saksena NK .** Drug resistance and viral evolution in plasma and peripheral blood cells during structured treatment interruption (STI) and non-interrupted HAART. *Curr HIV Res.* 2007; 5:235-250.
- Wessels E, Duijsings D, Lanke KH, Melchers WJ, Jackson CL, van Kuppeveld FJ.** Molecular determinants of the interaction between coxsackievirus protein 3A and guanine nucleotide exchange factor GBF1. *J. Virol.* 2007; 81:5238–5245.
- Westerlund M, Belin AC, Anvret A, Bickford P, Olson L, Galter D.** Developmental regulation of leucine-rich repeat kinase 1 and 2 expression in the brain and other

- rodent and human organs: implications for Parkinson's disease. *Neuroscience*. 2008; 152: 429–436
- Yamamoto A, DeWald DB, Boronenkov IV, Anderson RA, Emr SD, Koshland D.** Novel PI(4)P 5-kinase homologue, Fab1p, essential for normal vacuole function and morphology in yeast. *Mol Biol Cell*. 1995; 6: 525–539
- Yoo C; Yu GJ, Yang B, Robins LI, Verkman AS, Kurth MJ.** 4'-Methyl-4,5'-Bithiazole-based correctors of defective Δ F508- CFTR cellular processing. *Bioorg. Med. Chem. Lett*. 2008, 18: 2610–2614
- Yoshida S, Ohya Y, Goebel M, Nakano A, Anrakur Y.** A novel gene, STT4, encodes a phosphatidylinositol 4-kinase in the PKC1 protein kinase pathway of *Saccharomyces cerevisiae*. *J Biol Chem*. 1994; 269: 1166–1171
- Yun H, Heo HY, Kim HH, DooKim N, Seol W.** Identification of chemicals to inhibit the kinase activity of leucine-rich repeat kinase 2 (LRRK2), a Parkinson's disease-associated protein. *Bioorg Med Chem Lett*. 2011; 21:2953-2957.
- Zeitlmann L, Sirim P, Kremmer E, Kolanus W.** Cloning of ACP33 as a novel intracellular ligand of CD4. *J. Biol. Chem*. 2001; 276: 9123-9132.

List of original manuscripts



Cite this: DOI: 10.1039/c5md00462d

A multicomponent pharmacophore fragment-decoration approach to identify selective LRRK2-targeting probes†‡

Sabrina Tassini,^a Daniele Castagnolo,^{bc} Nicolò Scalacci,^{bc} Miroslava Kissova,^d Jorge I. Armijos-Rivera,^d Federica Giagnorio,^{ac} Giovanni Maga,^d Gabriele Costantino,^a Emmanuele Crespan^{§d} and Marco Radi^{§*a}

Herein we report the development of a new versatile chemical tool for the rapid identification of LRRK2-targeting probes as potential anti-Parkinson's agents. Based on the structure of recently identified inhibitors, we decided to develop a new multicomponent approach to explore the biologically relevant space around their key pharmacophore fragment. The combination of organo/metal catalysis and microwave-assisted technology, allowed us to quickly generate highly functionalized heteroaryl-hydrazone derivatives for biological investigation. Enzymatic studies on the synthesized compounds allowed the identification of promising compounds endowed with a good LRRK2 specificity index (wt/G2019S activity ratio), low affinity towards a small panel of selected kinases and a mixed-type inhibition against the pathogenic G2019S mutant. These results show how a diversity-oriented approach based on a privileged pharmacophore fragment may play a key role in the identification of novel biologically relevant chemical probes.

Received 9th October 2015,
Accepted 15th December 2015

DOI: 10.1039/c5md00462d

www.rsc.org/medchemcomm

The discovery of new first-in-class medicines to improve current treatment regimens or to treat unmet medical needs is one of the most challenging tasks for a medicinal chemist, both in academia and in big pharma. Despite the recent advancements in molecular biology and gene-to-medicine approaches, 37% of new small-molecule first-in-class drugs approved in the last 10 years came from phenotypic approaches, while only 23% were discovered by hypothesis-driven target-based approaches.^{1,2} In this scenario, repositioning the classical chemistry-based phenotypic approaches at the center of an integrated multidisciplinary drug-discovery platform could provide an important contribution to the discovery of new medicines. The recently launched Open Antimicrobial Drug Discovery initiative is an important example of how chemical diversity is currently considered as a key resource to discover new antibiotics.³ The availability of versatile chemical

approaches to rapidly produce highly functionalized molecules represents therefore an essential medicinal chemistry tool for different drug-discovery campaigns: diversity-oriented synthesis (DOS), combinatorial chemistry and biology-oriented synthesis (BIOS) are widely used to explore the biologically relevant chemical space.⁴⁻⁶ In particular, exploring the chemical space around a privileged scaffold (privileged-substructure-based diversity-oriented synthesis, pDOS) has been considered as a suitable strategy for the systematic enhancement of molecular diversity to discover new probes for chemical biology and drug discovery.⁷ In analogy with the pDOS approach and as a continuation of our interest in the development of microwave-assisted and multicomponent strategies for the synthesis of new chemical probes,⁸⁻¹² we decided to build a fast and versatile diversity-oriented synthesis around a key pharmacophore fragment. This pharmacophore fragment-decoration approach could be considered as a good compromise between a target-based and a phenotypic drug discovery approach. Specifically, we became interested in the biological versatility of the heteroaryl-hydrazone pharmacophore moiety and in its potential for the discovery of new anti-Parkinson agents.¹³ Among heteroaryl-hydrazones, 2-quinoline derivatives have been studied as antineoplastic drugs (1, 2, Fig. 1),^{14,15} while 2-pyridine derivatives displayed interesting anti-inflammatory (3, Fig. 1), anticancer (4, Fig. 1) and broad-spectrum antimicrobial activities (5, Fig. 1).¹⁶⁻¹⁸ Interestingly, a recent study identified (*E*)-2-(2-arylidenehydrazinyl)quinolone derivatives (6, Fig. 1) as selective inhibitors of leucine-rich repeat kinase 2 (LRRK2) that has been

^a P4T Group, Dipartimento di Farmacia, Università degli Studi di Parma, Viale delle Scienze, 27/A, 43124 Parma, Italy. E-mail: marco.radi@uni.pr.it

^b Institute of Pharmaceutical Science, King's College London, 150 Stamford Street, SE1 9NH London, UK

^c Northumbria University Newcastle, Department of Applied Sciences, Ellison Building, Ellison Place, NE1 8ST Newcastle upon Tyne, UK

^d Istituto di Genetica Molecolare, IGM-CNR, Via Abbiategrasso 207, 27100 Pavia, Italy

† The authors declare no competing interest.

‡ Electronic supplementary information (ESI) available: Experimental procedures and analytical data for compounds 9 and 10, *in vitro* LRRK2 inhibition assays, inhibition mechanism and kinase panel data. See DOI: 10.1039/c5md00462d

§ Co-last authors.

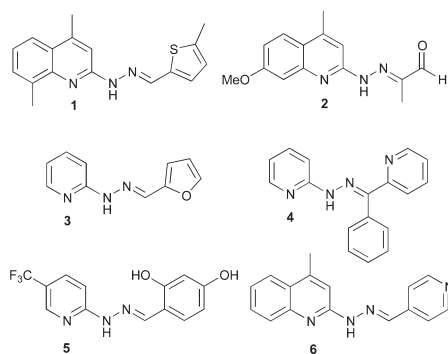
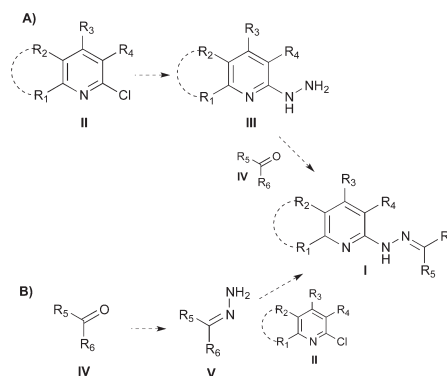


Fig. 1 Representative biologically relevant heteroaryl-hydrazones 1-6.

associated with both autosomal-dominant and late-onset sporadic Parkinson's disease (PD) cases.¹⁹ Inhibition of LRRK2 kinase activity, and in particular of the pathogenic mutant G2019S, has been proposed as an attractive therapeutic strategy for the treatment of PD.^{20,21} Despite a few LRRK2 inhibitors having been published in the last years,²²⁻³⁰ to the best of our knowledge, only a few reports have been published on the selective inhibition of the G2019S mutant over wild type LRRK2.³¹⁻³³ Considering that the physiological and pathological functions of this kinase remain poorly understood, it would be desirable to identify novel chemical probes able to selectively inhibit the pathogenic G2019S LRRK2 mutant. Herein we report the development of a microwave-assisted proline/Pd-catalysed multicomponent approach for the rapid synthesis of substituted heteroaryl-hydrazones and their biological evaluation as LRRK2 inhibitors, both WT and G2019S mutant. The classical approach for the synthesis of substituted heteroaryl-hydrazones **I** requires the conversion of heteroaryl halides **II** into hydrazino derivatives **III** by heating in an excess of hydrazine hydrate (approach A, Scheme 1).³⁴ Heteroaryl-hydrazones are finally obtained by coupling hydrazino derivatives **III** with the appropriate aldehydes or ketones **IV** in refluxing ethanol using acetic acid as catalyst.^{35,36} Alternatively, the less explored approach B (Scheme 1) requires the preliminary conversion of aldehydes or ketones **IV** into the corresponding hydrazones **V** followed by Pd-catalyzed coupling with heteroaryl halides **II** to give the desired heteroaryl-hydrazones **I**. Only a few examples on the application of the latter approach have been reported in the literature while, to the best of our knowledge, no multicomponent strategies for the synthesis of heteroaryl-hydrazones **I** have been reported so far.³⁷⁻³⁹

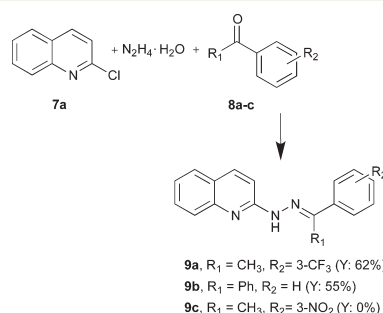
Multicomponent approaches display the advantage of atom and cost efficiency that, coupled with microwave irradiation, could permit the quick generation of compound libraries with high chemical variability for drug discovery purposes.⁴⁰ A new microwave-assisted multicomponent approach for the direct synthesis of substituted heteroaryl-hydrazones **I**



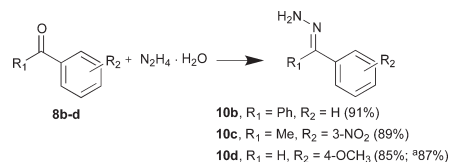
Scheme 1 Approaches for the synthesis of heteroaryl-hydrazones I.

could therefore represent a valuable tool to further explore the structure-activity relationships of quinolone-based LRRK2 inhibitors and to discover new active scaffolds.

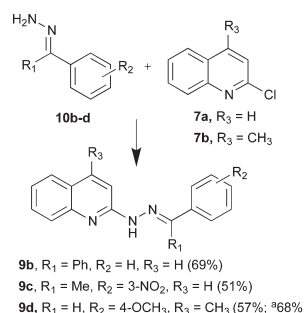
We initially focused our attention on the development of a single-step multicomponent procedure following the synthetic approach A: a mixture of 2-chloroquinoline **7a**, hydrazine monohydrate and ketones **8a-c** was irradiated in a sealed microwave tube at 120 °C (Scheme 2). Compounds **9a** and **b** were thus obtained in good yields after 15 min while compound **9c** was never obtained even under harsh reaction conditions. The same protocol also failed when we replaced the ketones **8a-c** with different aldehydes, giving a complex mixture of many side products. Given the poor versatility of the above approach, we decided to investigate the possibility of developing a microwave-assisted multicomponent strategy based on the synthetic approach B. As far as we know, the microwave-accelerated catalytic amination of heteroaryl halides with hydrazine derivatives has never been addressed before and could be exploited to quickly generate highly functionalized heteroaryl-hydrazones starting from commercially

Scheme 2 Three component synthesis of heteroaryl-hydrazones **9a-c**. Reaction conditions: EtOH, MW, 120 °C, 15 min.

available aldehydes/ketones, hydrazine and heteroaryl halides (see Scheme 5). We decided to optimize the first step of this new protocol in toluene because the following Pd-catalyzed amination of heteroaryl halides frequently requires this solvent.⁴¹ Different temperatures, reaction times and catalysts (sodium *tert*-butoxide, acetic acid and *L*-proline) were used in order to improve the conversion of aldehydes or ketones **IV** into the corresponding hydrazones **V**. After several attempts, the best reaction conditions were found to be the irradiation of ketones with hydrazine monohydrate in a sealed microwave tube at 300 W for 15 minutes in the presence of a catalytic amount of *L*-proline to give the hydrazones **10b–d** in good yields (Scheme 3). For the second step of the protocol we extensively evaluated the Pd-catalyzed coupling of aryl halides with benzophenone hydrazone reported by different research groups.^{42–44} In order to quickly obtain highly functionalized heteroaryl-hydrazones our preliminary experiments were inspired by the works published by Maes *et al.*, who developed a fast microwave-assisted Pd-catalyzed amination of aryl chlorides with aromatic and aliphatic amines.^{45,46} After different pivotal studies to choose the best catalyst system, we selected 2-dicyclohexylphosphino-2'-(*N,N*-dimethylamino)-biphenyl (DavePhos) as the ligand and Pd(OAc)₂ as the Pd(0) source. We applied the procedure proposed by Maes *et al.* to the coupling of hydrazones **10b–d** and 2-chloroquinolines **7a** and **b** using *t*-BuONa as a base in combination with a solution of 2% Pd(OAc)₂/4% DavePhos in toluene. The substituted heteroaryl-hydrazones **9b–d** were obtained by microwave heating at 150 °C for 10 minutes (Scheme 4). Finally we combined the optimized steps I and II in a single one-pot two-step protocol: this new organo/metal catalyzed strategy links the advantages of the multicomponent procedures with those of microwave-assisted reactions (Scheme 5). In the optimized protocol, a mixture of substituted aldehydes or ketones **8b–n** and hydrazine monohydrate in toluene was irradiated in the presence of a catalytic amount of *L*-proline. After that time, heteroaryl chlorides and *t*-BuONa were added to the same reaction vessel and the mixture was flushed under argon atmosphere for a few minutes before adding a toluene solution of 2% Pd(OAc)₂/4% DavePhos previously prepared. The desired heteroaryl-hydrazones **9b–n** were quickly obtained in moderate to good yields after microwave irradiation at 150–180 °C for 10–20 minutes (Table 1). To demonstrate the efficiency of

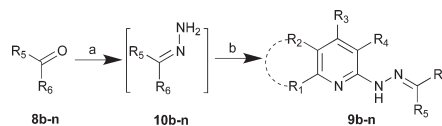


Scheme 3 First step optimization. Reaction conditions: *L*-proline, toluene, MW, 300 W, 15 min. ^aConventional heating, toluene, reflux, 90 min.



Scheme 4 Second step optimization. Reaction conditions: Pd(OAc)₂, DavePhos, *t*-BuONa, toluene, MW, 150 °C, 10 min. ^aConventional heating, toluene, 100 °C, 16 h.

our protocol, the synthesis of compound **9d** was also conducted step by step under conventional heating (CH) conditions: as reported in Schemes 3 and 4; the yield of each step is comparable with those obtained under microwave-assisted conditions but, in the latter case, compound **9d** was obtained in only 25 minutes (18 h under CH) after a single chromatographic purification. This protocol was efficiently applied to a series of cheap and commercially available building blocks, allowing us to easily decorate the aryl-hydrazone pharmacophore fragment. Different heteroaryl chlorides provided a different core scaffold to the final compounds: 2-chloroquinoline (compounds **9b**, **c**, **e**, **f**, **m**, **n**), 2-chloro-4-methylquinoline (compounds **9d**, **g**), substituted 2-chloropyridines (compounds **9h–j**) and substituted 2-chloro-5,6,7,8-tetrahydroquinoline (compounds **9k** and **l**). On the other hand, different aldehydes and ketones projected different functional groups in the surrounding space of the final compounds: substituted ketones (compounds **9b**, **c**, **e**, **f**) and benzaldehydes (compounds **9d**, **g–n**). Overall, the final compounds **9b–n** were obtained after only 25–35 min each followed by a single chromatographic purification, instead of multiple synthetic steps/purifications. In addition, aryl/heteroaryl-hydrazones can also be used as versatile key intermediates to increase their molecular complexity by easy conversion into different heterocycles, such as indoles, pyrazoles and triazolopyridines.^{37–39} We attempt this additional molecular complication on compound **9i**, since the chlorine in



Scheme 5 Optimized one-pot two-step protocol. Reaction conditions: (a) hydrazine monohydrate, *L*-proline, toluene, MW, 300 W, 15 min; (b) heteroaryl chloride, *t*-BuONa, Pd(OAc)₂, DavePhos, toluene, MW, 150–180 °C, 10–20 min.

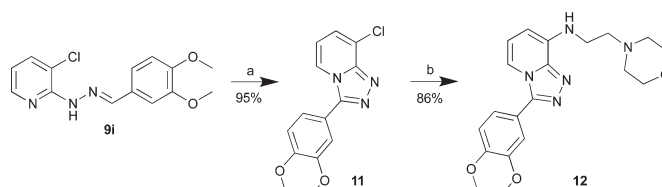
Table 1 Heteroaryl-hydrazone derivatives

Cpd							Yield ^a (%)
	R ₁	R ₂	R ₃	R ₄	R ₅	R ₆	
9b			H	H			53
9c			H	H	CH ₃		33
9d			CH ₃	H	H		39
9e			H	H	CH ₃		32
9f			H	H	CH ₃		41
9g			CH ₃	H	H		42
9h	H	H	H	H	H		45
9i	H	H	H	Cl	H		40
9j	CH ₃	H	CH ₃	CN	H		48
9k				CN	H		44
9l				CN	H		51
9m			H	H	H		38
9n			H	H	H		41

^a Isolated yield.

position C3 could be further displaced by different nucleophiles (Scheme 6). Copper-catalyzed oxidation⁴⁷ of 9i yielded the

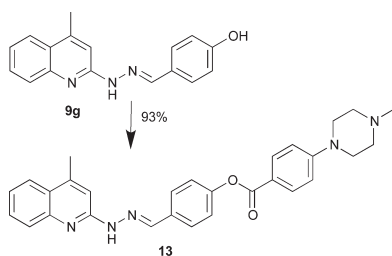
corresponding [1,2,4]triazolo[4,3-*a*]pyridine intermediate **11**, which was then submitted to a microwave-assisted Buchwald



Scheme 6 Synthesis of compound **12**. Reaction conditions: (a) CuCl_2 , DMF, 90 °C, 1 h; (b) 4-(2-aminoethyl)morpholine, *t*-OBuNa, Pd(OAc)₂, rac-BINAP, toluene, MW, 120 °C, 10 min.

amination with 4-(2-aminoethyl)morpholine to give the desired compound **12** in good overall yields. Finally, we also decided to modify one of the quinoline derivatives (**9g**) on the basis of the docking studies reported for similar compounds (**6**) on a LRRK2 homology model.¹⁹ Since the 4-pyridyl substituent of compound **6** was proposed to occupy a solvent-exposed region just outside the ATP-binding pocket, we decided to attach a polar methylpiperazine moiety, common to different kinase inhibitors, to the hydroxyl group of compound **9g**. Reacting the latter compound with 4-(4-methylpiperazin-1-yl)benzoic acid under standard coupling conditions afforded the desired derivative **13** in high yields, as described in Scheme 7.

The inhibition potency of the synthesized compounds (**9c**–**1**, **12** and **13**) towards both LRRK2 wild type (wt) and the G2019S mutated form was evaluated in cell-free assays: a preliminary screening was initially conducted to select the most promising compounds for additional biological studies (Fig. 2). Among the quinoline derivatives, the most interesting compounds were found to be those bearing a hydroxyl or methoxy substituent on the right part of the molecule (**9d**, **f**, **g**) while pyridine derivatives (**9h**–**j**) generally showed poor inhibitory potency. Despite its high micromolar activity, the novel tetrahydroquinoline-3-carbonitrile derivative **9k** could be also considered as an interesting starting point for future chemical exploration. Another promising result was obtained from the screening of the triazolo[4,3-*a*]pyridine derivative **12** while the complete loss of activity converting compound **9g** into **13**



Scheme 7 Synthesis of compound **13**. Reaction conditions: 4-(4-methylpiperazin-1-yl)benzoic acid, EDC HCl, DMAP, dry CH_2Cl_2 , 25 °C, 12 h.

may provide useful indications to refine the docking models. In the next phase, inhibition potencies of compounds **9d**, **f**, **g** and **12** were further investigated in dose-dependent experiments and ID_{50} values for LRRK2 wt and G2019S were determined. Furthermore, the specificity of the compounds was tested in a panel of selected kinases (Table 2). Two well-known kinase-targeting drugs (Bosutinib and Sorafenib), recently investigated as LRRK2 inhibitors,³² were also included in Table 2 for comparison purposes. It was interesting to note that, compared to Bosutinib and Sorafenib, our compounds showed a better selectivity profile as indicated by the higher wt/G2019S activity ratio (LRRK2 specificity index) and by the very low inhibitory potency against all the tested kinases. Although Bosutinib and Sorafenib were not developed as LRRK2 inhibitors, their good inhibitory efficacy against a few of the kinases reported in Table 2 is representative of the poor selectivity that characterizes most of the common kinase-targeting drugs. We then investigated the mechanism of inhibition of compounds **9d**, **f**, **g** and **12** toward the pathogenic G2019S mutant. LRRK2 G2019S kinase reactions were conducted by titrating ATP at different fixed doses of the compounds (Fig. 3, ESI† eqn (1)). Trends of the apparent affinities ($K_{m,app}$) and apparent maximal velocities ($V_{max,app}$) obtained from this analysis were then studied as a function of inhibitor concentration (Fig. 4 and 5). For all these

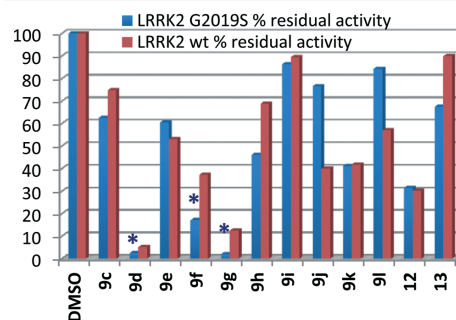


Fig. 2 Inhibitory effect of synthesized compounds against LRRK2 wt (red bars) and G2019S (blue bars) expressed as % residual activity at 100 μM concentration of the inhibitors. *% residual activity for compounds **9d**, **f**, **g** was reported at 50 μM .

Table 2 The potency of compounds **9d**, **f**, **g** and **12** against LRRK2 (wt and G2019S mutant) and their inhibitory effect on selected kinases

Kinase	ID ₅₀ (μM) ^a				K _i (μM) ^b	
	9d	9f	9g	12	Bosutinib	Sorafenib
LRRK2 wt	3.0 (4) ^c	32.6 (7.5) ^c	2.7 (2.4) ^c	32.0 (3.5) ^c	0.3 (1.5) ^c	0.7 (0.07) ^c
LRRK2 G2019S	0.9	4.8	1.3	9.1	0.2	9.7

Kinase	% Inhibition at 100 μM				K _d (nM) ^d	
	9d	9f	9g	12	Bosutinib	Sorafenib
Src	31	5	21	40	1	NA
GSK3β	0	1	0	14	NA ^e	NA
Hck	0	0	0	0	3.4	8500
FAK	11	1	13	8	8	570
DYRK1A	0	9	22	26	NA	NA
ABL	43	6	24	19	0.1	130
FLT3	50	3	62	0	2200	13
CDK2/cycA2	9	3	12	22	NA	8700
CDK9/cycT1	0	1	0	24	NA	NA
CDK9/cycK	53	2	24	38	NA	NA
CDK6/cycD1	42	1	40	18	ND ^f	ND
CDK4/cycD1	9	7	16	10	NA	NA
Pi4Kβ	32	0	31	3	NA	NA
Pim1	20	3	43	29	NA	NA

^a ID₅₀ values are the mean of at least three independent experiments. Standard errors were all within 10% of the mean. ^b K_i values were extrapolated from ref. 25. ^c wt/G2019S activity ratio (LRRK2 specificity index). ^d K_d values were extrapolated from ref. 48. ^e NA = not active. ^f ND = not determined.

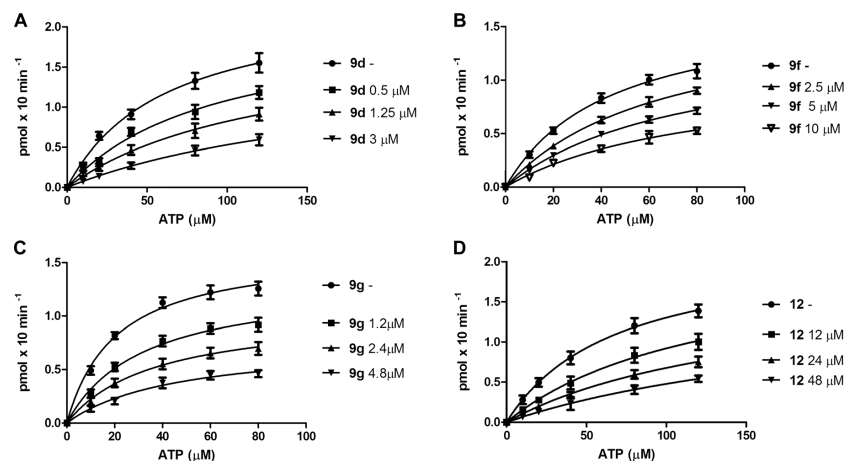


Fig. 3 Kinetic analysis of the kinase reaction in the presence of different concentrations of LRRK2 G2019S inhibitors **9d**, **f**, **g** and **12**. Variation of the reaction velocity of LRRK2 G2019S as a function of ATP concentration at different fixed concentrations of **9d** (A), **9f** (B), **9g** (C) and **12** (D). Each reaction was performed as described in the ESI. ‡ Values are the means of three independent experiments. Error bars represent ±S.D.

compounds, the $K_{m,app}$ values increased with increasing dose of inhibitor, underlying a competitive mechanism of action toward ATP. In particular, compound **12** inhibited the G2019S reaction without affecting the $V_{max,app}$ parameter (Fig. 5D), thus resulting in a pure ATP-competitive mechanism of inhibition. On the other hand, increasing the

concentration of compounds **9d**, **f** and **g** resulted in a decrease in $V_{max,app}$ values, revealing these compounds as mixed-type inhibitors against G2019S, being able to compete with ATP to form a complex with the free enzyme ($[E] \rightarrow [E:I]$) and also to bind to the enzyme in complex with ATP ($[E:ATP] \rightarrow [E:ATP:I]$). The affinity for the free enzyme (K_i') was

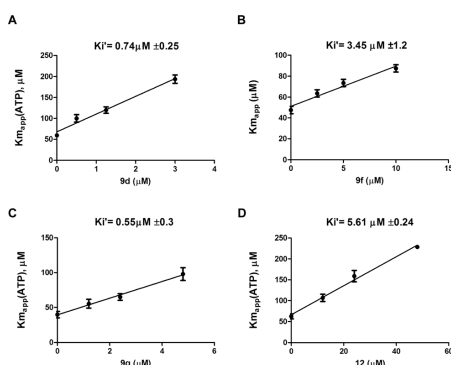


Fig. 4 Determination of inhibitors' affinities for the LRRK2 G2019S free enzyme complex. Variation of the $K_{m,app}$ values of LRRK2 G2019S determined as shown in Fig. 3 as a function of 9d (A), 9f (B), 9g (C) and 12 (D) concentration. K_i' values are reported at the top of each graph. Data analysis was performed as described in the ESI.† Values are the means of three independent experiments. Error bars represent \pm S.D.

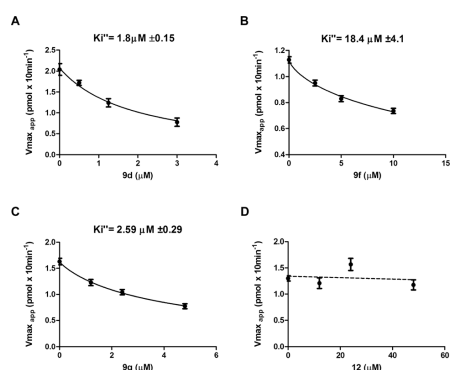


Fig. 5 Determination of inhibitors' affinities for the LRRK2 G2019S:ATP complex. Variation of the $V_{max,app}$ values of LRRK2 G2019S determined as shown in Fig. 3 as a function of 9d (A), 9f (B), 9g (C) and 12 (D) concentration. K_i'' values are reported at the top of each graph. Dotted line in (D) was obtained from data linear interpolation. Data analysis was performed as described in the ESI.† Values are the means of three independent experiments. Error bars represent \pm S.D.

calculated for each compound according to eqn (2) (see the ESI†) and reported in Fig. 4; the affinity for the binary complex was calculated according to eqn (3) (see the ESI†) and reported in Fig. 5. The mixed-type inhibitors 9f and 9g showed a higher affinity toward the free enzyme than toward the [E:ATP] complex, with K_i' values about 5-fold lower than their K_i'' . Interestingly, compound 9d, which exhibited the highest affinity toward the [E:ATP] complex among the tested compounds, showed also comparable K_i' and K_i''

values. This is of particular interest since the intracellular ATP concentration is quite higher than that used in the *in vitro* assays, and this could affect the activity of purely ATP-competitive inhibitors. The mixed-type inhibitor 9d (and to a lesser extent 9f and 9g) showed the ability to inhibit the catalytic activity of the LRRK2 G2019S mutant at low micromolar concentrations even when the enzyme is already bound to the ATP. This peculiar mechanism of action makes 9d a promising candidate for further biological investigations and an interesting tool to identify a possible allosteric pocket on the LRRK2 kinase.

Conclusions

We herein presented the application of a new pharmacophore fragment-decoration strategy for the identification of new LRRK2-targeting chemical probes as potential anti-Parkinson agents. Starting from the knowledge of a key pharmacophore substructure common to a few LRRK2 specific inhibitors, we develop a versatile microwave-assisted proline/Pd-catalyzed multicomponent approach for the rapid synthesis of substituted heteroaryl-hydrazone. This novel synthetic protocol was efficiently applied to a series of cheap and commercially available building blocks, allowing us to easily decorate the heteroaryl-hydrazone pharmacophore fragment. Additional molecular complication was also generated by simple modifications of the final compounds. *In vitro* biological evaluation of the synthesized compounds allowed us to quickly identify a few promising LRRK2 inhibitors (9d, f, g and 12) endowed with a low micromolar activity, good LRRK2 specificity index (wt/G2019S activity ratio), low affinity towards a small panel of selected kinases and a mixed-type inhibition against the pathogenic G2019S mutant. Among these compounds, 9d, 9f and 9g resulted in a mixed-type inhibition towards G2019S, being able to bind also to the enzyme in complex with the ATP substrate. This is of particular interest since, differently from purely ATP-competitive inhibitors, the inhibitory activity of these compounds should not be affected by the high intracellular ATP concentration. In summary, our results demonstrate how a diversity-oriented approach based on a key pharmacophore fragment could represent an efficient strategy for the identification of new chemical probes of biological interest. Further studies on the optimization of the identified compounds and on the comprehensive elucidation of their mechanism of action will be reported in due course.

Experimental

General

All commercially available chemicals were purchased from both Sigma-Aldrich and Alfa Aesar and, unless otherwise noted, used without any previous purification. Solvents used for work-up and purification procedures were of technical grade. TLC was carried out using Sigma-Aldrich TLC plates (silica gel on Al foils, SUPELCO Analytical). Where indicated, products were purified by silica gel flash chromatography on

columns packed with Merck Geduran Si 60 (40–63 μm). ^1H and ^{13}C NMR spectra were recorded on BRUKER AVANCE 300 MHz and BRUKER AVANCE 400 MHz spectrometers. Chemical shifts (δ scale) are reported in parts per million (ppm) relative to TMS. ^1H NMR spectra are reported in this order: multiplicity and number of protons; signals were characterized as follows: s (singlet), d (doublet), dd (doublet of doublets), ddd (doublet of doublet of doublets), t (triplet), m (multiplet), bs (broad signal). HPLC/MS analyses were conducted on an Agilent 1100 series equipped with a Waters Symmetry C18 column (3.5 μm , 4.6 \times 75 mm) and a MS detector (Applied Biosystem/MDS SCIEX, with API 150EX ion source). Elemental analyses were performed on a Perkin-Elmer PE 2004 elemental analyzer, and the data for C, H, and N were all within 0.4% of the theoretical values.

Microwave irradiation experiments

Microwave reactions were conducted using a CEM Discover Synthesis Unit (CEM Corp., Matthews, NC). The machine consists of a continuous focused microwave power delivery system with an operator-selectable power output from 0 to 300 W. The temperature inside the reaction vessel was monitored using a calibrated infrared temperature control mounted under the reaction vessel. All experiments were performed using a stirring option whereby the reaction mixtures are stirred by means of a rotating magnetic plate located below the floor of the microwave cavity and a Teflon-coated magnetic stir bar in the vessel.

General procedure for the one-pot two-step synthesis of functionalized heteroaryl-hydrazone derivatives (9b–n)

Substituted ketone/aldehyde (0.73 mmol), hydrazine monohydrate (0.73 mmol), *L*-proline (0.15 mmol) and 1 mL of anhydrous toluene were placed in a dried 10 mL microwave tube equipped with a magnetic stir bar and a septum, and the colorless mixture was irradiated at 300 W for 15 minutes in the microwave apparatus (maximum pressure: 250 psi; maximum temperature: 200 $^{\circ}\text{C}$; power max: OFF; stirring: ON). The solution became light yellow and the TLC, eluting with petroleum ether/ethyl acetate, 6/4 (vol/vol), showed the complete conversion of ketone/aldehyde into the corresponding hydrazone. Subsequently heteroaryl chloride (0.61 mmol) and *t*-BuONa (0.98 mmol) were added and the tube was flushed with argon for 1 minute. Then, 1 mL of a stock solution of the catalyst [Pd(OAc)₂ (27.0 mg, 0.12 mmol) plus DavePhos (96 mg, 0.24 mmol) in anhydrous toluene (10 mL) stored under Ar atmosphere] was added and the resulting mixture was stirred and flushed with argon for an additional 2 minutes. Next, the tube was heated under microwave irradiation at 150 $^{\circ}\text{C}$ for 10 minutes (for compounds 9b–g, j, m, n) or for 20 minutes (for compounds 9k, l) or at 180 $^{\circ}\text{C}$ for 20 minutes (for compounds 9h, i) (maximum power input: 300 W; maximum pressure: 250 psi; power max: OFF; stirring: ON). After cooling to room temperature the dark red reaction mixture was filtered over Celite and the resulting solution

was evaporated under reduced pressure. The residue was purified by silica gel flash chromatography (petroleum ether/ethyl acetate, from 9/1 to 7/3), affording pure, target heteroaryl-hydrazone (9b–n).

2-(2-(Diphenylmethylene)hydrazinyl)quinoline (9b)

Starting from benzophenone and 2-chloroquinoline, the title compound was obtained as a yellow solid (53% yield). ^1H NMR (300 MHz, CDCl_3) δ 8.59 (s, 1H), 8.11 (d, J = 8.9 Hz, 1H), 7.91 (d, J = 8.9 Hz, 1H), 7.69–7.66 (m, 4H), 7.62–7.59 (m, 3H), 7.44–7.30 (m, 7H). ^{13}C NMR (75 MHz, CDCl_3) δ 160.6, 155.5, 138.5, 137.9, 132.4, 129.9 (2C), 129.6, 129.1, 129.0 (2C), 128.8, 128.5, 128.3 (2C), 128.1, 127.9, 127.8, 126.9 (2C), 123.3, 110.1. MS (ESI) m/z 324.2 $[\text{M} + \text{H}]^+$, 346.3 $[\text{M} + \text{Na}]^+$.

(*E*)-2-(2-(1-(3-Nitrophenyl)ethylidene)hydrazinyl)quinoline (9c)

Starting from 3'-nitroacetophenone and 2-chloroquinoline, the title compound was obtained as a yellow solid (33% yield). ^1H NMR (400 MHz, CDCl_3) δ 8.67 (s, 1H), 8.21–8.12 (m, 3H), 7.75–7.64 (m, 5H), 7.58 (t, J = 7.6 Hz, 1H), 7.36 (bs, 1H), 2.38 (s, 3H). ^{13}C NMR (100.6 MHz, CDCl_3) δ 155.3, 148.6, 146.1, 140.4, 138.7, 136.2, 131.4, 130.2, 129.3, 128.8, 127.9, 126.2, 123.6, 122.9, 120.6, 109.9, 29.7. MS (ESI) m/z 307.2 $[\text{M} + \text{H}]^+$, 329.3 $[\text{M} + \text{Na}]^+$.

(*E*)-2-(2-(4-Methoxybenzylidene)hydrazinyl)-4-methylquinoline (9d)

Starting from 4-methoxybenzaldehyde and 2-chloro-4-methylquinoline, the title compound was obtained as a yellow solid (39% yield). ^1H NMR (400 MHz, $\text{DMSO}-d_6$) δ 11.12 (s, 1H), 8.03 (s, 1H), 7.88 (d, J = 7.4 Hz, 1H), 7.67 (d, J = 8.4 Hz, 2H), 7.61–7.55 (m, 2H), 7.49 (s, 1H), 7.31 (t, J = 6.8 Hz, 1H), 7.00 (d, J = 8.8 Hz, 2H), 3.81 (s, 3H), 2.65 (s, 3H). ^{13}C NMR (100.6 MHz, $\text{DMSO}-d_6$) δ 160.3, 156.0, 147.4, 145.9, 139.8, 129.9, 128.5, 128.1 (2C), 126.6, 126.1, 124.6, 122.6, 114.7 (2C), 110.3, 55.7, 19.1. MS (ESI) m/z 292.1 $[\text{M} + \text{H}]^+$, 314.3 $[\text{M} + \text{Na}]^+$.

(*E*)-2-(2-(1-Phenylethylidene)hydrazinyl)quinoline (9e)

Starting from acetophenone and 2-chloroquinoline, the title compound was obtained as a yellow solid (32% yield). ^1H NMR (400 MHz, CDCl_3) δ 8.11 (d, J = 9.0 Hz, 1H), 7.86 (d, J = 7.6 Hz, 2H), 7.81 (d, J = 8.9 Hz, 1H), 7.75 (t, J = 7.5 Hz, 2H), 7.64 (t, J = 7.4 Hz, 1H), 7.46–7.28 (m, 5H), 2.37 (s, 3H). ^{13}C NMR (100.6 MHz, CDCl_3) δ 155.3, 148.6, 138.7, 137.9, 132.1, 130.1, 129.8, 128.6, 128.4 (2C), 127.8 (2C), 125.9, 124.7, 115.7, 110.2, 29.7. MS (ESI) m/z 262.2 $[\text{M} + \text{H}]^+$, 284.1 $[\text{M} + \text{Na}]^+$.

(*E*)-2-(1-(2-(Quinolin-2-yl)hydrazono)ethyl)phenol (9f)

Starting from 2'-hydroxyacetophenone and 2-chloroquinoline, the title compound was obtained as a yellow solid (41% yield). ^1H NMR (300 MHz, CDCl_3) δ 12.35 (bs, 1H), 8.09 (d, J = 6.9 Hz, 1H), 7.73–7.63 (m, 3H), 7.48 (d, J = 7.4 Hz, 1H), 7.37–7.27 (m, 4H), 7.04 (d, J = 8.2 Hz, 1H), 6.92 (m, 1H), 2.41 (s, 3H). ^{13}C NMR (100.6 MHz, CDCl_3) δ 158.1, 154.4, 149.6,

146.8, 139.2, 130.6, 130.4, 127.8, 127.2, 126.1, 124.9, 123.8, 119.8, 119.1, 117.5, 108.9, 29.7. MS (ESI) m/z 278.4 $[M + H]^+$, 300.4 $[M + Na]^+$.

(E)-4-((2-(4-Methylquinolin-2-yl)hydrazono)methyl)phenol (9g)

Starting from 4-hydroxybenzaldehyde and 2-chloro-4-methylquinoline, the title compound was obtained as a yellow solid (42% yield). 1H NMR (400 MHz, DMSO- d_6) δ 11.05 (bs, 1H), 9.79 (s, 1H), 7.99 (s, 1H), 7.86 (d, $J = 7.9$ Hz, 1H), 7.60–7.58 (m, 2H), 7.55 (d, $J = 8.4$ Hz, 2H), 7.48 (s, 1H), 7.27 (t, $J = 7.4$ Hz, 1H), 6.83 (d, $J = 8.3$ Hz, 2H), 2.64 (s, 3H). ^{13}C NMR (100.6 MHz, DMSO- d_6) δ 158.7, 156.1, 147.8, 146.0, 140.3, 129.8, 128.2 (2C), 126.8, 126.6, 124.6, 124.4, 122.5, 116.1 (2C), 109.8, 19.1. MS (ESI) m/z 278.2 $[M + H]^+$, 300.1 $[M + Na]^+$.

(E)-2-(2-(4-Methoxybenzylidene)hydrazinyl)pyridine (9h)

Starting from 4-methoxybenzaldehyde and 2-chloropyridine, the title compound was obtained as a light yellow solid (45% yield). 1H NMR (400 MHz, $CDCl_3$) δ 8.90 (s, 1H), 8.16 (d, $J = 4.2$ Hz, 1H), 7.76 (s, 1H), 7.64 (d, $J = 8.7$ Hz, 2H), 7.62–7.60 (m, 1H), 7.38 (d, $J = 8.4$ Hz, 1H), 6.94 (d, $J = 8.7$ Hz, 2H), 6.78 (dd, $J = 6.4, 5.3$ Hz, 1H), 3.86 (s, 3H). ^{13}C NMR (100.6 MHz, $CDCl_3$) δ 160.3, 157.2, 147.3, 139.2, 138.2, 127.9 (2C), 127.8, 115.3, 114.2 (2C), 107.5, 55.4. MS (ESI) m/z 228.2 $[M + H]^+$, 250.3 $[M + Na]^+$.

(E)-3-Chloro-2-(2-(3,4-dimethoxybenzylidene)hydrazinyl)pyridine (9i)

Starting from 3,4-dimethoxybenzaldehyde and 2,3-dichloropyridine, the title compound was obtained as a yellow solid (40% yield). 1H NMR (300 MHz, $CDCl_3$) δ 8.48 (s, 1H), 8.26–8.25 (m, 1H), 8.00 (s, 1H), 7.57 (d, $J = 7.5$ Hz, 1H), 7.49 (s, 1H), 7.15 (d, $J = 7.9$ Hz, 1H), 6.87 (d, $J = 8.0$ Hz, 1H), 6.76–6.75 (m, 1H), 3.97 (s, 3H), 3.92 (s, 3H). ^{13}C NMR (75 MHz, $CDCl_3$) δ 150.6, 150.2, 149.3, 146.9, 144.2, 137.1, 127.2, 121.9, 115.6, 114.2, 110.6, 108.5, 56.1, 55.9. MS (ESI) m/z 292.2 $[M + H]^+$, 314.1 $[M + Na]^+$.

(E)-2-(2-(4-Methoxybenzylidene)hydrazinyl)-4,6-dimethylnicotinonitrile (9j)

Starting from 4-methoxybenzaldehyde and 2-chloro-4,6-dimethylpyridine-3-carbonitrile, the title compound was obtained as a yellow solid (48% yield). 1H NMR (400 MHz, $CDCl_3$) δ 8.49 (s, 1H), 7.76 (d, $J = 8.2$ Hz, 2H), 7.73 (s, 1H), 6.95 (d, $J = 8.2$ Hz, 2H), 6.60 (s, 1H), 3.85 (s, 3H), 2.50 (s, 3H), 2.43 (s, 3H). ^{13}C NMR (100.6 MHz, $CDCl_3$) δ 161.3, 160.8, 156.2, 154.7, 141.5, 130.1, 128.8 (2C), 127.1, 116.7, 116.5, 114.2 (2C), 55.3, 24.5, 20.8. MS (ESI) m/z 281.4 $[M + H]^+$, 303.3 $[M + Na]^+$.

(E)-2-(2-(4-Methoxybenzylidene)hydrazinyl)-4-phenyl-5,6,7,8-tetrahydroquinoline-3-carbonitrile (9k)

Starting from 4-methoxybenzaldehyde and 2-chloro-4-phenyl-5,6,7,8-tetrahydroquinoline-3-carbonitrile, the title compound

was obtained as an orange solid (44% yield). 2-Chloro-4-phenyl-5,6,7,8-tetrahydroquinoline-3-carbonitrile was prepared from 2-oxo-4-phenyl-1,2,5,6,7,8-hexahydroquinoline-3-carbonitrile, as previously described by our research group.⁸ 1H NMR (400 MHz, $CDCl_3$) δ 8.51 (s, 1H), 7.77 (s, 1H), 7.73 (d, $J = 8.2$ Hz, 2H), 7.53–7.46 (m, 3H), 7.30–7.28 (m, 2H), 6.91 (d, $J = 8.2$ Hz, 2H), 3.83 (s, 3H), 2.93–2.90 (m, 2H), 2.39–2.36 (m, 2H), 1.87–1.86 (m, 2H), 1.72–1.70 (m, 2H). ^{13}C NMR (100.6 MHz, $CDCl_3$) δ 161.3, 160.7, 156.6, 153.4, 141.6, 136.4, 132.4, 128.8 (2C), 128.7 (2C), 128.1, 127.2 (2C), 122.6, 116.8, 114.2 (2C), 113.6, 55.3, 33.3, 26.7, 22.8, 22.5. MS (ESI) m/z 383.3 $[M + H]^+$, 405.4 $[M + Na]^+$.

(E)-4-(2-Chlorophenyl)-2-(2-(4-methoxybenzylidene)hydrazinyl)-5,6,7,8-tetrahydroquinoline-3-carbonitrile (9l)

Starting from 4-methoxybenzaldehyde and 2-chloro-4-(2-chlorophenyl)-5,6,7,8-tetrahydroquinoline-3-carbonitrile, the title compound was obtained as an orange solid (51% yield). 2-Chloro-4-(2-chlorophenyl)-5,6,7,8-tetrahydroquinoline-3-carbonitrile was prepared from 4-(2-chlorophenyl)-2-oxo-1,2,5,6,7,8-hexahydroquinoline-3-carbonitrile, as previously described by our research group.⁸ 1H NMR (400 MHz, $CDCl_3$) δ 8.57 (s, 1H), 7.75 (d, $J = 8.4$ Hz, 2H), 7.71 (s, 1H), 7.56–7.53 (m, 1H), 7.45–7.39 (m, 2H), 7.25–7.21 (m, 1H), 6.91 (d, $J = 8.4$ Hz, 2H), 3.83 (s, 3H), 2.92–2.88 (m, 2H), 2.33–2.29 (m, 2H), 1.89–1.88 (m, 2H), 1.71–1.69 (m, 2H). ^{13}C NMR (100.6 MHz, $CDCl_3$) δ 161.2, 160.8, 156.4, 153.5, 141.8, 135.4, 132.2, 130.3, 129.9, 129.5, 128.8 (2C), 127.4, 127.2, 122.9, 116.4, 114.3 (2C), 114.1, 55.3, 33.1, 29.7, 25.9, 22.5. MS (ESI) m/z 417.2 $[M + H]^+$, 439.3 $[M + Na]^+$.

(E)-2-(2-(4-(Methylthio)benzylidene)hydrazinyl)quinoline (9m)

Starting from 4-(methylthio)benzaldehyde and 2-chloroquinoline, the title compound was obtained as a yellow solid (38% yield). 1H NMR (400 MHz, $CDCl_3$) δ 8.60 (s, 1H), 8.25–8.23 (m, 1H), 7.83–7.77 (m, 3H), 7.60–7.56 (m, 4H), 7.48 (t, $J = 7.6$ Hz, 1H), 7.21 (d, $J = 8.1$ Hz, 2H), 2.49 (s, 3H). ^{13}C NMR (100.6 MHz, $CDCl_3$) δ 154.5, 147.4, 139.3, 138.4, 130.1, 129.6, 128.7, 128.5, 127.9 (2C), 127.6, 127.3, 126.3 (2C), 126.2, 117.5, 15.6. MS (ESI) m/z 294.1 $[M + H]^+$, 316.2 $[M + Na]^+$.

(E)-N,N-Dimethyl-4-((2-(quinolin-2-yl)hydrazono)methyl)aniline (9n)

Starting from 4-(dimethylamino)benzaldehyde and 2-chloroquinoline, the title compound was obtained as a yellow solid (41% yield). 1H NMR (400 MHz, $CDCl_3$) δ 8.55 (s, 1H), 8.20 (d, $J = 8.2$ Hz, 2H), 7.83–7.77 (m, 3H), 7.61–7.55 (m, 3H), 7.45 (t, $J = 7.6$ Hz, 1H), 6.67 (d, $J = 8.0$ Hz, 2H), 2.98 (s, 6H), ^{13}C NMR (100.6 MHz, $CDCl_3$) δ 154.9, 151.2, 147.5, 142.3, 138.1, 129.4, 128.7, 128.3 (2C), 127.5, 126.3, 125.2, 123.5, 117.7 (2C), 112.0, 40.4 (2C). MS (ESI) m/z 291.2 $[M + H]^+$, 313.2 $[M + Na]^+$.

Synthesis of 8-chloro-3-(3,4-dimethoxyphenyl)-[1,2,4]triazolo-[4,3- α]pyridine (11)

A solution of CuCl₂ (369 mg, 2.74 mmol) in DMF (4.5 mL) was added to a stirred solution of **9i** (400 mg, 1.37 mmol) in DMF (4.5 mL) and the mixture was heated at 90 °C for an hour. After cooling to room temperature, 20 mL of water and 0.5 mL of 30% ammonia solution were added, followed by extraction with ethyl acetate (3 × 20 mL). The collected organic phases were washed with an aqueous solution of LiCl (5%) and brine, dried over Na₂SO₄ and evaporated under vacuum to give the product as a beige solid (95% yield). ¹H NMR (400 MHz, CDCl₃) δ 8.17 (d, J = 6.8 Hz, 1H), 7.30 (s, 1H), 7.25 (d, J = 8.4 Hz, 1H), 7.22 (d, J = 8.4 Hz, 1H), 6.97 (d, J = 7.2 Hz, 1H), 6.79 (t, J = 7.0 Hz, 1H), 3.91 (s, 3H), 3.88 (s, 3H). MS (ESI) m/z 290.2 [M + H]⁺, 312.3 [M + Na]⁺.

Synthesis of 3-(3,4-dimethoxyphenyl)-N-(2-morpholinoethyl)-[1,2,4]triazolo[4,3- α]pyridin-8-amine (12)

In a microwave tube a mixture of **11** (50 mg, 0.17 mmol), 4-(2-aminoethyl)morpholine (68 μ L, 0.51 mmol), *t*-OBuNa (33 mg, 0.35 mmol), rac-BINAP (32 mg, 0.051 mmol), Pd(OAc)₂ (8 mg, 0.034 mmol) and dry toluene (1 mL) were heated at 120 °C for 10 min in the microwave apparatus (maximum power input: 300 W; maximum pressure: 250 psi; power max: OFF; stirring: ON). After cooling to room temperature water was added, followed by extraction with ethyl acetate. The collected organic phases were washed with brine, dried over Na₂SO₄ and evaporated under vacuum. The residue was purified by silica gel flash chromatography (dichloromethane/methanol 96/4) to give the desired compound as a white solid (86% yield). ¹H NMR (400 MHz, CDCl₃) δ 7.63 (d, J = 6.9 Hz, 1H), 7.40 (s, 1H), 7.33 (d, J = 8.3 Hz, 1H), 7.02 (d, J = 8.3 Hz, 1H), 6.70 (t, J = 7.0 Hz, 1H), 6.04 (d, J = 7.3 Hz, 1H), 5.88–5.87 (m, 1H), 3.95 (s, 6H), 3.76–3.73 (m, 4H), 3.36 (dd, J = 11, 5.5 Hz, 2H), 2.74 (t, J = 6.0 Hz, 2H), 2.54–2.52 (m, 4H). ¹³C NMR (100.6 MHz, CDCl₃) δ 150.4, 149.6, 147.6, 145.5, 136.3, 120.5, 119.8, 115.9, 111.8, 111.3, 110.5, 97.3, 66.9 (2C), 56.6, 56.1, 56.0, 53.4 (2C), 39.4. MS (ESI) m/z 384.1 [M + H]⁺, 406.2 [M + Na]⁺.

Synthesis of (*E*)-4-((2-(4-methylquinolin-2-yl)hydrazono)methyl)phenyl 4-(4-methylpiperazin-1-yl)benzoate (13)

A solution of 4-(4-methylpiperazin-1-yl)benzoic acid (44 mg, 0.20 mmol), (*E*)-4-((2-(4-methylquinolin-2-yl)hydrazono)methyl)phenol **9g** (50 mg, 0.18 mmol), EDC HCl (63 mg, 0.33 mmol) and DMAP (37 mg, 0.30 mmol) in dry CH₂Cl₂ was stirred at room temperature overnight. At the end of the reaction water was added, followed by extraction with CH₂Cl₂. The collected organic phases were washed with brine, dried over Na₂SO₄ and evaporated under vacuum. The residue was purified by silica gel flash chromatography (dichloromethane/methanol 95/5) to give the desired compound as a yellow solid (93% yield). ¹H NMR (400 MHz, DMSO-*d*₆) δ 11.34 (s, 1H), 8.10 (s, 1H), 7.96 (d, J = 8.4 Hz, 2H), 7.91 (d, J = 8.0 Hz, 1H), 7.80 (d, J = 8.0 Hz, 2H), 7.64–

7.55 (m, 3H), 7.34–7.29 (m, 3H), 7.06 (d, J = 8.0 Hz, 2H), 3.37–3.35 (m, 4H), 2.67 (s, 3H), 2.47–2.45 (8s, 4H), 2.23 (s, 3H). ¹³C NMR (100.6 MHz, DMSO-*d*₆) δ 164.8, 156.0, 154.9, 151.6, 147.6, 146.3, 139.0, 133.3, 132.0 (2C), 129.9, 127.6 (2C), 126.8, 126.6, 124.8, 124.6, 122.9 (2C), 117.1, 113.8 (2C), 109.8, 54.7 (2C), 46.9 (2C), 46.2, 19.1. MS (ESI) m/z 480.2 [M + H]⁺, 502.1 [M + Na]⁺.

Acknowledgements

This work was supported by the University of Parma (to MR) and a Region of Lombardy-CNR grant (MbMM – basic methodologies for innovation in the diagnosis and treatment of multifactorial diseases) to EC. ST is supported by a fellowship from the Chiesi Foundation.

Notes and references

- 1 D. C. Swinney, *Clin. Pharmacol. Ther.*, 2013, 93, 299–301.
- 2 W. Zheng, N. Thorne and J. C. McKew, *Drug Discovery Today*, 2013, 18, 1067–1073.
- 3 M. A. Cooper, *Nat. Rev. Drug Discovery*, 2015, 14, 587–588.
- 4 C. J. O. Connor, H. S. G. Beckmann and D. R. Spring, *Chem. Soc. Rev.*, 2012, 41, 4444–4456.
- 5 J. Kim, H. Kim and S. B. Park, *J. Am. Chem. Soc.*, 2014, 136(42), 14629–14638.
- 6 H. van Hattum and H. Waldmann, *J. Am. Chem. Soc.*, 2014, 136(34), 11853–11859.
- 7 S. Oh and S. B. Park, *Chem. Commun.*, 2011, 47, 12754–12761.
- 8 M. Radi, G. P. Vallerini, A. Petrelli, P. Vincetti and G. Costantino, *Tetrahedron Lett.*, 2013, 54, 6905–6908.
- 9 M. Radi, L. Botta, G. Casaluce, M. Bernardini and M. Botta, *J. Comb. Chem.*, 2010, 12, 200–205.
- 10 M. Radi, V. Bernardo, B. Bechi, D. Castagnolo, M. Pagano and M. Botta, *Tetrahedron Lett.*, 2009, 50, 6572–6575.
- 11 M. Radi, S. Saletti and M. Botta, *Tetrahedron Lett.*, 2008, 49, 4464–4466.
- 12 M. Radi, E. Petricci, G. Maga, F. Corelli and M. Botta, *J. Comb. Chem.*, 2005, 7, 117–122.
- 13 M. Asif, *International Journal of Advanced Chemistry*, 2014, 2, 85–103.
- 14 L. Savini, P. Massarelli, L. Chiasserini, A. Segà, C. Pellarano, A. Barzi and G. Nocentini, *Eur. J. Med. Chem.*, 1995, 30, 547–552.
- 15 L. Savini, L. Chiasserini, V. Travagli, C. Pellarano, E. Novellino, S. Cosentino and M. B. Pisano, *Eur. J. Med. Chem.*, 2004, 39, 113–122.
- 16 A. R. Todeschini, A. L. P. de Miranda, K. C. M. da Silva, S. C. Parrini and E. J. Barreiro, *Eur. J. Med. Chem.*, 1998, 33, 189–199.
- 17 J. Easmon, G. Heinisch, G. Pürstinger, T. Langer, J. K. Österreicher, H. H. Grunicke and J. Hofmann, *J. Med. Chem.*, 1997, 40, 4420–4425.
- 18 J. Y. Lee, K. W. Jeong, S. Shin, J. U. Lee and Y. Kim, *Eur. J. Med. Chem.*, 2012, 47, 261–269.

- 19 H. Yun, H. Y. Heo, H. H. Kim, N. Dookim and W. Seol, *Bioorg. Med. Chem. Lett.*, 2011, **21**, 2953–2957.
- 20 M. R. Cookson, *Nat. Rev. Neurosci.*, 2010, **11**, 791–797.
- 21 T. Hatano, S. Kubo, S. Sato and N. Hattori, *J. Neurochem.*, 2009, **111**, 1075–1093.
- 22 T. Kramer, F. Lo Monte, S. Göring, G. M. O. Amombo and B. Schmidt, *ACS Chem. Neurosci.*, 2012, **3**, 151–160.
- 23 A. A. Estrada and Z. K. Sweeney, *J. Med. Chem.*, 2015, **58**(9), 3767–3793.
- 24 S. Ray and M. Liu, *Future Med. Chem.*, 2012, **4**, 1701–1713.
- 25 A. W. Garofalo, M. Adler, D. L. Aubele, S. Bowers, M. Franzini, E. Goldbach, C. Lorentzen, R. J. Neitz, G. D. Probst, K. P. Quinn, P. Santiago, H. L. Sham, D. Tam, A. P. Truong, X. M. Ye and Z. Ren, *Bioorg. Med. Chem. Lett.*, 2013, **23**, 71–74.
- 26 A. W. Garofalo, M. Adler, D. L. Aubele, E. F. Brigham, D. Chian, M. Franzini, E. Goldbach, G. T. Kwong, R. Motter, G. D. Probst, K. P. Quinn, L. Ruslim, H. L. Sham, D. Tam, P. Tanaka, A. P. Truong, X. M. Ye and Z. Ren, *Bioorg. Med. Chem. Lett.*, 2013, **23**, 1974–1977.
- 27 A. A. Estrada, X. Liu, C. Baker-Glenn, A. Beresford, D. J. Burdick, M. Chambers, B. K. Chan, H. Chen, X. Ding, A. G. DiPasquale, S. L. Dominguez, J. Dotson, J. Drummond, M. Flagella, S. Flynn, R. Fuji, A. Gill, J. Gunzner-Toste, S. F. Harris, T. P. Heffron, T. Kleinheinz, D. W. Lee, C. E. Le Pichon, J. P. Lyssikatos, A. D. Medhurst, J. G. Moffat, S. Mukund, K. Nash, K. Scearce-Levie, Z. Sheng, D. G. Shore, T. Tran, N. Trivedi, S. Wang, S. Zhang, X. Zhang, G. Zhao, H. Zhu and Z. K. Sweeney, *J. Med. Chem.*, 2012, **55**, 9416–9436.
- 28 J. Zhang, X. Deng, H. G. Choi, D. R. Alessi and N. S. Gray, *Bioorg. Med. Chem. Lett.*, 2012, **22**, 1864–1869.
- 29 A. D. Reith, P. Bamborough, K. Jandu, D. Andreotti, L. Mensah, P. Dossang, H. G. Choi, X. Deng, J. Zhang, D. R. Alessi and N. S. Gray, *Bioorg. Med. Chem. Lett.*, 2012, **22**, 5625–5629.
- 30 T. M. Kirrane, S. J. Boyer, J. Burke, X. Guo, R. J. Snow, L. Soleymanzadeh, A. Swinamer, Y. Zhang, J. B. Madwed, M. Kashem, S. Sugler and M. M. O'Neill, *Bioorg. Med. Chem. Lett.*, 2012, **22**, 738–742.
- 31 M. Franzini, X. M. Ye, M. Adler, D. L. Aubele, A. W. Garofalo, S. Gauby, E. Goldbach, G. D. Probst, K. P. Quinn, P. Santiago, H. L. Sham, D. Tam, A. Truong and Z. Ren, *Bioorg. Med. Chem. Lett.*, 2013, **23**, 1967–1973.
- 32 Z. Liu, R. A. Galleo Jr., K. B. Fraser, M. S. Moehle, S. Sen, L. A. Volpicelli-Daley, L. J. DeLucas, L. J. Ross, J. Valiyaveetil, O. Moukha-Chafiq, A. K. Pathak, S. Ananthan, H. Kezar, E. L. White, V. Gupta, J. A. Maddry, M. J. Suto and A. B. West, *J. Biol. Chem.*, 2014, **289**, 32937–32951.
- 33 C. A. Lang, S. S. Ray, M. Liu, A. K. Singh and G. D. Cuny, *Bioorg. Med. Chem. Lett.*, 2015, **25**, 2713–2719.
- 34 D. G. Calatayud, E. López-Torres and M. A. Mendiola, *Eur. J. Inorg. Chem.*, 2013, **1**, 80–90.
- 35 B. E. Sleebbs, W. J. A. Kersten, S. Kulasegaram, G. Nikolakopoulos, E. Hatzis, R. M. Moss, J. P. Parisot, H. Yang, P. E. Czabotar, W. D. Fairlie, E. F. Lee, J. M. Adams, L. Chen, M. F. van Delft, K. N. Lowes, S. Wei, D. C. S. Huang, P. M. Colman, I. P. Street, J. P. Baell, K. Watson and G. Lessene, *J. Med. Chem.*, 2013, **56**, 5514–5540.
- 36 M. N. Chaur, D. Collado and J. M. Lehn, *Chem. – Eur. J.*, 2011, **17**, 248–258.
- 37 S. Wagaw, B. H. Yang and S. L. Buchwald, *J. Am. Chem. Soc.*, 1999, **121**(44), 10251–10263.
- 38 N. Haddad, A. Salvagno and C. Busacca, *Tetrahedron Lett.*, 2004, **45**, 5935–5937.
- 39 O. R. Thiel, M. M. Achmatowicz, A. Reichelt and R. D. Larsen, *Angew. Chem., Int. Ed.*, 2010, **49**, 8395–8398.
- 40 A. Dömling, W. Wang and K. Wang, *Chem. Rev.*, 2012, **112**, 3083–3135.
- 41 C. Mauger and G. Mignani, *Adv. Synth. Catal.*, 2005, **347**, 773–782.
- 42 D. S. Surry and S. L. Buchwald, *Chem. Sci.*, 2011, **2**, 27–50.
- 43 J. P. Wolfe, H. Tomori, J. P. Sadighi, J. Yin and S. L. Buchwald, *J. Org. Chem.*, 2000, **65**, 1158–1174.
- 44 Q. Shen, S. Shekhar, J. P. Stambuli and J. F. Hartwig, *Angew. Chem., Int. Ed.*, 2005, **44**, 1371–1375.
- 45 B. U. W. Maes, K. T. J. Loones, G. L. F. Lemièrre and R. A. Dommissie, *Synlett*, 2003, **12**, 1822–1825.
- 46 B. U. W. Maes, K. T. J. Loones, S. Hostyn, G. Diels and G. Rombouts, *Tetrahedron*, 2004, **60**, 11559–11564.
- 47 M. Ciesielski, D. Pufky and M. Döring, *Tetrahedron*, 2005, **61**, 5942–5947.
- 48 M. I. Davis, J. P. Hunt, S. Herrgard, P. Ciceri, L. M. Wodicka, G. Pallares, M. Hocker, D. K. Treiber and P. P. Zarrinkar, *Nat. Biotechnol.*, 2011, **29**, 1046–1051.

Discovery of Multitarget Agents Active as Broad-Spectrum Antivirals and Correctors of Cystic Fibrosis Transmembrane Conductance Regulator for Associated Pulmonary Diseases

Sabrina Tassini,[†] Liang Sun,[‡] Kristina Lanko,[‡] Emmanuele Crespan,[§] Emily Langron,^{||} Federico Falchi,^{⊥,¶} Miroslava Kissova,[§] Jorge I. Armijos-Rivera,[§] Leen Delang,[‡] Carmen Mirabelli,[‡] Johan Neyts,^{*,‡} Marco Pieroni,[†] Andrea Cavalli,^{⊥,¶} Gabriele Costantino,[†] Giovanni Maga,[§] Paola Vergani,^{||} Pieter Leyssen,[‡] and Marco Radi^{*,†}

[†]P4T Group, Dipartimento di Scienze degli Alimenti e del Farmaco, Università degli Studi di Parma, Viale delle Scienze, 27/A, 43124 Parma, Italy

[‡]Laboratory of Virology and Experimental Chemotherapy, Rega Institute for Medical Research, KU Leuven, Minderbroedersstraat 10, 3000, Leuven, Belgium

[§]Istituto di Genetica Molecolare, IGM-CNR, Via Abbiategrasso 207, 27100 Pavia, Italy

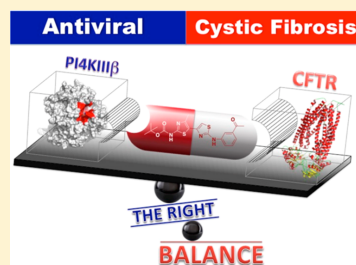
^{||}Department of Neuroscience, Physiology and Pharmacology, University College London, Gower Street, WC1E 6BT London, U.K.

[⊥]CompuNet, Istituto Italiano di Tecnologia, Via Morego 30, I-16163 Genova, Italy

[¶]Department of Pharmacy and Biotechnology, University of Bologna, Via Belmeloro 6, I-40126 Bologna, Italy

Supporting Information

ABSTRACT: Enteroviruses (EVs) are among the most frequent infectious agents in humans worldwide and represent the leading cause of upper respiratory tract infections. No drugs for the treatment of EV infections are currently available. Recent studies have also linked EV infection with pulmonary exacerbations, especially in cystic fibrosis (CF) patients, and the importance of this link is probably underestimated. The aim of this work was to develop a new class of multitarget agents active both as broad-spectrum antivirals and as correctors of the F508del-cystic fibrosis transmembrane conductance regulator (CFTR) folding defect responsible for >90% of CF cases. We report herein the discovery of the first small molecules able to simultaneously act as correctors of the F508del-CFTR folding defect and as broad-spectrum antivirals against a panel of EVs representative of all major species.



INTRODUCTION

Enteroviruses (EVs) are positive-sense single-stranded RNA viruses, classified into 12 species, including four human EV species (EV-A to EV-D), three species of human rhinoviruses (RV-A to RV-C), and five EV species that only infect animals.¹ EVs are responsible for a great variety of clinical manifestations, especially in young children, which may result in life-threatening neurological complications (e.g., encephalitis, meningitis, and poliomyelitis-like paralysis).^{2–4} Furthermore, RV infections are now considered one of the major causes of acute exacerbations in chronic pulmonary diseases like asthma, chronic obstructive pulmonary disorder (COPD), and cystic fibrosis (CF) in children and adults.⁵ Physicians pay particular attention to patients who already suffer from respiratory diseases, such as CF or asthma, as they could be particularly affected by an additional EV infection.⁶ An increasing number of studies also suggest that respiratory viruses, in particular, EV and RV, contribute significantly to CF pulmonary exacerbations, hospitalization,

decreased lung function, and predisposition to bacterial colonization.⁷ The mechanistic link between viral infections and deterioration of CF lung function is not fully understood, and their impact is probably underestimated, especially in young children.⁸ Despite their high clinical and socioeconomic impact, to date there is no approved antiviral therapy for the prophylaxis and/or treatment of EV infections, and the management of patients is currently limited to symptomatic treatment and supportive care. Therefore, there is an unmet need for broad-spectrum antiviral drugs as a rapid defense strategy against EV infections and virus-related exacerbations.

Nowadays, host factors are considered as very attractive targets for the development of antiviral drugs because they are unlikely to mutate and develop resistance in response to therapy.⁹ Moreover, since viruses belonging to the same genus or family

Received: October 18, 2016

Published: January 25, 2017

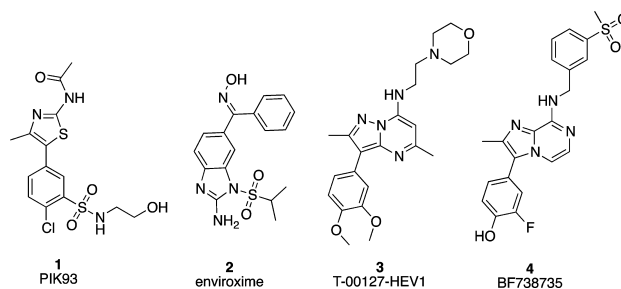
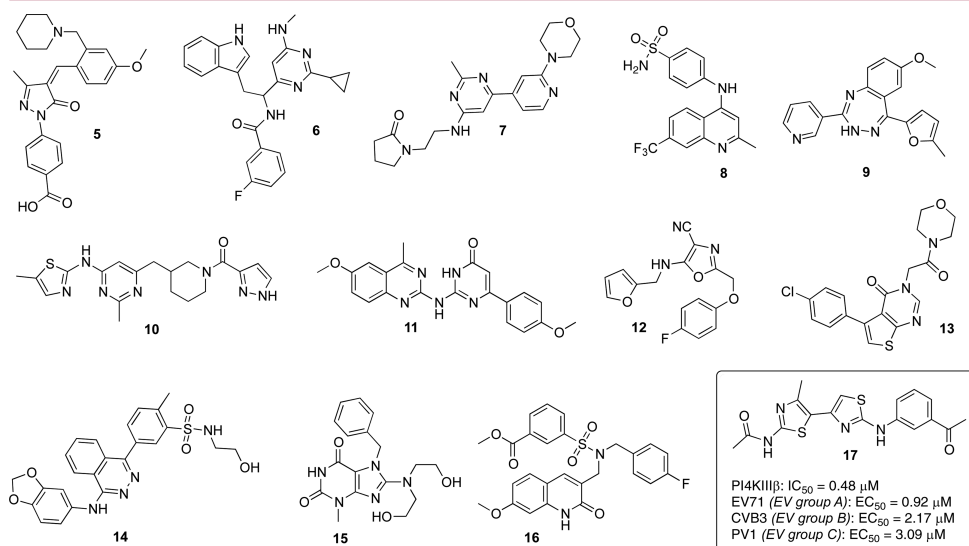
Figure 1. Representative PI4KIII β inhibitors.

Figure 2. Chemical structure of compounds selected by virtual screening and activity profile of the hit compound 17.

usually share the same cellular pathways for replication, targeting a host factor may allow the development of effective broad-spectrum antiviral compounds.¹⁰ Although some toxicity risks may be expected from inhibiting a host factor, it should be kept in mind that most drugs currently used in therapy target host proteins with excellent therapeutic outcomes and acceptable safety profiles. In particular, it has been well documented that the host lipid kinase phosphatidylinositol 4-kinase III β (PI4KIII β) is critical for RNA replication of several EVs.^{11–14} PI4KIII β belongs to the phosphatidylinositol 4-kinases (PI4Ks) that synthesize phosphatidylinositol 4-phosphate (PI4P) from phosphatidylinositol (PI). PI4P is involved in signaling and cellular trafficking mainly at the Golgi and trans-Golgi network (TGN), it contributes to defining the characteristics of plasma membranes, and it activates a variety of ion channels, including CFTR.^{15–18} Four PI4K isoforms have been identified in mammals, classified as type II (PI4KII α and PI4KII β) or type III (PI4KIII α and PI4KIII β) based on their primary sequences and catalytic properties.¹⁹ Type III PI4Ks are hijacked by several

ss(+)RNA viruses (especially from *Flaviviridae*, *Picornaviridae*, and *Coronaviridae* families) to remodel cellular membranes and generate PI4P lipid-enriched organelles specialized for viral replication.²⁰

A few PI4KIII β inhibitors with antiviral activity against a panel of picornaviruses have been reported recently (Figure 1).^{21–23} Generally, chemical inhibition of PI4KIII β does not influence cell viability.²⁴ One possible explanation might be that while the small amounts of PI4P produced by other PI4K isoforms could be enough to support cell trafficking and signaling, it would not be sufficient to sustain viral RNA synthesis.²⁰ A major aim in the development of PI4KIII β inhibitors is to achieve selective inhibition of the α or β isoforms. Among known PI4KIII β inhibitors, compound 1 (PIK93) is about 100-fold more potent against the PI4KIII β isoform, although it also has detectable activity toward PI3-kinases.^{25,26}

Considering the growing need for novel broad-spectrum antivirals to fight emerging epidemics and the link between respiratory viruses and pulmonary exacerbation in CF patients,

our aim was the development of a new class of multitarget agents active both as broad-spectrum antivirals (by targeting PI4KIII β) and as correctors of the F508del-CFTR folding defect responsible for >90% of CF cases. We here report the discovery of the first small-molecule compounds able to simultaneously act as moderately efficacious correctors of the F508del-CFTR folding defect and broad-spectrum antivirals against a panel of EVs (linked to CF pulmonary exacerbations).

RESULTS AND DISCUSSION

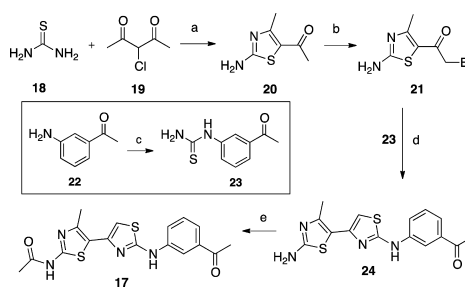
Drug repurposing and polypharmacology are two very attractive approaches in modern drug discovery. The first offers the possibility of recycling known drugs or advanced drug candidates developed for a different disease. The second results in simultaneous action on different targets/diseases with a single, rationally designed drug.^{27,28} In particular, polypharmacology aims at producing multitarget agents whose interference with multiple biochemical pathways offers an advantage—in terms of drug load, efficacy and safety—over combination therapy. This approach is well suited to complex diseases that generally require the simultaneous administration of many different drugs. Considering the increasing number of reports on the connection between EV infections and pulmonary exacerbations in CF patients, we reasoned that an ideal drug candidate for such closely related diseases might be a multitarget agent able to act, at the same time, on proteins/pathways implicated in EV replication (PI4KIII β) and on F508del-CFTR biogenesis. At the beginning of this work, the X-ray structures of the above targets were not available for a structure-based study. We therefore developed a PI4KIII β homology model to be used for the design of PI4KIII β inhibitors, selecting those whose chemical scaffolds resemble known CFTR correctors/potentiators. The structure of the complex of PI3K γ with compound **1** (PDB ID: 2CHZ)²⁶ has been used to build the homology model of PI4KIII β by using Prime software (see [Experimental Section](#)): this structure shows an identity of 30%, a positive of 52% and a score of 322. The presence of **1** in the structure of PI3K γ allowed us to identify its likely binding site in PI4KIII β and hypothesize its binding mode. A 10 ns molecular dynamics simulation on the modeled PI4KIII β protein containing compound **1** was performed using the software Desmond.²⁹ In the latter (equilibrated) part of the trajectory (last 2 ns) 100 frames were extracted and clustered on the basis of RMSD. Five clusters were obtained. All PI4K β inhibitors available in Pubchem³⁰ were docked in the compound **1** binding site of each cluster and the frame with the best correlation between docking score and enzymatic activity was selected for virtual screening. A high-throughput docking (HTD) approach was then applied to the compound **1** binding site in our PI4KIII β model to identify high affinity hits within the Asinex database collection.³¹ Compound selection was based on the ranking score and visual inspection of the PI4KIII β catalytic site, but also took into account the 2D similarity to known CFTR correctors/potentiators. Thirteen commercially available compounds (**5**–**17**, [Figure 2](#)), four of which (**6**, **11**, **16**, and **17**) resemble known CFTR correctors,^{32,33} were selected for biological investigation. These computational results were confirmed on the recently released crystal structure of PI4KIII β cocrystallized with compound **1**, and this structure (PDB ID: 4DOL) was used for all the following simulations.³⁴

These commercially available compounds were then tested both against the PI4KIII β enzyme and in a virus-cell-based replication assay. In particular these compounds were evaluated

for antiviral activity against a panel of EVs that are representative of all major species: EV group A (EV71), group B (coxsackievirus B3, CVB3, and echovirus 11, ECHO11), group C (poliovirus 1, PV1), group D (enterovirus 68, EV68), rhinovirus group A (RV02) and rhinovirus group B (RV14). Among the selected compounds, only the bithiazole **17** showed activity in cell-free and cell-based assays and possesses a chemical scaffold (the bithiazole) of a known family of CFTR correctors ([Figure 2](#)).^{33,35} Compound **17** was therefore selected as a promising starting point for further structure-based optimization.

Chemistry. Compound **17** was initially resynthesized to validate the biological activity of the commercial sample and to set up a synthetic protocol for its chemical diversification starting from cheap and commercially available building blocks ([Scheme 1](#)).

Scheme 1^a

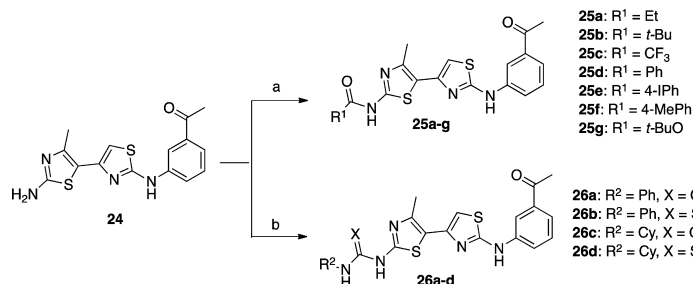


^aReagents and conditions: (a) EtOH, reflux, 12 h, 95%; (b) 48% aqueous HBr, Br₂, 1,4-dioxane, 60 °C, 3 h, 90%; (c) (i) benzoyl isothiocyanate, DCM, rt, 12 h, (ii) NaOH 1 N, THF, reflux, 3 h, 72%; (d) EtOH, reflux, 1 h, 84%; (e) acetyl chloride, Et₃N, DCM, rt, 15 h, 77%.

Thiourea **18** was condensed with 3-chloro-2,4-pentanedione **19** in refluxing ethanol to afford 1-(2-amino-4-methylthiazol-5-yl)ethanone **20** in nearly quantitative yield,³⁶ followed by bromination α to the carbonyl to give compound **21**. The subsequent condensation of intermediate **21** with 1-(3-acetylphenyl)thiourea **23** gave bithiazole **24** that was finally N-acetylated to obtain the desired compound **17**. Thiourea **23** was synthesized by the reaction of 3'-aminoacetophenone **22** with benzoyl isothiocyanate, followed by a basic hydrolysis to remove the benzoyl group.³⁷

Docking studies on compound **17** (see [Molecular Modeling and SAR](#) section) showed a pattern of interactions within the ATP-binding pocket of PI4KIII β very similar to that of the reference compound **1**. The proposed binding mode of **17** suggested that two main portions of this molecule could be functionalized to explore the biologically relevant chemical space: (i) the 2-amino group on the 4-methylthiazole ring (left part) and (ii) the phenyl ring (right part). We first explored the chemical space around the left part of compound **17**, introducing bulkier groups and urea/thiourea functions in place of the acetamide moiety. The intermediate **24** represents in fact an advanced intermediate that could be easily functionalized on the 2-amino group to give a series of functionalized derivatives (**25a–g** and **26a–d**) ([Scheme 2](#)).

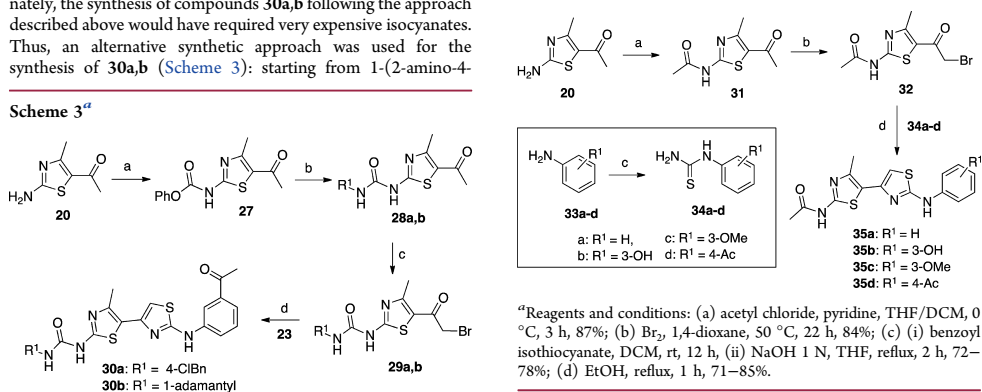
Compound **24** was first reacted with different acyl chlorides or anhydrides to obtain compounds **25a–g**, while the urea/thiourea

Scheme 2^{4a}

^{4a}Reagents and conditions: (a) method A (for **25a–c**), R¹COCl (for **25a,b**) or (R¹CO)₂O (for **25c**), Et₃N, DCM, rt, 12–15 h, 65–80%; method B (for **25d–f**) R¹COCl, Et₃N, DCM, reflux, 15 h, 65–75%; method C (for **25g**), (R¹CO)₂O, Et₃N, DMF, 50 °C, 12 h, 63%; (b) R²NCX, pyridine, reflux, 12–18 h, 52–69%.

derivatives **26a–d** were synthesized by reacting **24** with the appropriate isocyanates/isothiocyanates. We also decided to replace the acetamide moiety of compound **17** with chain-extended ureidic groups for the SAR development. Unfortunately, the synthesis of compounds **30a,b** following the approach described above would have required very expensive isocyanates. Thus, an alternative synthetic approach was used for the synthesis of **30a,b** (Scheme 3): starting from 1-(2-amino-4-

reacting **32** with substituted thioureas **34a–d**, previously synthesized from the corresponding amines **33a–d**.

Scheme 4^{4a}

^{4a}Reagents and conditions: (a) diphenyl carbonate, NaH, DMF, rt, 30 min, 67%; (b) 4-chlorobenzylamine (for **28a**) or 1-adamantylamine (for **28b**), THF, 50 °C, 5–6 h, 61–93%; (c) 48% aqueous HBr, Br₂, 1,4-dioxane, 60 °C, 3 h, 88–92%; (d) EtOH, reflux, 1 h, 78–83%.

^{4a}Reagents and conditions: (a) acetyl chloride, pyridine, THF/DCM, 0 °C, 3 h, 87%; (b) Br₂, 1,4-dioxane, 50 °C, 22 h, 84%; (c) (i) benzoyl isothiocyanate, DCM, rt, 12 h, (ii) NaOH 1 N, THF, reflux, 2 h, 72–78%; (d) EtOH, reflux, 1 h, 71–85%.

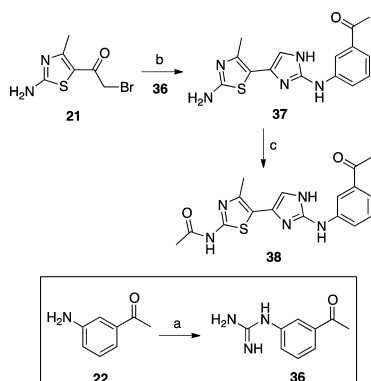
methylthiazol-5-yl)ethanone **20**, reaction with diphenyl carbonate gave good yields of the desired phenyl carbamate **27** that reacted readily with the appropriate amines to give the urea intermediates **28a,b**.³⁸ Similar to the synthesis of compound **17**, the bromination α to the carbonyl and the subsequent condensation of intermediates **29a,b** with the 1-(3-acetylphenyl)thiourea **23** gave the desired compounds **30a,b**.

We next explored the right part of compound **17**, keeping the 2-acetamido group on the left part of the molecule unchanged and modifying the substitution pattern of the phenyl ring on the right part. Since the acetamide moiety on the left part of the molecule was conserved, intermediate **20** was conveniently acetylated before the bromination α to the carbonyl (Scheme 4). Final compounds **35a–d** were quickly obtained in good yields by

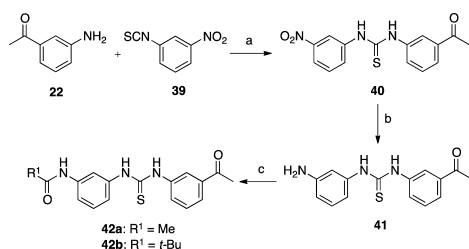
Then we decided to modify the central bithiazole scaffold of the hit compound **17**, to get additional SAR information. As described in Scheme 5, we first introduced an imidazole ring by reacting intermediate **21** with the 1-(3-acetylphenyl)guanidine **36**, obtained by treating 3'-aminoacetophenone **22** with cyanamide.³⁹ Compound **38** was thus synthesized by acylation of the intermediate **37** with acetyl chloride.

A scaffold hopping approach (FAF-drugs2 server)⁴⁰ was also employed to identify alternatives to the bithiazole scaffold: among the molecules proposed by the software, the asymmetrical *N,N'*-diarylthiourea scaffold was considered the most promising on the basis of its synthetic accessibility and the antiviral activity of some closely related analogues reported in the literature.⁴¹ Intermediate **41** was easily obtained by addition of 3'-aminoacetophenone **22** to 3-nitrophenyl isothiocyanate **39**, followed by reduction of the nitro group with iron powder in acidic ethanol (Scheme 6). The subsequent acylation of the amino group led to final compounds **42a,b**.

Moreover we noted high chemical similarity between compound **17** and compound **46**, a known inhibitor of DC-

Scheme 5^a

^aReagents and conditions: (a) cyanamide, HNO₃, EtOH/H₂O, reflux, 24 h, 73%; (b) Et₃N, EtOH, reflux, 12 h, 82%; (c) acetyl chloride, Et₃N, DCM, rt, 8 h, 47%.

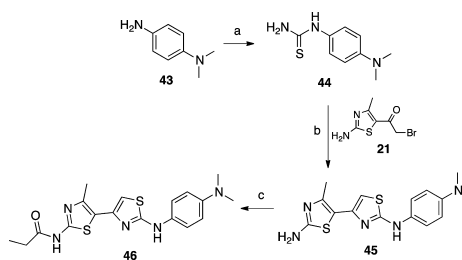
Scheme 6^a

^aReagents and conditions: (a) DCM, rt, 18 h, 88%; (b) Fe, HCl, EtOH, reflux, 2 h, 75%; (c) acetyl chloride (for 42a) or trimethylacetyl chloride (for 42b), pyridine, THF, rt, 2 h, 67–69%.

SIGN (dendritic cell (DC)-specific intercellular adhesion molecule-3 grabbing nonintegrin).⁴² The role of DC-SIGN in the binding and transmission of different pathogens, including EVs, has been well investigated.⁴³ So we decided to evaluate the antiviral effect of compound 46 in a virus-cell-based assay and its activity on PI4KIII β . As described in Scheme 7, compound 46 was synthesized following the procedure previously reported for compound 17.

Finally, we decided to prepare two compounds (related to the hit 17) known in the CFTR field to evaluate the potential role of the CFTR channel in viral replication: (i) compound 47a, which is active in correcting the F508del-CFTR defect and, (ii) compound 47b, which is inactive in correcting the F508del-CFTR defect (Figure 3). Compound 47a,b were synthesized following the procedure reported in the literature.⁴⁴

Biology. All the synthesized compounds were initially evaluated for their inhibitory potency against PI4KIII β kinase in vitro and for their cell-based antiviral activity: EV71 was used as the primary target for SAR exploration since compound 17 revealed the best and most reproducible antiviral activity against this virus. In particular, the antiviral activity against EV71 was evaluated in EV71-induced CPE-reduction assay in rhabdosar-

Scheme 7^a

^aReagents and conditions: (a) (i) benzoyl isothiocyanate, DCM, rt, 12 h, (ii) NaOH 1 N, THF, reflux, 3 h, 80%; (b) EtOH, reflux, 30 min, 77%; (c) propionyl chloride, Et₃N, DCM, rt, 8 h, 68%.

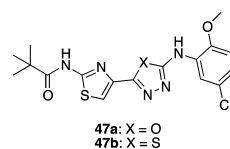


Figure 3. Chemical structures of compounds 47a,b.

coma (RD) cells. Both the EC₅₀ values and the CC₅₀ values were measured. Uninfected, treated cells were also inspected under the microscope to evaluate whether the compounds altered normal cell morphology. The EC₅₀ and CC₅₀ values allowed us to calculate the selectivity index (SI), defined as CC₅₀/EC₅₀. Compound 3 was used as a positive control. Results are summarized in Table 1.

A close correlation between the antiviral activity measured in the cell-based assay and the inhibitory potency of the PI4KIII β kinase was observed, with only a few exceptions. The best results were obtained via modifying the left part of the molecule. In particular, compounds 25a,b, bearing respectively a propanamide and a pivalamide moiety instead of the acetamide function of compound 17, showed a very promising antiviral activity.

Compounds 25a,b inhibited PI4KIII β and exhibited a significant antiviral effect at sub-micromolar concentrations, demonstrating a better activity than compound 17. Compound 25g, characterized by the Boc amino group, proved to be the most interesting compound of the entire series showing the highest selectivity index in the EV71 cell-based assay. Also changing the right portion of hit compound 17 gave interesting results (compounds 35a,c,d). The central bithiazole scaffold proved to be essential for antiviral activity, as changing it gave inactive compounds (compounds 38, 42a,b). Finally, the reported compounds 46, 47a,b were devoid of antiviral activity and PI4KIII β inhibition activity.

On the basis of these activity data, and considering that the SI of a promising antiviral candidate should be at least greater than 10, compounds 17, 25a–d, and 25g were selected for further studies. The broad-spectrum activity of the six selected compounds was evaluated against a panel of EVs representative of all major groups: EV group B (coxsackievirus B3 and echovirus11, ECHO11), group C (poliovirus 1), group D (enterovirus 68), rhinovirus group A (RV02), and rhinovirus group B (RV14) (see the Experimental Section for details). Results are reported in Table 2. The selected compounds showed

Table 1. Activity of Synthesized Derivatives in PI4KIII β Inhibition Assay and in Virus-Cell-Based EV71 Assay

compd	PI4K III β IC ₅₀ (μ M) ^a	EV71 EC ₅₀ (μ M)	EV71 CC ₅₀ (μ M) ^b	EV71 CC ₅₀ (μ M) ^c	SI ^d	SI ^d
17	0.48	0.92 \pm 2.75	16.5 \pm 9.04	9.73 \pm 0.87	17.9	10.6
25a	0.27	0.38 \pm 0.10	10.1 \pm 4.82	6.37 \pm 2.46	26.6	23.6
25b	0.32	0.27 \pm 0.05	7.94 \pm 1.24	8.83 \pm 0.89	29.4	32.7
25c	21.89	2.0 \pm 0.95	25.8 \pm 5.06	30.1 \pm 9.93	12.9	15.0
25d	18.85	0.51 \pm 0.14	5.75 \pm 2.12	11.8 \pm 4.56	11.3	23.1
25e	>50	>44.6	ND ^e	ND	ND	ND
25f	>50	>55.7	ND	ND	ND	ND
25g	4.67	1.42 \pm 0.04	42.3 \pm 4.94	101.0 \pm 15.8	29.7	71.1
26a	7.69	NA ^f	ND	ND	ND	ND
26b	>50	NA	ND	ND	ND	ND
26c	1.82	2 \pm 0.04	8.87 \pm 3.85	ND	4.4	ND
26d	>50	NA	ND	ND	ND	ND
30a	3.95	4.77 \pm 0.28	20.9 \pm 6.97	ND	4.4	ND
30b	12.40	NA	ND	ND	ND	ND
35a	2.48	1.93 \pm 0.81	18.6 \pm 6.01	ND	9.64	ND
35b	2.63	NA	ND	ND	ND	ND
35c	1.55	1.2 \pm 0.16	9.17 \pm 0.85	ND	5.9	ND
35d	3.71	0.68 \pm 0.04	5.59 \pm 0.32	ND	8.2	ND
38	>50	>90.2	85.7	64.2	ND	ND
42a	NA	NA	ND	ND	ND	ND
42b	NA	NA	ND	ND	ND	ND
46	50.00	8.58 \pm 0.77	51.6 \pm 27.1	142.0 \pm 62.8	6	ND
47a	NA	NA	ND	ND	ND	ND
47b	NA	NA	ND	ND	ND	ND
3 ^g	0.06	0.73	>125			

^aValues are the mean of at least three independent experiments. ^bCC₅₀ values were assessed by MTS method. ^cCC₅₀ values were determined by microscopically detectable alteration of cell morphology. ^dSelectivity index (SI = CC₅₀/EC₅₀). ^eND = not determined. ^fNA = not active. ^gRef 13.

Table 2. Evaluation of the Broad-Spectrum Antiviral Activity of the Most Potent Derivatives against a Representative Panel of Enteroviruses

compd	CVB3		ECHO11		PV1		EV68		RV14		RV02	
	EC ₅₀ (μ M)	CC ₅₀ (μ M)	EC ₅₀ (μ M)	CC ₅₀ (μ M)	EC ₅₀ (μ M)	CC ₅₀ (μ M)	EC ₅₀ (μ M)	CC ₅₀ (μ M)	EC ₅₀ (μ M)	CC ₅₀ (μ M)	EC ₅₀ (μ M)	CC ₅₀ (μ M)
17	2.17	101 \pm 33.6	1.57 \pm 0.23	>268	3.09	>269	NA ^a	ND ^b	>268	ND	NA ^b	ND
25a	2.16	89.1 \pm 16.2	0.97	12 \pm 4.07	<1.52	5.49 \pm 1.42	NA	ND	NA	ND	>259	ND
25b	ND	20.9 \pm 3.83	0.72 \pm 0.05	5.07 \pm 1.24	<1.41	5.07 \pm 1.3	1.38	3.09	4.85 \pm 1.09	ND	2.01 \pm 0.05	ND
25c	3.87 \pm 0.23	58.8 \pm 7.14	3.51	29.3 \pm 1.78	2.86 \pm 0.36	30.3 \pm 3.66	ND	ND	10.6 \pm 0.7	ND	10.6 \pm 0.2	ND
25d	2.19 \pm 0.23	45.1 \pm 4.44	1.77 \pm 0.13	145 \pm 27.6	2.23 \pm 0.4	145 \pm 27.6	NA	ND	>230	ND	2.05 \pm 0.36	ND
25g	2.74 \pm 0.17	80.1 \pm 6.97	2.93	124 \pm 7.94	13.3 \pm 1.9	124 \pm 7.94	ND	ND	>232	ND	ND	ND

^aNA = not active. ^bND = not determined.

micromolar and sub-micromolar activity against different EVs within the tested panel. In addition, the antiviral activity of the less toxic compound **25g** was confirmed against a representative panel of EV71 clinical isolates. As shown in Table 3, we could

Table 3. Evaluation of the Antiviral Activity of Compound 25g against EV71 Clinical Isolates

Genogroup	strain	Genbank	EC ₅₀ (μ M) ^a
			compd 25g
B2	11316	AB575927	<1.39
B5	TW/96016/08	GQ231942	21.00
	TW/70902/08	GQ231936	3.58
C2	H08300 461#812		0.97
C4	TW/1956/05	GQ231926	<1.39
	TW/2429/04	GQ231927	1.17

^aAll values are based on at least three independent dose-response curves.

confirm the activity of compounds **25g** against the clinically relevant EV71 specimens. Only the (sub)genogroup B5 appeared to be less sensitive. Furthermore, we evaluated the lipid kinase isoform selectivity of our best PI4KIII β inhibitors by testing them in an in vitro inhibition assay on the related enzyme PI4KIII α and PI3K- α /p85 α (Table 4).

Results showed a higher specificity of the tested thiazole derivatives for the PI4KIII β isoform with poor inhibition of both PI4KIII α and PI3K- α /p85 α at 100 μ M concentration of each compound. The specificity of compound **25g** was also tested on a small panel of unrelated kinases: it shows only a low inhibitory effect on Src and CDK6. Despite the latter enzymes being involved in cell cycle regulation and representing common targets of antitumor compounds, **25g** did not show any toxicity or morphology alteration at antiviral concentration in the tested cell lines. In addition, recent studies indicated that Src inhibitors have no effect on EV71 replication,⁴⁵ while CDK6 seems to be down-regulated in response to EV71 infection.⁴⁶ Finally, compounds reported in Table 4 were evaluated for their CFTR

Table 4. Inhibitory Effect of Selected Compounds against Members of PIK Family and Profiling of Compound 25g against a Small Panel of Unrelated Kinases

compd	PI4KIII β	PI4KIII α	PI3K- α /p85 α	compd	kinase	% residual activity at 100 μ M ^a
	IC ₅₀ (μ M) ^a	% residual activity at 100 μ M ^a				
17	0.48	52	37	25g	Src FL	32
25a	0.27	72	40		GSK3 β	79
25b	0.32	71	93		Hck FL	100
25c	21.89	73	85		FAK	82
25d	18.85	81	54		DYRK1A	88
25g	4.67	69	64		ABL FL	53
35a	2.48	58	81		FLT3	59
35c	1.55	71	51		CDK2/cA2	62
35d	3.71	73	100		CDK9/cT1	57
					CDK9/cK	49
					CDK6/cD1	25
					Pim1	70

^aValues are the mean of two independent replicates.

corrector/potentiator activity, to identify molecules that may be endowed with dual antiviral/CFTR modulator activity. As shown in Figure 4A, some of the compounds (25a, 25d, 25g) acted as CFTR correctors, increasing steady-state levels of F508del-CFTR at the plasma membrane after chronic (24 h) incubation. Compound 48 (Lumacaftor), the leading corrector drug,⁴⁷ was used as a benchmark. This increased CFTR plasma membrane density was measured with a recently developed assay exploiting a CFTR fusion to a pH-sensitive protein.⁴⁸ The improvement in biogenesis also led to increased anion permeability, estimated from fluorescence quenching of a CFTR-fused YFP probe following extracellular I⁻ addition (Figure 4B). None of the compounds acted as "potentiators" rapidly increasing anion permeability, when added only immediately prior to I⁻ addition (Figure 4C). The approved potentiator drug 49 (Ivacaftor) was used as a comparison.⁴⁹ Overall, the drug-induced changes in the iodide entry rate and in membrane density followed similar patterns, suggesting that the chemically corrected molecules of F508del-CFTR that reached the plasma membrane displayed an ion-channel function similar to those corrected by treatment with 48. However, compound 25d appears to increase CFTR membrane density more than expected from its effect on anion permeability (Figure 4D). Further studies will be required to understand the underlying mechanism. Overall, the collected biological data indicate that a fine chemical tuning of the bithiazole substituents is needed to generate compounds able to specifically inhibit the PI4KIII β kinase and block the replication of different EVs while also correcting the F508del-CFTR folding defect. It is interesting to note that the most promising CFTR correctors (25a, 25d, 25g) are also the most active broad-spectrum antivirals and represent the first example of multitarget agents for tightly associated pulmonary diseases like EV infection and CF.

Molecular Modeling and SAR. The hit compound 17 was docked with the Glide software⁵⁰ (SP) in the ATP binding site of the PI4KIII β crystal structure (PDB ID: 4D0L)³⁴ centering the grid on compound 1. The predicted binding mode and interaction profile of compound 17 is very similar to that of compound 1 (Figure 5). The NH-acetamide moiety of 17 is hydrogen bonded to VAL598, which also interacts with the thiazole nitrogen. The thiazole ring is involved in a Pi-Pi stacking with TYR583, while the phenyl ring is involved in a Pi-cation interaction with LYS549. The O carbonyl moiety is hydrogen bonded to LYS377. Moreover, the binding mode is

completed by a series of hydrophobic interactions involving LEU383, ALA602, VAL599, VAL602, LEU663, ILE595, TYR583, ILE671, ILE673, PRO381, and LEU374. The first series of derivatives of the hit compound 17 encompasses different substitution on the left part of the molecule (right part as per Figure 5–7 representation) by replacing the methyl group of the acetamide moiety with different groups. Changing the methyl of the acetamide with an ethyl or *tert*-butyl group (25a,b) caused a 2-fold increase of potency, but the substitution with more hydrophobic and therefore more sterically bulky groups first reduced the potency (25d) and then led to a complete loss of activity (25e,f). The limit seems to be a *tert*-butoxycarbonyl group (25g) which still maintains low micromolar activity (Figure 6).

The substitution of the acetamide methyl with a CF₃ (25c) weakened the inhibition (45-fold decrease) not due to steric reasons, but probably because of the electron withdrawing properties of the CF₃ group. Changing the acetamide moiety with a ureidic moiety caused a slight decrease in potency (26a,c and 30a,b). The ureidic portion seems to interact with a double hydrogen bond to VAL598, but at the same time, the hydrophobic NH substituent moves away from the protein resulting in a solvation penalty (Figure 6). Finally, modifying a ureidic group with a thioureidic moiety caused a complete loss of activity (26b,d).

The second series of derivatives of the hit compound 17 comprises different substitutions on the right part of the molecule (left part as per Figures 5–7 representation) by changing the substitution pattern of the phenyl ring. A change in the position of the acetyl group reduces the potency by about 10-fold (35d), and the same happens by introducing hydroxy and methoxy groups in the meta position (35b,c). The precise positioning of the hydrogen-bond acceptor on the phenyl ring seems therefore important in improving the affinity for the enzyme. Surprisingly, the deletion of the ketonic group reduces but does not abolish activity (35a). The lack of the substituent on the phenyl ring deletes a hydrogen bond, but allows optimization of the other interactions, in particular, the Pi-cation with lysine 549.

The last series of derivatives of the hit compound 17 encompasses modifications of the bithiazole scaffold and closely related analogues reported as DC-SIGN inhibitors and CFTR correctors. Replacement of the thiazole group of compound 17 with an imidazole (38) or conversion of the bithiazole scaffold

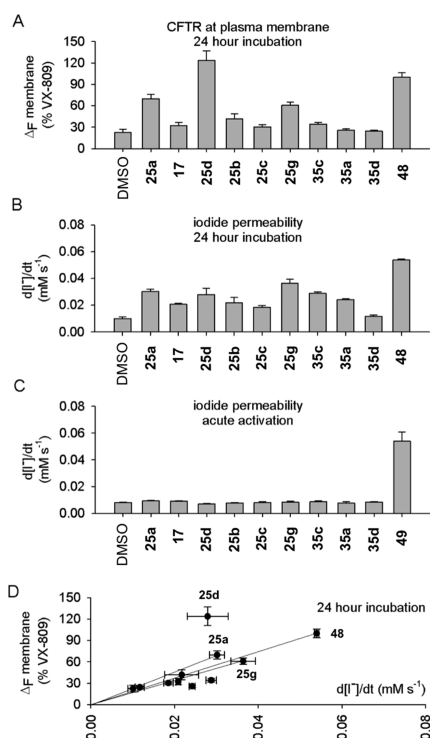


Figure 4. Effects of selected compounds on CFTR biogenesis and function. All treatments were carried out alongside low temperature incubation, known to improve F508del-CFTR membrane-localization and used to increase the fluorescence signal. (A) F508del-CFTR-pHTomato present at the plasma membrane was quantified following 24 h incubation in 10 μ M of each drug. Incubation with 48 (Lumacaftor) was assessed in parallel, as a positive control. (B) Anion permeability quantified using a YFP-F508del-CFTR probe following 24 h treatment as in (A). (C) Compounds (10 μ M) do not cause an immediate change in anion permeability. Potentiator compound 49 (Ivacaftor) was used as a positive control. (D) For most compounds, there is a similar ratio describing an increase in membrane density over anion permeability as caused by 48 (Lumacaftor).

into a N,N' -diarylthiourea (42a,b) changes the binding mode and abolishes the activity. Finally, also the DC-SIGN inhibitor 46 and CFTR correctors 47a,b presented a suboptimal interaction profile with PI4KIII β and resulted in a complete loss of activity. As reported by Warren et al.,⁵¹ docking programs and scoring functions present a few limitations in correlating subtle structural differences of active ligands with their enzymatic activity. This error is quite limited within homologous series of compounds, but it can be very important for structurally unrelated compounds.⁵² Our docking studies were in fact able to distinguish between active and inactive compounds, but it is no coincidence that the reference compound 3, whose scaffold is very different from those of our series, showed a docking score that is not in line with its enzymatic potency (Table S). The most active compounds 17, 25a, and 25b also showed the best

specificity for PI4KIII β over PI4KIII α , which seems to depend on the steric hindrance of the acetamide substitution. In fact, considering compounds 17, 25a, 25b, 25g, and 25d that differ only for the bulkiness of the amide substituents in position C2 of the thiazole (methyl, ethyl, *tert*-butyl, *tert*-butoxy, and phenyl, respectively), the affinity for PI4KIII α decreases going from 17 to 25d (see Table 4).

The higher the bulkiness in C2 of the thiazole, the lower the affinity for PI4KIII α over PI4KIII β with the phenyl substituent (25d) representing the highest tolerated hindrance after which the inhibition of PI4KIII β is also compromised. The reason for the specificity of these compounds toward PI4KIII β seems to depend on the different opening (compared to the α isoform) of a specific loop that in the β isoform goes from ILE595 to ILE604 (Figure 7). In fact, in this portion of protein, the sequence of PI4KIII β resembles more the sequence of PI3K (α , γ , and δ) than the sequence of PI4KIII α . In particular, the presence of a cysteine residue in position 30 of PI4KIII α (corresponding to proline 597 in PI4KIII β) could change the fold of this "selectivity loop".

CONCLUSIONS

An increasing number of reports suggest a causal link between EV infections and pulmonary exacerbations in CF patients. We report the discovery of a new class of multitarget agents active as broad-spectrum antivirals and correctors of the F508del-CFTR folding defect. To identify these drug candidates, we first carried out a virtual screening on the PI4KIII β (a host protein involved in EV replication) catalytic site to select commercially available compounds: our choice was based on the best-predicted affinity for the target kinase and 2D similarity (in a few cases) to known CFTR correctors/potentiators. Among the selected compounds, hit 17 showed activity in cell-free PI4KIII β inhibition assay and cell-based EV replication assays and was therefore considered a promising starting point for further structure-based optimization. A small collection of analogues of compound 17 was then designed, synthesized, and biologically evaluated for their (i) activity against panel of EVs representative of all major groups; (ii) inhibition of lipid kinases PI4KIII β , PI4KIII α , and PI3K- α /p85 α ; (iii) corrector/potentiator activity on F508del-CFTR. Three compounds (25a, 25d, 25g) were finally identified as novel multitarget agents able to act as broad-spectrum antivirals (EV family) and as correctors of F508del-CFTR folding defect. These compounds represent a valuable starting point to develop a novel polypharmacological approach for the treatment of closely related pulmonary diseases such as CF and EV infections with a single pill.

EXPERIMENTAL SECTION

Molecular Modeling. Homology Modeling. The structure of PI4KIII β was built with the Prime⁵³ 38013 software on the basis of the crystal structure 2CHZ using ClustalW for sequence alignment and knowledge-based as the building method. The structure of PI4KIII α was built with the online server 3D-JIGSAW⁵⁴ on the basis of the crystal structure 4D0L.

Molecular Dynamics. The structure of modeled PI4KIII β was aligned to the 2CHZ structure. Compound 1 was extracted from 2CHZ and was manually introduced in the structure of PI4KIII β . A molecular dynamics simulation of the resulting complex was performed using Desmond v40013. The complex was neutralized using sodium counterions. The complex and the counterions were immersed in a orthorhombic periodic SPC water bath that extended about 10 Å in each direction. After an initial default relaxation protocol, a MD production run was performed for 10 ns with a time step of 2 fs.

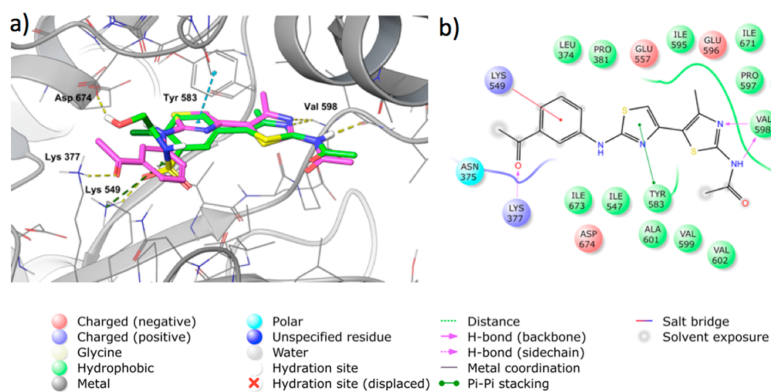


Figure 5. (a) Predicted binding mode of the hit 17 (magenta sticks) superimposed to compound 1 (green sticks) into the binding site of PI4KIII β . (b) 2D ligand interaction diagram of 17.

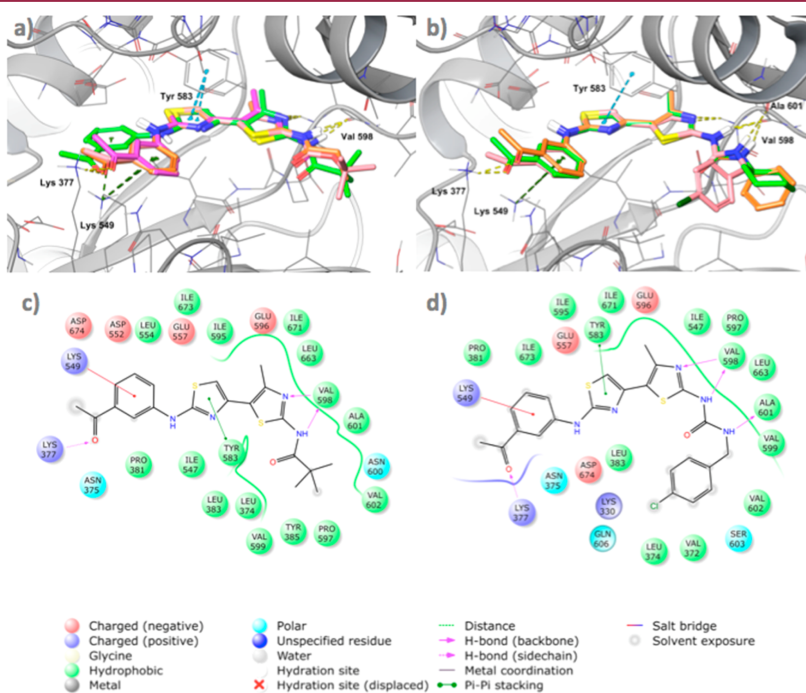


Figure 6. (a) Superimposed binding modes of compounds 17 (purple sticks), 25a (orange sticks), 25b (green sticks), and 25g (pink sticks) into the binding site of PI4KIII β . (b) Superimposed binding modes of compounds 26a (orange sticks), 26c (green sticks), and 30a (pink sticks) into the binding site of PI4KIII β . (c) 2D ligand interaction diagram of 25b. (d) 2D ligand interaction diagram of 30a.

Virtual Screening. From the last 2 ns of the dynamics simulation 100 frames were extracted and clustered on the basis of RMSD. Five clusters were generated. The protein representative of each cluster was processed with the Schrödinger Suite 2014-3⁵⁵ Protein Preparation Wizard tool. On each structure a grid was generated with the software

Glide 65013 centering the grid on compound 1, and then all PI4KIII β ligands available from the Pubchem database were docked with the SP protocol. Structures were selected for virtual screening on the basis of their enrichment factor. The Mid Asinx database was extracted from the ZINC database⁵⁶ and docked in the binding site of compound 1

Table 5. Correlation between IC₅₀ and Docking Score for the Synthesized Compounds

compd	PI4K IIIβ IC ₅₀ (μM) ^a	docking score ^b	compd	PI4K IIIβ IC ₅₀ (μM) ^a	docking score ^b
35d	3.71	-8.297	25e	>50	-7.431
30b	12.40	-8.222	26d	>50	-7.4
26a	7.69	-8.172	25f	>50	-7.356
26c	1.82	-8.108	38	>50	-7.355
17	0.48	-8.035	42a	>50	-7.251
25a	0.27	-8.012	26b	>50	-7.144
25d	18.85	-7.983	42b	>50	-7.052
30a	3.95	-7.97	25c	21.90	-6.678
35b	2.63	-7.726	3 ^c	0.06	-6.553
46	50.00	-7.644	47b	>50	-6.424
25g	4.67	-7.63	47a	>50	-6.148
35c	1.55	-7.605	25e	>50	-7.431
35a	2.48	-7.6			
25b	0.32	-7.484			

^aValues are the mean of at least three independent experiments.

^bDocking score was calculated by the software Gold and expressed as kcal/mol. ^cRef 13.

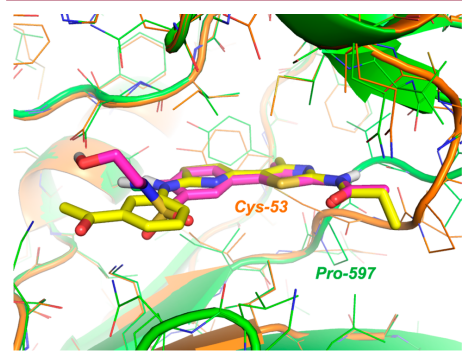


Figure 7. Observed binding mode of 25a (yellow sticks) superimposed to compound 1 (magenta sticks) into the binding site of PI4KIIIβ (green ribbons). The orange ribbons represent the modeled structure of PI4KIIIα.

using compound 1 as the center of the grid. The software Glide 65013 with the SP protocol was used for high throughput docking. The best 1000 compounds in terms of the docking score were selected and submitted to one more docking cycles of docking with the XP protocol. On the basis of the docking score and a visual inspection, 25 compounds were selected and 13 compounds were purchased.

Ligand Preparation. Ligands were prepared with the LigPrep⁵⁷ tool available in the Schrödinger Suite 2015-4. Ionization states were generated at pH 7.0 ± 2.0 with Epik.

Ligand Docking. The X-ray coordinates of PI4KIIIβ in complex with compound 1 were extracted from the Protein Data Bank (PDB code 4D0L). The structure was then processed with the Schrödinger Suite 2015-4 Protein Preparation Wizard tool.⁵⁸ The A Chain was selected, water molecules were removed, and an exhaustive sampling of the orientations of groups, whose hydrogen bonding network needs to be optimized, was performed. Finally, the protein structure was refined to relieve steric clashes with a restrained minimization with the OPLS3 force field⁵⁹ until a final RMSD of 0.30 Å with respect to the input protein coordinates.

Docking studies were performed using Glide⁶⁰ 69017 with the SP protocol. The protein structure, prepared as described above, was used

to build the energy grid. The enclosing box was centered on the cocrystallized ligand. All parameters were set to their default value. The docking protocol was validated by redocking the cocrystallized ligand (compound 1).

Chemistry. General. All commercially available chemicals were purchased from both Sigma-Aldrich and Alfa Aesar and, unless otherwise noted, used without any previous purification. Solvents used for workup and purification procedures were of technical grade. Dry solvents used in the reactions were obtained by distillation of technical grade materials over appropriate dehydrating agents. Reactions were monitored by thin layer chromatography on silica gel-coated aluminum foils (silica gel on Al foils, SUPELCO Analytical, Sigma-Aldrich) at 254 and 365 nm. Where indicated, products were purified by silica gel flash chromatography on columns packed with Merck Geduran Si 60 (40–63 μm). ¹H and ¹³C NMR spectra were recorded on BRUKER AVANCE 300 MHz and BRUKER AVANCE 400 MHz spectrometers. Chemical shifts (δ scale) are reported in parts per million relative to TMS. ¹H NMR spectra are reported in this order: multiplicity and number of protons; signals were characterized as *s* (singlet), *d* (doublet), *t* (triplet), *q* (quadruplet), *m* (multiplet), and *bs* (broad signal). ESI-mass spectra were recorded on an API 150EX apparatus and are reported in the form of (*m/z*). Elemental analyses were performed on a PerkinElmer PE 2004 elemental analyzer. Melting points were taken using a Gallenkamp melting point apparatus and were uncorrected. All final compounds showed chemical purity ≥95% as determined by elemental analysis data for C, H, and N (within 0.4% of the theoretical values).

Synthesis of *N*-(2-((3-Acetylphenyl)amino)-4'-methyl-[4,5'-bithiazol]-2'-yl)acetamide (17). Et₃N (84 μL, 0.60 mmol) was added to a stirred suspension of intermediate 24 (100 mg, 0.30 mmol) in dry DCM (4 mL) at 0 °C. After 15 min acetyl chloride (32 μL, 0.45 mmol), diluted in dry DCM (0.5 mL), was added dropwise. The resulting solution was warmed to room temperature and stirred for 15 h. Next, H₂O and DCM were added and the aqueous phase was extracted twice with DCM. The combined organic phases were washed with brine, dried over Na₂SO₄ and evaporated. The crude was purified by flash chromatography using DCM/MeOH (98/2) as eluent to afford compound 17 as a yellow solid. Yield 77%; mp 244–246 °C. MS (ESI) [*M* + *H*]⁺: 373.3 *m/z*. ¹H NMR (DMSO-*d*₆ 300 MHz): δ 2.14 (s, 3H), 2.51 (s, 3H), 2.63 (s, 3H), 6.95 (s, 1H), 7.48 (t, 1H, *J* = 7.9 Hz), 7.56 (d, 1H, *J* = 7.9 Hz), 7.77 (d, 1H, *J* = 7.9 Hz), 8.51 (s, 1H), 10.56 (s, 1H), 12.06 (s, 1H). ¹³C NMR (DMSO-*d*₆ 100.6 MHz): δ 17.56, 22.92, 27.42, 103.25, 116.75, 120.52, 121.44, 121.65, 129.79, 138.11, 141.81, 143.21, 143.29, 155.58, 162.92, 168.73, 198.28. Anal. (C₁₇H₁₆N₄O₂S₂) C, H, N.

Synthesis of 1-(2-Amino-4-methylthiazol-5-yl)ethanone (20). A solution of thiourea 18 (283 mg, 3.72 mmol) and 3-chloro-2,4-pentanedione 19 (419 μL, 3.72 mmol) in ethanol (20 mL) was heated at reflux for 12 h, and then the reaction mixture was cooled down to 0 °C. The precipitate was separated by filtration over a Buchner funnel and washed with cold ethanol and ether to afford the product 20 as a white solid. Yield 95%. MS (ESI) [*M* + *H*]⁺: 157.2 *m/z*. ¹H NMR (DMSO-*d*₆ 400 MHz): δ 2.44 (s, 3H), 2.52 (s, 3H), 9.49 (bs, 2H).

Synthesis of 1-(2-Amino-4-methylthiazol-5-yl)-2-bromoethanone (21). A suspension of intermediate 20 (500 mg, 3.20 mmol) in 48% HBr solution in water (10 mL) was warmed to 60 °C. A solution of Br₂ (148 μL, 2.88 mmol) in 1,4-dioxane (10 mL) was added dropwise, and the reaction mixture was heated at 60 °C for 3 h. After being cooled to room temperature, saturated aqueous NaHCO₃ solution and ethyl acetate were added, and the aqueous phase was extracted three times with ethyl acetate. The combined organic phases were washed with brine, dried over Na₂SO₄, and concentrated under a vacuum to obtain compound 21, used in the next step without any further purification. Yield 90%. MS (ESI) [*M* + *H*]⁺: 235.0 *m/z*, [*M* + 2 + *H*]⁺: 237.1 *m/z*. ¹H NMR (DMSO-*d*₆ 400 MHz): δ 2.46 (s, 3H), 4.48 (s, 2H), 9.18 (bs, 2H).

Synthesis of 1-(3-Acetylphenyl)thiourea (23). Benzoyl isothiocyanate (547 μL, 4.07 mmol) was added dropwise to a solution of 3'-aminoacetophenone 22 (500 mg, 3.70 mmol) in dry DCM (12 mL), and the mixture was stirred at room temperature for 12 h. The solvent of reaction was evaporated, the residue was dissolved in THF/NaOH 1 N (1/1, 15 mL), and the mixture was refluxed for 3 h. After being cooled to

room temperature, H₂O and ethyl acetate were added, and the aqueous phase was extracted twice with ethyl acetate. The combined organic phases were dried over Na₂SO₄ and evaporated. The resulting solid was crystallized from ether. Yield 72%. MS (ESI) [M + H]⁺: 195.1 *m/z*. ¹H NMR (DMSO-*d*₆ 400 MHz): δ 2.57 (s, 3H), 7.46 (t, 1H, *J* = 7.9 Hz), 7.55 (bs, 2H), 7.70–7.73 (m, 2H), 8.03 (s, 1H), 9.89 (s, 1H).

Synthesis of 1-(3-((2'-Amino-4'-methyl-[4,5'-bithiazol]-2-yl)amino)phenyl)ethanone (24). Intermediates **21** (200 mg, 0.85 mmol) and **23** (165 mg, 0.85 mmol) were suspended in ethanol (5 mL), and the mixture was heated at reflux for 1 h. Then saturated aqueous NaHCO₃ solution and ethyl acetate were added to the mixture, and the aqueous phase was extracted three times with ethyl acetate. The combined organic phases were washed with brine, dried over Na₂SO₄, and concentrated under a vacuum. Ether was added to the crude, and the solid obtained was filtered over a Buchner funnel, washed with ether, and used in the following step without any further purification. Yield 84%. MS (ESI) [M + H]⁺: 331.3 *m/z*. ¹H NMR (DMSO-*d*₆ 300 MHz): δ 2.35 (s, 3H), 2.60 (s, 3H), 6.67 (s, 1H), 7.09 (bs, 2H), 7.46 (t, 1H, *J* = 7.9 Hz), 7.55 (d, 1H, *J* = 7.9 Hz), 7.75 (d, 1H, *J* = 7.9 Hz), 8.40 (s, 1H), 10.55 (s, 1H).

General Procedure for the Synthesis of Compounds 25a–g. (a) Method A (for 25a–c). Et₃N (84 μL, 0.60 mmol) was added to a stirred suspension of intermediate **24** (100 mg, 0.30 mmol) in dry DCM (4 mL) at 0 °C. After 15 min the proper acyl chlorides or anhydride (0.45 mmol), diluted in dry DCM (0.5 mL), were added dropwise. The resulting solution was warmed to room temperature and stirred for 12–15 h. Next, H₂O and DCM were added, and the aqueous phase was extracted twice with DCM. The combined organic phases were washed with brine, dried over Na₂SO₄, and evaporated. The crude was purified by flash chromatography using DCM/MeOH (98/2) as eluent.

(b) *N*-(2-((3-Acetylphenyl)amino)-4'-methyl-[4,5'-bithiazol]-2'-yl)propionamide (**25a**). Yield 75%; mp 244–246 °C. MS (ESI) [M + H]⁺: 387.1 *m/z*. ¹H NMR (DMSO-*d*₆ 400 MHz): δ 1.11 (t, 3H, *J* = 7.5 Hz), 2.45 (q, 2H, *J* = 7.5 Hz), 2.52 (s, 3H), 2.64 (s, 3H), 6.95 (s, 1H), 7.50 (t, 1H, *J* = 7.9 Hz), 7.57 (d, 1H, *J* = 7.9 Hz), 7.82 (d, 1H, *J* = 7.9 Hz), 8.47 (s, 1H), 10.56 (s, 1H), 12.03 (s, 1H). ¹³C NMR (DMSO-*d*₆ 100.6 MHz): δ 9.63, 17.56, 27.43, 28.69, 103.25, 116.72, 120.47, 121.49, 121.63, 129.82, 138.11, 141.82, 143.24, 143.33, 155.62, 162.94, 172.36, 198.28. Anal. (C₁₈H₁₉N₄O₃S₂) C, H, N.

(c) *N*-(2-((3-Acetylphenyl)amino)-4'-methyl-[4,5'-bithiazol]-2'-yl)pyridaldehyde (**25b**). Yield 80%; mp 232–234 °C. MS (ESI) [M + H]⁺: 415.4 *m/z*. ¹H NMR (DMSO-*d*₆ 400 MHz): δ 1.25 (s, 9H), 2.53 (s, 3H), 2.63 (s, 3H), 6.95 (s, 1H), 7.50 (t, 1H, *J* = 7.9 Hz), 7.57 (d, 1H, *J* = 7.9 Hz), 7.85 (d, 1H, *J* = 7.9 Hz), 8.43 (s, 1H), 10.57 (s, 1H), 11.79 (s, 1H). ¹³C NMR (DMSO-*d*₆ 100.6 MHz): δ 16.45, 26.90, 27.05 (3x), 39.24, 102.80, 117.29, 120.96, 122.25, 122.46, 129.67, 138.02, 140.79, 142.33, 143.58, 156.98, 163.28, 176.67, 198.36. Anal. (C₂₀H₂₂N₄O₃S₂) C, H, N.

(d) *N*-(2-((3-Acetylphenyl)amino)-4'-methyl-[4,5'-bithiazol]-2'-yl)-2,2,2-trifluoroacetamide (**25c**). Yield 65%; mp 254–256 °C. MS (ESI) [M + H]⁺: 427.1 *m/z*. ¹H NMR (DMSO-*d*₆ 400 MHz): δ 2.54 (s, 3H), 2.63 (s, 3H), 7.14 (s, 1H), 7.50 (t, 1H, *J* = 7.9 Hz), 7.58 (d, 1H, *J* = 7.9 Hz), 7.75 (d, 1H, *J* = 7.9 Hz), 8.47 (s, 1H), 10.64 (s, 1H), 14.05 (s, 1H). ¹³C NMR (DMSO-*d*₆ 100.6 MHz): δ 15.84, 27.41, 105.27, 115.80, 116.68, 120.50, 121.44, 121.79, 129.86, 138.12, 141.59, 143.31, 143.48, 155.43, 163.45, 168.73, 198.21. Anal. (C₁₇H₁₃F₃N₄O₃S₂) C, H, N.

(e) **Method B (for 25d–f).** Et₃N (84 μL, 0.60 mmol) was added to a stirred suspension of intermediate **24** (100 mg, 0.30 mmol) in dry DCM (4 mL) at 0 °C. After 15 min the proper acyl chlorides (0.45 mmol), diluted in dry DCM (0.5 mL), were added dropwise. The resulting solution was warmed to room temperature and heated at reflux for 15 h. Next, H₂O and DCM were added, and the aqueous phase was extracted twice with DCM. The combined organic phases were washed with brine, dried over Na₂SO₄, and evaporated. The crude was purified by flash chromatography using DCM/MeOH (99/1) as eluent.

(f) *N*-(2-((3-Acetylphenyl)amino)-4'-methyl-[4,5'-bithiazol]-2'-yl)benzamide (**25d**). Yield 75%; mp 199–200 °C. MS (ESI) [M + H]⁺: 435.3 *m/z*. ¹H NMR (DMSO-*d*₆ 400 MHz): δ 2.58 (s, 3H), 2.66 (s, 3H), 7.02 (s, 1H), 7.49–7.66 (m, 5H), 7.83 (d, 1H, *J* = 7.9 Hz), 8.12 (d, 2H, *J* = 7.8 Hz), 8.50 (s, 1H), 10.59 (s, 1H), 12.62 (s, 1H). ¹³C NMR (DMSO-*d*₆ 100.6 MHz): δ 17.42, 27.44, 103.60, 116.76, 121.52, 121.66, 128.61,

129.02, 129.06 (2x), 129.83 (2x), 132.59, 133.31, 138.12, 141.82, 143.23, 143.29, 155.72, 163.02, 167.79, 198.30. Anal. (C₂₂H₁₈N₄O₃S₂) C, H, N.

(g) *N*-(2-((3-Acetylphenyl)amino)-4'-methyl-[4,5'-bithiazol]-2'-yl)-4-iodobenzamide (**25e**). Yield 65%; mp 220–223 °C. MS (ESI) [M + H]⁺: 561.3 *m/z*. ¹H NMR (DMSO-*d*₆ 400 MHz): δ 2.58 (s, 3H), 2.66 (s, 3H), 7.01 (s, 1H), 7.50 (t, 1H, *J* = 7.9 Hz), 7.58 (d, 1H, *J* = 7.9 Hz), 7.81 (d, 1H, *J* = 7.9 Hz), 7.88 (d, 2H, *J* = 8.5 Hz), 7.94 (d, 2H, *J* = 8.5 Hz), 8.50 (s, 1H), 10.58 (s, 1H), 12.70 (s, 1H). ¹³C NMR (DMSO-*d*₆ 100.6 MHz): δ 17.33, 27.45, 101.14, 103.65, 116.77, 121.03, 121.51, 121.67, 129.82, 130.44 (2x), 132.34, 137.95 (2x), 138.12, 141.81, 143.16, 143.29, 154.99, 163.02, 165.15, 198.30. Anal. (C₂₂H₁₇IN₄O₃S₂) C, H, N.

(h) *N*-(2-((3-Acetylphenyl)amino)-4'-methyl-[4,5'-bithiazol]-2'-yl)-4-methylbenzamide (**25f**). Yield 72%; mp 243–244 °C. MS (ESI) [M + H]⁺: 449.2 *m/z*. ¹H NMR (DMSO-*d*₆ 400 MHz): δ 2.40 (s, 3H), 2.58 (s, 3H), 2.66 (s, 3H), 7.01 (s, 1H), 7.36 (d, 2H, *J* = 8.0 Hz), 7.50 (t, 1H, *J* = 7.9 Hz), 7.57 (d, 1H, *J* = 7.9 Hz), 7.82 (d, 1H, *J* = 7.9 Hz), 8.02 (d, 2H, *J* = 8.0 Hz), 8.50 (s, 1H), 10.58 (s, 1H), 12.55 (s, 1H). ¹³C NMR (DMSO-*d*₆ 100.6 MHz): δ 17.76, 21.55, 27.44, 103.55, 116.75, 120.52, 121.51, 121.66, 128.63 (2x), 129.62 (2x), 129.83, 131.51, 138.13, 141.42, 141.83, 143.26, 143.39, 155.78, 163.00, 168.09, 198.31. Anal. (C₂₃H₂₀N₄O₃S₂) C, H, N.

(i) **Method C (for 25g).** Et₃N (84 μL, 0.60 mmol) was added to a stirred suspension of intermediate **24** (100 mg, 0.30 mmol) in dry DMF (4 mL) at 0 °C. After 15 min Boc anhydride (0.60 mmol), diluted in dry DMF (0.5 mL), was added dropwise under vigorous stirring. The resulting solution was warmed to room temperature and heated at 50 °C for 12 h. Next, H₂O and ethyl acetate were added, and the aqueous phase was extracted twice with ethyl acetate. The combined organic phases were washed with brine, dried over Na₂SO₄, and evaporated. The crude was purified by flash chromatography using DCM/MeOH (98/2) as eluent.

(j) *tert*-Butyl 2-((3-acetylphenyl)amino)-4'-methyl-[4,5'-bithiazol]-2'-yl)carbamate (**25g**). Yield 63%; mp 235–236 °C. MS (ESI) [M + H]⁺: 431.5 *m/z*. ¹H NMR (DMSO-*d*₆ 400 MHz): δ 1.50 (s, 9H), 2.47 (s, 3H), 2.63 (s, 3H), 6.92 (s, 1H), 7.49 (t, 1H, *J* = 7.9 Hz), 7.56 (d, 1H, *J* = 7.9 Hz), 7.80 (d, 1H, *J* = 7.9 Hz), 8.50 (s, 1H), 10.54 (s, 1H), 11.39 (s, 1H). ¹³C NMR (DMSO-*d*₆ 100.6 MHz): δ 17.51, 27.42, 28.37 (3x), 79.61, 103.15, 116.70, 120.03, 121.24, 121.65, 128.34, 138.55, 141.83, 143.41, 143.62, 155.67, 157.03, 168.39, 198.32. Anal. (C₂₀H₂₂N₄O₃S₂) C, H, N.

General Procedure for the Synthesis of Compounds 26a–d. A solution of intermediate **24** (100 mg, 0.30 mmol) and the proper isocyanate or isothiocyanate (0.45 mmol) in pyridine (2 mL) was heated at reflux for 12–18 h. The mixture was cooled to room temperature and diluted with ethyl acetate. The organic phase was washed with saturated aqueous NH₄Cl solution and brine, dried over Na₂SO₄, and concentrated under a vacuum. The crude was purified by flash chromatography using DCM/MeOH (98/2) as eluent.

(a) 1-(2-((3-Acetylphenyl)amino)-4'-methyl-[4,5'-bithiazol]-2'-yl)-3-phenylurea (**26a**). Yield 59%; mp 236–239 °C. MS (ESI) [M + H]⁺: 450.3 *m/z*. ¹H NMR (DMSO-*d*₆ 400 MHz): δ 2.51 (s, 3H), 2.64 (s, 3H), 6.92 (s, 1H), 7.05 (t, 1H, *J* = 7.4 Hz), 7.33 (t, 2H, *J* = 7.4 Hz), 7.48–7.52 (m, 3H), 7.57 (d, 1H, *J* = 7.8 Hz), 7.80 (d, 1H, *J* = 7.8 Hz), 8.47 (s, 1H), 8.99 (s, 1H), 10.52 (s, 1H), 10.55 (s, 1H). ¹³C NMR (DMSO-*d*₆ 100.6 MHz): δ 17.29, 27.43, 102.86, 116.73, 119.02 (2x), 121.46, 121.62, 123.17, 128.20, 129.39 (2x), 129.83, 138.10, 139.17, 139.43, 141.83, 143.36, 151.90, 155.68, 162.92, 198.35. Anal. (C₂₂H₁₉N₅O₃S₂) C, H, N.

(b) 1-(2-((3-Acetylphenyl)amino)-4'-methyl-[4,5'-bithiazol]-2'-yl)-3-phenylthiourea (**26b**). Yield 65%; mp 217–218 °C. MS (ESI) [M + H]⁺: 466.4 *m/z*. ¹H NMR (DMSO-*d*₆ 400 MHz): δ 2.54 (s, 3H), 2.64 (s, 3H), 6.99 (s, 1H), 7.07 (t, 1H, *J* = 7.4 Hz), 7.32 (t, 2H, *J* = 7.4 Hz), 7.48 (t, 1H, *J* = 7.8 Hz), 7.57 (d, 1H, *J* = 7.8 Hz), 7.69 (d, 1H, *J* = 7.8 Hz), 7.73 (d, 2H, *J* = 7.4 Hz), 8.57 (s, 1H), 10.20 (s, 1H), 10.59 (s, 1H), 12.68 (s, 1H). ¹³C NMR (DMSO-*d*₆ 100.6 MHz): δ 17.30, 27.60, 103.92, 116.74, 121.50, 121.77, 122.48, 127.80, 128.20 (2x), 128.84 (2x), 129.81, 138.12, 138.30, 139.89, 141.73, 142.96, 155.60, 163.20, 176.12, 198.28. Anal. (C₂₂H₁₉N₅OS₂) C, H, N.

(c) 1-(2-((3-Acetylphenyl)amino)-4'-methyl-[4,5'-bithiazol]-2'-yl)-3-cyclohexylurea (**26c**). Yield 69%; mp 197–198 °C. MS (ESI) [M + H]⁺: 456.4 m/z. ¹H NMR (DMSO-*d*₆ 400 MHz): δ 1.14–1.38 (m, 6H), 1.52–1.56 (m, 1H), 1.64–1.68 (m, 2H), 1.80–1.83 (m, 2H), 2.45 (s, 3H), 2.61 (s, 3H), 6.53 (d, 1H, *J* = 7.8 Hz), 6.84 (s, 1H), 7.48 (t, 1H, *J* = 7.8 Hz), 7.56 (d, 1H, *J* = 7.8 Hz), 7.85 (d, 1H, *J* = 7.8 Hz), 8.41 (s, 1H), 10.09 (s, 1H), 10.52 (s, 1H). ¹³C NMR (DMSO-*d*₆ 100.6 MHz): δ 17.53, 24.67, 25.58, 27.41 (2x), 33.12 (2x), 48.44, 102.47, 116.67, 120.57, 121.45, 121.57, 129.81, 138.07, 141.85, 143.61, 147.01, 155.38, 157.13, 162.82, 198.29. Anal. (C₂₂H₂₅N₃O₂S₂) C, H, N.

(d) 1-(2-((3-Acetylphenyl)amino)-4'-methyl-[4,5'-bithiazol]-2'-yl)-3-cyclohexylthiourea (**26d**). Yield 52%; mp 234–236 °C. MS (ESI) [M + H]⁺: 472.3 m/z. ¹H NMR (DMSO-*d*₆ 400 MHz): δ 1.24–1.37 (m, 6H), 1.52–1.56 (m, 1H), 1.63–1.67 (m, 2H), 1.85–1.93 (m, 2H), 2.49 (s, 3H), 2.63 (s, 3H), 6.96 (s, 1H), 7.47 (t, 1H, *J* = 7.8 Hz), 7.56 (d, 1H, *J* = 7.8 Hz), 7.85 (d, 1H, *J* = 7.8 Hz), 8.41 (s, 1H), 9.55 (s, 1H), 10.57 (s, 1H), 11.41 (s, 1H). ¹³C NMR (DMSO-*d*₆ 100.6 MHz): δ 17.84, 24.38, 25.56, 27.50 (2x), 31.80 (2x), 52.62, 103.47, 116.67, 121.45, 121.58, 121.74, 129.79, 137.20, 138.11, 141.65, 142.93, 146.01, 163.00, 171.90, 198.11. Anal. (C₂₂H₂₅N₃O₂S₂) C, H, N.

Synthesis of Phenyl (5-Acetyl-4-methylthiazol-2-yl)carbamate (27). 1-(2-Amino-4-methylthiazol-5-yl)ethanone **20** (1000 mg, 6.40 mmol) was added to a suspension of NaH 60% dispersion in mineral oil (768 mg, 19.20 mmol) in DMF (15 mL) at 0 °C. Diphenyl carbonate (3428 mg, 16.0 mmol) was added while cooling, and the reaction mixture was stirred for additional 30 min at room temperature. H₂O and ethyl acetate were added and the aqueous phase was extracted three times with ethyl acetate. The combined organic phases were washed twice with an aqueous solution of LiCl (5% w/w) and brine, dried over Na₂SO₄, and concentrated under vacuum. Ether was added to the crude and the white solid obtained was filtered over a Buchner funnel, washed with ether, and used in the following step without any further purification. Yield: 67%. MS (ESI) [M + H]⁺: 277.2 m/z. ¹H NMR (DMSO-*d*₆ 400 MHz): δ 2.52 (s, 3H), 2.57 (s, 3H), 7.27–7.34 (m, 3H), 7.44–7.48 (m, 2H), 12.71 (s, 1H).

General Procedure for the Synthesis of Compounds 28a,b. The proper amine (1.09 mmol) was added to a solution of intermediate **27** (300 mg, 1.09 mmol) in dry THF (15 mL). The mixture was heated at 50 °C for 5–6 h, after which H₂O and ethyl acetate were added, and the reaction mixture was cooled down to room temperature. The aqueous phase was extracted twice with ethyl acetate, the combined organic phases were washed with brine, dried over Na₂SO₄, and concentrated under a vacuum. The crude was purified by flash chromatography using DCM/MeOH (97/3) as eluent.

(a) 1-(5-Acetyl-4-methylthiazol-2-yl)-3-(4-chlorobenzyl)urea (**28a**). Yield: 61%. MS (ESI) [M + H]⁺: 324.2 m/z. ¹H NMR (DMSO-*d*₆ 300 MHz): δ 2.49 (s, 3H), 2.62 (s, 3H), 4.34 (d, 2H, *J* = 5.7 Hz), 7.18 (bs, 1H), 7.33 (d, 2H, *J* = 8.2 Hz), 7.40 (d, 2H, *J* = 8.2 Hz), 11.02 (s, 1H).

(b) 1-(5-Acetyl-4-methylthiazol-2-yl)-3-(adamantan-1-yl)urea (**28b**). Yield: 93%. MS (ESI) [M + H]⁺: 334.5 m/z. ¹H NMR (DMSO-*d*₆ 300 MHz): δ 1.64–1.65 (m, 6H), 1.93–1.95 (m, 6H), 2.05–2.06 (m, 3H), 2.49 (s, 3H), 2.63 (s, 3H), 6.42 (s, 1H), 10.21 (s, 1H).

General Procedure for the Synthesis of Compounds 29a,b. A suspension of the proper intermediate **28a,b** (0.62 mmol) in 48% HBr solution in water (2 mL) was warmed to 60 °C. A solution of Br₂ (42 μL, 0.81 mmol) in 1,4-dioxane (2 mL) was added dropwise, and the reaction mixture was heated at 60 °C for 3 h. After being cooled down to room temperature, saturated aqueous NaHCO₃ solution and ethyl acetate were added, and the aqueous phase was extracted three times with ethyl acetate. The combined organic phases were washed with brine, dried over Na₂SO₄, and concentrated under a vacuum. Intermediates **29a,b** were used in the next step without any further purification.

(a) 1-(5-(2-Bromoacetyl)-4-methylthiazol-2-yl)-3-(4-chlorobenzyl)urea (**29a**). Yield: 88%. MS (ESI) [M + H]⁺: 402.4 m/z. [M + 2 + H]⁺: 404.3 m/z. [M + 4 + H]⁺: 406.3 m/z. ¹H NMR (DMSO-*d*₆ 300 MHz): δ 2.49 (s, 3H), 4.34 (d, 2H, *J* = 5.7 Hz), 4.46 (bs, 2H), 7.18 (bs, 1H), 7.36 (d, 2H, *J* = 8.2 Hz), 7.43 (d, 2H, *J* = 8.2 Hz), 11.23 (s, 1H).

(b) 1-(Adamantan-1-yl)-3-(5-(2-bromoacetyl)-4-methylthiazol-2-yl)urea (**29b**). Yield: 92%. MS (ESI) [M + H]⁺: 412.3 m/z. [M + 2 + H]⁺: 414.3 m/z. ¹H NMR (DMSO-*d*₆ 300 MHz): δ 1.65–1.67 (m, 6H), 1.93–1.95 (m, 6H), 2.06–2.08 (m, 3H), 2.49 (s, 3H), 4.49 (bs, 2H), 6.43 (s, 1H), 10.31 (s, 1H).

General Procedure for the Synthesis of Compounds 30a,b. A suspension of intermediate **23** (100 mg, 0.51 mmol) and the proper compound **29a,b** (0.51 mmol) in ethanol (6 mL) was heated at reflux for 1 h. After being cooled down to room temperature, saturated aqueous NaHCO₃ solution, H₂O, and ethyl acetate were added, and the aqueous phase was extracted three times with ethyl acetate. The combined organic phases were washed with brine, dried over Na₂SO₄, and concentrated under a vacuum. The crude was purified by flash chromatography using DCM/MeOH (97/3) as eluent.

(a) 1-(2-((3-Acetylphenyl)amino)-4'-methyl-[4,5'-bithiazol]-2'-yl)-3-(4-chlorobenzyl)urea (**30a**). Yield 78%; mp 240–241 °C. MS (ESI) [M + H]⁺: 498.2 m/z. ¹H NMR (DMSO-*d*₆ 400 MHz): δ 2.47 (s, 3H), 2.61 (s, 3H), 4.34 (d, 2H, *J* = 5.7 Hz), 6.86 (s, 1H), 7.09 (bs, 1H), 7.33 (d, 2H, *J* = 8.2 Hz), 7.40 (d, 2H, *J* = 8.2 Hz), 7.48 (t, 1H, *J* = 7.8 Hz), 7.55 (d, 1H, *J* = 7.8 Hz), 7.83 (d, 1H, *J* = 7.8 Hz), 8.42 (s, 1H), 10.51 (s, 1H), 10.53 (s, 1H). ¹³C NMR (DMSO-*d*₆ 100.6 MHz): δ 17.50, 27.41, 42.73, 102.57, 116.67, 120.01, 121.45, 121.58, 128.78 (2x), 129.54 (2x), 129.82, 131.89, 138.08, 139.25, 141.84, 143.21, 143.55, 154.41, 157.67, 162.84, 198.30. Anal. (C₂₃H₂₀ClN₃O₂S₂) C, H, N.

(b) 1-(2-((3-Acetylphenyl)amino)-4'-methyl-[4,5'-bithiazol]-2'-yl)-3-(adamantan-1-yl)urea (**30b**). Yield 83%; mp 227–230 °C. MS (ESI) [M + H]⁺: 508.5 m/z. ¹H NMR (DMSO-*d*₆ 400 MHz): δ 1.65–1.67 (m, 6H), 1.93–1.95 (m, 6H), 2.05–2.06 (m, 3H), 2.49 (s, 3H), 2.63 (s, 3H), 6.78 (s, 1H), 6.97 (s, 1H), 7.49 (t, 1H, *J* = 7.8 Hz), 7.56 (d, 1H, *J* = 7.8 Hz), 7.81 (d, 1H, *J* = 7.8 Hz), 8.46 (s, 1H), 10.21 (bs, 1H), 10.59 (s, 1H). ¹³C NMR (DMSO-*d*₆ 100.6 MHz): δ 16.39, 27.47, 29.29 (3x), 36.32 (3x), 41.73 (3x), 51.16, 103.55, 116.76, 119.09, 121.49, 121.63, 129.83, 138.08, 139.61, 141.76, 142.58, 152.13, 158.27, 163.05, 198.32. Anal. (C₂₆H₂₉N₃O₂S₂) C, H, N.

Synthesis of N-(5-Acetyl-4-methylthiazol-2-yl)acetamide (31). Intermediate **20** (1000 mg, 6.40 mmol) was suspended in THF/DCM (3/2, 12 mL), and the mixture was cooled down to 0 °C. Pyridine (1.3 mL) was added, followed by the dropwise addition of acetyl chloride (683 μL, 9.60 mmol). The reaction mixture was stirred at 0 °C for 3 h. Next, H₂O and ethyl acetate were added, and the aqueous phase was extracted three times with ethyl acetate. The combined organic phases were washed three times with saturated aqueous NH₄Cl solution and brine, dried over Na₂SO₄, and concentrated under a vacuum. Intermediate **31** was used in the next step without any further purification. Yield: 87%. MS (ESI) [M + H]⁺: 199.3 m/z. ¹H NMR (DMSO-*d*₆ 400 MHz): δ 2.17 (s, 3H), 2.46 (s, 3H), 2.56 (s, 3H), 12.44 (s, 1H).

Synthesis of N-(5-(2-Bromoacetyl)-4-methylthiazol-2-yl)acetamide (32). A solution of Br₂ (388 μL, 7.6 mmol) in 1,4-dioxane (8.6 mL) was added dropwise to a stirred solution of intermediate **31** (1200 mg, 6.05 mmol) in 1,4-dioxane (23 mL). The mixture was heated at 50 °C for 22 h. After being cooled down to room temperature, saturated aqueous NaHCO₃ solution and ethyl acetate were added, and the aqueous phase was extracted three times with ethyl acetate. The combined organic phases were washed with brine, dried over Na₂SO₄, and concentrated under a vacuum. The crude was purified by flash chromatography using DCM/acetone (95/5) as eluent. Yield 84%. MS (ESI) [M + H]⁺: 277.3 m/z. [M + 2 + H]⁺: 279.4 m/z. ¹H NMR (DMSO-*d*₆ 400 MHz): δ 2.11 (s, 3H), 2.46 (s, 3H), 4.52 (bs, 2H), 12.44 (s, 1H).

General Procedure for the Synthesis of Intermediates 34a–d. Benzoyl isothiocyanate (547 μL, 4.07 mmol) was added dropwise to a solution of the appropriate aniline **33a–d** (3.70 mmol) in dry DCM (12 mL), and the mixture was stirred at room temperature for 12 h. The solvent of reaction was evaporated, the solid was dissolved in THF/NaOH 1 N (1/1, 15 mL), and the mixture was refluxed for 2 h. Next, H₂O and ethyl acetate were added, and the aqueous phase was extracted three times with ethyl acetate. The combined organic phases were dried over Na₂SO₄ and evaporated. Crystallization from ether afforded intermediates **34a–d**.

(a) 1-Phenylthiourea (**34a**). Yield 72%. MS (ESI) [M + H]⁺: 153.1 *m/z*. ¹H NMR (DMSO-*d*₆ 300 MHz): δ 7.09–7.14 (m, 1H), 7.30–7.42 (m, 6H), 9.67 (s, 1H).

(b) 1-(3-Hydroxyphenyl)thiourea (**34b**). Yield 74%. MS (ESI) [M + H]⁺: 169.2 *m/z*. ¹H NMR (DMSO-*d*₆ 300 MHz): δ 6.50–6.54 (m, 1H), 6.74–6.77 (m, 1H), 6.87–6.88 (m, 1H), 7.09 (t, 1H, *J* = 8.0 Hz), 7.32–7.36 (bs, 2H), 9.45 (s, 1H), 9.58 (s, 1H).

(c) 1-(3-Methoxyphenyl)thiourea (**34c**). Yield 75%. MS (ESI) [M + H]⁺: 183.3 *m/z*. ¹H NMR (DMSO-*d*₆ 300 MHz): δ 3.74 (s, 3H), 6.67–6.70 (m, 1H), 6.90–6.94 (m, 1H), 7.11–7.13 (m, 1H), 7.22 (t, 1H, *J* = 8.1 Hz), 7.46–7.49 (bs, 2H), 9.73 (s, 1H).

(d) 1-(4-Acetylphenyl)thiourea (**34d**). Yield 78%. MS (ESI) [M + H]⁺: 195.4 *m/z*. ¹H NMR (DMSO-*d*₆ 300 MHz): δ 2.49 (s, 3H), 7.79–7.83 (m, 2H), 7.87–8.03 (m, 4H), 10.69 (s, 1H).

General Procedure for the Synthesis of Compounds 35a–d. A solution of intermediate **32** (50 mg, 0.18 mmol) and the proper thiourea **34a–d** (0.18 mmol) in ethanol (2.5 mL) was heated at reflux for 1 h. After being cooled down to room temperature, saturated aqueous NaHCO₃ solution, H₂O and ethyl acetate were added, and the aqueous phase was extracted three times with ethyl acetate. The combined organic phases were washed with brine, dried over Na₂SO₄, and concentrated under a vacuum. The crude was purified by flash chromatography using DCM/MeOH (97/3) as eluent.

(a) *N*-(4'-Methyl-2-(phenylamino)-[4,5'-bithiazol]-2'-yl)-acetamide (**35a**). Yield 85%; mp 187–189 °C. MS (ESI) [M + H]⁺: 331.1 *m/z*. ¹H NMR (CDCl₃ 400 MHz): δ 2.19 (s, 3H), 2.57 (s, 3H), 6.58 (s, 1H), 7.10–7.12 (m, 1H), 7.36–7.42 (m, 4H), 8.18 (s, 1H), 11.94 (s, 1H). ¹³C NMR (CDCl₃ 100.6 MHz): δ 17.00, 23.07, 102.63, 118.50 (2x), 121.29, 123.32, 129.54 (2x), 140.15, 142.70, 143.31, 156.66, 164.76, 167.92. Anal. (C₁₅H₁₄N₄O₂S₂) C, H, N.

(b) *N*-(2-((3-Hydroxyphenyl)amino)-4'-methyl-[4,5'-bithiazol]-2'-yl)acetamide (**35b**). Yield 71%; mp 148–149 °C. MS (ESI) [M + H]⁺: 347.2 *m/z*. ¹H NMR (acetone-*d*₆ 400 MHz): δ 2.26 (s, 3H), 2.51 (s, 3H), 6.52–6.54 (m, 1H), 6.78 (s, 1H), 7.15–7.18 (m, 2H), 7.27 (s, 1H), 8.45 (s, 1H), 9.30 (s, 1H), 10.85 (s, 1H). ¹³C NMR (acetone-*d*₆ 100.6 MHz): δ 16.51, 21.90, 101.85, 104.58, 108.75, 109.12, 120.91, 129.81, 142.39, 143.14, 143.95, 155.28, 158.21, 163.25, 167.72. Anal. (C₁₅H₁₄N₄O₂S₂) C, H, N.

(c) *N*-(2-((3-Methoxyphenyl)amino)-4'-methyl-[4,5'-bithiazol]-2'-yl)acetamide (**35c**). Yield 74%; mp 118–119 °C. MS (ESI) [M + H]⁺: 361.2 *m/z*. ¹H NMR (DMSO-*d*₆ 400 MHz): δ 2.14 (s, 3H), 2.48 (s, 3H), 3.82 (s, 3H), 6.53 (d, 1H, *J* = 8.2 Hz), 6.90 (s, 1H), 6.98 (s, 1H, *J* = 8.2 Hz), 7.20 (t, 1H, *J* = 8.2 Hz), 7.71 (s, 1H), 10.42 (s, 1H), 12.06 (s, 1H). ¹³C NMR (DMSO-*d*₆ 100.6 MHz): δ 17.53, 22.93, 55.52, 102.71, 105.60, 107.78, 109.65, 120.81, 130.02, 142.77, 142.90, 143.12, 155.59, 160.40, 162.96, 168.75. Anal. (C₁₆H₁₆N₄O₂S₂) C, H, N.

(d) *N*-(2-((4-Acetylphenyl)amino)-4'-methyl-[4,5'-bithiazol]-2'-yl)acetamide (**35d**). Yield 79%; mp 233–235 °C. MS (ESI) [M + H]⁺: 373.2 *m/z*. ¹H NMR (DMSO-*d*₆ 400 MHz): δ 2.15 (s, 3H), 2.51 (s, 3H), 2.54 (s, 3H), 7.07 (s, 1H), 7.77 (d, 2H, *J* = 8.7 Hz), 7.97 (d, 2H, *J* = 8.7 Hz), 10.79 (s, 1H), 12.11 (s, 1H). ¹³C NMR (DMSO-*d*₆ 100.6 MHz): δ 17.49, 22.93, 26.82, 104.38, 116.33 (2x), 120.33, 130.34, 130.42 (2x), 143.41, 145.48, 152.60, 155.63, 162.37, 168.83, 196.63. Anal. (C₁₇H₁₆N₄O₂S₂) C, H, N.

Synthesis of 1-(3-Acetylphenyl)guanidine (36). Nitric acid (164 μL, 3.70 mmol) was added to a solution of 3'-aminoacetophenone **22** (500 mg, 3.70 mmol) in ethanol (10 mL), followed by addition of a solution of cyanamide (778 mg, 18.5 mmol) in a minimal amount of water. The mixture was heated at reflux for 24 h and concentrated in a vacuum. After being cooled to 0 °C, ether was added and the precipitate was separated by filtration over a Buchner funnel. Then saturated aqueous NaHCO₃ solution and ethyl acetate were added to the solid, and the aqueous phase was extracted three times with ethyl acetate. The combined organic phases were washed with brine, dried over Na₂SO₄ and concentrated under a vacuum to obtain compound **36**, used in the next step without any further purification. Yield 73%. MS (ESI) [M + H]⁺: 178.2 *m/z*. ¹H NMR (DMSO-*d*₆ 300 MHz): δ 2.57 (s, 3H), 7.49 (bs, 3H), 7.58–7.60 (m, 2H), 7.76–7.78 (m, 1H), 7.88 (s, 1H), 9.67 (bs, 1H).

Synthesis of 1-(3-((4-(2-Amino-4-methylthiazol-5-yl)-1H-imidazol-2-yl)amino)phenyl)ethanone (37). A solution of intermediate **36** (150 mg, 0.85 mmol) in ethanol (5 mL) was added dropwise to a solution of compound **21** (200 mg, 0.85 mmol) and Et₃N (118 μL, 0.85 mmol) in ethanol (10 mL). The mixture was heated at reflux for 12 h, after which H₂O and ethyl acetate were added. The organic phase was washed with saturated aqueous NH₄Cl solution and brine, dried over Na₂SO₄, and concentrated under a vacuum to obtain compound **37**, used in the next step without any further purification. Yield 82%. MS (ESI) [M + H]⁺: 314.3 *m/z*. ¹H NMR (DMSO-*d*₆ 400 MHz): δ 2.37 (s, 3H), 2.64 (s, 3H), 7.09 (s, 1H), 7.65 (t, 1H, *J* = 7.9 Hz), 7.79 (d, 1H, *J* = 7.9 Hz), 7.94 (d, 1H, *J* = 7.9 Hz), 8.04 (s, 1H), 9.50 (bs, 2H), 10.56 (s, 1H), 12.01 (s, 1H).

Synthesis of *N*-(5-(2-((3-Acetylphenyl)amino)-1H-imidazol-4-yl)-4-methylthiazol-2-yl)acetamide (38). Et₃N (89 μL, 0.64 mmol) was added to a stirred suspension of intermediate **37** (100 mg, 0.32 mmol) in dry DCM (4.5 mL) at 0 °C. After 15 min acetyl chloride (34 μL, 0.48 mmol), diluted in dry DCM (0.5 mL), was added dropwise. The resulting solution was warmed to room temperature and stirred for 8 h. Next, H₂O and DCM were added, and the aqueous phase was extracted three times with DCM. The combined organic phases were washed with brine, dried over Na₂SO₄, and evaporated. The crude was purified by flash chromatography using DCM/MeOH (97/3) as eluent. Yield 47%; mp 222–225 °C. MS (ESI) [M + H]⁺: 356.2 *m/z*. ¹H NMR (DMSO-*d*₆ 400 MHz): δ 2.14 (s, 3H), 2.37 (s, 3H), 2.65 (s, 3H), 7.11 (s, 1H), 7.66 (t, 1H, *J* = 7.9 Hz), 7.79 (d, 1H, *J* = 7.9 Hz), 7.94 (d, 1H, *J* = 7.9 Hz), 8.05 (s, 1H), 10.56 (s, 1H), 11.84 (s, 1H), 12.06 (s, 1H). ¹³C NMR (DMSO-*d*₆ 100.6 MHz): δ 17.56, 22.56, 27.42, 116.75, 119.9, 120.51, 121.65, 127.71, 129.79, 138.10, 140.81, 143.21, 143.28, 154.98, 162.89, 168.63, 198.32. Anal. (C₁₇H₁₇N₅O₂S) C, H, N.

Synthesis of 1-(3-Acetylphenyl)-3-(3-nitrophenyl)thiourea (40). 3'-Aminoacetophenone **22** (300 mg, 2.22 mmol) was added to a solution of 3-nitrophenyl isothiocyanate (400 mg, 2.22 mmol) in dry DCM (6.50 mL). The solution was stirred at room temperature for 18 h. The precipitate was separated by filtration over a Buchner funnel and washed with ether, affording compound **40** as a white solid. Yield 88%. MS (ESI) [M + H]⁺: 316.2 *m/z*. ¹H NMR (DMSO-*d*₆ 400 MHz): δ 2.58 (s, 3H), 7.52 (t, 1H, *J* = 7.9 Hz), 7.63 (t, 1H, *J* = 8.1 Hz), 7.76–7.78 (m, 2H), 7.92 (d, 1H, *J* = 7.9 Hz), 7.98 (d, 1H, *J* = 8.1 Hz), 8.07 (s, 1H), 8.56 (s, 1H), 10.31 (bs, 1H), 10.33 (bs, 1H).

Synthesis of 1-(3-Acetylphenyl)-3-(3-aminophenyl)thiourea (41). Iron powder (1490 mg, 26.67 mmol), water (7 mL), and concentrated HCl (4 drops) were added to a solution of compound **40** (400 mg, 1.27 mmol) in ethanol (35 mL). After heating at reflux for 2 h, the mixture was filtrated hot, washed with ethanol, and concentrated in a vacuum. The crude was purified by flash chromatography using DCM/MeOH (98/2) as eluent. Yield 75%. MS (ESI) [M + H]⁺: 286.1 *m/z*. ¹H NMR (CDCl₃ 400 MHz): δ 2.58 (s, 3H), 3.20–3.51 (bs, 2H), 6.59–6.62 (m, 2H), 6.68 (d, 1H, *J* = 7.7 Hz), 7.18 (t, 1H, *J* = 7.8 Hz), 7.45 (t, 1H, *J* = 7.8 Hz), 7.74–7.79 (m, 2H), 7.95 (s, 1H), 8.05 (s, 1H), 8.38 (s, 1H).

General Procedure for the Synthesis of Compounds 42a,b. The proper acyl chloride (0.53 mmol) was added to a stirred solution of intermediate **41** (100 mg, 0.35 mmol) and pyridine (56 μL, 0.70 mmol) in dry THF (4 mL). The resulting solution was stirred at room temperature for 2 h, after which H₂O and ethyl acetate were added, and the aqueous phase was extracted three times with ethyl acetate. The combined organic phases were washed with brine, dried over Na₂SO₄ and concentrated under a vacuum. The crude was purified by flash chromatography using DCM/MeOH (99/1) as eluent.

(a) *N*-(3-(3-(3-Acetylphenyl)thioureido)phenyl)acetamide (**42a**). Yield 67%; mp 171–173 °C. MS (ESI) [M + H]⁺: 328.1 *m/z*. ¹H NMR (DMSO-*d*₆ 400 MHz): δ 2.04 (s, 3H), 2.57 (s, 3H), 7.16–7.19 (m, 1H), 7.25 (t, 1H, *J* = 7.9 Hz), 7.35–7.37 (m, 1H), 7.47 (t, 1H, *J* = 7.9 Hz), 7.71–7.79 (m, 3H), 8.07 (bs, 1H), 9.89 (s, 1H), 9.96 (s, 1H), 9.98 (s, 1H). ¹³C NMR (DMSO-*d*₆ 100.6 MHz): 23.43, 27.23, 116.20, 117.10, 119.38, 123.64, 124.55, 128.90, 128.98, 129.04, 136.97, 139.64, 140.17, 140.52, 168.56, 180.27, 197.97. Anal. (C₁₇H₁₇N₃O₂S) C, H, N.

(b) *N*-(3-(3-(3-Acetylphenyl)thioureido)phenyl)pivalamide (**42b**). Yield 69%; mp 157–159 °C. MS (ESI) [M + H]⁺: 370.3 *m/z*. ¹H NMR (DMSO-*d*₆ 300 MHz): δ 1.22 (s, 9H), 2.57 (s, 3H), 7.14 (d, 1H, *J* = 7.9

Hz), 7.25 (t, 1H, $J = 7.9$ Hz), 7.42–7.50 (m, 2H), 7.71–7.80 (m, 3H), 8.06 (bs, 1H), 9.25 (s, 1H), 9.89 (s, 1H), 9.94 (s, 1H). ^{13}C NMR (DMSO- d_6 , 100.6 MHz): δ 27.23, 27.65 (3x), 30.90, 116.29, 117.14, 119.35, 123.68, 124.71, 128.88, 128.92, 129.10, 137.43, 139.65, 140.20, 140.52, 176.96, 180.27, 197.97. Anal. ($\text{C}_{20}\text{H}_{23}\text{N}_3\text{O}_2\text{S}$) C, H, N.

Synthesis of 1-(4-(Dimethylamino)phenyl)thiourea (44). Benzoyl isothiocyanate (543 μL , 4.04 mmol) was added dropwise to a solution of *N,N*-dimethyl-*p*-phenylenediamine 43 (500 mg, 3.67 mmol) in dry DCM (12 mL), and the mixture was stirred at room temperature for 12 h. The solvent of reaction was evaporated, the solid was dissolved in THF/NaOH 1 N (1/1, 15 mL), and the mixture was refluxed for 3 h. Next, H_2O and ethyl acetate were added, and the aqueous phase was extracted three times with ethyl acetate. The combined organic phases were dried over Na_2SO_4 and evaporated. The resulting solid was crystallized from ether. Yield 80%. MS (ESI) $[\text{M} + \text{H}]^+$: 196.4 m/z . ^1H NMR (DMSO- d_6 , 300 MHz): δ 2.88 (s, 6H), 6.69 (d, 2H, $J = 8.7$ Hz), 7.08 (d, 2H, $J = 8.7$ Hz), 7.55 (bs, 2H), 9.58 (s, 1H).

Synthesis of *N'*-(4-(Dimethylamino)phenyl)-4'-methyl-[4,5'-bithiazole]-2,2'-diamine (45). Intermediates 21 (150 mg, 0.64 mmol) and 44 (125 mg, 0.64 mmol) were suspended in ethanol (6 mL), and the mixture was heated at reflux for 30 min. Then saturated aqueous NaHCO_3 solution and ethyl acetate were added to the mixture, and the aqueous phase was extracted three times with ethyl acetate. The combined organic phases were washed with brine, dried over Na_2SO_4 , and concentrated under a vacuum. Ether was added to the crude and the solid obtained was filtered over a Buchner funnel, washed with ether and used in the following step without any further purification. Yield 77%. MS (ESI) $[\text{M} + \text{H}]^+$: 332.2 m/z . ^1H NMR (DMSO- d_6 , 400 MHz): δ 2.47 (s, 3H), 2.86 (s, 6H), 6.72 (s, 1H), 6.76 (d, 2H, $J = 8.8$ Hz), 7.43 (d, 2H, $J = 8.8$ Hz), 9.21 (bs, 2H), 10.58 (s, 1H).

***N*-(2-(4-(Dimethylamino)phenyl)amino)-4'-methyl-[4,5'-bithiazole]-2'-yl)propionamide (46).** Et_3N (84 μL , 0.60 mmol) was added to a stirred suspension of intermediate 45 (100 mg, 0.30 mmol) in dry DCM (4 mL) at 0 $^\circ\text{C}$. After 15 min propionyl chloride (39 μL , 0.45 mmol), diluted in dry DCM (0.5 mL), was added dropwise. The resulting solution was warmed to room temperature and stirred for 8 h. Next, H_2O and DCM were added and the aqueous phase was extracted twice with DCM. The combined organic phases were washed with brine, dried over Na_2SO_4 , and evaporated. The crude was purified by flash chromatography using DCM/MeOH (98/2) as eluent. Yield 68%; mp 222–224 $^\circ\text{C}$. MS (ESI) $[\text{M} + \text{H}]^+$: 388.3 m/z . ^1H NMR (DMSO- d_6 , 400 MHz): δ 1.10 (t, 3H, $J = 7.6$ Hz), 2.43 (q, 2H, $J = 7.6$ Hz), 2.47 (s, 3H), 2.86 (s, 6H), 6.73 (s, 1H), 6.76 (d, 2H, $J = 8.8$ Hz), 7.43 (d, 2H, $J = 8.8$ Hz), 9.90 (s, 1H), 11.98 (s, 1H). ^{13}C NMR (DMSO- d_6 , 100.6 MHz): δ 8.78, 16.88, 30.43, 40.46 (2x), 101.02, 113.74 (2x), 120.67 (2x), 121.44, 131.54, 143.10, 144.02, 147.72, 155.12, 165.29, 171.76. Anal. ($\text{C}_{18}\text{H}_{21}\text{N}_5\text{O}_2\text{S}_2$) C, H, N.

Biology. Antiviral Assays—Materials and Methods Assay Preparation. Enterovirus (EV). Rhabdosome (RD) cells, Vero cells and Hela-Rh cells, subcultured in cell growth medium [MEM Rega3 (Cat. No. 19993013; Invitrogen) supplemented with 10% FCS (Integro), 5 mL of 200 mM L-glutamine (25030024) and 5 mL of 7.5% sodium bicarbonate (25080060)] at a ratio of 1:4 and grown for 7 days in 150 cm^2 tissue culture flasks (Techno Plastic Products), were harvested and seeded in a 96-well plate at a cell density of 20 000 cells/well in assay medium (MEM Rega3, 2% FCS, 5 mL L-glutamine and 5 mL sodium bicarbonate) to perform standardized antiviral assay against EV71 and EVD68, CV and PV, RV02 and RV14, respectively.

Antiviral Activity and Cytotoxicity Determinations. Compounds were prepared as DMSO stock solution with a final compound concentration of 10 mM. The compound profiling setup was performed employing a Freedom EVO200 liquid handling platform (Tecan). The evaluation of the cytosstatic/cytotoxic as well as the antiviral effect of each compound was performed in parallel within one run. Three 8-step 1-to-5 dilution series were prepared (starting from 100 μM) in assay medium added to empty wells (picornaviruses: 96-well microtiter plates, Falcon, BD) or in the medium present on top of preseeded cells. Subsequently, 50 μL of a 4x virus dilution in assay medium (assay medium supplemented with 15 mL MgCl_2 , 1 M (Sigma, M1028) in case of RV) was added followed by 50 μL of cell suspension. The assay plates

were returned to the incubator for 2–3 (picornavirus, 35 $^\circ\text{C}$ for RV) days, a time at which maximal cytopathic effect (CPE) for picornaviruses is observed.

For the evaluation of cytosstatic/cytotoxic effects and for the evaluation of the antiviral effect in the case of PV, CV, RV, the assay medium was replaced with 75 μL of a 5% MTS (Promega) solution in phenol red-free medium and incubated for 1.5 h (37 $^\circ\text{C}$, 5% CO_2 , 95–99% relative humidity). Absorbance was measured at a wavelength of 498 nm (Safire2, Tecan) and optical densities (OD values) were converted to percentage of untreated controls.

Analysis of the raw data, quality control of each individual dose–response curve and calculation, if possible, of the EC_{50} , EC_{90} and CC_{50} values was performed employing ViroDM, a custom-made data processing software package. The EC_{50} and EC_{90} (values derived from the dose–response curve) represent the concentrations at which respectively 50% and 90% inhibition of viral replication would be observed. The CC_{50} (value derived from the dose–response curve) represents the concentration at which the metabolic activity of the cells would be reduced to 50% of the metabolic activity of untreated cells.

The EC_{50} , EC_{90} and $\text{CC}_{50} \pm \text{SD}$ were, whenever possible, calculated respectively as the median of all the EC_{50} , EC_{90} , or CC_{50} values derived from the three individual dose–response curves. The selectivity index (SI), indicative of the therapeutic window of the compound, was calculated as $\text{CC}_{50}/\text{EC}_{50}$. No further statistical analysis was performed.

CFTR Assays. The effects of compounds on CFTR biogenesis and function were measured using newly developed assays exploiting CFTR fusion probes with anion-sensitive YFP⁶¹ and pH-sensitive pHTomato.⁶² Lipofectamine transfection was used for transient transfection of HEK293 cells. Cells plated in 96-well plates were incubated with the YFP-CFTR- or CFTR-pHTomato-encoding plasmid⁶⁶ using Lipofectamine 2000 (Life Technologies), according to manufacturer's instructions. Following transfection, cell plates were returned to the 37 $^\circ\text{C}$ incubator for 24 h. Plates were further incubated at 30 $^\circ\text{C}$ for 24 h prior to imaging, with or without additional drug treatment.

All imaging was carried out using ImageXpress (ImageXpress Micro XLS, Molecular Devices); an image-acquisition system equipped with wide-field inverted fluorescence microscope and fluidics robotics. Images were obtained with a 20x objective, using excitation/emission filters 472 \pm 30 nm and 520 \pm 35 nm, for YFP-CFTR and 531 \pm 20 nm, and 592 \pm 20 nm for CFTR-pHTomato. In the latter assay, eGFP and Hoechst nuclear stain images were also acquired for each well, using excitation/emission filters 472 \pm 30 nm and 520 \pm 35 nm, and 377 \pm 25 nm and 447 \pm 30 nm, respectively. For each plate, the laser intensity and exposure were optimized to achieve the highest possible fluorescence while avoiding both photobleaching and saturation (illumination intensity 100–150/225 cd, and exposure 0.1–0.2 s).

For the YFP-CFTR assays, before imaging, cells were washed twice with 100 μL of standard buffer (140 mM NaCl, 4.7 mM KCl, 1.2 mM MgCl_2 , 5 mM HEPES, 2.5 mM CaCl_2 , 1 mM glucose, pH 7.4). Images were taken for 150 s at a frequency of 0.5 Hz. A total of 50 μL extracellular Γ^- (as standard buffer with 140 mM NaCl replaced with 300 mM NaI; resulting in 100 mM final $[\Gamma^-]$) was added at 20 s, and activating compounds (50 μM Forskolin alone or together with 10 μM compounds for acute treatment) were added at 60 s.

For the CFTR-pHTomato assay, before imaging, cells were washed twice with 100 μL of standard buffer (as above). During imaging, extracellular pH was changed using addition of 50 μL of pH 6 buffer (as standard buffer, with 5 mM HEPES replaced with 10 mM MES: final [MES] 3.3 mM, \sim pH 6.5), and 50 μL pH 9 buffer (as standard buffer, with 5 mM HEPES replaced with 100 mM Tris: final [Tris] 25 mM, \sim pH 8.8). Two pHTomato images (acquisition frequency 0.5 Hz) were taken in each condition. To account for variation in transfection efficiency the pHTomato fluorescence was normalized using average fluorescence intensity of a soluble eGFP, coexpressed in the cytosol. Because the rise in pHTomato fluorescence falls largely within the 6.5–8.8 pH range,⁶³ the change in fluorescence obtained upon increasing extracellular pH ($\Delta F_{\text{membrane}}$) was used as an estimate of membrane-exposed CFTR.

In Vitro Kinase Inhibition Assays. Recombinant full length, HIS6-tagged PI4KIII β was purchased from ProQinase (Germany);

recombinant full-length, GST tagged PI4KIII α was from Life Technologies. Recombinant full-length, HIS6-tagged (PI3K- α) and full-length, myc-tagged (p85 α) PI3K- α /p85 α was purchased from ProQinase (Germany).

Assay Conditions. PI4KIII β , PI4KIII α , and PI3K- α /p85 α reactions were performed in 10 μ L using 20 mM Tris-HCl pH 7.5, 0.125 mM EGTA, 2 mM DTT, 0.04% Triton, 3 mM MgCl₂, 3 mM MnCl₂, 20 μ M ATP, 0.01 μ Ci γ -P33 ATP, 200 μ M Pi:3PS, 10% DMSO, 0.4 ng/ μ L of PI4KIII β , 16 ng/ μ L of PI4KIII α , and 7.6 ng/ μ L of PI3K- α /p85 α . All reactions were performed at 30 °C for 10 min. Reactions were stopped by adding 5 μ L of phosphoric acid 0.8%. Aliquots (10 μ L) were then transferred into a P30 Filtermat (PerkinElmer) and washed five times with 0.5% phosphoric acid and four times with water for 5 min. The filter was dried and transferred to a sealable plastic bag, and scintillation cocktail (4 mL) was added. Spotted reactions were read in a scintillation counter (Trilux, PerkinElmer). IC₅₀ values were obtained according to eq 1, where v is the measured reaction velocity, V is the apparent maximal velocity in the absence of inhibitor, I is the inhibitor concentration, and IC₅₀ is the 50% inhibitory concentration.

$$v = V / \{1 + (I/IC_{50})\} \quad (1)$$

Lipidic Substrate Preparation. Phosphatidylinositol (PI, Sigma) and 2-oleoyl-1-palmitoyl-*sn*-glycero-3-phospho-L-serine (PS, Sigma) were dissolved in chloroform/methanol 9:1 and mixed at a 1:3 ratio. After chloroform/methanol evaporation, water was added to 1:62.5 w/v and the mixture was sonicated to clarity.

Kinase Panel. All tyrosine- and serine/threonine kinase reactions were performed according to the manufacturer's instructions, using 10–50 ng of enzyme. Details on the nature of the substrates and their concentration are reported elsewhere.⁶³ For some kinases, NP-40 or BSA was added. All reactions were performed in 10 μ L at 30 °C for 10 min using protein low-binding tubes. Reactions were stopped, transferred to filter, and counted as reported in ref 59. PI4KIII β was purchased from ProQinase. Reactions were performed according to the manufacturer's instructions and detected using ADP-Glo lipid kinase assay (Promega).

■ ASSOCIATED CONTENT

■ Supporting Information

The Supporting Information is available free of charge on the ACS Publications website at DOI: 10.1021/acs.jmedchem.6b01521.

3D coordinates of the PI4KIII β and PI4KIII α homology models (PDB1, PDB2)
Molecular formula strings (CSV)

■ AUTHOR INFORMATION

■ Corresponding Authors

*(M.R.) E-mail: marco.radi@unipr.it; phone: +39 0521 906080; fax: +39 0521 905006.

*(J.N.) E-mail: johan.neyts@kuleuven.be; phone: +32 163 21893; fax: +32 163 37340.

■ ORCID

Marco Pieron: 0000-0001-9190-3712

Marco Radi: 0000-0002-0874-6697

■ Notes

The authors declare no competing financial interest.

■ ACKNOWLEDGMENTS

Work in the P4T group has been supported by the Chiesi Foundation (Bando Dottorati di Ricerca 2014) and by the University of Parma (to M.R.). Work in the IGM laboratory has been supported by the Italian Cancer Research Association (AIRC), Grant IG15868. E.L.'s work was supported by the Cystic Fibrosis Trust (CFT Project No RS31). S.L. is funded by

the China Scholarship Council (CSC) (Grant 201403250056) and K.L. is supported by the European Union as a Marie-Sklodowska Curie European Training Network ANTIVIRALS (GA 642434).

■ ABBREVIATIONS

CF, cystic fibrosis; CFTR, cystic fibrosis transmembrane conductance regulator; COPD, chronic obstructive pulmonary disorder; CPE, cytopathic effect; CVB3, coxsackievirus B3; DC-SIGN, dendritic cell-specific intercellular adhesion molecule-3 grabbing nonintegrin; ECHO11, Echovirus 11; EV, enterovirus; F508del, deletion of Phe 508; RV, human rhinovirus; HTD, high-throughput docking; PI, phosphatidylinositol; PI4K, phosphatidylinositol 4-kinase; PIP₂, phosphatidylinositol 4,5-bisphosphate; PIP₃, phosphatidylinositol 3,4,5-trisphosphate; PI4P, phosphatidylinositol 4-phosphate; PV1, poliovirus 1; TGN, trans-Golgi network

■ REFERENCES

- (1) Adams, M. J.; King, A. M. Q.; Carstens, E. B. Ratification Vote on Taxonomic Proposals to the International Committee on Taxonomy of Viruses (2013). *Arch. Virol.* **2013**, *158*, 2023–2030.
- (2) Tapparel, C.; Siegrist, F.; Petty, T. J.; Kaiser, L. Picornavirus and Enterovirus Diversity with Associated Human Diseases. *Infect. Genet. Evol.* **2013**, *14*, 282–293.
- (3) Sabanathan, S.; Tan, L. V.; Thwaites, L.; Wills, B.; Qui, P. T.; Rogier van Doorn, H. Enterovirus 71 Related Severe Hand, Foot and Mouth Disease Outbreaks in South-East Asia: Current Situation and Ongoing Challenges. *J. Epidemiol. Community Health* **2014**, *68*, 500–502.
- (4) Esposito, S.; Bosis, S.; Niesters, H.; Principi, N. Enterovirus D68 Infection. *Viruses* **2015**, *7*, 6043–6050.
- (5) Leigh, R.; Proud, D. Virus-Induced Modulation of Lower Airway Diseases: Pathogenesis and Pharmacologic Approaches to Treatment. *Pharmacol. Ther.* **2015**, *148*, 185–198.
- (6) Wat, D. Impact of Respiratory Viral Infections on Cystic Fibrosis. *Postgrad. Med. J.* **2003**, *79*, 201–203.
- (7) (a) Waters, V.; Ratjen, F. Pulmonary Exacerbations in Children with Cystic Fibrosis. *Ann. Am. Thorac. Soc.* **2015**, *12* (Suppl. 2), S200–S206. (b) Singanayagam, A.; Joshi, P. V.; Mallia, P.; Johnston, S. L. Viruses Exacerbating Chronic Pulmonary Disease: The Role of Immune Modulation. *BMC Med.* **2012**, *10*, 27. (c) Goffard, A.; Lambert, V.; Salleron, J.; Herwegh, S.; Engelmann, I.; Pinel, C.; Pin, I.; Perrez, T.; Prévotat, A.; Dewilde, A.; Delhaes, L. Virus and Cystic Fibrosis: Rhinoviruses Are Associated with Exacerbations in Adult Patients. *J. Clin. Virol.* **2014**, *60*, 147–153. (d) Esther, C. R.; Lin, F. C.; Kerr, A.; Miller, M. B.; Gilligan, P. H. Respiratory Viruses Are Associated with Common Respiratory Pathogens in Cystic Fibrosis. *Pediatr. Pulmonol.* **2014**, *49*, 926–931.
- (8) van Ewijk, B. E.; van der Zalm, M. M.; Wolfs, T. F. W.; Fleer, A.; Kimpen, J. L. L.; Wilbrink, B.; van der Ent, C. K. Prevalence and Impact of Respiratory Viral Infections in Young Children With Cystic Fibrosis: Prospective Cohort Study. *Pediatrics* **2008**, *122*, 1171–1176.
- (9) Debing, Y.; Neyts, J.; Delang, L. The Future of Antivirals: Broad-Spectrum Inhibitors. *Curr. Opin. Infect. Dis.* **2015**, *28*, 596–602.
- (10) de Chasse, B.; Meyniel-Schicklin, L.; Aublin-Gex, A.; André, P.; Lotteau, V. New Horizons for Antiviral Drug Discovery from Virus-Host Protein Interaction Networks. *Curr. Opin. Virol.* **2012**, *2*, 606–613.
- (11) Delang, L.; Paeshuysse, J.; Neyts, J. The Role of Phosphatidylinositol 4-Kinases and Phosphatidylinositol 4-Phosphate during Viral Replication. *Biochem. Pharmacol.* **2012**, *84*, 1400–1408.
- (12) Hsu, N. Y.; Illytska, O.; Belov, G.; Santiana, M.; Chen, Y. H.; Takvorian, P. M.; Pau, C.; van der Schaar, H.; Kaushik-Basu, N.; Balla, T.; Cameron, C. E.; Ehrenfeld, E.; van Kuppeveld, F. J. M.; Altan-Bonnet, N. Viral Reorganization of the Secretory Pathway Generates Distinct Organelles for RNA Replication. *Cell* **2010**, *141*, 799–811.

- (13) Arita, M.; Kojima, H.; Nagano, T.; Okabe, T.; Wakita, T.; Shimizu, H. Phosphatidylinositol 4-kinase III Beta Is a Target of Enviroxime-Like Compounds for Antipoliiovirus Activity. *J. Virol.* **2011**, *85*, 2364–2372.
- (14) van der Schaar, H. M.; Leyssen, P.; Thibaut, H. J.; de Palma, A.; van der Linden, L.; Lanke, K. H. W.; Lacroix, C.; Verbeke, E.; Conrath, K.; MacLeod, A. M.; Mitchell, D. R.; Palmer, N. J.; van de Poël, H.; Andrews, M.; Neyts, J.; van Kuppeveld, F. J. M. A Novel, Broad-Spectrum Inhibitor of Enterovirus Replication That Targets Host Cell Factor Phosphatidylinositol 4-Kinase III β . *Antimicrob. Agents Chemother.* **2013**, *57*, 4971–4981.
- (15) Di Paolo, G.; De Camilli, P. Phosphoinositides in Cell Regulation and Membrane Dynamics. *Nature* **2006**, *443*, 651–657.
- (16) Clayton, E. L.; Minogue, S.; Waugh, M. G. Mammalian Phosphatidylinositol 4-Kinases as Modulators of Membrane Trafficking and Lipid Signaling Networks. *Prog. Lipid Res.* **2013**, *52*, 294–304.
- (17) Balla, T. Phosphoinositides: Tiny Lipids With Giant Impact on Cell Regulation. *Physiol. Rev.* **2013**, *93*, 1019–1137.
- (18) Himmel, B.; Nagel, G. Protein Kinase-Independent Activation of CFTR by Phosphatidylinositol Phosphates. *EMBO Rep.* **2004**, *5*, 85–90.
- (19) Balla, A.; Balla, T. Phosphatidylinositol 4-Kinases: Old Enzymes with Emerging Functions. *Trends Cell Biol.* **2006**, *16*, 351–361.
- (20) Altan-Bonnet, N.; Balla, T. Phosphatidylinositol 4-Kinases: Hostages Harnessed to Build Panviral Replication Platforms. *Trends Biochem. Sci.* **2012**, *37*, 293–302.
- (21) Boura, E.; Nencka, R. Phosphatidylinositol 4-Kinases: Function, Structure, and Inhibition. *Exp. Cell Res.* **2015**, *337*, 136–145.
- (22) Mejdrová, I.; Chalupská, D.; Kögler, M.; Šála, M.; Pláčková, P.; Baumlová, A.; Hřebabec, H.; Procházková, E.; Dejmeke, M.; Guillon, R.; Struin, D.; Weber, J.; Lee, G.; Birkus, G.; Mertlíková-Kaiserová, H.; Boura, E.; Nencka, R. Highly Selective Phosphatidylinositol 4-Kinase III β Inhibitors and Structural Insight into Their Mode of Action. *J. Med. Chem.* **2015**, *58*, 3767–3793.
- (23) MacLeod, A. M.; Mitchell, D. R.; Palmer, N. J.; Van de Poël, H.; Conrath, K.; Andrews, M.; Leyssen, P.; Neyts, J. Identification of a Series of Compounds with Potent Antiviral Activity for the Treatment of Enterovirus Infections. *ACS Med. Chem. Lett.* **2013**, *4*, 585–589.
- (24) LaMarche, M. J.; Borawski, J.; Bose, A.; Capacci-Daniel, C.; Colvin, R.; Dennehy, M.; Ding, J.; Dobler, M.; Drumm, J.; Gaitner, L. A.; Gao, J.; Jiang, X.; Lin, K.; McKeever, U.; Puyang, X.; Raman, P.; Thohan, S.; Tommasi, R.; Wagner, K.; Xiong, X.; Zabawa, T.; Zhu, S.; Wiedmann, B. Anti-Hepatitis C Virus Activity and Toxicity of Type III Phosphatidylinositol-4-Kinase Beta Inhibitors. *Antimicrob. Agents Chemother.* **2012**, *56*, 5149–5156.
- (25) Balla, A.; Tuymetova, G.; Toth, B.; Szentpetery, Z.; Zhao, X.; Knight, Z. A.; Shokat, K.; Steinbach, P. J.; Balla, T. Design of Drug-Resistant Alleles of Type-III Phosphatidylinositol 4-Kinases Using Mutagenesis and Molecular Modeling. *Biochemistry* **2008**, *47*, 1599–1607.
- (26) Knight, Z. A.; Gonzalez, B.; Feldman, M. E.; Zunder, E. R.; Goldenberg, D. D.; Williams, O.; Loewith, R.; Stokoe, D.; Balla, A.; Toth, B.; Balla, T.; Weiss, W. A.; Williams, R. L.; Shokat, K. M. A Pharmacological Map of the PI3-K Family Defines a Role for p110 α in Insulin Signaling. *Cell* **2006**, *125*, 733–747.
- (27) Anighoro, A.; Bajorath, J.; Rastelli, G. Polypharmacology: Challenges and Opportunities in Drug Discovery: Miniperspective. *J. Med. Chem.* **2014**, *57*, 7874–7887.
- (28) Reddy, A. S.; Zhang, S. Polypharmacology: Drug Discovery for the Future. *Expert Rev. Clin. Pharmacol.* **2013**, *6*, 41–47.
- (29) Bowers, K. J.; Chow, E.; Xu, H.; Dror, R. O.; Eastwood, M. P.; Gregersen, B. A.; Klepeis, J. L.; Kolossvary, I.; Moraes, M. A.; Sacerdoti, F. D.; Salmon, J. K.; Shan, Y.; Shaw, D. E. Scalable Algorithms for Molecular Dynamics Simulations on Commodity Clusters. Proceedings of the 2006 ACM/IEEE conference on Supercomputing; ACM: New York, 2006.
- (30) Wang, Y.; Suzek, T.; Zhang, J.; Wang, J.; He, S.; Cheng, T.; Shoemaker, B. A.; Gindulyte, A.; Bryant, S. H. PubChem BioAssay: 2014 update. *Nucleic Acids Res.* **2014**, *42* (Database issue), D1075–D1082.
- (31) <http://www.asinex.com/> accessed on February 14, 2014.
- (32) Pedemonte, N.; Sonawane, N. D.; Taddei, A.; Hu, J.; Zegarar-Moran, O.; Suen, Y. F.; Robins, L. I.; Dicus, C. W.; Willenbring, D.; Nantz, M. H.; Kurth, M. J.; Galletta, L. J.; Verkman, A. S. Phenylglycine and Sulfonamide correctors of Defective Delta F508 and G551D Cystic Fibrosis Transmembrane Conductance Regulator Chloride-Channel Gating. *Mol. Pharmacol.* **2005**, *67*, 1797–1807.
- (33) Pedemonte, N.; Lukacs, G. L.; Du, K.; Caci, E.; Zegarar-Moran, O.; Galletta, L. J.; Verkman, A. S. Small-molecule Correctors of Defective DeltaF508-CFTR Cellular Processing Identified by High-Throughput Screening. *J. Clin. Invest.* **2005**, *115*, 2564–2571.
- (34) Burke, J. E.; Inglis, A. J.; Perisic, O.; Masson, G. R.; McLaughlin, S. H.; Rutaganira, F.; Shokat, K. M.; Williams, R. L. Structures of PI4KIII β Complexes Show Simultaneous Recruitment of Rab11 and Its Effectors. *Science* **2014**, *344*, 1035–1038.
- (35) Yoo, C. L.; Yu, G. J.; Yang, B.; Robins, L. I.; Verkman, A. S.; Kurth, M. J. 4'-Methyl-4,5'-Bithiazole-Based Correctors of Defective Δ F508-CFTR Cellular Processing. *Bioorg. Med. Chem. Lett.* **2008**, *18*, 2610–2614.
- (36) Donald, M. B.; Rodriguez, K. X.; Shay, H.; Phuan, P. W.; Verkman, A. S.; Kurth, M. J. Click-Based Synthesis of Triazolobithiazole Δ F508-CFTR Correctors for Cystic Fibrosis. *Bioorg. Med. Chem.* **2012**, *20*, 5247–5253.
- (37) Haydon, D. J.; Bennett, J. M.; Brown, D.; Collins, I.; Galbraith, G.; Lancett, P.; Macdonald, R.; Stokes, N. R.; Chauhan, P. K.; Sutariya, J. K.; Nayal, N.; Srivastava, A.; Beanland, J.; Hall, R.; Henstock, V.; Noula, C.; Rockley, C.; Czaplowski, L. Creating an Antibacterial with in Vivo Efficacy: Synthesis and Characterization of Potent Inhibitors of the Bacterial Cell Division Protein PtsZ with Improved Pharmacological Properties. *J. Med. Chem.* **2010**, *53*, 3927–3936.
- (38) De Luca, G. V.; Kim, U. T.; Vargo, B. J.; Duncia, J. V.; Santella, J. B.; Gardner, D. S.; Zheng, C.; Liauw, A.; Wang, Z.; Emmett, G.; Wacker, D. A.; Welch, P. K.; Covington, M.; Stowell, N. C.; Wadman, E. A.; Das, A. M.; Davies, P.; Yelawaram, S.; Graden, D. M.; Solomon, K. A.; Newton, R. C.; Trainor, G. L.; Decicco, C. P.; Ko, S. S. Discovery of CC Chemokine Receptor-3 (CCR3) Antagonists with Picomolar Potency. *J. Med. Chem.* **2005**, *48*, 2194–2211.
- (39) Diab, S.; Teo, T.; Kumarasiri, M.; Li, P.; Yu, M.; Lam, F.; Basnet, S. K. C.; Sykes, M. J.; Albrecht, H.; Milne, R.; Wang, S. Discovery of 5-(2-(Phenylamino)pyrimidin-4-yl)thiazole-2(3H)-one Derivatives as Potent Mnk2 Inhibitors: Synthesis, SAR Analysis and Biological Evaluation. *ChemMedChem* **2014**, *9*, 962–972.
- (40) Sperandio, O.; Petitjean, M.; Tuffery, P. wwwLigCSRre: a 3D Ligand-Based Server for Hit Identification and Optimization. *Nucleic Acids Res.* **2009**, *37*, W504–W509.
- (41) (a) Radi, M.; Falchi, F.; Garbelli, A.; Samuele, A.; Bernardo, V.; Paolucci, S.; Baldanti, F.; Schenone, S.; Manetti, F.; Maga, G.; Botta, M. Discovery of the First Small Molecule Inhibitor of Human DDX3 Specifically Designed to Target the RNA Binding Site: Towards the next Generation HIV-1 Inhibitors. *Bioorg. Med. Chem. Lett.* **2012**, *22*, 2094–2098. (b) Bloom, J. D.; Digrandi, M. J.; Dushin, R. G.; Curran, K. J.; Ross, A. A.; Norton, E. B.; Terefenko, E.; Jones, T. R.; Feld, B.; Lang, S. A. Thiourea Inhibitors of Herpes Viruses. Part 1: Bis-(Aryl)thiourea Inhibitors of CMV. *Bioorg. Med. Chem. Lett.* **2003**, *13*, 2929–2932.
- (42) Borrok, M. J.; Kiessling, L. Non-Carbohydrate Inhibitors of the Lectin DC-SIGN. *J. Am. Chem. Soc.* **2007**, *129*, 12780–12785.
- (43) Ren, X. X.; Ma, L.; Liu, Q. W.; Li, C.; Huang, Z.; Wu, L.; Xiong, S. D.; Wang, J. H.; Wang, H. B. The Molecule of DC-SIGN Captures Enterovirus 71 and Confers Dendritic Cell-Mediated Viral Trans-Infection. *Viral J.* **2014**, *11*, 47.
- (44) Ye, L.; Hu, B.; El-Badri, F.; Hudson, B. M.; Phuan, P. W.; Verkman, A. S.; Tantillo, S. J.; Kurth, M. J. Δ F508-CFTR Correctors: Synthesis and Evaluation of Thiazole-Tethered Imidazolones, Oxazolones, Oxadiazoles, and Thiadiazoles. *Bioorg. Med. Chem. Lett.* **2014**, *24*, 5840–5844.
- (45) Ford Siltz, L. A.; Viktorova, E. G.; Zhang, B.; Kouivaskaia, D.; Dragunsky, E.; Chumakov, K.; Isaacs, L.; Belov, G. A. New Small-Molecule Inhibitors Effectively Blocking Picornavirus Replication. *J. Virol.* **2014**, *88*, 11091–11107.

- (46) Leong, W. F.; Chow, V. T. Transcriptomic and Proteomic Analyses of Rhabdomyosarcoma Cells Reveal Differential Cellular Gene Expression in Response to Enterovirus 71 Infection. *Cell. Microbiol.* **2006**, *8*, 565–580.
- (47) Van Goor, F.; Hadida, S.; Grootenhuis, P. D. J.; Burton, B.; Stack, J. H.; Straley, K. S.; Decker, C. J.; Miller, M.; McCartney, J.; Olson, E. R.; Wine, J. J.; Frizzell, R. A.; Ashlock, M.; Negulescu, P. A. Correction of the F508del-CFTR Protein Processing Defect in Vitro by the Investigational Drug VX-809. *Proc. Natl. Acad. Sci. U. S. A.* **2011**, *108*, 18843–18848.
- (48) Langron, E.; Simone, M. I.; Delalande, C. M. S.; Reymond, J.-L.; Selwood, D. L.; Vergani, P. Improved Fluorescence Assays to Measure the Defects Associated with F508del-CFTR Allow Identification of New Active Compounds. *Br. J. Pharmacol.* doi: **201710.1111/bph.13715**.
- (49) Van Goor, F.; Hadida, S.; Grootenhuis, P. D. J.; Burton, B.; Cao, D.; Neuberger, T.; Turnbull, A.; Singh, A.; Joubran, J.; Hazlewood, A.; Zhou, J.; McCartney, J.; Arumugam, V.; Decker, C.; Yang, J.; Young, C.; Olson, E. R.; Wine, J. J.; Frizzell, R. A.; Ashlock, M.; Negulescu, P. Rescue of CF Airway Epithelial Cell Function in Vitro by a CFTR Potentiator, VX-770. *Proc. Natl. Acad. Sci. U. S. A.* **2009**, *106*, 18825–18830.
- (50) Friesner, R. A.; Banks, J. L.; Murphy, R. B.; Halgren, T. A.; Klicic, J. J.; Mainz, D. T.; Repasky, M. P.; Knoll, E. H.; Shaw, D. E.; Shelley, M.; Perry, J. K.; Francis, P.; Shenkin, P. S. Glide: A New Approach for Rapid, Accurate Docking and Scoring. 1. Method and Assessment of Docking Accuracy. *J. Med. Chem.* **2004**, *47*, 1739–1749.
- (51) Warren, G. L.; Andrews, C. W.; Capelli, A.-M.; Clarke, B.; LaLonde, J.; Lambert, M. H.; Lindvall, M.; Nevins, N.; Semus, S. F.; Senger, S.; Tedesco, G.; Wall, I. D.; Woolven, J. M.; Peishoff, C. E.; Head, M. S. A Critical Assessment of Docking Programs and Scoring Functions. *J. Med. Chem.* **2006**, *49*, 5912–5931.
- (52) Manetti, F.; Falchi, F.; Crespan, E.; Schenone, S.; Maga, G.; Botta, M. N-(Thiazol-2-yl)-2-Thiophene Carboxamide Derivatives as Abl Inhibitors Identified by a Pharmacophore-Based Database Screening of Commercially Available Compounds. *Bioorg. Med. Chem. Lett.* **2008**, *18*, 4328–4331.
- (53) Jacobson, M. P.; Pincus, D. L.; Rapp, C. S.; Day, T. J. F.; Honig, B.; Shaw, D. E.; Friesner, R. A. A Hierarchical Approach to All-Atom Protein Loop Prediction. *Proteins: Struct., Funct., Genet.* **2004**, *55*, 351–367.
- (54) Bates, P. A.; Kelley, L. A.; MacCallum, R. M.; Sternberg, M. J. E. Enhancement of Protein Modeling by Human Intervention in Applying the Automatic Programs 3D-JIGSAW and 3D-PSSM. *Proteins: Struct., Funct., Genet.* **2001**, *45* (Suppl. 5), 39–46.
- (55) Schrödinger Release 2014-3: Maestro, version 9.9; Schrödinger, LLC: New York, NY, 2014.
- (56) Irwin, J. J.; Sterling, T.; Mysinger, M. M.; Bolstad, E. S.; Coleman, R. G. ZINC: a Free Tool to Discover Chemistry for Biology. *J. Chem. Inf. Model.* **2012**, *52*, 1757–1768.
- (57) Schrödinger Release 2015-4: LigPrep, version 3.6; Schrödinger, LLC: New York, NY, 2015.
- (58) (a) Schrödinger Release 2015-4: Schrödinger Suite 2015-4 Protein Preparation Wizard, Epik version 3.4; Schrödinger, LLC: New York, NY, 2015. (b) Impact version 6.9; Schrödinger, LLC: New York, NY, 2015; Prime version 4.2, Schrödinger, LLC, New York, NY, 2015.
- (59) Harder, E.; Damm, W.; Maple, J.; Wu, C.; Reboul, M.; Xiang, J. Y.; Wang, L.; Lupyan, D.; Dahlgren, M. K.; Knight, J. L.; Kaus, J. W.; Cerutti, D. S.; Krilov, G.; Jorgensen, W. L.; Abel, R.; Friesner, R. A. OPLS3: A Force Field Providing Broad Coverage of Drug-like Small Molecules and Proteins. *J. Chem. Theory Comput.* **2016**, *12*, 281–296.
- (60) Small-Molecule Drug Discovery Suite 2015-4: Glide, version 6.9; Schrödinger, LLC: New York, NY, 2015.
- (61) Galiotta, L. J. V.; Haggie, P. M.; Verkman, A. S. Green Fluorescent Protein-Based Halide Indicators with Improved Chloride and Iodide Affinities. *FEBS Lett.* **2001**, *499*, 220–224.
- (62) Li, Y.; Tsien, R. W. pHTomato, a Red, Genetically Encoded Indicator That Enables Multiplex Interrogation of Synaptic Activity. *Nat. Neurosci.* **2012**, *15*, 1047–1053.
- (63) Tassini, S.; Castagnolo, D.; Scalacci, N.; Kissova, M.; Armijos-Rivera, J. I.; Giagnorio, F.; Maga, G.; Costantino, G.; Crespan, E.; Radi, M. A multicomponent pharmacophore fragment-decoration approach to identify selective LRRK2-targeting probes. *MedChemComm* **2016**, *7*, 484–494.